APPENDIX A

DRILLCORE LOGS

Scope of the Logging

Fifty six drillholes, representative of all drilling sections established by North Broken Hill Limited in the Northern Leases, were logged in July 1975. A total of 51,096 metres was studied and logged in varying detail. The general approach was to log all significant changes in structure within each drillhole. In practice this involved logging zones of constant (or in some cases constantly varying) foliation (bedding, schistosity and gneissosity), logging the relative strengths of different schistosities and any associated overprinting criteria, logging other structures observed, e.g. graded bedding, layering/schistosity relationships, small folds, lineations, etc., and logging all significant lithological changes. The lattermost operation varied in its scale, depending on the importance attached to the various categories of lithology. Except for unusual lithologies, e.g. those with potential as marker units, the rock types are given brief field names without further description of their mineralogy. For detailed petrological descriptions see Chapter 2. For example, in some drillholes all pegmatite bodies (to a minimum width of approximately 0.5m) were logged, while in other drillholes none but the largest pegmatites were logged individually. The detail with which each drillhole was studied is indicated at the beginning of each log.

In addition, several holes were superficially examined with a view to observing any graded bedding present.

Layout of the Drillcore Logs

First column : Depth interval down drillhole, in metres.

Second column : Orientation of any foliations present, expressed as the angle (to within 5^{o}) between the foliation and the drill-core axis, i.e. the angle $|\ 90^{o}-\delta\ |$ where δ is defined as in Appendix B.

Third column : Information on lithology, schistosity development, facing evidence, etc.

Basis of Field Rock Names

Layered micaceous rocks

Sillimanite-bearing

Pelitic schist - dominantly sillimanite and a strong "mica" component (biotite-muscovite-chlorite). Layering is generally bedding.

Psammitic schist - at least 40% (quartz + K-feldspar), generally > 60%. Sillimanite and garnet generally as abundant as "mica" component. Layering is generally bedding. Tough, indurate rocks.

Lacking sillimanite

Quartz-mica schist[1] - lacks sillimanite (0-10%). May be prograde or retrograde. Generally pale green-grey. Layering is generally fine and of uncertain origin.

Quartzite - little mica (may have a poor schistosity), dominantly quartz + K-feldspar. Layering is generally bedding.

Retrograde

Retrograde schist, chloritic schist, chloritoid schist - variations on a muscovite + sericite + chlorite + (biotite) + (Quartz) + (chloritoid) schist, generally with a strong foliation which is retrograde in origin. Fine-grained rocks, green-grey to dark green or almost black.

Granite gneiss - quartz + K-feldspar + biotite + plagioclase gneiss with strong gneissosity defined by thin biotite versus quartzofeldspathic layers.

Potosi gneiss - general name for garnet-bearing granite gneiss, commonly rich in a pink or orange K-feldspar. Gradational into Potosi quartzite.

Potosi quartzite - quartzite with abundant quartz + feldspar veins, commonly ptygmatically folded.

Pegmatite - coarse, quartz + K-feldspar + (muscovite) rock with idiomorphic texture, commonly showing cuneiform and perthitic textures, and discordant

---

[1] Note the specific difference in classification between the sillimanite rocks ("pelitic" and "psammitic" schist) on the one hand and "quartz-mica" schist on the other: the former reflect original rock-type (muddy versus sandy); the latter refers to a rock of either pelitic or psammitic parentage, depending on the ratio of quartz to mica.

Pegmatite (cont'd)
to foliation.

Amphibolite - dark green to black, basic rock containing hornblende (+ pyroxene), with a granoblastic, generally gneissic texture. Fine gneissic layering may or may not be present. Commonly chloritized to a varying degree.

Garnet amphibolite - as above but with appreciable garnet content.

Black schist - retrograde, fine schist, $\pm$ garnets. Almost always adjacent to amphibolite or garnet amphibolite.

Mineralized - containing primary sulphide minerals (generally split core).

LIST OF DRILLHOLES LOGGED

Section	Hole Number	Length(m)
No. 2 Shaft	DD 508	1,248
	2084	316
	2088	524
	3176	271
	3178	705
	3190	587
No. 3 Shaft	2003	797
	2030	762
	2034	41
	2042	478
	2043	274
	4012	1,080
	4018	1,307
East of Mine	3188	263
	3192	263
	3195	317
Cosgroves	833	616
	3133	1,488
	3183	352
	3185	304
	4017	2,136
Imperial Ridge	3182	1,959
Potosi	3109	595
	3117	498
	3167	1,540
Round Hill	3105	1,032
	3105A	475
	3105B	368
	3115	449
	3115A	364
	3156	812
	3157	1,676
	3157A	1,843
	3179	2,135
	3194	561
Flying Doctor	3031	246
	3033	182
	3034	360

LIST OF DRILLHOLES LOGGED (cont'd)

Section	Hole Number	Length(m)
Flying Doctor (cont'd)	3036	265
	3074	1,596
	3155	1,285
	3170	1,449
	3186	1,902
Globe	956	679
	961	980
	963	519
	969	615
	970	431
Carbonate Ridge	15N-2	305
	15N-4	515
	3099	870
	3113	1,262
	3154	1,343
	3154A	450
	3160	2,254
	3160A	921
	3163	374
	3164	444
Alpha	3043	213
	3046	172
	3158	712
	3181	1,326
	3181/D2	210
Between Carbonate Ridge and Alpha	3175	450
Rupee	3184	330
Total length:		51,096 metres

DD 508 — No. 2 Shaft Section

Reconnaissance — Logged 10-2-76

0-1050	S||S_0 var. av. 50^o-90^o	
1050-1248	S||S_0 fairly constant, 70^o-90^o near base 90^o	
0- 61		PSAMMITIC SCHIST. Pink/white/grey. Graded bedding, younging downhole: 54m mod.good
61		RETROGRADE SCHIST. Thin.
61- 560		PELITIC SCHIST. Greyish (chloritic l/P). Graded bedding, younging uphole: 81m moderate. Graded bedding, younging downhole: 151m " Graded bedding, younging uphole: 279m poor " " " " : 310m mod. good " " " " : 321m good " " " " : 323m mod. good " " " " : 325m " " " " " " : 326m good " " " " : 335m moderate " " " " : 409m mod. good " " " " : 524m " "
560- 642		PSAMMITIC SCHIST. Graded bedding, younging uphole: 587m good
642- 645		AMPHIBOLITE. Non-garnetiferous.
645- 885		PSAMMITIC SCHIST. Graded bedding, younging downhole: 668m poor " " " " 674m good - is corebox correctly ordered?.
885- 960		PELITIC SCHIST.
960-1099		PSAMMITIC SCHIST.
1099-1151		AMPHIBOLITE. Non-garnetiferous.
1151-1153		GRANITE GNEISS. Foliated quartz-feldspar-biotite gneiss- ?Potosi lithology.
1153-1170		PSAMMITIC SCHIST.

1170-1201		AMPHIBOLITE; detailed logging: Milky quartz, chlorite and garnet: 2m Non-garnetiferous amphibolite : 28m Milky quartz, chlorite and garnet: 1m
1201-1248		PSAMMITIC SCHIST.
1248		END OF HOLE.

DD 2084 — No. 2 Shaft Section

Reconnaissance — Logged 13-2-76

0-316	$S \| \| S_0$ av. 20^0-50^0	Drillhole in psammopelitic schist at top, becoming more pelitic with depth. $S \| \| S_0$ folded l/P. S_2 rarely oblique to $S_1 \| \| S_0$.
	GRADED BEDDING DATA:	
7	$S \| \| S_0$ 30^0	Younging downhole, mod. good
13	S_{2-3} 0^0-30^0 (partly retrogressed)	" " , moderate
22	$S \| \| S_0$ 40^0	" " , good
169		" " , moderate
170-200	S_2 0^0-30^0	Strongly folded section with S_2 oblique to $S_1 \| \| S_0$ in many places.
171	$S \| \| S_0$ 50^0	Younging downhole, very good
		Specimen: 681 garnets graded in size.
179		Younging uphole, very good
181		Younging uphole, moderate to poor
183-194		Many "semi-graded" layers in this section, lacking distinct tops and/or bottoms.
187		Younging downhole, moderate
191		" " , good
316		End of detailed search for graded bedding.
316	S_R 40^0-70^0 av. 55^0	RETROGRADE SCHIST commences, with QUARTZ-MICA SCHIST interspersed.
643	$S \| \| S_0$ 45^0	Graded bedding, younging downhole: mod.good.

DD 2088 No. 2 Shaft Section

Reconnaissance Logged 13-2-76

0-435		PSAMMITIC SCHIST. Pink/white. Quartzitic rocks appear below 315m.

GRADED BEDDING DATA:

17	$S \| \| S_0$ 40^0	Younging downhole, moderate
54	$S \| \| S_0$ var.	" " , good, S_2 strongly oblique
	S_2 0^0-15^0	to visibly folded $S \| \| S_0$.
61- 70	$S_1 \| \| S_0$ 60^0-90^0	PSAMMITIC SCHIST. Well graded, layered schist,
	S_2 0^0-20^0	S_2 strongly oblique to $S_1 \| \| S_0$.
67.5		Younging downhole, mod. good.
68.0		" " , " "
68.3		" " , " "
73.8	$S \| \| S_0$ 35^0	Younging uphole, moderate
98-110	$S_1 \| \| S_0$ 45^0-90^0	PSAMMITIC SCHIST. Well graded, layered schist,
	S_2 0^0-30^0	S_2 strongly oblique to $S_1 \| \| S_0$.
99		Younging downhole, moderate
101-104		Younging uphole, good series of graded beds.
		Specimen: 682 graded bed with S_2 schistosity.

Interpretation: If 61-70m, facing downward on S_{2-3}, is correlated with 98-110, facing upward on S_{2-3}, we have two possibilities: (1) F_1 fold. The oblique schistosity in specimen 682 would be S_2 (or S_3).

(2) F_2 fold. The oblique schistosity in specimen 682 would be necessarily S_3.

110-435	$S \| \| S_0$ var. commonly 0^0.	
435	S_R gradation 50^0 top 45^0 base	RETROGRADE SCHIST commences.
524		END OF HOLE.

DD 3176 No. 2 Shaft Section

Moderate detail Logged 27-7-75

0- 54	Gneissosity S_1 strongly var. S_2 axial plane to folds in S_1 60^o-90^o	GRANITE GNEISS. Altered to orange/pink K feldspar assemblages 1/P, and strongly veined with quartz-feldspar segregations. Gneissosity strongly folded, with the segregations in the axial plane S_2. The latter indicate F_2 synform to east: 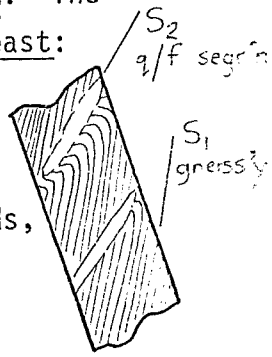 Several sillimanite schist bands, up to 2m thick, are strongly folded and sheared.
54- 81	$S_1 \| \| S_0$ av. 0^o S_2 axial plane to folds in $S_1 \| \| S_0$ av. 60^o.	SILLIMANITE SCHIST, biotite rich. Black/white/pink, "psammite" lithology with unusual enrichment in biotite. $S_1 \| \| S_0$ strongly contorted in kinks and open folds, with little S_2 schistosity. Interpretation: broad F_2 hinge area. Specimen: 638
81-136	Gneissosity S_1 55^o S_2 axial plane to folds in S_1 45^o	GRANITE GNEISS. Altered to orange/pink K feldspar but not as strongly veined as 0-54m. Gneissosity relatively constant (folded 1/P). Folds indicate F_2 synform to west: 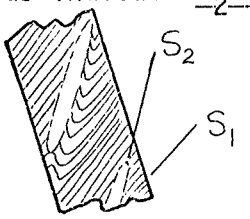
136-138		SILLIMANITE SCHIST. As 54-81; variable $S_1 \| \| S_0$, with little S_2 schistosity. Specimen: 639 F_2 fold.
138-142	Gneissosity S_1 parallel to schistosity S_{1-2} appr. 70^o	GRANITE GNEISS.

Strong shearing at and near contacts between granite gneiss and sillimanite schist in this drillhole.

DD 3176 (cont'd)

Moderate detail

142-253	$S \| \| S_0$ 60^0-90^0 S_2 axial plane to folds in $S \| \| S_0$ 60^0-90^0	PSAMMITIC SCHIST. Pink/white psammopelite, becoming partly retrogressed with depth. S_2 oblique to $S_1 \| \| S_0$ in places. GARNETIFEROUS AMPHIBOLITE. Fairly altered; also some sillimanite schist: 187-189m.
253-269	S_1 65^0-70^0	AMPHIBOLITE, garnetiferous in part. Margins strongly altered to quartz-garnet assemblages. Gradational into basal 7m which is QUARTZ-GARNET-BIOTITE GNEISS; possible ?Potosi lithology. <u>Specimen</u>: 640 ?orthopyroxene present.
269-272	$S \| \| S_0$ 60^0-65^0	PSAMMITIC SCHIST. END OF HOLE. <u>No graded bedding observed</u>.

DD 3178 | No. 2 Shaft Section

Moderate detail | Logged 27-7-75 and 13-2-76

0-466	$S_1 \| \| S_0$ strongly var 0-145: 0^o-45^o av. 145-466: 0^o-30^o av. S_2 30^o-45^o	PSAMMITIC SCHIST. Classic S_2 regime with S_2 strongly oblique to $S_1 \| \| S_0$ in most places. $S_1 \| \| S_0$ strongly folded, with F_2 folds and S_0/S_2 relations indicating <u>F_2 synform to east</u>: 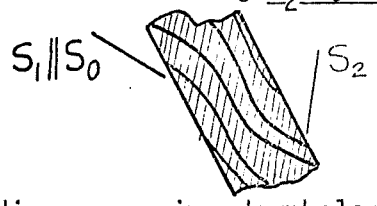 <u>Graded bedding, younging downhole</u>: 15m mod. good <u>" " " "</u>: 69m " " <u>" " " "</u>: 72m " " This section is strongly folded by F_2 folds (S_2 oblique to $S_1 \| \| S_0$). <u>Graded bedding, younging normal to core</u>: 117 mod. good <u>Graded bedding, younging downhole</u>: 207m good 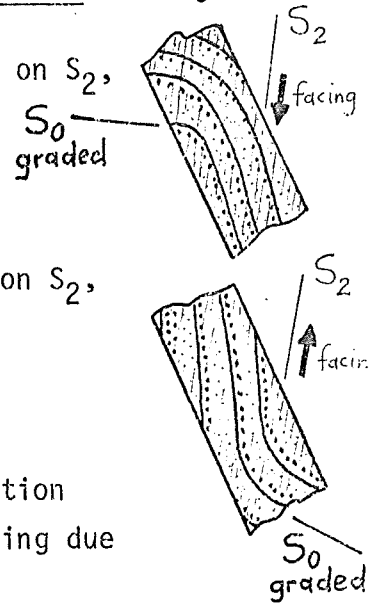 69m example: faces downward on S_2, consistent with <u>F_2 synform</u>, <u>inverted, to east</u>. 117m example: faces upward on S_2, consistent with <u>F_2 synform, right way up</u>, <u>to east</u>. <u>Interpretation</u>: one explanation is a local inversion of facing due to an F_1 fold.
466-704	$S \| \| S_0$ 60^o-70^o generally 625-645m: 80^o-90^o	PSAMMITIC SCHIST. Lithology as above, with quartzites becoming prominent toward base. Abrupt change in $S \| \| S_0$ angles is main feature of boundary with overlying unit, the angles in this interval remaining fairly constant throughout. Sequence becomes slightly retrogressed toward base. GARNETIFEROUS AMPHIBOLITE: 483-486m. Zone of strong alteration :486-497m AMPHIBOLITE, garnetiferous in part :497-511.

DD 3178

Moderate detail (cont'd)

466-704 (cont'd)		As found in DD 3176, 253-269m: basal 7m strongly altered to a QUARTZ-GARNET-BIOTITE GNEISS; possible ?Potosi lithology. GARNETIFEROUS AMPHIBOLITE; quartz present: 529-532m. Graded bedding, younging downhole: 563m moderate only.
704		END OF HOLE.

DD 3190 — No. 2 Shaft Section

Moderate detail — Logged 27-7-75 and 23-2-76

0- 69	Gneissosity S_1 30^0	POTOSI GNEISS. Coarse granite gneiss with abundant garnets. Many segregations and veins of quartz-feldspar, and strong orange feldspathic alteration, particularly near the top. Some sillimanite-rich patches.
69-284	$S \| \| S_0$ 40^0-50^0	PSAMMITIC SCHIST. Pink/white, becoming more psammitic with depth. Some pegmatites. Base of orange feldspathic alteration: 170m A yellowish, slight alteration l/P persists below 170m. Graded bedding, younging downhole: 177m mod.good " " " " : 218m moderate " " " " : 267m v.good " " " " : 273m v.good POTOSI QUARTZITE: ptygmatic veins in fine, pale grey quartzite, few garnets: 268-272m.
284-356	Amphib. S_1 55^0-60^0	AMPHIBOLITE, garnetiferous l/P. Detailed logging: Garnet-quartz-chlorite altered zone : 2m Non-garnetiferous amphibolite : 39m Garnet-quartz rich gneiss : 2m Chlorite-garnet banded, grey quartite: 5m Garnet-quartz-chlorite altered zone : 3m Amphibolite; plagioclase-garnet rich near top : 21m
356-361		MILKY QUARTZ and "APLITE". Intermixed phases with a coarse quartz-feldspar-biotite pegmatite at the base. The "aplite" is a fine, structureless quartz-feldspar rock with a pale creamy pink colour. Upper and lower contacts discordant. Specimen: 685 aplite
361-367	Amphib. S_1 60^0	AMPHIBOLITE. Slightly garnetiferous near base.
367-369		QUARTZITE, garnetiferous. Graded bedding, younging uphole: 369m mod. good.
369-372		PSAMMITIC SCHIST.

DD 3190 (cont'd)

Moderate detail

372-376	S_R 40°	RETROGRADE SCHIST. Ironstained, generally as DD 3195, 154-166m.
376-396	$S \| \| S_0$ 60°	QUARTZ MICA SCHIST.
396	S_R 50°	RETROGRADE SCHIST, 30cm thick. Black, with several small feldspar/quartz augen.
396-401	S_1 55°	POTOSI GNEISS. Fine grained.
401-409	S_R 70°-80°	MYLONITIC ZONE. Black and white, biotite granite gneiss and retrograde schist. Some relict sillimanite. Mylonitic gneissosity best developed at top and base, with S_R the main foliation in the centre.
	Comment:	Compare with DD 3195, 146-154m.
409-489	$S \| \| S_0$ 60°-70°	PSAMMITIC SCHIST. Graded bedding, younging uphole: 420m moderate " " " " : 428m mod. good " " " " : 488m mod. good Chloritic, black, non-dense rock with pyrite: 448-449m.
489-492		GARNETIFEROUS AMPHIBOLITE. Variable quartz-chlorite-plagioclase component.
492-549	$S \| \| S_0$ 60°-80°	PSAMMITIC SCHIST.
	0°: 532-535m	POTOSI GNEISS. Some S_R present: 516-527m, 542-549m
	Gneissosity S_1 80°.	
549-560	S_R 60°-80°	RETROGRADE SCHIST
560-584	S_1 80°-90°	POTOSI GNEISS. Transitional lithology to granite gneiss (variable garnet content).
584-586		AMPHIBOLITE. Non-garnetiferous. Sharp upper contact.
586		END OF HOLE.

DD 2003 | No. 3 Shaft Section

Moderate detail | Logged 10-2-76

0-210		UNDIFFERENTIATED SCHIST. Pink/white sillimanite schist, partly retrogressed. Graded bedding, younging uphole: 37m mod. good. " " " " : 204m v. good.
210-225		QUARTZ MICA SCHIST, chloritoid-bearing. Chloritoids fine to medium elongate, and generally randomly oriented within S_R.
225-315	S_R 60^o-80^o	RETROGRADE SCHIST.
315-435		BIOTITE SCHIST. S_R grades into S_{3R} and S_3 with many F_3 folds visible. S_{3R} and S_3 biotitic, particularly 315-421m. Section similar to DD 2042, 281-344m. Patchy retrograde schist 1/P. Specimen: 679 biotitic S_3 crosscutting $S \| \| S_0$.
435-489	Fracture 90^o	QUARTZITIC GNEISS. White, becoming slightly more micaceous with depth. A very strong fracture is characteristic, crosscutting $S \| \| S_0$. Gneissosity very weakly developed. Grades into unit beneath.
489-538	Gneissosity S_1 and schistosity S_{1-2} var. 0^o-30^o mainly. Fracture 90^o.	POTOSI GNEISS. White, fine to medium grained granite gneiss (quartz and K feldspar in approximately equal proportion), with numerous small (av. 0.5 cm) garnets rimmed by ?chlorite or biotite (dark green to black). Gneissosity only weakly developed. Specimen: 680
538-615	Gneissosity S_1 and schistosity S_{1-2} var. 0^o-30^o mainly. Fracture 90^o.	GRANITE GNEISS. As Potosi gneiss above but without garnets. White rock with weak to moderate gneissosity.
615-618		AMPHIBOLITE. Non-garnetiferous, party chloritic.
618-698		GRANITE GNEISS. As 538-615m; minor garnets rimmed with ?chlorite or biotite.
698-725		RETROGRESSED GRANITE GNEISS. Chloritic.
725-728		AMPHIBOLITE. Non-garnetiferous, strongly chloritic.

DD 2003 (cont'd)
Moderate detail

728-797		QUARTZ MICA SCHIST. Strongly retrogressed, cream-green sericite-chlorite assemblage. Some retrogressed quartzites. Unit similar to 698-725 but more retrogressed.
797		END OF LOGGING.

DD 2030 — No. 3 Shaft Section

Reconnaissance — Logged 10-2-76

NOTES

1. RETROGRADE SCHIST in middle of drillhole (Globe-Vauxhall Shear Zone) contains many of Hobbs' Group 3 folds, with S_R axial plane 80^o-90^o.

   Specimen: 677

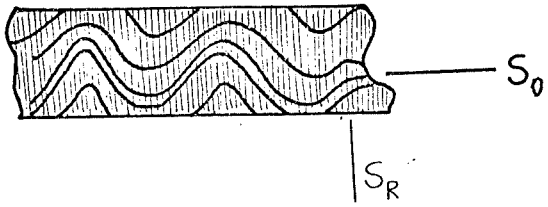

2. Below the Globe-Vauxhall Shear Zone is a dominantly quartzitic sequence:

   Graded bedding, younging downhole: 332m mod. good; S_0 35^o, variable locally around $?F_3$ folds.

   Graded bedding, younging downhole: 654m moderate to poor.

762m END OF HOLE.

DD 2034 — No. 3 Shaft Section

Reconnaissance — Logged 10-2-76

0-41m		PSAMMITIC SCHIST. Pink/white; no graded beds observed.
Below 41m		CORE INACCESSIBLE.

DD 2042 No. 3 Shaft Section

Moderate detail Logged 10-2-76

0-155		UNDIFFERENTIATED SCHIST.
155-170	$S_R \| \| S_0$ 60^o	QUARTZ MICA SCHIST, chloritoid-bearing. Large garnets present.
170-183	S_R 60^o	RETROGRADE SCHIST.
183-184		GARNET "SANDSTONE". Almost 100% orange garnet, fine grained, dense, with some pits and cavities.
184-188		RETROGRADE SCHIST.
188-196		MINERALIZED section. Massive and disseminated sulphide, principally galena/sphalerite/pyrite, in gangue of calcite/hedenbergite/bustamite.
196-260	S_R 70^o	RETROGRADE SCHIST. Very strong metamorphic layering parallel to S_R, which is kinked in numerous places.
260-281	S_{3R}/S_3 80^o-90^o	BIOTITE SCHIST. Black/white/grey schist, very rich in biotite, with layering S_0 strongly crenulated about axial planes. Subperpendicular to core - S_{3R} or S_3?
281-344	S_{3R}/S_3 80^o-90^o	PSAMMITIC SCHIST. As above but with less biotite, generally more quartzitic.
344-366		RETROGRADE SCHIST, some psammitic schist. Sharp top, diffuse base.
366-435		PSAMMITIC SCHIST. As 281-344m.
435-475		PSAMMITIC SCHIST. Some pink/white sillimanite/garnet patches, with S_2 oblique to $S_1 \| \| S_0$. Generally as above.
475-478		RETROGRADE SCHIST.
478		END OF HOLE.
		No graded bedding observed.

DD 2043 | No. 3 Shaft Section

Reconnaissance | Logged 10-2-76

0-186		PSAMMITIC SCHIST. Pink/white, quartzitic l/P. Graded bedding, younging uphole: 12m mod. good. Graded bedding, younging uphole: 27m moderate. Graded bedding, younging downhole: 70m mod. good.
186-195		QUARTZ MICA SCHIST, chloritoid bearing.
195-207		UNDIFFERENTIATED SCHIST.
207-213		QUARTZ MICA SCHIST, chloritoid-bearing. Fine, elongate chloritoid laths lying in S_R, defining a strong L_M in places. Also large, euhedral chloritoid grains also appear to be concordant with S_R, although bulky in cross-section.
213-274	S_R 60^o-55^o	RETROGRADE SCHIST. Very strong. Many of Hobbs' Group 4 folds present, folding S_R and L_M without an axial plane structure.
		Specimen: 678
274		END OF HOLE.

DD 4012 | No. 3 Shaft Section

Moderate detail | Logged 31-7-75

0-152	$S \| \| S_0$ 45^o-90^o av. 60^o S_3 0^o-40^o av. 25^o.	PELITIC SCHIST. S_3 dominant. S_2 becomes stronger downhole. S_2 oblique to $S_1 \| \| S_0$ 1/P.
152-312	$S_1 \| \| S_0$ var. S_2 50^o-90^o av. 70^o	PSAMMO-PELITIC SCHIST. S_2 strong, oblique to $S_1 \| \| S_0$ esp. 163m (S_2 90^o) 198-207m 229-256m } Negligible S_3. Specimens: 664 665 Graded bedding, younging uphole: 199m mod. good
312-433	$S_1 \| \| S_0$ var. S_2 70^o-90^o	PSAMMITIC SCHIST, quartzitic. Very sharp boundary with overlying pelitic and psammopelitic schist. S_2 regime.
433-439	Amphib. S_1 65^o	AMPHIBOLITE.
439-460	S_{2R} 45^o-60^o	PSAMMITIC SCHIST, quartzitic. Gradational boundaries above and below. Retrogressed schistosity oblique to $S \| \| S_0$ appears to be S_2.
460-506	S_R 0^o-30^o Av. 15^o	RETROGRADE SCHIST. Strong.
506-625	$S_1 \| \| S_0$ var. S_2 45^o-90^o av. 60^o	PSAMMITIC SCHIST, quartzitic. S_2 regime, with S_2 oblique to $S_1 \| \| S_0$ esp. 604-686m. Specimen: 666 S_1 stronger than S_2.
625-725	$S_1 \| \| S_0$ var. 0^o-90^o S_2 45^o-60^o	PSAMMITIC SCHIST, quartzitic. As above. Specimens: 667 S_2 oblique to $S_1 \| \| S_0$ 668 " " " "
725-745	S_{2-3} 40^o	PSAMMITIC SCHIST, quartzitic. S_3 appearing, but difficult to determine whether the general retrogressed schistosity is S_2 or S_3.
745-792	S_R 20^o	RETROGRADE SCHIST. Several bands. Garnet rich.
792-1079	S_2 var. mainly 45^o-90^o	PSAMMITIC SCHIST, quartzitic. General S_2 regime but S_3 1/P.
1079		END OF HOLE

DD 4018 — No. 3 Shaft Section

Reconnaissance — Logged 31-7-75 and 10-2-76

0- 168	$S \| \| S_0$ av. 45^0	PELITIC SCHIST. Little S_2 oblique to $S_1 \| \| S_0$.
168- 200	$S \| \| S_0$ av. 45^0	PSAMMITIC SCHIST, quartzitic.
200- 847	$S \| \| S_0$ var. 45^0-90^0	PSAMMITIC SCHIST, quartzitic.
	Amphib. S_1 50^0	AMPHIBOLITE, slightly garnetiferous :c.351m
	Amphib. S_1 55^0	AMPHIBOLITE, moderately garnetiferous :c.418m
		S_2 oblique to $S_1 \| \| S_0$ first visible : 445m
	S_{3R} 0^0-10^0	Patch of S_{3R} developed : 663m
		GARNETIFEROUS AMPHIBOLITE; thick: 847m.
847- 922	Schistosity 40^0	top QUARTZ MICA SCHIST. Retrogressed schistosity.
	70^0	base
922- 949		Drillcore inaccessible.
949-1160	S_R 60^0-90^0	RETROGRADE SCHIST. Incorporates bodies of:
1041-1079	S_R 55^0-80^0	GRANITE GNEISS, mylonitic, biotite rich.
		Specimens: 669 coarse augen gneiss
		670 medium grained gneiss
1088-1106		GRANITE GNEISS, mylonitic, more chloritic and sericitic, with less feldspar than the above. Also slightly finer. Generally more retrogressed.
		Specimen: 671
1160-1240	S_R var.	QUARTZ MICA SCHIST. Upper and lower boundaries very transitional into retrograde schist. Graded bedding, younging uphole: 1228m mod. poor, layering is retrogressed and may not be bedding.
1240-1305	S_R av. 60^0	RETROGRADE SCHIST.
1305		END OF HOLE.

DD 3188 — Between No. 3 Shaft and Cosgroves Sections

Moderate detail — Logged 26-7-75 and 23-2-76.

0- 21	Amphib. S_1 65^0	AMPHIBOLITE.
21- 47	Q/f segregations 50^0	POTOSI GNEISS. Garnet rich, pale gneiss, quartz-feldspar veins and milky quartz.
47- 66	Amphib. S_1 45^0-60^0	AMPHIBOLITE. ?Orthopyroxene present (brown, poikiloblastic). Unit very similar to DD 3185, 0-20m. Specimen: 622
66-254	S_{1-2} 60^0-90^0	PSAMMITIC SCHIST. S_2 rarely oblique to $S_1 \| \| S_0$. Orange feldspathic alteration: 66-137m including ?POTOSI GNEISS. Yellow, less intense alteration patches throughout. Specimen: 683 orange feldspathic alteration. The feldspathic alteration occurs in S_2 axial plane segregations e.g. 105m, 109m. Graded bedding, younging uphole: 177m mod. good. " " " " 178m " " " " " " 232m " "
254-263	Amphib. S_1 90^0	GARNETIFEROUS AMPHIBOLITE. Chloritic l/P. More altered than amphibolites above.
263		END OF HOLE. In quartzite.

DD 3192 — Adjacent to No. 3 Shaft Section

Moderate detail — Logged 26-7-75 and 23-2-76.

0- 11		AMPHIBOLITE, As DD 3185, 0-20m.
11-180	S_{1-2} 65°	PSAMMITIC SCHIST. S_2 rarely oblique to $S_1 \| \| S_0$. Orange feldspathic alteration: 11-110 m including ?POTOSI GNEISS. Yellow, less intense alteration patches throughout. S_{1-2} becomes partly retrogressed toward base. Graded bedding, younging uphole: 110m mod. good " " " " : 115m moderate " " " " : 120m mod. good " " " " : 144m v. good " " " " : 177m good
	S_1 65°	AMPHIBOLITE. Non garnetiferous: 133-134m.
180-185	Amphib. S_1 60°-70°	AMPHIBOLITE, garnetiferous over 15 cm at top and bottom. Chloritic.
185-263	$S_{1-2} \| \| S_0$ 60°-75°	QUARTZ MICA SCHIST. Partly retrogressed S_{1-2} parallel to S_0.
263		END OF HOLE.

DD 3195 Between British Shear and No. 2 Shaft Section

Moderate detail Logged 26-7-75

0- 41	S_1 or S_R 25^0-40^0	GRANITE GNEISS, mylonitic. Variable shearing evident, with granite gneiss unrecognizable as such in places. Also patches of sheared amphibolite 1-3m thick, sillimanite schist and quartzite. Some orange feldspathic alteration. Specimen: 623 granite gneiss/amphibolite contact, with strong S_R in latter changing orientation away from contact. 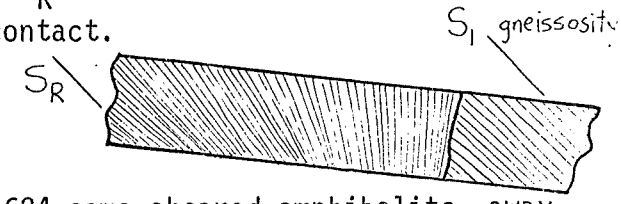 Specimen: 624 same sheared amphibolite, away from contact. POTOSI GNEISS phase: 36-42m.
41-200	$S \mid\mid S_0$ 41-120m: 30^0-40^0 150m: 45^0 180m: 50^0 200m: 55^0 (retr.)	PSAMMITIC SCHIST. Contact with above unit is gradational, defined by rapid increase in sillimanite content. Below 180m: the schistosity parallel to S_0 gradually becomes retrogressed. Specimen: 625 strong sillimanite + garnet in chloritic schistosity. NB. No orange feldspathic alteration in this drillhole.
	Gneissosity, S_R 60^0 S_R 60^0-80^0	Mylonitic section: 146-154m strong biotite gneiss and partly retrogressed schist. 154-166m fine grained retrograde schist; iron stained, sericite-chlorite-epidote. A relict sillimanite schistosity is strongly kinked, with a retrograde schistosity axial plane. Some small, brecciated, epidote rich fragments within S_R. Specimen: 684
200-213	S_R 50^0-65^0	QUARTZ MICA SCHIST. Gradational from overlying unit as a retrogressed "equivalent". Discordant chloritoid in appropriate bands, exhibiting strong lithological control.

DD 3195 (cont'd)

Moderate detail

200-213 (cont'd)		Specimens: 626 relict sillimanite 627 " " 628 " "
213-218	S_R 60°-70°	RETROGRADE SCHIST. As 154-166m.
218-249	Amphib. S_1 50°	AMPHIBOLITE. Variable mineralogy. An epidosite patch near the base contains fine chalcopyrite. Garnetiferous at top.
249-261	S_R 85°	QUARTZ MICA SCHIST. As 200-218m. Relict sillimanite and garnet present.
261-297	Amphib. S_1 55°	AMPHIBOLITE. More homogeneous than 218-249. 10m patch at top, rich in chlorite and magnetite. Specimen: 629 magnetite rich.
297-317	S ||S_0 50°	PSAMMITIC SCHIST. Slightly retrogressed.
317		END OF HOLE.
		No graded bedding observed.

DD 833 Cosgroves Section

Reconnaissance (mainly for graded bedding) Logged 13-2-76

NOTES

1. The thick, upper amphibolite is strongly garnetiferous I/P.

2. The granite gneiss has strong S_1 at 60^o-70^o, with no visible folds and a relatively constant orientation.

   There is 1 metre of fine grained ("aplitic") granite gneiss at the base.

3. Psammitic or psammopelitic schist generally throughout, with $S||S_0$ averaging 60^o-80^o. No unequivocal graded bedding observed; four occurrences of moderate to poor graded bedding are visible, 2 younging uphole and 2 younging downhole.

DD 3133 Cosgroves Section

Moderate detail Logged 23-7-75

0-150	S_3 0^o-20^o	PELITIC SCHIST. S_0 fairly poor, variable development. Chloritic (grey/green/cream) rocks. S_3 regime.
150-188	$S \| \| S_0$ 50^o-80^o	PELITIC SCHIST. Some quartzite bands. Transitional regime with $S_{1-2} \| \| S_0$ stronger than S_3, but strongly retrogressed.
188-380	$S \| \| S_0$ 70^o-90^o v. constant S_2 90^o	PELITIC SCHIST. $S_{1-2} \| \| S_0$ the dominant foliation, not retrogressed (pink/white/grey rocks). Rare patches of S_3 overprint $S_{1-2} \| \| S_0$.

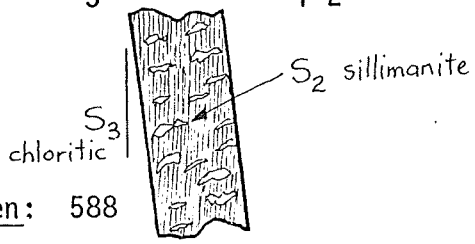

Specimen: 588

S_2 rarely visible oblique to $S_1 \| \| S_0$

Specimen: 589 S_1 in quartzite, S_2 in biotite layer with garnets parallel to S_1.

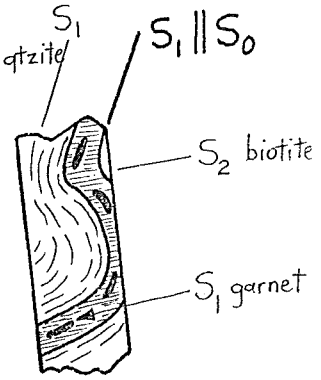

Comment: The general transition from S_3 to S_2 regime over the above three units is diagrammatically as follows:

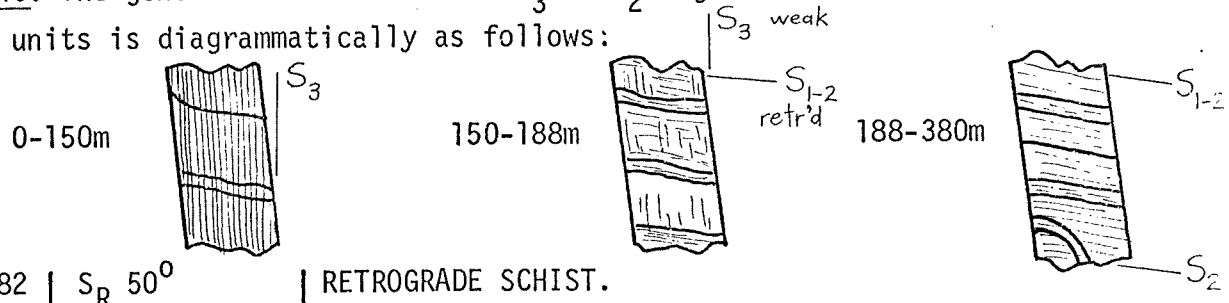

380-382	S_R 50^o	RETROGRADE SCHIST.
382-385	S_2 var. S_R 10^o-35^o	QUARTZ MICA SCHIST. Transition zone from retrograde schist above, to S_2 regime below. S_2 crenulated and crosscut by S_3.

Specimen: 598 S_3 overprinting $S_{1-2} \| \| S_0$
590 " " "

Comment: The sequence in this drillhole on both sides of the retrograde shear zone 380-382m, illustrates how a halo of mimetic retrogression of S_{1-2} surrounds the zone marked by a new retrograde S_{3R} fabric which in turn borders the retrograde shear zone itself.

DD 3133

Moderate detail (cont'd)

385- 421	S_{1-2} 80^{o}-90^{o}	PSAMMITIC SCHIST. S_{1-2} partly retrogressed, strongly crenulated I/P.
421- 545	S_{1-2} 80^{o}-90^{o}	MINERALIZED ZONE. Core altered and broken, with quartz veins; core split l/P.
545- 561	Amphib. S_1 60^{o}-90^{o}	GARNETIFEROUS AMPHIBOLITE. Boundaries gradational. less garnetiferous with depth.
		Specimens: 591 592 partly chloritised
561- 571		POTOSI QUARTZITE. Ptygmatic veins; grey-white.
571- 579		AMPHIBOLITE, strongly altered. Unusual unit, quartz-feldspar abundant, with orange ?feldspathic alteration. Garnet or chlorite aggregates visible.
579-1065	$S \| \| S_0$ var. top: $S_2 60^{o}$-70^{o} base: $S_2 45^{o}$-70^{o}	PSAMMITIC SCHIST, quartzitic, particularly near base. Partly retrogressed l/P. S_2 oblique to to $S_1 \| \| S_0$ in many places. Green feldspar and lode horizon characteristics in places.
		Specimen: 593 green feldspar vein folded about F_2 fold with S_2 axial plane.
		GARNETIFEROUS AMPHIBOLITE: 710-716m
	S_R 50^{o}-65^{o} S_{3R} base 70^{o}	RETROGRADE SCHIST, quartzitic: 730-740m S_R penetrative; 740-750m S_R non-penetrative. Base transitional to S_{3R}.
1065-1277	$S \| \| S_0$: 1065-1200m:var 1220-1277m: 70^{o}-90^{o} f.constant.	QUARTZ MICA SCHIST. Schistosity retrogressed, variable; becomes stronger near base. Some pegmatites.
1277-1291	S_R 85^{o}	CHLORITIC SCHIST. Numerous small garnets.
		Specimen: 594

1291-1372	Amphib. S_1 70^o-85^o	AMPHIBOLITE. Chloritic near top, some plagioclase. Plagioclase rich in centre. Specimen: 595 Chlorite rich near base. Specimen: 596 Last 5m is strongly schistose (S_R). Specimen: 597
1372-1487	S_R 80^o-90^o	RETROGRADE SCHIST. Very strong metamorphic layering in S_R, strongest 1372-1460m.
1487		END OF HOLE.

DD 3183 Cosgroves Section

Reconnaissance Logged 26-7-75

0-353	$S \| \| S_0$ var. 90-150m: 0^o common S_2: top : 60^o 90m : 70^o 120m : 75^o Below 120m : 75^o-90^o	PSAMMITIC SCHIST. Excellent oblique relations between S_2 and $S_1 \| \| S_0$, particularly 90-150m. Strong $S_1 \| \| S_0$. Specimen: 630 S_1 in quartzite, S_2 in pelite Specimen: 631 F_2 fold nose with S_1 in quartzite, S_2 in pelite and grey-green ?cordierite. Specimen: 632
	Contacts top : 36^o bottom: 38^o	DOLERITE : 187m 40cm thick. Both contacts strongly discordant. Specimen: 633 contact discordant to S_2 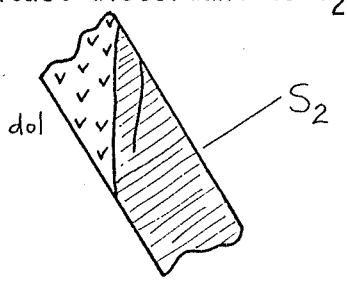 NB. The psammitic schist shows many strong quartz-feldspar segregations in S_2 and in the axial plane of F_2 folds.
353		END OF HOLE.

DD 3185 — Cosgroves Section

Moderate detail — Logged 26-7-75 and 23-2-76.

0- 20	Amphib. S_1 60^o	AMPHIBOLITE. Partly chloritic. Specimen: 612
20- 70	$S_1 \| \| S_0$ var. S_2 60^o	PSAMMITIC SCHIST. S_2 regime, $S_1 \| \| S_0$ strongly folded. Orange/pink feldspathic alteration strong 1/P.
70-213	S_2 70^o-80^o	PSAMMITIC SCHIST. As above, but $S_1 \| \| S_0$ not strongly folded, S_2 oblique to $S_1 \| \| S_0$ 1/P. Orange/pink feldspathic alteration to 137m. Specimen: 613 S_2 in pelite and quartzite, with ?cordierite. Specimen: 614. As 613 but ?cordierite coarser (grey grains).
213-250	S_{1-2} 80^o-90^o	PSAMMITIC SCHIST. As 70-213m. Specimens: Strong S_1 with variable development of S_2 and L_2. (a) 615 S_1 dominant, patchy S_2; L_2 weak (b) 616 S_1 and S_2 equally; L_2 strong 617 S_2 dominant, S_1 only preserved in porphyroblasts; L_2 very strong. 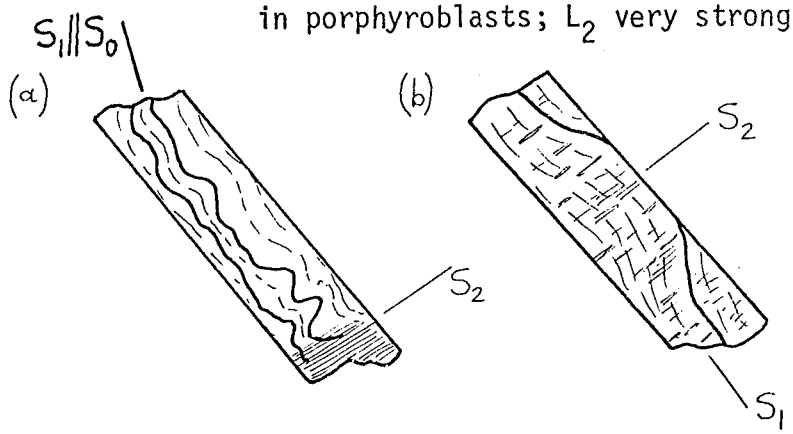
250-265	Amphib. S_1 90^o	AMPHIBOLITE. Strongly variable mineralogy. Specimens: 618 garnet-quartz-plag. 619 ?orthopyroxene-hornblende 620 dark green and pale green chloritic 621 ?orthopyroxene
265-304		PSAMMITIC SCHIST. As 213-250m. Milky quartz: 271-273m.
304		END OF HOLE. No graded bedding observed.

DD 4017 — Cosgroves Section

Moderate detail — Logged 31-7-75

0- 120		PELITIC SCHIST. Regrogressed, ?S_3 regime.
120- 375	S_2 0^o-30^o av. 15^o	PSAMMOPELITIC SCHIST. Very characteristic, large dark green chloritic aggregates are common. Appears to be S_2 regime.
	U. contact 25^o	Dolerite dyke: 193m, discordant, 40cm thick.
375-460	Schistosity var.	QUARTZ MICA SCHIST. Contains bands, 1-10cm thick, with characteristic feldspar porphyroblasts in a fine retrogressed matrix. The schistosity is fine grained, retrogressed, and generally parallel to S_0. The schistosity is very irregular, and the unit contains no planar, constant schistosity oblique to S_0.
		Specimen: 649
460-610	S_2 top 20^o base 50^o	PSAMMOPELITIC SCHIST, similar to 120-375m except S_2 distinctly oblique to S_0 l/P.
		"Aplitic dyke": 567m, crosscuts schistosity; fine, pale brown, granular rock with no foliation.
		Specimen: 650
610-670		PELITIC SCHIST. Large dark green chloritic aggregates; unit combines features of 0-120m and 120-375m.
		Dolerite dyke: 614-619m.
670-802	S_2 av. 40^o	PELITIC SCHIST. Generally as 120-375m.
802		Sharp boundary between dominantly pelitic rocks above and psammitic units below.
802-1190	S_2 av. 40^o	PSAMMITIC SCHIST, quartzitic.
	S_R 70^o	RETROGRADE SCHIST: 903-908m.
		1042m: First appearance of "intrusive" quartz-feldspar bands 0.3 to 1m thick.
		Specimen: 651
1190-1250	Schistosity var.	QUARTZ MICA SCHIST. Generally as 375-460m, pelitic in nature, but lacking the bands of feldspar porphyroblasts in fine matrix. Schistosity very variable in orientation and intensity, and retrogressed.

1250-1355	S_{3R} top 35° below 1280m: 50°-55°	QUARTZ MICA SCHIST and RETROGRADE SCHIST. Upper boundary gradational. Patches of S_R throughout. GARNETIFEROUS AMPHIBOLITE: 1333-1335m, within retrograde schist proper.
1355-1436	S_2 30°-50° av. 40°	PSAMMOPELITIC SCHIST. S_2 regime, S_2 fairly strong, oblique to $S_1 \| \| S_0$ l/P. Also crenulated l/P and folded. Example of S_2 oblique to $S_1 \| \| S_0$ at 1419m.
1436-1483	S_3 and S_R top 45° base 70°	QUARTZ MICA SCHIST. Becoming more retrogressed with depth; S_3 grades into S_R which is segregated l/P in a metamorphic layering parallel to S_R. S_3 is oblique to S_0 l/P.
1483-1516	Amphib. S_1 50°	AMPHIBOLITE. Chloritic, dark green, negligible plagioclase and quartz. Garnetiferous alteration, black schist: 1495-1510m. The unit is strongly sheared at the base.
1516-1585	S_R top av. 50° base av. 70°	RETROGRADE SCHIST. Strong, S_R segregated l/P, and folded in places with a later S_R axial plane to the folds.
1585-1675	S_{1-2} var., commonly 0° S_3 70°-90° av. 80°	PSAMMOPELITIC SCHIST. S_3 (chloritic) dominant at top but S_{1-2} visible with depth (pink/white garnet/sillimanite). S_0 is folded about S_3 axial plane. S_{1-2} crenulated l/P about axial planes probably S_3. Unit fairly quartzitic. Specimens: 652 S_0 folded about S_3 653 S_{1-2} tightly crenulated 654 S_{1-2} openly crenulated
1675-1768	$S_1 \| \| S_0$ var. S_2 0° S_3 70°-90°	PSAMMITIC SCHIST. S_2 regime, S_2 oblique to $S_1 \| \| S_0$ in many places. S_3 overprints S_2. Specimens: 655 no S_3 656 S_3 incipient 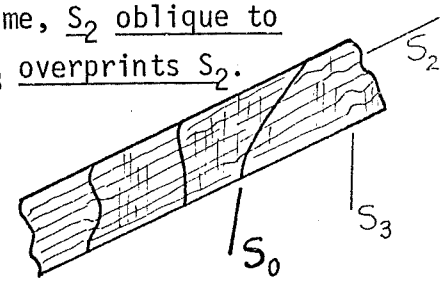 Interpretation: S_2 dips shallowly to west, strongly oblique to $S_1 \| \| S_0$, and is overprinted by subvertical S_3 and F_3.

1768-1785	Margins: S_2 0^o S_3 70^o-90^o Centre: S_R 80^o	RETROGRADE SCHIST. Transition from S_2 regime, at both margins, via S_3 becoming stronger and more retrogressive inwards into S_R. S_2 and S_3 present: 1760-1768m S_R only : 1768-1785m S_2 and S_3 present: 1785-1787m Specimens to illustrate transition: 1762-1786m 657 S_2 strong, partly retrogressed 658 S_2 and S_3 present (S_3 chloritic) 659 S_{3R}, no sillimanite left, some S_2 garnet 660 strong S_R with small retrograde garnets 661 " " " " " " 662 very strong S_R, sericite-chlorite (no garnet) 663 S_2 and S_3 present
1785-2018	$S \| \| S_0$ var. S_2 var. 0^o-90^o S_3 60^o-90^o	PSAMMITIC SCHIST. S_{1-2} regime with lesser S_3. S_2 crenulated by F_3 1/P.
2018-2025	S_3 60^o-90^o	QUARTZ MICA SCHIST. As 1436-1483m. Transitional from unit above into retrograde schist below.
2025-2041	S_R 90^o	RETROGRADE SCHIST, chloritic. Transition on margins similar to 1768-1785m.
2041-2072	S_3 60^o-90^o	QUARTZ MICA SCHIST. As 2018-2025m.
2072-2136		PSAMMITIC SCHIST, quartzitic. $S \| \| S_0$ disrupted, no visible S_2.
2136		END OF HOLE.

DD 3182 — Imperial Ridge Section

Moderate detail — Logged 27-7-75 and 10-2-76

0-1292

PELITIC SCHIST. Pelite: quartzite ratio 80:20, typical of pelitic schist generally. Pink/white

$S||S_0$

$S_{1-2}||S_0$ visible l/P. S_2 and S_3 have variable intensity; S_3 disruption of S_2 visible l/P:

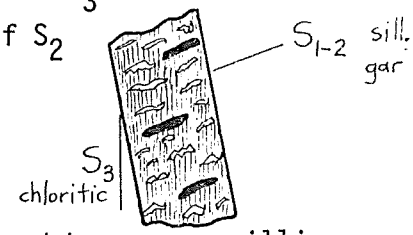

0-335m: av.70°

f. constant

?Chiastolite relicts replaced by coarse sillimanite, garnet and chlorite, at 354-355m.

Specimens: 642 ?chiastolite preserved

643

$S||S_0$:

335-460m: 85°

460-865m: 50°-70°

865-1292m: 60°-80°

S_{1-2} parallel to S_0 except rare sections with S_2 oblique to $S_1||S_0$:

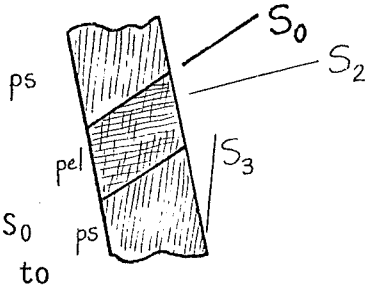

S_3:

0-180m: 0°-10°

180-1292m: 0°-30°

example at 23m:

At 574m, S_2 is oblique to S_0 with S_1 preserved parallel to S_0 in quartzite. Criteria used to verify S_2 not S_3:

(1) orientation (S_2 55° hence flatlying)

(2) sillimanite-garnet

(3) in adjacent core it is overprinted by chloritic S_3, 0°-20°, hence subvertical.

At 789m, excellent example of S_3 transitional to S_R, both overprinting S_2:

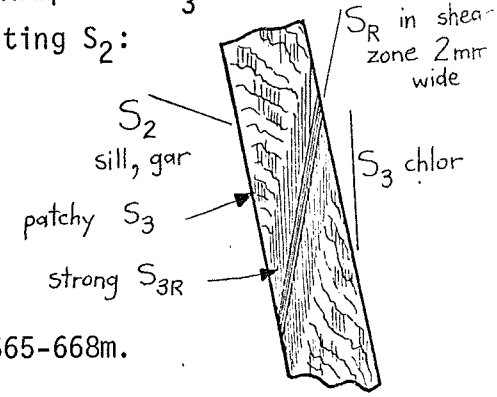

Specimen: 645

S_R 30°

RETROGRADE SCHIST: 665-668m.

Specimen: 644 slightly sheared quartzite.

Below 865m: quartzite bands increasing.

Pelite: quartzite ratio 50:50.

1292-1317	S_R top 70^o base 35^o	RETROGRADE SCHIST. Strong.
1317-1500	$S \|\| S_0$ v.var. 0^o-90^o	PSAMMOPELITIC SCHIST. S_2 regime, S_{1-2} generally parallel to S_0, except at 1422m, 1470-1480m. S_{1-2} is folded, probably by F_3 folds, but negligible S_3. Graded bedding, younging uphole : 1401m v. good " " " " : 1418m mod.good " " " " : 1423m good Graded bedding, younging downhole : 1473m mod.good Graded bedding, younging uphole : 1476m moderate Graded bedding, younging downhole : 1479m good " " " " : 1481m good

Interpretation: The interval 1400-1500m shows strongly oblique relations between S_2 and $S_1 || S_0$, which taken with the reversals of younging indicate a small macroscopic F_2 fold:

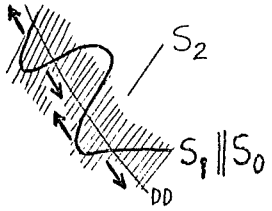

		Specimen: 675 graded bedding
1500-1959	S_0 v. var. S_2 av. 45^o	PSAMMITIC SCHIST. Many patches where S_2 is oblique to $S_1 \|\| S_0$, in places at high angles. Graded bedding, younging downhole: 1519m good
	S_R 55^o	RETROGRADE SCHIST: 1617-1623m. DOLERITE: 1763m 45cm thick, discordant margins, biotite enriched on margins.
		Specimen: 676
	S_R av. 50^o-70^o	RETROGRADE SCHIST and QUARTZ MICA SCHIST: 1792-1846m.
		GARNETIFEROUS AMPHIBOLITE: 1897-1899m.
1959		END OF HOLE.

DD3109 Potosi Section

Moderate detail Logged 23-7-75

0-160	S_3 av. 30^o	PELITIC SCHIST. Bedding very poor; S_3 decreases toward base and a very constant, retrogressed $S \| \| S_0$ appears. Traces of S_3 in transition area indicate F_3 synform to west. 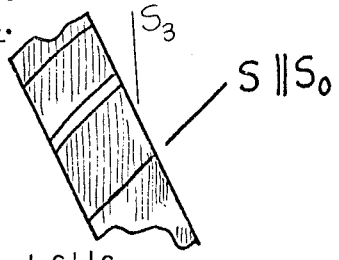 Specimen: 578 ?Retrogressed $S \| \| S_0$

Transition (quartz veins, etc.) to underlying Potosi gneiss.

160-178	Gneissosity S_1 60^o	SHEARED POTOSI GNEISS. Ptygmatic veins. Gneissosity not cut by any schistosity. Specimen: 579 Gneissosity-cross-cut by Schistosity?
178-188		PEGMATITE, massive.
188-211	S_R 60^o(top)	QUARTZ-MICA SCHIST. Constant S_R MINERALIZED: 205-211m (split)
211-229	40^o 70^o (base)	RETROGRADE SHEAR ZONE
229-261	$S_{2(-3)}$ 70^o-90^o S_0 var. mainly 70^o-90^o	QUARTZ-MICA SCHIST. $S_{2(-3)}$ is strongly retrogressed, generally layer-parallel. Specimen: 580 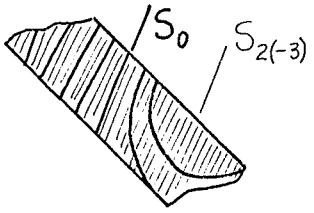
261-264		PEGMATITE
264-270	Ptyg. fold axial planes var.	POTOSI QUARTZITE. Strong ptygmatic veins with biotite schistosity S_1 parallel to folded quartz veins. Sillimanite patches l/P, esp. near base.
270-276		PEGMATITE.
276-293		QUARTZ-MICA SCHIST. S_3 dominant. Transition zone to underlying S_2 regime.
293-416	$S_1 \| \| S_0$ var. S_2, axial plane to folds in $S_1 \| \| S_0$ 70^o-90^o, mainly 85^o	PSAMMITIC SCHIST. Classic example of S_2 overprinting $S_1 \| \| S_0$, featuring (1) pink (garnet)/white (sillimanite)/grey (quartz + K feldspar) schist (2) may F_2 fold hinges

293-416 (cont'd)		(3) S_2 dominant in pelitic bands, S_1 remnant in quartzitic bands. (4) Orientation of S_2 precludes interpretation as S_3. Best examples 293-335m. <u>Specimens</u>: 581 582 583 PEGMATITE: 348-355m 386-395m MINERALIZED: 399-416m (split) 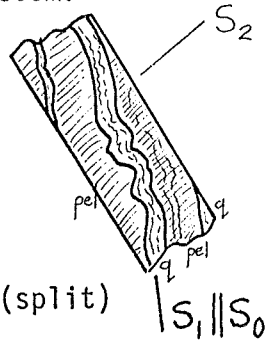
416-429		GARNET AMPHIBOLITE. Very poor schistosity S_1.
429-518	$S_1 \| \| S_0$ var. S_2 90^o	PSAMMITIC SCHIST. Classic S_2 regime as 293-416m, pink/white/grey schist. Best examples around 442m. <u>Specimen</u>: 584
518-577	$S_1 \| \| S_0$ var. S_2 90^o	PSAMMITIC SCHIST. S_2 overprinting $S_1 \| \| S_0$ but green-grey, retrogressed.
577-592		BLACK GARNETIFEROUS SCHIST. Some patches as 518-577m. Rich in quartz veins; toward base more chloritic.
592-604	Moderate S_1 80^o	GARNET AMPHIBOLITE. Chloritic. Upper contact gradational from strongly altered at top to amphibolite at end of hole; illustrated as follows: <u>Specimen</u>: 585 garnet-quartzite schist 586 (garnet)-chlorite-hornblende 587 chlorite-hornblende-plagioclase amphibolite
604		END OF HOLE.

DD3117 Potosi Section

Moderate detail Logged 23-7-75

0-181	S_0 0-30° S_{3R} 0-30°	PELITIC SCHIST. Silky schistosity with poor S_0. Minor pegmatites (less than 1m thick).
181-184	Boundaries 35°	MILKY QUARTZ VEIN.
184-220	S_2 30°-40° S_3 0°-30°	QUARTZ-MICA SCHIST. As 0-181m; also S_2 present, retrogressed, with strong thin quartz veins parallel to S_2 near base.
220-266	S_2, axial plane to ptyg. folds 30°-70°, av. 45° S_3 10°-30°	POTOSI GNEISS and QUARTZITE. Garnet common; strong ptygmatic quartz-feldspar veins crosscut by retrogressed schistosity S_3. Schistosity S_1 parallel to folded veins. Specimen: 576 Ptygmatic vein with axial plane ?S_3.
266-345	S_R 30° (top) 50° (base)	QUARTZ-MICA SCHIST. Becomes more quartzitic toward base. S_R semi penetrative, very planar. PEGMATITE; 320-323m 328-331m 336-339m
345-357		BLACK GARNETIFEROUS SCHIST and PEGMATITE. Some broken core.
357-375	Poor S_1 50°-60°	GARNET AMPHIBOLITE. Specimen: 577
375-395	S_R 50°	QUARTZ-MICA SCHIST.
395-410	S_R, fractures 55°-70°	PEGMATITE, massive.
410-418		Transition to unit below, gradual.
418-506	S_R 60°	RETROGRADE SCHIST. Contains appreciable quartz. BLACK GARNETIFEROUS SCHIST with quartz veins: 488-500m.
506		END OF HOLE.

DD 3167 — Potosi Section

Moderate detail — Logged 11-7-75

0-100		No core.
100-323	$S \| \| S_0$ 30^0-90^0 S_3 0^0-30^0	PELITIC SCHIST. S_3 prominent, green-grey. S_0 poor, has schistosity parallel. No graded bedding observed. PEGMATITE: 261-267m.
323-357	S_R 0^0-10^0	RETROGRADE SCHIST. Chloritic S_R is strongly crenulated about axial planes at 45^0-90^0 Crenulations (L_C) oblique as: 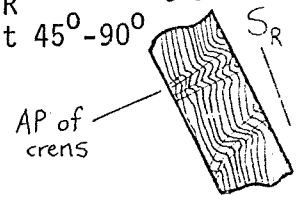 Specimen: 515
357-412	S_{3R} 0^0-30^0	PELITIC SCHIST with RETROGRADE SCHIST in places, 50:50. S_3 regime in former ($S \| \| S_0$ poorly visible), S_R in latter unit. PEGMATITE : 360-367m
613-770		Depths approximate only.
613-704	Gneissosity S_1 var. (top) 0^0-45^0 (generally) av. 0^0-10^0 40^0 (below 640) S_R 30^0	POTOSI GNEISS with abundant quartz-feldspar veins and segregations. RETROGRADE SCHIST: 690-694m.
704-745	S_3 45^0	PELITIC SCHIST. Some pink/white S_2.
745		QTZITE, MINERALIZED. Garnet quartzite (split).
745-793	$S \| \| S_0$ 45^0 S_3 0^0-30^0	PSAMMITIC SCHIST. Strong $S \| \| S_0$, patchy S_3. Specimen: 516 PEGMATITE: 770-778m.
793-832	S_R 0^0-25^0	RETROGRADE SCHIST, strongly chloritic. Large garnet eyes in S_R.
832-898	S_R 30^0	QUARTZ-MICA SCHIST. Chloritic, green-grey schistosity, S_0 lacking.
898-911		PEGMATITE with MINERALIZATION near top (split).

DD 3167 (cont'd)

Moderate detail

911-1006	S_R 30°	QUARTZ-MICA SCHIST. Very strong, constant, chloritic S_R with L_M and fine metamorphic layering parallel to S_R. S_R not completely penetrative due to psammitic nature of schist. Specimen: 517
1006-1073	S_R 40°	RETROGRADE SCHIST, more pelitic than unit above. S_R strongly layered, and crenulated I/P.
793-1073	INTERPRETATION: A large shear zone, in dominantly psammitic rocks.	
1073-1189	$S_{1-2}\|\|S_0$ 50° S_2 50°	PSAMMITIC SCHIST with quartzites. S_2 regime in pink/white/grey schist, with S_{1-2} schistosity generally parallel to S_0 but S_2 oblique to $S_1\|\|S_0$ locally. Negligible S_3; one piece of core with chloritic S_3 crosscutting S_2: 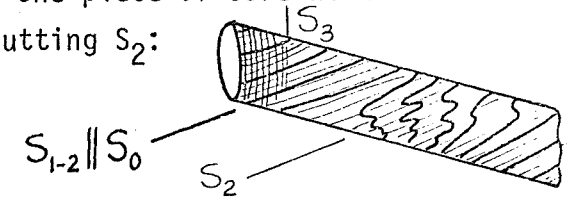
1189-1238	Gneissosity S_1 60° S_2(axial plane to F_2 folds) 55°	GRANITE GNEISS. Gneissosity at boundary is at 50° but within 3-4m is constant at 60°. Specimen: 672
1238-1242	S_1 80°	AMPHIBOLITE, chloritic I/P Specimen: 518
1242-1248		GRANITE GNEISS
1248-1253	S_1 70°	AMPHIBOLITE, chloritic I/P.
1253-1288	Gneissosity S_1 70°-80° S_2 65°	GRANITE GNEISS. ZONE OF W-STYLE FOLDS: 1282-1288m Axial planes (S_2) contain quartz-feldspar segregations. Specimen: 519
1288-1409	Gneissosity S_1 60°-90°	GRANITE GNEISS. Gneissosity more variable in orientation.

DD 3167 (cont'd)
Moderate detail

1409-1436	S_2 90°	PSAMMITIC SCHIST, quartzitic. S_0 poor. CHLORITIC AMPHIBOLITE with BLACK GARNETIFEROUS SCHIST on margins: 1413-1414m.
1436-1439	S_R 85°	RETROGRADE SCHIST. Black, green and grey.
1439-1494	S_2 60°	PSAMMITIC SCHIST. Pink/white/grey schist, with S_{1-2} parallel S_0 but locally S_2 overprinting S_1S_0. No S_3. Specimen: 520
1494-1542	S_0 90° S_3 90°	PSAMMITIC SCHIST in which S_3 (green-grey) increases with depth. S_2 difficult to see; some "S_3" may be mimetically retrogressed-S_2 (their orientations are very close). Specimen: 521 ?S_3
1542-1550	S_R 90°	QUARTZ-MICA SCHIST. Transitional from unit above, with S_3 becoming stronger and more retrograde (no sillimanite). At base a true RETROGRADE SCHIST.
1550		END OF HOLE.

DD 3105 — Round Hill Section

Moderate detail — Logged 8,8-7-75

0- 244	$S \| \| S_0$ 0^o-45^o S_3 0^o-20^o	PELITIC SCHIST. S_3 strong. PEGMATITE: 49-66m 155-186m
244- 275	$S \| \| S_0$ 45^o	PELITIC SCHIST. S_3 becoming weaker.
275- 372	$S_1 \| \| S_0$ 45^o-60^o	PELITIC and PSAMMITIC SCHIST. S_3 weak, S_1 more visible (pink/white) esp. in psammitic rocks.
372- 402		PEGMATITE.
402- 545	$S \| \| S_0$ 60^o	PSAMMITIC SCHIST. Poor S_3, S_1 strong.
545- 556		PEGMATITE.
556- 684	$S \| \| S_0$ var. 80^o-90^o	PSAMMITIC SCHIST. $S \| \| S_0$ is folded throughout.
684- 692	S_0 90^o	PSAMMITIC SCHIST. "Herringbone" texture l/P, generally S_3 (grey-green) dominant over S_2.
692- 704	S_0 90^o S_2 70^o S_3 70^o not parallel	PSAMMITIC SCHIST. Strong "herringbone" texture with grey-green. chloritic S_3 in alternate layers with white, sillimanite-rich S_2. S_2 is finely crenulated about an axial plane parallel to S_3. Both schistosities are moderately oblique (av. 20^o) to S_0, which has similar characteristics to bedding in general (i.e. is not a metamorphic layering). S_3 contains a muscovite, chlorite lineation L_M. With core orientated correctly, S_3 is vertical, L_M is vertical (downdip) and S_2 dips west at approximately 45^o. Specimens: 506 507 508 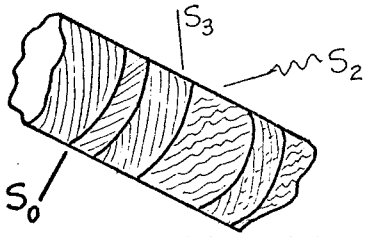
704- 706	S_0 90^o	PSAMMITIC SCHIST. Sillimanite schist with "herringbone" texture grades into quartzite lacking "herringbone".

DD 3105 (cont'd)
Moderate detail

706- 778	Gneissosity S_1 90° (60°-70° 1/P) S_R 45°	GRANITE GNEISS. No "herringbone" texture. Some thin (1 cm) shear zones cut the core (S_R) at moderate angles; with these orientated in a vertical position the gneissosity S_1 dips moderately west.
778- 900	Gneissosity S_1 80°-60°	GRANITE GNEISS. As above.
900- 991	Gneissosity S_1 45°-60° variable	GRANITE GNEISS. Gneissosity variable, some pieces showing S_1 parallel to core. Probably a W-style fold zone.
991-1003	S_1 mylonitic 60°	SHEARED GRANITE GNEISS. Gradual transition with depth into "mylonitic" granite gneiss: increasing biotite content defining a strong schistosity which appears to be parallel to the original gneissosity (nowhere is a cross-cutting relationship observed). Numerous augen and relicts of quartz-feldspar aggregates and large grains, are enveloped by the schistosity. Specimen: 510 partly mylonitized. With depth the rock becomes more chloritic and micaceous (i.e. darker), the schistosity becomes strongly and finely segregated into layers approx. 1mm thick, and the rock completely loses its granitic and gneissic characteristics. The mylonitic schistosity is crenulated 1/P. Specimen: 511 completely mylonitized.
1003-1028		RETROGRADE SCHIST. Chloritic, segregated schistosity containing small (1-5mm) garnets and wrapping around large (1-5cm) garnets. S_R crenulated 1/P, and shows a strong, very fine crenulation. Lineation L_C, Specimen: 512. ?MINERALISATION: near base (core split).
1028		END OF HOLE.

DD 3105A — Round Hill Section

Reconnaissance (mainly for pegmatites) — Logged 9-7-75

154		Wedged hole commences.
154-376		PELITIC SCHIST.
158-187	$S \| \| S_0$ 60^o near top of hole	PEGMATITE, with schist inclusions (to 1.5 m) esp. near base.
199-		PEGMATITE, lower boundary missing.
206-211		PEGMATITE.
217-234	$S \| \| S_0$ 60^o-80^o	PEGMATITE, minor schist inclusions.
254-256	$S \| \| S_0$ 60^o-80^o	PEGMATITE.
293		?POTOSI unit.
351-361		PEGMATITE.
370-376		PEGMATITE.
376-475	$S \| \| S_0$ 60^o-80^o S_2 60^o-80^o	PSAMMITIC SCHIST appears; pink/white. S_2 slightly oblique to $S_1 \| \| S_0$ in places but generally parallel (i.e. S_{1-2}). $S_1 \| \| S_0$ is commonly folded or crenulated. PEGMATITE: 443-448m 450-452m Graded bedding, younging uphole: two definite examples, at 464, 465m. Specimens: 513 514
475		END OF HOLE.

DD 3105B — Round Hill Section

Reconnaissance (mainly for pegmatites) — Logged 9-7-75

260		Wedged hole commences.
260-295	$S \| \| S_0$ 60^o	PSAMMITIC SCHIST. PEGMATITE: 266-268m
295-305		POTOSI unit (thickness approximate)
305-392	$S \| \| S_0$ 80^o	PSAMMITIC SCHIST
392		END OF HOLE.

DD 3115A — Round Hill Section

Reconnaissance (mainly for pegmatites) — Logged 9-7-75

125		Wedged hole commences
125-364	S_0 80^o-90^o	SCHIST, undifferentiated PEGMATITE : 165-183m POTOSI unit: 260-275m (approx.) PEGMATITE : 279-290m
364		END OF HOLE.

Note change in schist from pelitic at top to psammitic at base of hole.

DD 3115 — Round Hill Section

Reconnaissance (mainly for pegmatites) — Logged 9-7-75

0- 44	$S \| \| S_0$	0^o-45^o	SCHIST, undifferentiated. S_3 weak.
	S_3	0^o-30^o	
44-105	$S \| \| S_0$	45^o-60^o	As above.
	S_3	0^o-30^o	PEGMATITE: 44-55m 67-72m 76-78m
	$S \| \| S_0$	60^o	SCHIST, undifferentiated. $S_1 \| \| S_0$ folded, some S_2 oblique to S_0; S_3 weak.
	S_3	0^o-30^o	PEGMATITE: 105-109m
162-350	$S \| \| S_0$	70^o-90^o	SCHIST, undifferentiated. S_3 weak.
			PEGMATITE: 162-181m 220-227m (several schist slices). 247-250m 262-269m
			POTOSI GNEISS, large quartz-feldspar veins: 269-280m
			PEGMATITE: 280-283m
350-449	$S \| \| S_0$	90^o	SCHIST, undifferentiated. S_3 weak.
			PEGMATITE: 420-427m
449			END OF HOLE.

Note change in schist from pelitic at top to psammitic at base of hole.

DD 3156 Round Hill Section

Reconnaissance Logged 8-7-75

0-812	$S \| \| S_0$ var., av. 45^o-60^o S_3 0^o-20^o S_R 0^o-20^o	PELITIC SCHIST. Long representative section through this unit, consisting of interlayered pelitic schist and lesser quartzitic schists, in the ratio 60:40. The rocks are generally garnetiferous, and S_0 is well preserved. Two schistosities show variable development: The pelitic layers show green-grey S_3, the psammopelitic layers show both S_{1-2} (pink/white) and S_3, and the quartzite layers show S_{1-2}. The S_{1-2} is not observed oblique to S_0, and very characteristically contains garnets parallel to the schistosity. S_3 commonly grades mineralogically and geometrically into S_R in discrete shear zones. 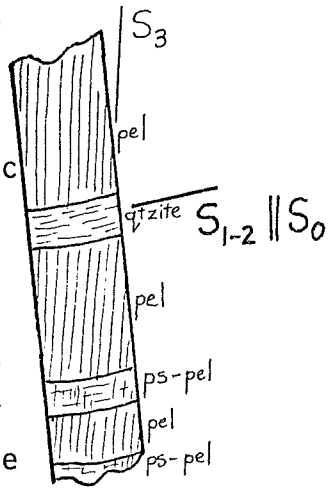 Specimens: 504 pelitic schist, S_3 stronger than S_{1-2} 505 quartzitic with (biotitic) S_{1-2} only. No graded bedding observed.
812		END OF HOLE.

DD 3157 — Round Hill Section

Reconnaissance (mainly for pegmatites) — Logged 9-7-75

0- 600	$S \| \| S_0$ 0^o-45^o S_3 0^o-30^o	PELITIC SCHIST. S_3 prominent.
600-1038	$S \| \| S_0$ av. 45^o	PELITIC SCHIST. S_3 decreases and is almost absent below approx. 800m. S_0 highly folded throughout. PEGMATITE: 850- 866m 892- 901m 917- 929m 1033-1038m
1038-1129	$S \| \| S_0$ 60^o-70^o	PELITIC SCHIST. S_0 highly folded throughout. PEGMATITE: 1086-1097m
1129-1281	$S \| \| S_0$ 45^o-60^o	PELITIC SCHIST. S_0 highly folded throughout. PEGMATITE: 1254-1259m
1281-1372		PELITIC and PSAMMITIC SCHIST. Transition zone. GREEN FELDSPAR VEIN, mineralized (core split, 40 cm): 1333m
1372-1670	$S \| \| S_0$ 50^o	PSAMMITIC SCHIST. PEGMATITE: 1510-1517m 1586-1591m Graded bedding, younging uphole: 1492m.
1670		END OF HOLE.

DD 3157A — Round Hill Section

Reconnaissance (mainly for pegmatites) — Logged 9-7-75

754			Wedged hole commences.
754-1130		S_{1-2} 45° S_3 0°-20°	PELITIC SCHIST. So poor, S_{1-2} moderately strong, S_3 strong, 1/P. PEGMATITE: 845- 866m 895- 904m 911- 930m 933- 936m (diffuse) 978- 983m 1040-1044m (schist inclusions 50%) 1052-1061m 1094-1097m 1103-1130m
1130-1190		S_{1-2} 50°-80° av. 70°	PELITIC SCHIST.
1190-1370		$S \| \| S_0$ var. av. 45°	PELITIC and PSAMMITIC SCHIST. Transition zone. GREEN FELDSPAR/QUARTZ VEIN, diffuse: 1200-1204m BANDED IRON FORMATION, 2 pods, 15cm and 5cm : 1240m PEGMATITE: 1242-1245m 1283-1287m GREEN FELDSPAR zone: 1320-1323m
1370-1573		$S \| \| S_0$ var. ?av. 45°	PSAMMITIC SCHIST Graded bedding, younging uphole (series of beds): 1497m Specimen: 673 graded bedding PEGMATITE: 1514-1523m 1525-1533m
		S_R 50°	RETROGRADE SCHIST, chloritic: 1524-1532m ?POTOSI QUARTZITE, ptygmatic veins: 1533-1550m
1573-1588	Wallrock S_{1-2} 60° Amphib. S_1 mainly 90° (to 60°) (poor-moderate)		GARNETIFEROUS AMPHIBOLITE; detailed logging: Garnet-rich, quartz-veined amphib: 6m Amphib.(garnet, quartz 1/P) : 2m Milky quartz vein : 1m Amphib.(garnet, quartz 1/P) : 6m The lower contact, with quartzite, is sharp.

DD 3157A (cont'd)
Reconnaissance (mainly for pegmatites)

1588-1843	S||S_0 60°	PSAMMITIC SCHIST. PEGMATITE : 1708-1714m Graded bedding, younging uphole, strongly developed : 1723m
1730-1743	Wallrock S_{1-2} 55°-80° Amphib. S_1 60° (strong)	GARNETIFEROUS AMPHIBOLITE; detailed logging: Amphibolite (garnet, quartz l/P): 7m Milky quartz vein : 1m Amphibolite (garnet,quartz l/P) : 3m Garnet-rich,black (chloritic) amphibolite : 3m
1843		END OF HOLE

Note symmetry of the two garnetiferous amphibolites: interpreted as the same unit around a small fold.

DD 3179 Round Hill Section

Detailed logging Logged 7,8,11 and 26-7-75

0- 96		No core.
96- 152	$S \| \| S_0$ 45^0-90^0 S_3 0^0-20^0 S_R 0^0-20^0	PELITIC and PSAMMITIC SCHIST. Interbands of both types contain S_3 in pelite and $S \| \| S_0$ in psammite. S_3 grades into S_R in places.
152- 335	$S \| \| S_0$ 45^0-90^0	PSAMMITIC SCHIST. Pink/white schist with strong S_{1-2}; generally parallel to S_0 (hence S_{1-2}) but oblique to $S_1 \| \| S_0$ in many places (hence S_2). Poor S_3 but S_2 folded in places, and S_{1-2} has a general crenulated aspect. S_0 well developed, but no graded bedding observed. Specimen: 501 S_2 oblique to S and ?S_1.
335- 732	$S \| \| S_0$ 30^0-50^0 S_3 0^0-10^0	PELITIC SCHIST. S_{1-2} poorly preserved, S_3 strong (green-grey); some fibrolite observed in S_3 but also chloritic, and grades into S_R in discrete shear zones. S_0 variable.
732- 884	$S \| \| S_0$ 50^0-90^0	PELITIC SCHIST. As above.
884- 914		PELITIC SCHIST with quartzite appearing l/P. S_3 prominent.
914-1067	$S \| \| S_0$ var. S_3 45^0	PSAMMITIC SCHIST. S_3 prominent, constant. Fault; puggy weathered rock: 1004 m. Graded bedding, younging uphole: 934 m strong.
1067-1370	$S_1 \| \| S_0$ var., commonly 0^0 S_2 90^0	PSAMMITIC SCHIST. S_2 weak to strong, crosscuts $S_1 \| \| S_0$ in places. Where S_2 is absent or weak, kinks and open folds in $S_1 \| \| S_0$ have axial planes parallel to the S_2 schistosity elsewhere. Specimen: 522 fold in quartzite with unusual orientation parallel to core - F_1 fold? Interpretation: high angle relationships between S and S_2 suggest a local F_2 hinge area.
1370-1431		RETROGRADE SCHIST. Position and width approximate.

1431-1461	S_2 80^0-90^0	POTOSI ?QUARTZITE. Ptygmatic quartz S_1 parallel to vein, folded about an axial plane S_2 which develops a schistosity in the hinge zones of the folds. No garnet or biotite clots observed in this unit. 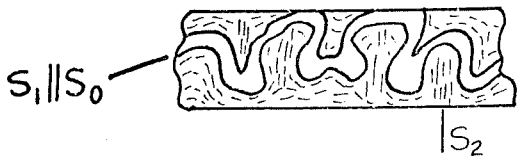
1461-1490	$S \| S_0$ var. S_{2-3} 80^0-90^0	PSAMMITIC SCHIST. Oblique schistosity difficult to label, either S_2 or S_3. Probably the latter, since grey-green and fibrolitic.
1490-1508	Wallrock S_0 45^0 Amphib. S_1 45^0	GARNETIFEROUS AMPHIBOLITE; detailed logging: Milky quartz vein, chloritic schist : 2m Amphibolite, massive, garnetiferous : 15m Black, garnet-rich chloritic schist : 1m (quartz 1/P)
1508-1592	$S \| S_0$ var. S_{2-3} 80^0-90^0	PSAMMITIC SCHIST. As 1461-1490m Graded bedding, younging uphole: 1562m strong.
1592-1595	Wallrock-schistosity 63^0 Amphib. S_1 63^0	GARNETIFEROUS AMPHIBOLITE; detailed logging: Black,garnet-rich chloritic amphib.: 1m Amphibolite (garnet 1/P) : 1m Garnet-rich, quartz-veined amphib. : 1m This unit enclosed by retrograde schist.
1595-1676	$S \| S_0$ 80^0-90^0(top) $S \| S_0$ 45^0 (base) S_3 90^0	PSAMMITIC SCHIST. Transition zone in $S \| S_0$ orientation. Near top is patchy S_3 development.
1676-2080	$S_{1-2} \| S_0$ 45^0 S_2 45^0	PSAMMITIC SCHIST. Only one schistosity, S_{1-2} present, generally parallel to S_0, but occasional folds in S_0 have "S_{1-2}" axial plane, hence S_2 in these cases. This S_2 is folded and kinked 1/P, by F_3 folds. S_2 is visibly segregated in one piece 2070-2080m.

2080-2085	S_{1-2}||S_0 var. mainly 0^o-45^o S_2 45^o	PSAMMITIC SCHIST. Folds in S_1||S_0 (S_1 visible l/P) with S_2 axial plane; S_1||S_0 generally closer to core than S_2, hence <u>interpretation</u>: with S_2 dipping 45^oW (approx.), the structural location is on the right-way-up limb of an F_2 synform above and to the west (see pictorial log interpretation). <u>Specimen</u>: 502 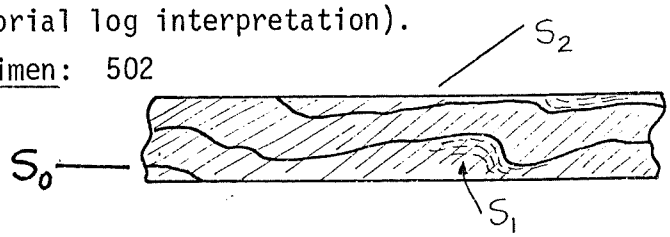
2085-2090	S_1||S_0 0^o S_2 0^o	PSAMMITIC SCHIST. Generally the schistosity is parallel to S_0, hence S_{1-2}. F_3 fold has flattened S_2 in this interval.
2090-2098	S_{1-2}||S_0 var. mainly 0^o-45^o S_2 0^o-45^o S_3 90^o	PSAMMITIC SCHIST. Can trace S_2 from F_2 fold (where it crosscuts S_1||S_0) to a flattened position around an F_3 fold, with incipient S_3 (green-grey, chloritic) crosscutting S_2. <u>Specimen</u>: 503 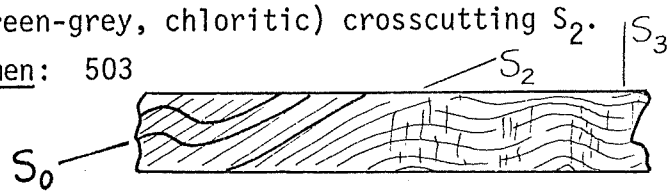
2098-2134	S_{1-2} 45^o S_3 85^o-90^o	PELITIC SCHIST. S_3 strong, has disrupted S_1||S_0 and S_2 into individual fibrolite and mica flakes crenulated about the chloritic S_3. <u>Specimens</u>: 634 635 636 637 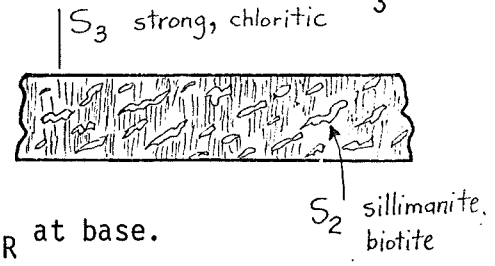 S_3 gradational into S_R at base.
2134		END OF HOLE.

DD 3179 (cont'd)
Detailed logging

PEGMATITE LOGGING from 731m to 1754m:

Depth	Thickness
758	1
792- 804	12
812	3
825	2
829- 838	9
931	2
940	1
991	3
1006	2
1014	2
1475-1486	11
1566-1583	17
1631-1635	4
1751-1754	3

NB. NBHL oriented core sampling yields the following true dips on undifferentiated foliation:

2001m $42^{o} \rightarrow 350^{o}$ Interpreted as S_{1-2}, probably S_2.
2018m $42^{o} \rightarrow 350^{o}$ " " " " "

Wedged section below DD3179:
1495m $22^{o} \rightarrow 245^{o}$ " " S_2

DD 3194 — Round Hill Section

Moderate detail — Logged 11-7-75

0-400	$S \| \| S_0$ 45^o	PELITIC SCHIST. Pink/white $S \| \| S_0$ observed, crenulated and folded to 200m, below which it becomes planar. S_3 fairly weak (green-grey). Rocks becoming more quartzitic with depth.
	S_0 80^o	Graded bedding, younging uphole: 368m.
	$S_R \| \| S \| \| S_0$ 45^o	Thin shear zones observed, parallel to S_0.
400-450	$S \| \| S_0$ 60^o-80^o	PELITIC SCHIST. Planar $S \| \| S_0$.
450-560	$S \| \| S_0$ 80^o-90^o	PELITIC SCHIST. Planar $S \| \| S_0$.
560-561	S_R 80^o	RETROGRADE SCHIST. Thin patch.
561		END OF HOLE.

Note change in schist from pelite at top to more quartzitic pelite at base of hole.

DD 3031 — Flying Doctor Section

Reconnaissance — Logged 24-7-75

0- 80	$S \| \| S_0$ 60^0-70^0	PELITIC SCHIST. S_{1-2} and S_3 equally prominent, S_3 seen overprinting S_{1-2} I/P.
80-246	S_R 50^0	RETROGRADE SCHIST. Very strong, constant S_R.
246		END OF HOLE.

DD 3033 — Flying Doctor Section

Moderate detail — Logged 24-7-75

0- unknown	$S \| \| S_0$ 45^0 S_3 0^0-20^0	PELITIC SCHIST. S_2 and S_3 equally prominent, S_3 seen overprinting S_{1-2} I/P.
	Strong boundary between pelitic and psammitic schist, but position unknown because of missing depth markers.	
unknown-182	$S \| \| S_0$ 45^0-70^0 S_3 10^0-30^0	PSAMMITIC SCHIST.
182		END OF HOLE.

DD 3034 — Flying Doctor Section

Moderate detail — Logged 24-7-75

0- 82	$S \| \| S_0$ 45^0	PELITIC SCHIST. S_3 strong near top, pink/white S_{1-2} strong in lower part. Several good examples of S_3 overprinting $S_{1-2} \| \| S_0$ e.g. 81m: 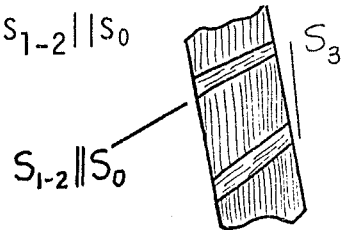 Graded bedding, younging downhole: in specimen 599, 36m.
82-290	$S \| \| S_0$ 50^0 top 70^0 base	PSAMMITIC SCHIST. Regular S_0. Contains mineralised (split) sections and several thin amphibolite bands. S_{1-2} becomes retrogressed at depth.

DD 3034 (cont'd)

Moderate detail

290-360	S_R 65°	RETROGRADE SCHIST. Very strong.
360		END OF HOLE.

DD 3036 Flying Doctor Section

Moderate detail Logged 14-7-75

0- 21	S_3 0^o	PELITIC SCHIST. S_3 prominent.
21- 30		PEGMATITE.
30- 58	$S_1 \| \| S_0$ var. $>40^o$ S_2 35^o-40^o S_3 0^o	PSAMMITIC and PELITIC SCHIST. S_0 well developed. S_2 occurs oblique to $S_1 \| \| S_0$ in many places; S_1 is particularly visible in quartzitic bands. S_3 rare, seen overprinting S_{1-2} at 49m.
	$S \| \| S_0$ 90^o	Specimen: 538 S_2 oblique to $S_1 \| \| S_0$
	S_2 10^o	Graded bedding, younging uphole: in specimen 538 at 38m

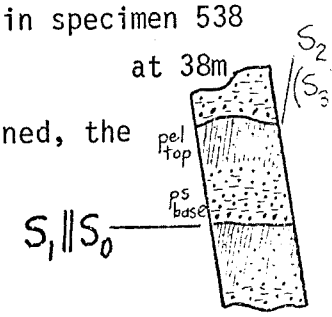

INTERPRETATION: If this interpretation is maintained, the facing evidence of specimen 538 indicates that F_2 folds in this locality at least, are inverted (diagram A or D), or that this locality is on the right-way-up limb of an F_1 fold (contrary to the overwhelming inverted facing encountered generally in this region), (Diagram B & C).

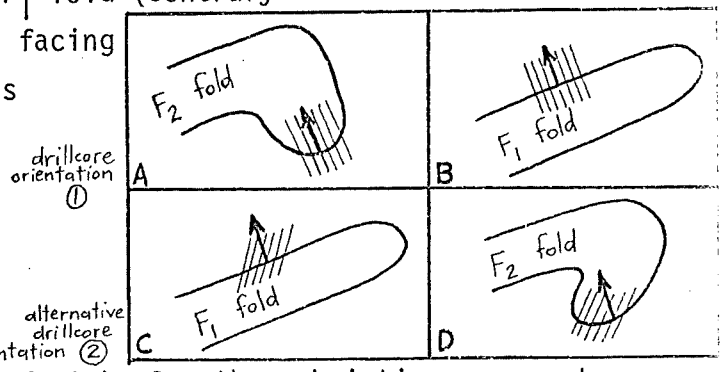

Alternatively, the S_2 may in fact be S_3, thus obviating any need for these explanations with their far reaching implications. See petrological description.

58-108	S_3 0^o-20^o	PELITIC SCHIST. S_3 very strong, S_0 weak. S_{1-2} disrupted and largely obliterated by S_3 except for patches of pink/white S_{1-2} I/P. Specimen: 674

Comment: A remarkable example, in the previous two units, of the lithological control on S_3 schistosity development (i.e. S_3 strong in pelitic schist, weak in psammitic schist).

108-168	$S \| \| S_0$ 40^o	QUARTZ MICA SCHIST. Constant, retrogressed schistosity, parallel to S_0. Orientation inconsistent with S_3 hence a retrogressed S_1 or S_2. Near the base is S_3 overprinting this schistosity.
168-265	$S \| \| S_0$ 55^o S_3 20^o	
265		END OF HOLE

DD 3074 Flying Doctor Section

Moderate detail Logged 13-7-75

0- 691	$S \| \| S^0$ 45^0-90^0	PELITIC SCHIST. Two schistosities present: S_3 (green-grey, chloritic) and S_{1-2} (pink/white). $S_{1-2} \| \| S_0$ is planar and constant in orientation. PEGMATITE: 631m (thin).
691- 744	S_R 20^0-35^0	RETROGRADE SCHIST interspersed with PELITIC SCHIST; former ironstained, chloritic.
744- 773	$S \| \| S_0$ 45^0	PELITIC SCHIST. $S \| \| S_0$ constant.
773		END OF HOLE.
640		Wedged hole commences.
640- 678	$S \| \| S_0$ 45^0 S_3 45^0	PELITIC SCHIST.
678- 732	S_R 30^0	RETROGRADE SCHIST interspersed with PELITIC SCHIST.
732- 945	$S \| \| S_0$ 45^0 S_3 45^0	PELITIC SCHIST. PEGMATITE: 818-829m.
945- 987	$S \| \| S_0$ 60^0-70^0	PELITIC SCHIST.
987-1001	Gneissosity || schistosity S_1 60^0-65^0, constant	BIOTITIC ?POTOSI GNEISS. Quartz-feldspar biotite-garnet-sillimanite gneiss with strong gneissosity and parallel biotite schistosity; dark in colour.
1001-1049	$S_{3R} \| \| S_0$ 60^0-70^0 constant.	QUARTZ-MICA SCHIST.
1049-1067	S_R 50^0-60^0, constant.	RETROGRADE SCHIST, transitional from above unit. Fairly quartz rich.
1067-1174	$S \| \| S_0$ 60^0-65^0, constant.	PSAMMITIC SCHIST. Schistosity green-grey, retrogressed, very constant. Thin pegmatitic segregations to 2m thick are common. Interpretation: retrogressed S_{1-2} and S_2 regime.
1174-1212	$S \| \| S_0$ var. av. 45^0	SCHIST, undifferentiated. Variable angles indicate folded $S \| \| S_0$.
1212-1247	Gneissosity S_1 60^0-70^0 near middle var. to 0^0.	GRANITE GNEISS. Altered I/P to green-grey chloritic assemblages. Gneissosity folded I/P esp. near middle.

DD 3074 (cont'd)
Moderate detail

1247-1280	$S_1 \| \| S_0$ var. 0^o-90^o, commonly 0^o S_3 80^o-90^o	PSAMMITIC SCHIST. Green-grey (S_3) with many patches of pink/white (S_1). $S_1 \| \| S_0$ strongly folded. Little S_2 visible (i.e. the pink/white schistosity is parallel to S_0 and is S_1).
1280-1311	$S_1 \| \| S_0$ var. 0^o-90^o S_2 crenulated, 0^o I/P S_3 80^o	PSAMMITIC SCHIST. As above but with strong S_2 (pink/white) oblique to S_0. S_2 is crenulated and overprinted by chloritic S_3. The partial restriction of S_3 to pelitic layers gives the rock an incipient herringbone texture (see DD 3105, Round Hill Section). Specimens: 525, 526, 527 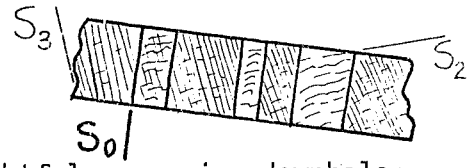 Graded bedding, doubtful, younging downhole: in Specimen 526, 1300m.
1311-1409	$S \| \| S_0$ 0^o-45^o fairly constant	PSAMMITIC SCHIST.
1409-1430	$S_1 \| \| S_0$ var. S_2 45^o	PSAMMITIC SCHIST. Strong S_2 oblique to S_0, negligible S_3. $S_1 \| \| S_0$ strongly folded. Typical core as: 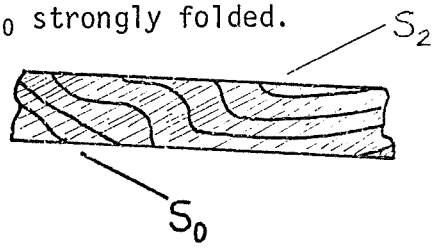 Specimens: 528, 529, 530
1430-1529	Gneissosity S_1 25^o-30^o top var. toward base 30^o-45^o	GRANITE GNEISS. Partly schistose in middle, chloritic. Specimen: 531
1529-1552	S_R 55^o constant	QUARTZ-MICA SCHIST.
1552-1595	S_R 60^o-65^o top 70^o-90^o base	RETROGRADE SCHIST. Sericite-chlorite with quartz veins. L_M pitches obliquely across core ellipse. Specimen: 532
1595		END OF HOLE.

Comment: an important drillhole for demonstrating
(1) S_2 oblique to $S_1 \| \| S_0$ and axial plane to a large F_2 fold

DD 3074 (cont'd)
Moderate detail

Comment: (1) (cont'd) (synform, see pictorial log) in granite gneiss.

(2) S_3 overprinting an S_2 which is oblique to $S_1 || S_0$.

DD 3155 Flying Doctor Section

Moderate detail Logged 14-7-75

0- 341	$S \| \| S_0$ $0^0(-20^0)$	PSAMMITIC SCHIST. Strong pink/white S_{1-2}, negligible S_3. Specimen: 533 S_3 overprinting S_2.
341- 349	S_R 40^0	RETROGRADE SCHIST, ?chloritoid-bearing. Black mineral present either biotite or chloritoid, also presence of pink/white minerals (garnet/ sillimanite) suggest amphibolite facies assemblage.
349- 366	$S \| \| S_0$ 0^0-20^0	PSAMMITIC SCHIST. As 0-341 m.
366- 442	$S \| \| S_0$ var. 0^0-40^0	PSAMMITIC SCHIST. As above.
442- 471	$S \| \| S_0$ 40^0-50^0	PSAMMITIC SCHIST. As above.
471- 486	Amphib. S_1 45^0-50^0	AMPHIBOLITE. Large hornblende grains. Specimens: 534 535 black ?pyroxene
486- 518	$S \| \| S_0$ 60^0	PSAMMITIC SCHIST. As 0-341 m.
518- 625	$S \| \| S_0$ 0^0-70^0 mainly 45^0-70^0	PSAMMITIC SCHIST. Strongly folded S_0. $S_{1-2} \| \| S_0$ but S_2 oblique to S_0 in places.
625- 723	$S \| \| S_0$ 60^0	PSAMMITIC SCHIST. More planar than above but some folded zones (one of which shows S_2 oblique to S_0). Possibly more quartzitic than unit above.
723- 762	$S_R \| \| S_0$ 60^0	QUARTZ MICA SCHIST. Strong blackish schistosity $?S_R$.
762- 799	S_R 85^0 constant	RETROGRADE SCHIST. Strong S_R, fine metamorphic layering and quartz veins parallel to S_R.
799-1105	$S \| \| S_0$ var. top 0^0-90^0 av. 45^0; constant 50^0-60^0 base.	PSAMMITIC SCHIST. Pink/white S_{1-2} regime. $S \| \| S_0$ folded near top.
1105-1116	Amphib. S_1 55^0-60^0	AMPHIBOLITE. Moderate foliation I/P, defined by hornblende/?pyroxene bands (dark green to black) versus mid green, finer bands (chloritic). Foliation 2-5 mm thick. Specimen: 536

DD 3155 (cont'd)

Moderate detail

1116-1125	$S \| \| S_0$ 60^o	PSAMMITIC SCHIST. Pink/white S_{1-2} regime.
1125-1136	Amphib. S_1 70^o	AMPHIBOLITE. Near base becomes chloritic and garnetiferous. Base transitional to unit below.
1136-1149	$S \| \| S_0$ 70^o	PSAMMITIC SCHIST. As 1116-1125m.
1149-1184		PEGMATITE.
1184-1244	$S_R \| \| S_0$ 70^o-80^o	QUARTZ-MICA SCHIST. Dark retrograde schistosity.
		Specimen: 537
	Amphib. S_R 70^o-80^o	
1244-1285	$S_R \| \| S_0$ 80^o-90^o	QUARTZ-MICA SCHIST and RETROGRADE SCHIST. True S_R at base.
1285		END OF HOLE.

DD 3170 Flying Doctor Section

Reconnaissance Logged 14-7-75

0- 610	S_0 moderate angles S_3 0^o-20^o S_R 0^o-20^o	PELITIC SCHIST. S_3 dominant schistosity, gradational into S_R I/P.
610- 945	S_R 0^o-5^o	RETROGRADE SCHIST and PELITIC SCHIST.
945-1160	S_3 10^o-40^o	PELITIC SCHIST. As 0-610.
1160-1458	$S \| \| S_0$ var. 40^o	PSAMMITIC SCHIST. S_{1-2} dominant, rarely observed as S_2 oblique to S_0 (e.g. 1220-1250 I/P). Some S_3 developed in middle.
1458		END OF HOLE.

DD 3186 — Flying Doctor Section

Moderate detail — Logged 14-7-75, 13-2-76 and 23-2-76

0- 90	$S \| \| S_0$ 30^0-35^0 constant	PSAMMITIC SCHIST. S_{1-2} prominent, S_2 in places is oblique to $S_1 \| \| S_0$ but generally $S_{1-2} \| \| S_0$. Specimen: 539
91- 111	Gneissosity S_1 30^0-35^0	POTOSI GNEISS. Garnetiferous grey gneiss with numerous quartz-feldspar segregations and veins. Rare sillimanite.
111- 133	Gneissosity S_1 30^0	GRANITE GNEISS. Grey and cream, abundant quartz-feldspar segregations and veins.
133- 146	Gneissosity S_1 30^0 S_{2-3} 0^0	GRANITE GNEISS. As above but with a moderate to strong, planar sillimanite schistosity S_{2-3} cross-cutting the gneissosity. Specimen: 540
146	S_R 30^0	RETROGRADE SCHIST, 0.5m thick.
146- 152	S_1 35^0	GARNETIFEROUS AMPHIBOLITE. Chloritic I/P.
152- 251	$S \| \| S_0$ var. S_3 0^0-30^0 S_R 0^0-30^0 at depth	SCHIST, undifferentiated, grading downward into RETROGRADE SCHIST. Garnetiferous sillimanite schist with $S_{1-2} \| \| S_0$ crosscut by green-grey S_3. With depth S_3 becomes more retrograde and more penetrative, i.e. grades into S_R.
		INTERPRETATION: An example of S_3 overprinting this limb of the Broken Hill Synform and grading into a retrograde schist zone. A stage more retrograde than the similar occurrence of S_{2-3} in 133-146; both comparable to outcrop on Rasp Ridge, in which S_3 (sillimanite-bearing I/P) overprints this limb of the Broken Hill Synform.
251- 305		RETROGRESSED GRANITE GNEISS. Muscovite-chlorite rich, white granite gneiss in which gneissosity is almost obliterated. Cut by chloritic retrograde shear zones I/P.

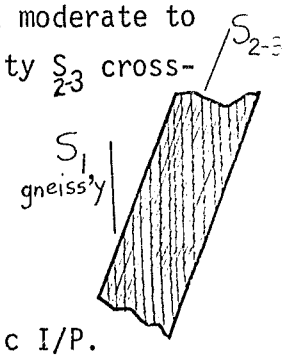

DD 3186 (cont'd)

Moderate detail

305-1044	Gneissosity S_1 305-350m 40° 350-565m 0°-40° 565-750m 0°-10° 750-1044m var., some high angles.	GRANITE GNEISS. Sharp upper contact. Parasitic folds in S_1 at 349m indicate axial plane S_2 flatter than S_1; see diagram. Several retrograde schist zones and altered amphibolites occur, as well as pegmatites. Specimen: 573, 574. F_2 folds in S_1 with quartz-feldspar segregation in axial plane. 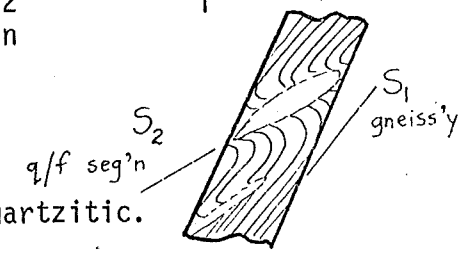
1044-1068	S_3 45°-70°	QUARTZ-MICA SCHIST, quartzitic.
1068-1323	Gneissosity S_1 1068-1120m: var. 1120-1220m: 60°-70° 1220-1323m: var. 45°-70°	GRANITE GNEISS. Basal 40m has some S_R patches with S_R at high angles.
1323-1390	S_R 1323-1335m: 45°-90° 1335-1390m: 90°	QUARTZ-MICA SCHIST. Fairly strong S_R. S_R kinked in lower part. AMPHIBOLITE, altered: 1328-1332m.
1390-1450	$S \| \| S_0$ var. S_2 var. 0°-40°	PSAMMITIC SCHIST. Pink/white/grey, S_2 regime with S_2 oblique to $S_1 \| \| S_0$ in many places. $S_1 \| \| S_0$ variable (folded). No definite S_3. No graded bedding observed. Specimen: 575 ?S_1 in quartzite, S_2 in pelite band oblique to S_0. Comment: The parallelism of S_2 with the drill-core precludes the possibility of it being S_3.
1450-1730	$S \| \| S_0$ 30°-50° S_2 45° approx.	PSAMMITIC SCHIST. S_{1-2} dominant, S_2 rarely oblique to $S_1 \| \| S_0$. Graded bedding; younging downhole: 1479m moderate only 1480m moderately good 1481m moderate only 1533m moderate only.

DD 3186 (cont'd)

Moderate detail

1730-1750	$S \| \| S_0$ var., 0^o I/P S_2 45^o approx.	PSAMMITIC SCHIST. As above.
1750-1810	$S \| \| S_0$ 60^o-80^o S_2 45^o approx.	PSAMMITIC SCHIST. As above.
1810-1896	S_R 70^o-80^o	QUARTZ-MICA SCHIST and RETROGRADE SCHIST.
	MINERALIZATION: 1894m 15cm semi-massive galena in S_R.	
1896-1902	S_R 80^o	RETROGRADE SCHIST.
	Below 1902: NBHL core logging indicates granite gneiss. Drilling still proceeding.	

NB. NBHL oriented core sampling yields the following <u>true dips on undifferentiated foliation</u>.

1406m $27^o \rightarrow 075^o$ interpreted as $S_1 \| \| S_0$ } Intersection ($?F_2$ fold axis) plunges $25^o \rightarrow 055^o$.

1451m $49^o \rightarrow 349^o$ " " $S_1 \| \| S_0$ }

1705.5m $46^o \rightarrow 297^o$ " " $?S_2$

DD 956 | Globe Section

Moderate detail | Logged 15-7-75

0 - 113	S_{1-2} 60^{o}	PELITIC SCHIST. Poor S_0. Strong S_{1-2} is sillimanite-garnet-?cordierite, strongly lineated (SW-plunging). S_{1-2} becomes clearer toward base. Specimens: 549 strong lineation 550 ?cordierite, strong lineation PEGMATITE: 54-63m
113 - 198		Core inaccessible.
198 - 305	S_0 80^{o}-90^{o}	PSAMMITIC SCHIST. Strong $S_{1-2}\|\|S_0$, poor S_3. Relations indicate F_3 synform to west: 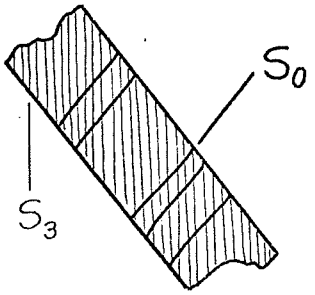
305 - 366	S_0 60^{o}-70^{o} S_3 45^{o}	PSAMMITIC SCHIST. As above. Specimen: 551 fold in $S_{1-2}\|\|S_0$ with S_3 axial plane.
366 - 454		Core inaccessible.
454 - 476	$S\|\|S_0$ $60^{o}(-90^{o})$ S_3 60^{o}	PSAMMOPELITIC SCHIST. Mixed $S_{1-2}\|\|S_0$ and S_3 regimes (S_3 patchy). Relations indicate F_3 synform to west (as diagram above). Specimen: 552 S_3 crosscutting S_0 S_3 becomes stronger and more sericitic downhole, S_{1-2} becomes weaker. Base thus transitional to retrograde schist zone.
476 - 555	S_R 40^{o}-45^{o} top 80^{o} base	RETROGRADE SCHIST. Contains pegmatites. Upper and lower boundaries transitional.
555 - 679	S_{3R} 80^{o}-90^{o}	QUARTZ-MICA SCHIST. Cross-cutting chloritoids abundant; chlorite-sericite with large garnets containing oblique fabric: 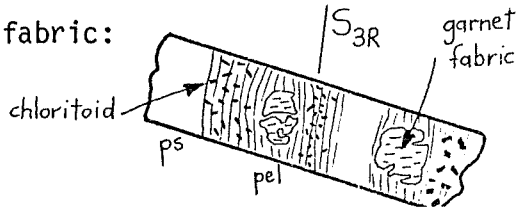 Specimen: 553
679		END OF HOLE.

DD 961 Globe Section

Moderate detail Logged 15-7-75

0- 18	S||S_0 var. 45^0-60^0 S_3 0^0	PELITIC SCHIST. Classic two-schistosity rocks: Specimens: 554 555 556 grey clots- ?cordierite 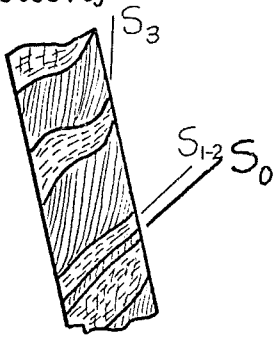
18- 50	S_3 0^0-10^0	PELITIC SCHIST. S_3 strong.
50- 82	S||S_0 60^0-65^0	PELITIC SCHIST. S_{1-2} strong (white/pink/grey), S_3 very weak. Specimen: 557
82-137	S||S_0 50^0-60^0 S_3 0^0-10^0	UNDIFFERENTIATED SCHIST. Patchy S_3. PEGMATITE: 112-136m
137-194		Core inaccessible.
194-357	S||S_0 $>50^0$	PSAMMOPELITIC SCHIST. Reconnaissance shows S_3 in places, with relations indicating F_3 synform to west: 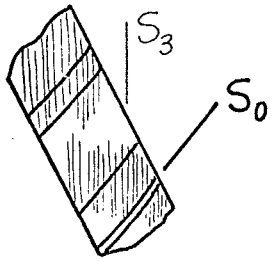
357-433		Core inaccessible.
433-509	S||S_0 70^0-90^0 S_3 approx.50^0	PSAMMOPELITIC SCHIST. As above. Specimen: 558 S_3 Graded bedding, younging uphole: 479m v. good Specimen: 559 graded beds Lower part of section shows folded S||S_0, with F_3 vergence varying.
509-526	S_1 70^0-80^0	AMPHIBOLITE. Rich in plagioclase (40-50%), with strong S_1.
526-558	S||S_0 var.	PSAMMOPELITIC SCHIST. Folded S||S_0.
558-561		GARNETIFEROUS AMPHIBOLITE. Specimen: 560
561-634	S||S_0 60^0-70^0	PSAMMOPELITIC SCHIST. S_{1-2} dominant, with patches of S_3, particularly in pelite layers. Graded bedding, younging uphole: 628m moderate.

DD 961 (cont'd)
Moderate detail

634-701		Core inaccessible.
701-836	$S \| \| S_0$ 70^o-90^o S_3 50^o	PSAMMOPELITIC SCHIST. S_3 in pelitic bands; relations indicate <u>F_3 synform to west</u>. <u>Specimen</u>: 561 F_3 fold with S_3
836-902		Core inaccessible.
902-966	$S \| \| S_0$ var. 45^o-90^o S_3 45^o-60^o	PSAMMOPELITIC SCHIST. S_3 slightly stronger.
966-976		RETROGRADE SCHIST. Over this interval (i) S_2 disappears; (ii) S_3 grades into S_R mineralogically; (iii) S_0 becomes parallel to S_R.
976		END OF HOLE

<u>Comment</u>: This drillhole provides an example of the transition from S_3 to S_R downhole. Control is gained from the orientation of S_3 mapped at the surface which is then extended down the drillhole (as the core shallows) by the method outlined in Chapter 8.

DD 963 — Globe Section

Moderate detail — Logged 15-7-75

0- 58	S_3 and S_{3R}: 35^o-65^o	PELITIC SCHIST. S_0 fairly poor. Dark green, coarse, biotite-rich; partly retrogressed, with patchy chloritoid cross-cutting S_3 and S_{3R}. S_{1-2} visible I/P as relict patches of sillimanite-garnet between "microlithons" of micaceous material associated with S_3: 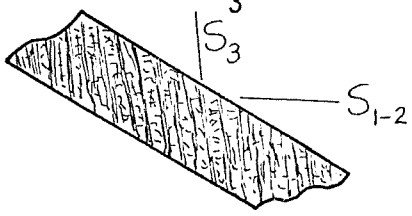 Specimen: 541 The S_{3R} contains L_M plunging moderately or steeply to the NE.
58-166	S_R var. 10^o-50^o av. 20^o-30^o	RETROGRADE SCHIST. Generally chloritic, with coarse biotite in places, but quartz-rich I/P.
166-470	?S_3 50^o-90^o av. 60^o	PELITIC SCHIST. S_0 poor. Green, moderately coarse, biotite-rich, with chloritoids cross-cutting a partly retrograde biotite-sillimanite schistosity which is inferred to be S_3. There are local patches of earlier high-grade S_{1-2}. Some quartzites. Specimens: 542 543
	?S_{1-2} 70^o-80^o	Below 320m : PSAMMITIC SCHIST becomes evident over a very transitional boundary, with S_{1-2} regime more prominent. Dark green biotite still present in the schistosity.
470-497	S_1 80^o	AMPHIBOLITE. Chloritic, hornblende-?pyroxene-plagioclase. Specimens: 544 545
497-508	Sch 90^o	CHLORITE-BIOTITITE. Appears to be an altered, retrogressed amphibolite. Becomes finer toward base. Specimens: 546 547 548
508-519	S_R 80^o	QUARTZ-MICA SCHIST. Retrograde zone.
519		END OF HOLE. No graded bedding observed.

DD 969 Globe Section

Moderate detail Logged 16-7-75

0- 95	S||S_0 30^0-45^0 S_3 0^0 -30^0	PELITIC SCHIST. Patches of white/pink S_{1-2} with strong S_3.
95-124		RETROGRADE SCHIST. Upper boundary transitional from S_3.
124-156		PEGMATITE.
156-260	S||S_0 50^0-60^0 S_3 0^0-10^0	PELITIC SCHIST. S_{1-2} partly retrogressed.
260		Boundary pelitic/psammitic schist; fairly sharp.
260-490	260-445m: 60° S||S_0 constant, S_3 10^0-45^0 av. 40^0 445-490m: S||S_0 70^0-90^0 S_3 60^0	PSAMMITIC SCHIST. S_{1-2} stronger than S_3. S_3 relations with S_0 indicate F_3 synform to west: Specimen: 562 S_3 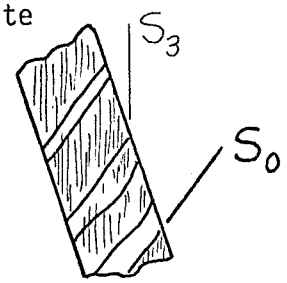
	Comment:	The drillhole is inferred to be perpendicular to F_3, because the apices of the ellipses formed respectively by S_0 and S_3 coincide in the drillcore (see Chapter 8): 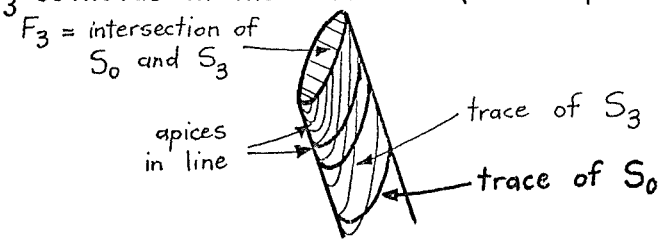
490-615	S||S_0 var. 45^0-60^0 S_{3R} 20^0-45^0 S_R (base) 10^0	PSAMMITIC SCHIST. S_0 changes orientation, is more variable. S_3 becomes stronger downhole, at base is S_R.
615		END OF HOLE.

DD 970 Globe Section

Moderate detail Logged 16-7-75

0- 44	$S \| \| S_0$ 45^0-60^0 S_3 0^0-10^0	PELITIC SCHIST. S_3 stronger than S_{1-2}, the latter being generally parallel to S_0 but one specimen showing $S_1 \| \| S_0$, S_2 oblique, and S_3 overprinting both: Specimen: 563 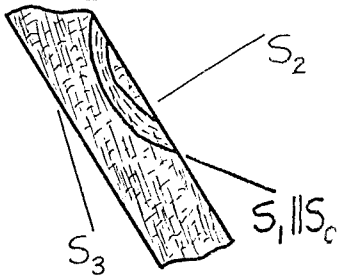
44- 58	$S_1 \| \| S_0$ var. S_2 60^0-65^0 S_3 0^0-20^0	PSAMMOPELITIC SCHIST. Strong S_2 regime with S_2 (constant orientation) cross-cutting $S_1 \| \| S_0$ (variable orientation). S_3 negligible. Specimens: 564 pelitic S_2 565 graded bedding with S_1 in psammitic band Graded bedding, younging uphole: 52m good
58-110	$S \| \| S_0$ 45^0-60^0 S_3 0^0-20^0	PSAMMOPELITIC SCHIST. S_{1-2} parallel to S_0.
110-116		PEGMATITE.
116-156	$S \| \| S_0$ 50^0-70^0 S_3 $<50^0$	PSAMMOPELITIC SCHIST. S_3 relations with S_0 indicate F_3 synform to west.
156-207		Core inaccessible. Pelitic/psammitic schist boundary in this interval.
207-304	$S \| \| S_0$ 90^0 (top) 70^0 (base)	PSAMMITIC SCHIST. S_3 relations with S_0 indicate F_3 synform to west.
304-350		Core inaccessible.
350-431	$S \| \| S_0$ 60^0-90^0	PSAMMITIC SCHIST. S_{1-2} parallel to S_0.
431		END OF HOLE.

DD 15N-2 — Carbonate Ridge Section

Moderate detail — Logged 16-7-75

0- 45	Gneissosity S_1 0^0-20^0 av. 10^0 S_R 0^0-15^0	GRANITE GNEISS. Cut by strong retrograde schist in places.
45-185	S_R 15^0-25^0	RETROGRADE SCHIST, chloritic. Very strong, core broken; S_R completely penetrative.
185-267	S_R 15^0-30^0	RETROGRADE SCHIST, quartzitic. S_R not completely penetrative. Below 267m: Core split and sampled; quartzitic. S_R present with some pelitic retrograde schist I/P. Below 300m: Core inaccessible.

DD 15N-4 — Carbonate Ridge Section

Moderate detail — Logged 16-7-75

0-299	S_1 gneissosity 0^0-30^0 AP to folds in S_1 30^0-40^0	GRANITE GNEISS. Numerous tight, asymmetric folds in S_1 gneissosity (e.g. 40-43m), with quartzofeldspathic veinlets in their axial plane. Sense of folds indicates <u>F_2 synform to east</u>:
299-371		Core inaccessible.
371-448	$S \| \| S_0$ var. 0^0-45^0 S_3/S_R 0^0-10^0	QUARTZ-MICA SCHIST. $S \| \| S_0$ very variable. Crosscut or paralleled by grey-green S_3 or S_R.
448-498	S_R 30^0	QUARTZ-MICA SCHIST. There is an abrupt change at 448m, marked by a weak retrograde schist zone, below which the schistosity changes orientation and becomes sericitic, chloritic and fine grained S_R. Thin amphibolites also occur, partly schistose. <u>Specimen</u>: 566 amphibolite.
498-515	Gneissosity S_1 20^0-25^0	GRANITE GNEISS. Transitional boundary from quartz-mica schist above. Below 575m: core inaccessible.

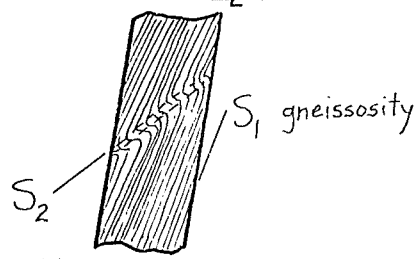

DD 3099 — Carbonate Ridge Section

Moderate detail — Logged 25-7-75

0-443	$S \| \| S_0$ and S_2: 0-180m 60^0 180-443m 70^0-90^0 S_3 0^0-30^0	PSAMMOPELITIC SCHIST. Pelitic near top, becoming psammitic toward base; S_3 strong near top, but generally S_{1-2} regime with minor patches of S_3. S_{1-2}, parallel to S_0 but S_2 is oblique to $S_1 \| \| S_0$ in places. S_2 is partly retrogressed near the base.
443-486		PEGMATITE. Three narrow schist bands.
486-688		PSAMMOPELITIC SCHIST. As above, slightly retrogressed. A number of thin (av. 1-2m) pegmatites occur, in contrast to above section. PEGMATITE: 654-661m.
688-744	S_R 50^0 top 60^0 base	RETROGRADE SCHIST. Strong. Upper and Lower boundaries transitional.
744-794	S_{3R} 60^0-80^0	QUARTZ-MICA SCHIST. Non-penetrative, grey-green S_{3R}. Several thick pegmatites as follows: 750-751m 755-758m 762-766m 774-780m 786-794m
794		END OF WEDGED HOLE.

DD 3099 continues:

656-694	S_{3R} 65^0	PSAMMOPELITIC SCHIST. Partly retrogressed. PEGMATITE: 666-670m.
694-750	S_R 45^0 top 50^0 base	RETROGRADE SCHIST. Boundaries transitional.
750-870	S_{3R} 50^0-90^0	QUARTZ-MICA SCHIST. As 744-794m above. Pegmatites as follows: 758-759m 765-769m 778-783m 789-790m 792-798m 807-810m 815-819m
870		END OF HOLE.

DD 3113 — Carbonate Ridge Section

Moderate detail — Logged 16-7-75

0- 500	Gneissosity S_1 0-250m 0^o-10^o 250-370m av. 10^o 370-430m av. 15^o 430-500m av. 20^o S_2 0^o	GRANITE GNEISS. Gneissosity S_1 fairly constant, with some small folds with geometric axial plane S_2.
500- 580		GRANITE GNEISS. Grey-green schistosity S_3 or S_R gives the gneiss a slightly dirty appearance.
580- 631	S_3/S_R 50^o	GRANITE GNEISS. Gneissosity partly obliterated by a chloritic schistosity, giving the rock a grey, finer grained aspect.
630- 790	S_R: 630m 50^o 660m 70^o 720m 85^o 760m 80^o 790m 70^o	RETROGRADE SCHIST. Abrupt upper boundary. AMPHIBOLITE: 734-736m, variably schistose: Specimens: 567 fine grained, from edge of amphibolite. 568 coarser, relatively unsheared, from middle.
790- 825	S_R 70^o	RETROGRADE SCHIST grading into PELITIC SCHIST. Very distinctive changes, comprising (i) appearance of small chloritoid grains (ii) " " coarser green biotite/chlorite (iii) general coarsening (incl. sericite → muscovite) (iv) "waviness" and crenulation of S_R The rock has a cream-green colour.
825-1000	S_R var. $> 45^o$	RETROGRADE SCHIST and PELITIC SCHIST. As above, with cream-green, "coarse" pelitic schist containing discrete zones of finer retrograde schist.
1000-1261	S_{3R} 60^o below 1200m 80^o-90^o	QUARTZ-MICA SCHIST. S_{3R} (cream-green, fine-grained) crosscuts S_0 in many places. A less retrogressed, more quartz-rich type than previous unit. Specimens: 569 pelitic type 570 quartz-pelite 571 garnetiferous S_R
1261		END OF HOLE.

DD 3154 — Carbonate Ridge Section

Reconnaissance; detailed pegmatites — Logged 21-7-75

0-1210	S||S_0 f. constant 60^o S_3 0^o-20^o mostly 0^o-5^o S_R 0^o-5^o	PELITIC SCHIST. S_{1-2} and S_3 similar in strength. RETROGRADE SCHIST: 540-548m, with S_R gradational into S_3 on each side. Pegmatites as follows: 606-611m 616-619m 1150-1165m 1190-1195m
1210-1228		RETROGRADE SCHIST, white quartz, brecciated pegmatite.
1228-1285	S||S_0 45^o	PSAMMITIC SCHIST. Altered I/P, some brecciation. Pegmatites as follows: 1242-1266m (broken near top) 1279-1285m
1285-1295	Sch, qtz veins constant 50^o-55^o	BLACK, ALTERED SCHIST. Zone of black, garnetiferous schist, green chloritic garnetiferous schist (?altered amphibolite) and numerous fine quartz veins parallel to the schistosity.
1295-1340	S||S_0 constant 50^o-55^o	PSAMMITIC SCHIST. Pegmatites (1m thick) at 1308m, 1317m
1340		END OF HOLE.

No graded bedding observed.

Comment: The zone 1210-1295m contains altered and brecciated rocks, and may represent a faulted area.

DD 3154A — Carbonate Ridge Section

Reconnaissance; detailed pegmatites — Logged 21-7-75

990-1146	$S \| \| S_0$ 45^o-80^o av. 60^o	PELITIC SCHIST. Becomes more psammitic with depth. PEGMATITE: 1141-1146 diffuse boundaries.
1146-1162		Pelitic/psammitic schist boundary probably occurs in this interval.
1162-1171		PEGMATITE. Centre section split.
1171-1351	$S \| \| S_0$ constant approx. 60^o	PSAMMITIC SCHIST. PEGMATITE: 1177-1200m brecciated near base 1202-1214m 50% core loss 1241-1246m BLACK GARNETIFEROUS SCHIST and white quartz: 1262-1265m PEGMATITE; 1280-1281m 1347-1351m
1351-1427	S_R 60^o	RETROGRADE SCHIST, quartzitic. Gradational from psammitic schist.
1427-1439	S_{2-3} 45^o-70^o	PSAMMITIC SCHIST. S_2 regime (white/pink/grey) with patches of S_3 (green-grey).
1439		END OF HOLE.

DD 3160 — Carbonate Ridge Section

Moderate detail; detailed pegmatites — Logged 21-7-75

0- 326	$S \| \| S_0$ var. S_3 0^o-20^o	PELITIC SCHIST. Typical Browne Hills schist sequence, with interlayered pelite and quartzite bands on the scale of 5cm-1m, in the approximate ratio 60:40. S_{1-2} generally parallel to S_0 but in places S_2 is oblique to $S_1 \| \| S_0$. S_3 is generally poorer than S_{1-2} but in places forms a classic two-schistosity rock (particularly near the top), with S_{1-2} in the quartzite and S_3 in the pelite bands.
326- 333	S_3 0^o (top) S_R 0^o-30^o (base)	TRANSITION from S_3 to S_R downhole. Evident in: (i) mineralogy: chlorite prominent below 326m, sillimanite disappears at 333m. 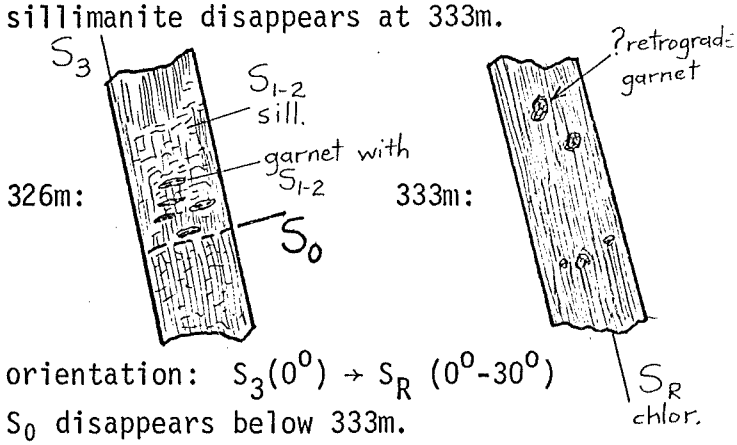 (ii) orientation: $S_3(0^o) \rightarrow S_R$ $(0^o$-$30^o)$ (iii) S_0 disappears below 333m.
333- 354	S_R 0^o-30^o	RETROGRADE SCHIST, chloritic.
		<u>Specimen</u>: 572 S_R in different lithologies
	Narrow transition	zone to pelitic schist, as 326-333m.
354- 570	$S \| \| S_0$ 45^o-90^o S_3 0^o-30^o S_R 0^o-10^o	PELITIC SCHIST. Dominantly S_3 regime. In places S_R occurs, with L_M. RETRO GRADE SCHIST: 485-490m.
570- 631	$S \| \| S_0$ 45^o-60^o	PELITIC SCHIST. Dominantly S_{1-2} regime.
631-1186	S_3 0^o-20^o	PELITIC SCHIST. S_3 variable from strong to absent.
		<u>Graded bedding younging uphole</u>: 673m moderate
	$S \| \| S_0$: 631-825m 60^o-90^o 825-950m var. 950-1186m 45^o-60^o	

DD 3160 (cont'd)

Moderate detail; detailed pegmatites

1186-1509	$S \| \| S_0$ var. av. 50^0-55^0	PSAMMOPELITIC SCHIST. Approximately equal proportion pelite: psammite in this interval. PEGMATITE: 1431-1444m 1471-1478m 1493-1495m
1509m		Clean quartzite units appear. Pelitic/psammitic schist boundary.
1509-2140	$S \| \| S_0$ var., high angles S_R 35^0 (top) 80^0 (base)	PSAMMITIC SCHIST. RETROGRADE SCHIST; quartzitic: 1526-1530m PEGMATITE: 1610-1617m 1625-1628m 1669-1670m 1686-1692m 1717-1719m 1745-1755m 1779-1784m 1795-1798m 1811-1817m with retr. schist 1820-1845m 1856-1874m schist bands 1896-1899m 1913-1922m schist bands 1962-1971m brecciated 1977-1982m brecciated 1995-2002m Below 1950m: schist iron-stained, broken, quartz-veined I/P. $?S_3$ 90^0 2098-2140m
2140-2180	Gneissosity and AP of ptyg.veins 80^0-90^0	POTOSI GNEISS. Fine-moderate grained, garnetiferous; ptygmatic veins common.
2180-2184		PEGMATITE
2184-2235	$?S_3$ 80^0-90^0	QUARTZ-MICA SCHIST. Grades into unit below.
2235-2253	S_R 60^0-90^0	RETROGRADE SCHIST.
2253		END OF HOLE.

DD 3160A — Carbonate Ridge Section

Moderate detail; detailed pegmatites — Logged 21-7-75

1019		Start of wedged hole.
1019-1497	S||S_0: 1019-1190m 50°-90° 1190-1340m var. 1340-1497m >45° S_2 70°-80°	PSAMMOPELITIC SCHIST. S_{1-2} regime, with S_2 oblique to S_1||S_0 in places. Negligible S_3. PEGMATITE, diffuse: 1242-1252m 1258-1264m 1280-1290m
	Comment: Zone 1200-1325m is rich in diffuse pegmatitic material, possibly of F_2 origin..	
		PEGMATITE: 1385-1387m 1390-1394m schist bands 1423-1430m first sharp
1497-1555	S_0 var. S_2 90°	Pelitic/psammitic schist boundary in this interval, probably at 1497m (first significant quartzite).
1555-1677	S_0 var. S_2 high angles	PSAMMITIC SCHIST. S_3 very poor. PEGMATITE, sharp: 1615-1620m 1634-1637m 1651-1653m
1677-1723	S_3 80°-90°	PSAMMITIC SCHIST. S_3 fairly strong. PEGMATITE: 1684-1707m
1723-1876	S_2 45°-60° S_R 60° Fractures 90° Fractures 90°	PSAMMITIC SCHIST. S_{1-2} regime, with S_2 oblique to S_1||S_0 in many places. RETROGRADE SCHIST: 1816-1823m, broken PEGMATITE. PEGMATITE: 1823-1849m, two schist bands (2m). 1853m: sheared pegmatite boundary - FAULT? PEGMATITE: 1853-1876m
1876-1939	S_0 var. S_3 >50° Fractures 90°	PSAMMITIC SCHIST. S_{1-2} and S_3 equally developed. PEGMATITE: 1927-1932m.
1939		END OF HOLE.

DD 3163 — Carbonate Ridge Section

Moderate detail — Logged 25-7-75

0-373	S_3, S_R 0^o-30^o S_R 0^o-10^o S_R 0^o-10^o	PELITIC SCHIST. S_3 regime with S_3 developed in retrograde schist zones. RETROGRADE SCHIST: 137-177m strong 210-247m strong 244-373m: S_3 and S_{3R} oblique to $S \| \| S_0$ in many places, which is strongly folded. Specimen: 600 F_3 fold showing S_{1-2} parallel to folded S_0, with axial-plane S_3 (?sillimanite-chlorite) Specimens: 601, 602, 603 chloritic S_{3R} cross-cutting $S \| \| S_0$ NB. The four specimens (600 to 603) show increasingly retrograde $S_3 \rightarrow S_{3R}$ downhole. GREEN FELDSPAR PEGMATITE: 274m.
373		END OF HOLE.

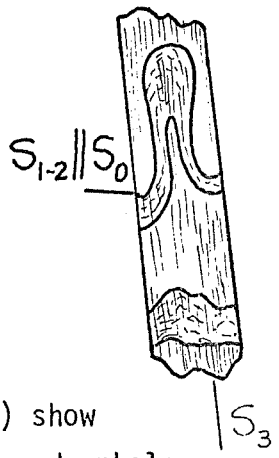

Comment: This hole provides many examples of the transitional relationship (orientation and mineralogical) between S_3 and S_R via S_{3R}.

DD 3164 — Carbonate Ridge Section

Moderate detail — Logged 25-7-75

0-107	$S \| \| S_0$ 70°	PELITIC SCHIST. S_2 and S_3 both developed. Numerous pegmatites. S_{1-2} generally parallel to S_0.
107-245	$S_1 \| \| S_0$ var. S_2: 107-180m 70° 180-245m 75°-90°	PSAMMITIC SCHIST. S_2 oblique to $S_1 \| \| S_0$ in many places. S_2 relations with S_0 indicate <u>F_2 synform downhole to east</u>: <u>Specimen</u>: 604 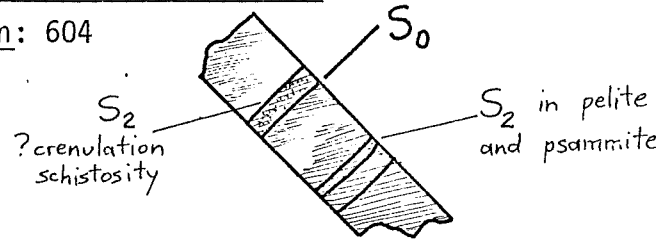 <u>Specimen</u>: 605 S_2 cross-cutting $S_1 \| \| S_0$ <u>Specimen</u>: 606 F_2 dragfold giving vergence as above: 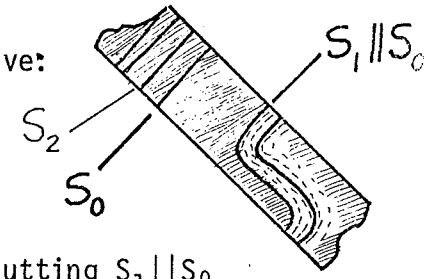 <u>Specimens</u>: 607, 608 S_2 cross-cutting $S_1 \| \| S_0$
	<u>Comment</u>: The orientation of the drillhole and the perpendicularity of S_2 with the core axis (hence unique orientation of S_2) prove that the schistosity is S_2 not S_3.	
245-354	S_2 75°-90° S_3 25°	PSAMMITIC SCHIST. S_2 patchily retrogressed, S_3 appearing in places. <u>Specimen</u>: 609 S_3 cross-cutting S_0
354-415	S_0 60°	PSAMMITIC SCHIST. S_2 patchily retrogressed, S_3 becoming stronger, esp. toward base. <u>Specimen</u>: 610 S_3 cross-cutting S_0.
	S_3 80°	?POTOSI GNEISS: 357-368m ptygmatic veins.
415-444	S_R 75° (top) 60° (base)	RETROGRADE SCHIST. Upper boundary gradational. AMPHIBOLITE, chloritic: 424m, 0.6m thick.
444		END OF HOLE.
	<u>Comment</u>: An excellent drillhole illustrating relationships between S_1 and S_2 (upper part) and S_{1-2} and S_3 (lower part).	

DD 3043 — Alpha Section

Moderate detail — Logged 25-7-75

0-146	S_R: 0m 0^o-20^o; 60m 30^o; 90m 40^o; 120m 50^o; 146m 55^o	RETROGRADE SCHIST, chloritic. S_R changes core angle downhole as shown.
146-213	S_R: 150m 60^o; 180m 65^o; 210m 70^o-80^o	QUARTZ-MICA SCHIST. Contains a non-penetrative schistosity S_R, always parallel to layering. Gradational from unit above (more quartzitic). Some pegmatites. Specimen: 611 S_R - possibly slightly oblique to layering.
213		END OF HOLE.

Interpretation: The change in S_R orientation can be inferred to represent a steepening of S_R from the centre of the Globe-Vauxhall shear zone (see pictorial log), at the top of the drill-hole, to its SE margin, at 146m. See Chapter 5 for further interpretation.

DD 3046 — Alpha Section

Moderate detail — Logged 25-7-75

0- 72	S_R slightly var. 20^o-40^o	RETROGRADE SCHIST, chloritic.
72-171	S_R: 90m 40^o; 120m 50^o; 150m 60^o; 170m 70^o	QUARTZ-MICA SCHIST. As 146-213m, DD 3043.
171		END OF HOLE.

DD 3158 | Alpha Section

Moderate detail | Logged 25-7-75

0-210	S_3 0^o-10^o	PELITIC SCHIST. Poor S_0, negligible S_{1-2}, Strong S_3.
210-400	$S \| \| S_0$ 50^o-90^o S_3 10^o-30^o	PELITIC SCHIST. More quartzitic bands than above. S_{1-2} now evident, but S_3 still stronger. S_3 relations with S_0 indicate <u>F_3 synform to west</u>: 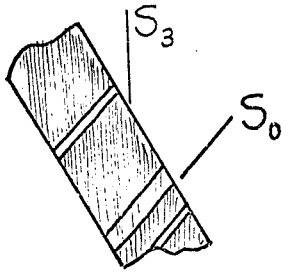 Some pegmatites.
400-460	$S \| \| S_0$ 50^o-90^o S_3 45^o	PELITIC SCHIST. As above. $S \| \| S_0$ retrogressed. S_3 grades into S_R of unit below.
460-543	S_R 45^o (top) 60^o (base)	RETROGRADE SCHIST. Upper boundary sharp, lower boundary gradational. Thick PEGMATITE in middle (15m thick).
543-712	S_{3R} 80^o	QUARTZ-MICA SCHIST. Non-penetrative schistosity S_{3R} appears to be parallel to layering. Several thick pegmatites.
712		END OF HOLE.

<u>No graded bedding observed</u>.

DD 3181 Alpha Section

Detailed logging; summary only Logged 15, 16-5-74 and 25-7-75

0-939	S_{1-2} || S_0	S_2	S_3
113	50^0		
116	60^0		
119	70^0-90^0		
122	90^0		0^0
127	35^0		5^0
130	85^0		0^0
134	55^0		10^0
137	70^0		0^0
139	60^0		10^0
142	20^0		10^0
144	85^0		5^0
147	70^0		0^0
150	70^0		0^0
171	60^0		10^0
180	50^0		10^0
201	45^0		0^0
215	55^0		0^0
265	75^0	50^0	
317	60^0		0^0
352	60^0		
378	70^0		0^0
396-427	70^0-90^0		
432	45^0		25^0
454	40^0		
472	70^0		
485	65^0		0^0
502	70^0		$<45^0$
511	80^0		
525	70^0		
537	80^0	70^0	
546	70^0	55^0	
568	60^0	70^0	
580		50^0	
582	60^0		
595	70^0		0^0
610	70^0		0^0-20^0

PELITIC SCHIST. Variations in strength of S_{1-2}, S_2 and S_3 are closely related to lithology (pelitic vs. psammitic bands). S_{1-2} generally parallel to S_0 except in sections noted below.

The core angles are listed in detail to show their variation.

Main units listed below:

113-213m: Dominantly PELITIC with strong S_0, strong S_3 and weak to moderate S_{1-2}. The latter is segregated in places.

Graded bedding, younging uphole: 134m good

" " " " : 145m good

" " " " : 150m good

" " " " : 171m moderate

Specimens: 686 fold in quartzite band with S_3 AP

687 ptygmatic quartz vein and parallel S_1 folded about S_3

688 S_3 (chloritic)

213-442m: PSAMMOPELITIC with many grey quartzite bands. Moderate S_0, S_{1-2} strong esp. toward base, with S_3 weak and patchy. S_2 oblique to S_1||S_0 in places.

Specimens: 689 segregated S_{1-2}

690 S_{1-2}

691 segregated S_{1-2} cross-cut by chlorite and ?biotite of S_3

692 as 691:

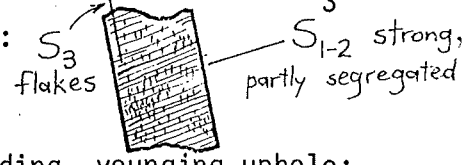

Graded bedding, younging uphole: 246m excellent

Graded bedding, younging uphole: 284m excellent

Graded bedding, younging uphole: 338m 6 beds - v.good.

DD 3181 (cont'd)

Detailed logging; summary only

618	70^0		0^0-20^0
622			0^0
623	55^0		15^0
628	45^0		20^0
630	85^0		0^0
644	70^0		0^0-10^0
651	75^0		20^0-30^0
657	60^0		30^0
663	55^0		5^0
671	55^0		0^0
677	60^0-90^0		30^0
689	55^0		30^0
696	55^0		5^0
699	45^0		
704	55^0		20^0
715			30^0
720	60^0		30^0
732			0^0
734	60^0-70^0		0^0-5^0
749	60^0		15^0
764			25^0
765	50^0		0^0
778	30^0		0^0
782	35^0		0^0
791	30^0		10^0
815	45^0		5^0
820	50^0		15^0
828	50^0		
857	40^0		20^0
878	40^0		0^0-15^0
888	15^0		0^0
899	15^0		
909	15^0		5^0
925	25^0		15^0
935	15^0		10^0

<u>442-534m</u>: PSAMMOPELITIC, white/pink/grey, S_0 moderate; S_{1-2} strong in psammitic and pelitic bands with S_3 absent. S_{1-2} displays a strong sillimanite lineation.

A fracture at 483m:

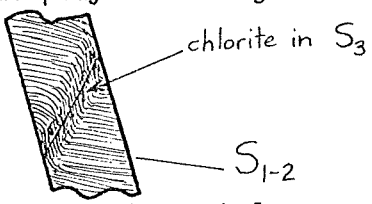

<u>Graded bedding, younging uphole</u>:
488m excellent

<u>Graded bedding, younging uphole</u>:
490m v. good

<u>Graded bedding, younging uphole</u>:
499m moderate

<u>Specimens</u>: 693 strong S_{1-2}
694 strong S_{1-2}
695 strong S_{1-2} and sillimanite lineation

<u>534-580m</u>: PSAMMOPELITIC as above, but <u>S_2 cross-cuts $S_1 || S_0$</u>

<u>Specimen</u>: 696 S_2 cross-cuts $S_1 || S_0$

<u>580-625m</u>: PSAMMOPELITIC as 213-442m.
S_{1-2} dominant but S_3 increasing toward base.
S_{1-2} parallel to S_0.

<u>Specimens</u>: 697 S_1 (garnet) in quartzite
698 S_{1-2} in psammite (retrogressed)
S_2 in pelite
699 as 698

<u>625-939m</u>: PELITIC SCHIST with S_3 now dominant over S_{1-2} and becoming more penetrative with depth; the chlorite and mica "pods" defining S_3 become more elongate and the grainsize becomes finer. A strong L_M appears on S_3, which generally becomes S_{3R} at depth.

900m: S_{1-2} disappears, S_0 becomes rare.

939m: S_0 disappears.

DD 3181 (cont'd)

Detailed logging; summary only

		The general relationship between S_3 and S_0 or S_{1-2} indicates <u>F_3 synform to west</u>: 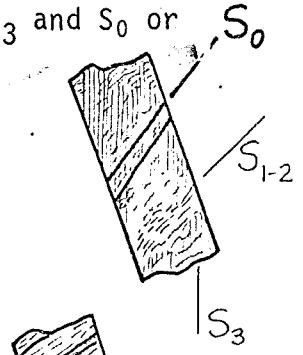 <u>Graded bedding, younging uphole</u>: 826m moderate <u>Specimens</u>: 700 biotites in S_3 701 S_{1-2} (psammite) and S_3 (pelite) with garnets in pelite preserving S_{1-2}: 702 S_3 in pelite and psammite 703 S_3 strong; S_{1-2} preserved in quartzite patches and in garnets 704 strong S_3 enclosing round garnets 705 F_3 fold in $S_{1-2}\|\|S_0$ with S_3 AP; 706 S_{1-2} (biotite) overprinted by S_3 (chlorite) 707 S_3 strong with ?S_{1-2} in garnets 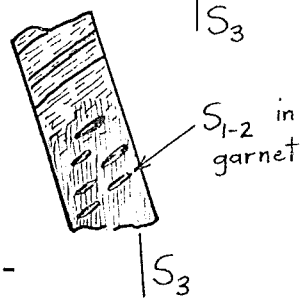 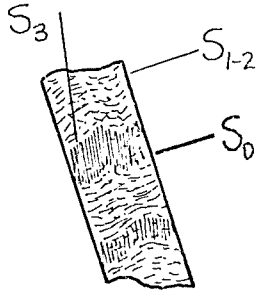 NB. S_{3R} has a strong L_M which pitches steeply NE: 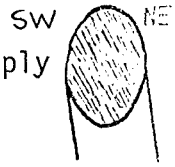
939-1098	S_R 0^o-10^o (top) 20^o-30^o (middle) 30^o-45^o (base)	RETROGRADE SCHIST. Boundary somewhat arbitrary, marked by disappearance of S_0 and appearance of iron staining, milky quartz augen in S_R, and strong fracturing parallel to S_R. Garnets decrease and chlorite/sericite continues to increase down hole. L_M (chlorite and sericite) lies at about 20^o to the core axis, and thus pitches steeply in S_R. 994m : Disappearance of large garnets. 1006m: Commencement of silky schist.
1098		END OF HOLE.

<u>Comments</u>: Over most of the drillhole the apices of the S_0 and S_3 ellipses in the core coincide, indicating that <u>F_3 fold axes are generally subhorizontal</u> (see Chapter 8).

DD 3181/D2 Alpha Section

Reconnaissance Logged 25-7-75

520		Start of wedged hole.
520-588	S_2 70^0-80^0	PSAMMOPELITIC SCHIST. S_2 regime (white/pink/grey) with S_2 oblique to $S_1 \| \| S_0$ in many places.
588		Very sharp boundary between abundant sillimanite (above) and negligible sillimanite (below, replaced by chlorite/mica).
588-729	$S \| \| S_0$ var. 50°-90° S_3 0°-40°	PSAMMOPELITIC SCHIST. Some relict S_2 (retrogressed). Dominantly S_3, strongly oblique to $S \| \| S_0$.
		Specimen: 641 S_2 (psammite) and S_3 (pelite)
729		END OF HOLE.
		No graded bedding observed.

DD 3175 — Between Carbonate Ridge and Alpha Sections

Graded bedding search — Logged 3-8-75

Logged between 250m and 700m:

Graded bedding, younging uphole: 625-629m good, series of graded beds

Graded bedding, younging uphole: 639m good

DD 3184 — Line 48S, Rupee Section

Graded bedding search — Logged 2-8-75

Graded bedding, younging downhole: 33m good

Specimen: 708

Graded bedding, younging downhole: 194m moderate

Graded bedding, younging uphole : 259m moderately good

APPENDIX B

STRUCTURAL INTERPRETATION OF DRILLCORE FROM FOLDED AND CLEAVED ROCKS

by

W. P. Laing

(Manuscript of a paper published in

Economic Geology, vol. 72, no. 4, 1977)

TABLE OF CONTENTS

ABSTRACT

Published research on drillcore interpretation has been confined to the simple case involving multiple drillholes penetrating a planar sequence of layers. This paper investigates the more general situation applicable to deformed terrains, in which the rocks are folded. The analysis is applicable to single, non-linear drillholes. Fold cylindricity is assumed in some parts of the analysis.

Methods are developed in which the relationship of bedding to cleavage and other small scale structures in drillcore is used to determine the orientation of the fold axis, the angle between bedding and cleavage, the vergence with respect to major fold hinges, and the stratigraphic facing of the sequence. The assumptions in each case are clearly spelled out and discussed.

These structural parameters may be expressed quantitatively in terms of easily measured drillcore parameters, viz. the angle of inclination of the drillhole, the core angles of bedding, cleavage and lineation, and the direction of younging of any sedimentary structures present in the drillcore. This quantified approach permits the introduction of computer programming as an important aid to structural interpretation of drillcore.

INTRODUCTION

Geological literature contains many papers dealing with the structural interpretation of drillcore in layered rocks. Virtually all are restricted to a specific, albeit fundamental, problem, namely the calculation of the dip of a planar surface intersected by one or more drillholes. This paper is an attempt to expand the scope of drillcore interpretation, in the following ways:

1. By examining the more general case in which the bedding or layering is folded. Parts of the analysis assume that the folding is cylindrical.
2. By developing methods which are applicable to single drillholes. The drillholes are generally assumed to be curved, i.e. flattening or steepening with depth, which is the most commonly encountered situation in practice.

Folded layering in strongly deformed terrains is conveniently analyzed by considering the disposition of small scale structures. This paper develops methods of utilizing cleavage, fold axes, fold vergence, interlimb fold angles, and younging directions in drillcore, in the same way as they are used in mapping deformed rocks on the surface.

PREVIOUS LITERATURE

Discussion to date on structural interpretation from drillcore has been concerned almost exclusively with determining the attitude of bedding planes in a planar sequence lacking marker units, from non-oriented drillcore. Combinations of one, two and three drillholes, with or without surface information, have been analyzed. Early workers used instrumental, graphical, and mathematical techniques (Mead, 1921; Haddock, 1931; Wisser, 1932; Stein, 1941; Mertie, 1943). The stereographic projection was then introduced and became established as the standard technique (Johnson, 1939; Fisher, 1941; Bucher, 1943; Gilluly, 1944; McClellan, 1948; Addie, 1962; Mills, 1963). Summaries of the stereographic method are contained in Badgley (1959), Phillips (1971), and Ragan (1973).

Calculation of the attitude of bedding planes from oriented drillcore is discussed in McClellan (1948) and at length in Zimmer (1963). An alternative method is presented in an unpublished report of North Broken Hill Limited, Australia (1975).

The only paper which attempts to analyze folded layering is that of Mertie (1943). This treatment fits an algebraic function to the coordinates of a marker unit in a large number of drillholes.

No published method of analyzing folded layering in drillcore, independently of marker units, has been found.

THE APPROACH IN THIS PAPER

The analysis is developed for non-oriented drillcore, from a drillhole whose orientation is known at every point. The principles are equally relevant to oriented drillcore. Different parts of the analysis are applicable in different circumstances, depending on:

1. whether the folds are cylindrical;
2. fold style and the scale of folding;
3. the presence or absence of an axial plane structure;
4. the presence of sedimentary facing criteria.

For the purposes of this paper we will hereafter use the term bedding to denote the folded surface (in practice this may be bedding, cleavage, schistosity, metamorphic foliation, etc.) and the term cleavage to denote the axial plane structure (in practice this may be slaty cleavage, crenulation cleavage, schistosity, metamorphic foliation etc.). The following symbols will be used:

S_0	bedding
S_1	cleavage
P_0	pole to bedding
P_1	pole to cleavage
F	fold axis
D	angle of dip of S_0 or S_1

δ angle between core axis and P_0 or P_1

β angle of inclination of drillhole, measured downward from the horizontal

ϕ angle between S_0 and S_1

α angle between S_0 and S_1 in a plane perpendicular to drillcore

γ angle between lineation and drillcore axis

ϵ angle between lineation and minor axis of the elliptical face formed where cleavage cuts the drillcore.

The analysis is presented in two sections. Discussed first is the problem of bedding attitude and the determination of the fold axis. Then follows a discussion on the use of bedding/cleavage relationships and small folds to determine vergence with respect to major fold hinges, and the concomitant use of sedimentary younging criteria to determine stratigraphic facing.

DETERMINATION OF THE FOLD AXIS

METHOD OF BEDDING-POLES

Importance of fold style

Before we look at this method of determining the fold axis it is necessary to consider the role of fold style, which has an important limiting effect on the usefulness of the method.

For the purpose of this discussion we may consider fold style in terms of two parameters: the interlimb angle (Fleuty, 1964) which we shall call L, and a parameter R (Ramsay, 1967, p. 350*) which broadly expresses the ratio of limb area to hinge area. The folds shown in Figure 1 represent the spectrum of fold styles most commonly found in nature, with corresponding values of the parameters L and R. The equal area projection shown below each fold represents the contoured pattern of bedding-pole orientations measured around the folded surface.

---

*Ramsay called the parameter P_1 but it is denoted R in this paper to avoid confusion with the pole to cleavage. R is defined as the ratio of the lengths of projection of the limbs versus the hinge, on to the join of the inflexion points on each side of the fold.

The method discussed in this section is applied most readily to folded rocks in which the bedding occupies all possible orientations about the fold axis. This corresponds to folds showing the full girdle pattern in Figure 1. In practical terms this means folds with a tight interlimb angle (L close to 0^{o}) with a hinge area of similar size to the limb area (R = 0 to 1). Folds of more open style (two point maxima and partial girdle), or with the limb area much greater than the hinge area (two point maxima and single point maximum) are amenable to treatment, but will generally provide less information than the ideal, full girdle fold style. We shall first investigate the full girdle case, and subsequently look at the partial girdle case as an example of the non-ideal fold styles.

A necessary assumption of the method is that the folding is cylindrical.

Method applied to "full girdle" folds

Let us assume that the drillhole penetrates a sequence of rocks cylindrically folded on all scales, in a manner yielding a full girdle of bedding-pole orientations. Figure 2 shows the general case, where the fold axis F is plunging at some angle. The poles to bedding may assume any orientation A,B,C,.....within the great circle perpendicular to the fold axis F. Furthermore, because the folding occurs on all scales, any arbitrary segment of drillcore (whose orientation is represented by the point DH in Figure 2) will contain this same range of bedding orientations A,B,C,.....Let us consider for a moment this single segment of drillcore. Where the core is unoriented, we will not obtain unique pole orientations A,B,C,....., rather these will be situated somewhere on the surface of a group of coaxial cones of varying apical half-angles $\delta_A,\delta_B,\delta_C,.....$, whose axis coincides with the drillhole axis DH. These cones are represented on the stereographic net of Figure 2 by small circles of angular radii $\delta_A,\delta_B,\delta_C,.....$, centered on the point DH and passing through the points A,B,C,....

All the small circles intersect the great circle of bedding poles (hereafter termed the bedding-pole girdle for convenience), at two points (B and

B', C and C', etc.) which represent alternate bedding attitudes for a given δ, except for one small circle which is tangential to the bedding-pole girdle, at the point A. This point occurs at the intersection of the bedding-pole girdle with the plane DH-F, containing the drillhole and the fold axis. It is evident that the angular distance DH-A, i.e. δ_A, represents the minimum possible angle between the drillhole and all poles to bedding, hence this angle will be denoted δ_{min}. Its value is the complement of the angle DH-F between the drillhole and the fold axis.

The existence of a particular δ_{min} for any particular drillhole orientation DH provides a method of determining the orientation of the fold axis F, provided that we have at least two values of δ_{min} and DH. The method thus requires data from two or more non-parallel drillholes or from a curved single drillhole. A linear drillhole will provide only a single δ_{min}, whose corresponding small circle will have an infinite number of great circles tangential to it, representing various possible bedding-pole girdles. Selection of the correct bedding-pole girdle, hence the determination of F, will depend on the availability of other information. With a curved drillhole or a number of linear non-parallel drillholes, it is possible to define a unique great circle representing the correct bedding-pole girdle. The pole to this great circle then constitutes the fold axis F.

The general case of a curved drillhole intersecting a fold representative of a full bedding-pole girdle is illustrated in Figure 3A. The fold is abstracted in Figure 3B into its components, the fold axis and the plane containing the poles to bedding. These components are mutually perpendicular for a cylindrical fold. The main point of the diagram is to demonstrate that in the general case, there is one point in the drill path (point 5) which is parallel to the plane containing the poles to bedding, and therefore parallel to one particular bedding pole PP'; this direction also is coincident with the intersection QQ' of the plane containing the poles to bedding and the plane of the drillhole.

Figure 4 contains the stereographic representation of Figures 3A and 3B, and illustrates the principles involved in determining the fold axis by the method of bedding-poles. For a range of drillhole orientations downhole (1 to 7, Fig. 4), we plot the corresponding small circles of radii δ_{min} around each drillhole orientation. This gives a series of small circles which must all be tangential to the great circle representing the bedding-pole girdle. The series of small circles actually gives rise to two great circles (Fig. 4), symmetrically disposed about the plane of the drillhole. One of the great circles is spurious. Selection of one great circle as the correct bedding-pole girdle will depend on other information. This is most likely to be a knowledge of the approximate trend of the fold axis in the area (e.g. easterly versus north-westerly in Figure 4). A unique solution will also be provided if the drillhole deviates from lying in a plane. A drillhole deviation from 6 to 7a in Figure 4 will give a δ_{min} for 7a which is tangential (at δ_{7a}) to the correct bedding-pole girdle but not to the other.

To apply the method we must divide the drillhole into small linear sections and find the δ_{min} for each section. The angles between bedding and core must be converted to δ pole angles as shown in Figure 5A. To obtain δ_{min} we must search for bedding at a maximum angle to the drillcore axis (i.e. maximum core angles) as shown in Figure 5B.

In general we need only consider a small number of sections, preferably representing drillhole orientations furthest apart. If the drillhole passes through the bedding-pole girdle (path 1 to 6 in Figure 6A), the envelope around the small circles has a "nodal point" where $\delta_{min} = 0$. This point corresponds to the bedding pole PP' in Figure 3B. If the drillhole does not pass through the bedding-pole girdle (path 1 to 4 in Figure 6B), then no nodal point exists. The use of only two δ_{min} small circles which do not intersect, complicates the selection of the correct bedding-pole girdle, because four great circles can be drawn tangential to any pair of non-intersecting small circles. In the case of a drillhole passing through the bedding-pole girdle (Fig. 6A), the two great

circles "outside" the nodal point are spurious. If the drillhole does not pass through the bedding-pole girdle (Fig. 6B), there will be a spurious nodal point through which pass two spurious great circles. These considerations indicate that at least three δ_{min} small circles should be used to avoid unnecessary ambiguity.

If it is found that a great circle cannot be fitted tangential to the group of small circles, we may conclude either that the folding is non-cylindrical, or that at least one of the δ_{min} is not the true δ_{min} for that particular drillhole orientation. Assuming that the folding is cylindrical, and that the sampling has been sufficiently dense, this result indicates that the scale of folding has not been sufficiently small in part of the drillhole to provide layering in an attitude corresponding to δ_{min}. It is clear that the method is most powerful in areas of small scale folding.

Method applied to "partial girdle" folds

This group of folds forms the most general category of folds in which the interlimb angle is non-zero. For our purposes the important feature of these folds is that the bedding-pole girdle is only part of a great circle (see Figure 1). We shall now analyze this situation, which is more generally encountered in folded rocks than full girdle-type folding.

With bedding-poles occupying only part of a great circle (AC in Figure 7), there is only a restricted section of drillcore orientations (XY) which can be projected on to this partial girdle by the shortest angular route, i.e. along a great circle passing through the fold axis F. Because the projections from it on to the bedding-pole girdle are the only true δ_{min} values that can be obtained, this restricted section of drillcore orientations is termed the effective drillhole arc. That portion of the bedding-pole girdle on to which the effective drillhole arc projects (BC) is termed the common arc.

Outside the effective drillhole arc, the drillcore orientation cannot be projected along a great circle containing F, on to the fold arc. Thus the minimum δ angles measured from core orientations outside the effective drillhole arc

will not be the true δ_{min} which would be obtained from a full girdle pattern. Minimum δ angles measured in the drillhole arc YZ will decrease from the point Y to a minimum at Y', with an angular length Y'C, then increase from Y' to Z. These minimum δ angles will yield small circles all of which will intersect at the endpoint C of the common arc. This latter feature will allow the correct interpretation to be made, and furthermore provides useful information on the angular extent of the bedding-pole girdle and thus on the tightness of the folding.

Effectiveness of the method

It is apparent that the most significant restraint on the effectiveness of the method of bedding-poles is the length of the common arc. The method is most effective when the length of the common arc is at a maximum, which occurs in the case of full girdle-type folding. If, however we consider a general case of folding, with an arbitrary interlimb angle, the length of the common arc will be maximized by obtaining the maximum possible curvature of the drillhole. A linear drillhole (zero curvature) provides a common arc of length 0^o, i.e. a common "point" only.

BEDDING/CLEAVAGE INTERSECTION METHOD

Applicability of the method

Calculation of the fold axis by this method is more useful than the previous method, in that it requires only one piece of drillcore for the determination. Hence a large number of separate determinations may be made down the drillhole. It does not depend on whether the drillhole is linear or curved, nor does it depend on an assumption that the folding is cylindrical. It does, however, assume that the fold axis is parallel to the bedding/cleavage intersection, which is an assumption inherent in most surface structural analysis. The method also relies on two factors not necessary in the previous method:

1. The presence of measurable cleavage and a measurable bedding/cleavage intersection in the drillcore.
2. That the orientation of cleavage is known, or (in one case) that at least the strike of cleavage is known.

These are both reasonable suppositions, because many deformed terrains demonstrate an axial plane cleavage whose attitude is uniform over areas at least comparable in size to those involved in extrapolation from surface to drillhole. It is also reasonable to assume that in most situations it is possible to measure the attitude of cleavage, or at least the strike lines of the cleavage, at the surface.

Given these conditions, there are two alternate ways of applying the method to unoriented drillcore. Measurement of the bedding/cleavage intersection observed on the bedding surface in drillcore leads to two solutions for the fold axis. Other information is necessary to find the appropriate solution. On the other hand, measurement of the bedding/cleavage intersection on the cleavage surface provides a unique solution for the fold axis.

Method employing bedding/cleavage intersection on the bedding surface

The ellipse formed by bedding in drillcore is shown in Figure 8A. I represents the trace of the cleavage on the bedding surface. This intersection lineation is at an angle γ to the drillcore axis. For unoriented core the possible orientations of P_0 and I lie on the small circles shown in Figure 8B. The orientation of cleavage is shown by the great circle labelled S_1.

The intersection of the great circle S_1 and the small circle I will in general give two solutions, I and I'. Selection of the appropriate solution to give the fold axis will depend on other information (e.g. steep versus shallow plunge of fold axis, in the example depicted). Once the fold axis is known, we also may determine the two alternative possible orientations of bedding corresponding to the intersection lineation I. The alternative possible bedding-poles consist of the two points located on the small circle P_0 at 90^o to I.

Method employing bedding/cleavage intersection on the cleavage surface

The ellipse formed by cleavage in drillcore is shown in Figure 9A. The diagram is analogous to Figure 8A, except that an extra measurement is made, being the angle ε, the angle between the intersection lineation and the minor

axis E of the cleavage ellipse. The convention is made that ε is measured anticlockwise from the minor axis. This is to distinguish between two possible intersection lineations, I and I' in Figure 9A, which possess the same angle γ and superficially the same angle "ε" (in the case of I', "ε" being measured clockwise from the minor axis).

Figure 9B illustrates the construction used to determine the fold axis from unoriented core. The method consists of (a) plotting S_1 on the stereographic net, (b) finding the orientations of the lineations E, I and I' in the plane of S_1, then (c) selecting the appropriate I or I' to give the fold axis.

If the orientation of S_1 is already known, we plot it as a great circle and proceed with step (b) as set out below. However, if only the strike of S_1 is known, and the approximate angle of dip able to be estimated, we may construct S_1 as shown in Figure 9C. From the known strike of S_1 and the P_1 small circle constructed about DH, we derive two alternate poles P_1 and P_1' as shown. One of the corresponding cleavage orientations S_1 or S_1' will be closer to the estimated orientation than the other, so we select this orientation.

Step (b) is commenced by plotting the small circle I about DH, with an angular radius γ. The alternative solutions I and I' lie at the intersection of the small circle I with the cleavage plane S_1. We then plot the great circle E at 90^0 to DH. This represents the locus of the minor axis of the ellipse, the latter being perpendicular to the drillcore axis. The minor axis E of the cleavage ellipse lies at the intersection of the great circles E and S_1.

Step (c), viz. selection of the correct orientation of the fold axis, simply consists in measuring the angle ε anticlockwise from E, along the S_1 great circle to the appropriate position I or I'.

The procedure is greatly simplified if we know the approximate orientation of the fold axis before we start. Once I and I' are located (step (b)) we then choose the appropriate solution for the fold axis. This abbreviates step (b) and also obviates the need for measuring the angle ε.

Summary

We assume that the area being investigated has a penetrative, uniformly oriented cleavage whose attitude is known. If the very approximate orientation of the fold axis is also known, we may determine its exact orientation, at any number of points down the drillhole, by measuring pairs of (δ,γ) angles on either bedding or cleavage surfaces in the drillcore. If the approximate orientation of the fold axis cannot be estimated, we may determine its orientation, at any number of points down the drillhole, by measuring triplets of $(\delta,\gamma,\varepsilon)$ angles on cleavage surfaces in the drillcore.

As an adjunct to the method employing the bedding/cleavage intersection on the bedding surface, it is possible to obtain some information on the attitude of bedding itself. As described above, this method yields alternative orientations of bedding corresponding to each possible fold axis orientation. If a number of these alternative bedding solutions are obtained down the drillhole, they may ultimately be rationalized, and a unique set of bedding orientations selected, on the basis of a consistent, or consistently varying, orientation of one of the alternatives, as opposed to inconsistency in the other orientation. On the other hand, we may be able to discriminate between the alternative bedding orientations using some external information, such as results from surface mapping.

An interesting result of the general analysis which has great practical significance, is that if the drillhole is perpendicular to the fold axis, the extremities of the major axes of the bedding and cleavage ellipses appear "in line" along the drillcore as shown in Figure 10. This provides a rapid visual check on the approximate fold axis orientation with respect to the drillhole. Generally, the greater the departure from an "in line" appearance (i.e. as α increases from 0^{o} to 90^{o} in Figure 12) the greater is the departure from perpendicularity.

It is important to observe that the bedding/cleavage intersection method may actually be used to test cylindricity of folding in the area under investigation, by allowing the comparison of a number of fold axis measurements down

the drillhole. The twin features of non-dependence on cylindricity assumptions and applicability to linear as well as curved drillholes, characterize the bedding/cleavage intersection method as a widely applicable and powerful tool for determining the fold axis in drillholes.

DETERMINATION OF VERGENCE AND FACING

The interpretation of strongly folded rocks is greatly facilitated by mapping vergence and facing relationships. For a full discussion of the respective principles involved see Wilson (1961) and Shackleton (1958), and as an example of their use in field mapping see Means (1963).

Vergence, or broadly the relationship between bedding and the axial plane of folds, may be assessed using two parameters:

1. The angle between bedding and the axial plane, normally measured as the angle between bedding and cleavage, ϕ (see "a" in Figure 11).
2. The direction in which synformal and antiformal closures are located. This parameter can be determined in two ways, as the asymmetry or "sense" of the bedding/cleavage relationship at a particular point ("b" in Figure 11), or as the "sense" of rotation of parasitic folds ("c" in Figure 11).

Once vergence is established at a given location it is then possible to use sedimentary younging criteria to determine whether the folds face upward or downward, i.e. whether the stratigraphic sequence is right way up or inverted.

The following section investigates the application of these principles to folded rocks in drillcore.

ANGLE BETWEEN BEDDING AND CLEAVAGE

This parameter may be divided into two categories: cleavage parallel to bedding, and cleavage oblique to bedding.

Where cleavage is parallel to bedding, we may conclude that the drillcore is passing through the limb of an isoclinal fold ($\phi = 0^{o}$ in Figure 11).

Where cleavage is oblique to bedding, we may use the magnitude of the angle ϕ to assess position around large folds. ϕ reaches a maximum of 90^{o} in

fold hinges (Figure 11). The method is essentially statistical, because parasitic folds give locally anomalous values of ϕ whose effect must be minimized by taking a large number of measurements.

Two non-parallel planar surfaces appear in drillcore as two ellipses (Fig. 12), whose mutual relationship is described by three angles. If the planes are bedding and cleavage, the angles are δ_0, δ_1, and α, the latter being the angle between S_0 and S_1 in a plane perpendicular to the core axis. α is measured around the drillcore between the major axes of the two ellipses.

A stereographic method of calculating ϕ is outlined in Zimmer (1963), and a variation on this is contained in an unpublished report of North Broken Hill Limited, Australia (1975). The algebraic solution, modified from Zimmer, is as follows:

$$\phi = \cot^{-1}\left[\frac{\cot \delta_0}{\text{Sin} \tan^{-1}\left(\frac{\cot \delta_1 - \cos \alpha \cot \delta_0}{\text{Sin } \alpha \cot \delta_0}\right)}\right] + \cot^{-1}\left[\frac{\cot \delta_1}{\text{Sin} \tan^{-1}\left(\frac{\cot \delta_0 - \cos \alpha \cot \delta_1}{\text{Sin } \alpha \cot \delta_1}\right)}\right]$$

Eq. 1.

Zimmer omitted to point out that the formula breaks down under any of the following conditions:

1. $\delta_0 = 0^o$
2. $\delta_1 = 0^o$
3. $\delta_0 = \delta_1 = 90^o$
4. $\alpha = 0^o$ and $\delta_0 = \delta_1$

In order to obtain a large number of ϕ measurements, the use of a flexible template, described by Zimmer, permits rapid measurement of (δ_0, δ_1, α) angle triplets down the drillcore. It will be found that the stereographic method of calculating a large number of angles between bedding and cleavage is prohibitively slow. The formula presented above can be readily incorporated into a computer program, provided that the limiting conditions are taken into account.

VERGENCE AND FACING

Visual Method

In the general case of a drillhole intersecting a cylindrical fold at an arbitrary angle, we cannot determine the sense of bedding and cleavage, hence the vergence, in unoriented drillcore. There is, however, a special case which is amenable to treatment: that is where the drillhole is oriented approximately perpendicular to the fold axis and to the strike of the axial plane. If the fold axis is not subhorizontal this condition applies to a linear drillhole only, but where the fold axis is subhorizontal (i.e. subparallel to the strike of the axial plane) the condition is fulfilled for a curved drillhole lying in a plane subperpendicular to the fold axis. Hence the method described below is most applicable to terrains characterized by subhorizontal fold axes. This includes the typical slate belts (Hobbs, Means and Williams, 1976, p. 403), as well as more complex metamorphic terrains in which the large scale fold axes are subhorizontal. The techniques described below were developed during a study of the latter type of terrain, namely the Willyama Complex of western New South Wales (Laing, 1977). The complexity of the fold history in this area, with three phases of folding and schistosity development, is offset by the fact that the major folds (which belong to the second and third phases) generally possess subhorizontal fold axes.

It has been shown that where the drillcore is perpendicular to the fold axis, the extremities of the major axes of the bedding and cleavage ellipses are "in line" down the drillcore (Fig. 10). Hence a rapid scan down the core will establish that the necessary condition holds. A sufficient condition for the method to be then applied is that the very approximate attitude of cleavage be known.

Because the drillcore is perpendicular to the fold axis, hence to the strike of the cleavage, we may visually place the segment of core in either of two permitted orientations, as illustrated in the example shown in Figure 13. Knowledge of the approximate dip of the cleavage (e.g. steep versus flatlying

in Figure 13), will then enable us to select the correct orientation and hence determine the vergence appropriate to that segment of core. The vergence may be expressed as "antiform uphole" or "antiform downhole", meaning that as we go uphole or downhole respectively, the cleavage planes in the drillcore progressively approach the geometrical axial plane of an antiform. This is illustrated clearly in Figure 13.

Having determined the vergence, it is a simple matter to relate it to occurrences of sedimentary younging which may be observed in the drillcore, and so determine the facing of the folds (Shackleton, 1958). If the vergence coincides with the sedimentary younging, i.e. the antiforms are anticlines (e.g. in Figure 13A, the layering may contain graded bedding which youngs to the right), we may conclude that the sequence is stratigraphically right way up in the folds associated with the cleavage. If the vergence and sedimentary facing are opposite, then the sequence is inverted, and the folds are said to be downward facing.

In terrains where cleavage is absent or only sporadically developed, we may use parasitic folds to determine the vergence. Figure 11 shows how the relationship between long limb and axial plane of parasitic folds is geometrically equivalent to the relationship between bedding and cleavage around a large fold. Again, provided we know the approximate attitude of the axial plane of the regional folds, we may thus determine vergence from small parasitic folds in drillcore.

Quantified Method

In the preceding section we have discussed the determination of vergence from bedding/cleavage relationships in an individual piece of drillcore. However, like the use of the bedding-cleavage angle to determine position around a fold, the application of vergence to locate large scale fold hinges is a statistical process. Parasitic folds on the limbs of large folds yield anomalous vergence in their short limbs (Figure 11), whose effect must be counteracted by considering a large number of vergence determinations. In this section we de-

velop a quantified version of the visual method, and discuss the merits of the quantified method as an aid to the statistical use of vergence in drillcore. The same conditions apply, that the drillhole must be subperpendicular to the fold axis, which generally means that the fold axis should be subhorizontal.

The quantified method takes the observable parameters β, δ_0, and δ_1 and transforms them into two sets of dip data (D_0, D_1) describing the two permitted orientations of drillcore. Each set of dip data has a corresponding vergence, calculated by applying the principles shown in Figure 13. The boundary conditions describing the attitude of cleavage D_1 are then invoked to select the correct set of dip data, and hence the appropriate vergence. The observable parameter "younging" is then read in and the stratigraphic facing determined by comparison of the vergence and the younging.

Figure 14 illustrates how the two permitted drillcore orientations give rise to two sets of (δ_0,δ_1) readings. To commence the method, either of the angle pairs (δ_0,δ_1) or (δ_0',δ_1') may be measured in the field. The dip pairs corresponding to these two sets, namely (D_0, D_1) and (D_0' D_1') are then obtained used the relationship

$$D = \beta + \delta \pm 90^{o} \qquad \text{Eq. 2.}$$

From this relationship we obtain the corollaries

$$\delta' = 180 - \delta \qquad \text{Eq. 3.}$$

$$D' = 2\beta - D \qquad \text{Eq. 4.}$$

Two conventions are observed in obtaining these results. These are:

1. δ angles must be measured clockwise from the top of the drillhole to the bottom (Fig. 14). Hence $0^{o} \leqslant \delta < 180^{o}$, contrary to normal drill logging practice in which δ is measured from 0^{o} to 90^{o}. An important practical corollary is that the latter convention, if used without care, leads to the sort of ambiguity shown in Figure 15. As can be seen, normal logging practice yields identical core angles for two situations which are structurally quite distinct: in A the vergence is "antiform

uphole" whereas in B the vergence is neutral, because we are at a fold hinge. However, insertion of the angles measured using the new convention, into Equation 2 and thence into Table 2, as explained below, provides the correct solution. Figure 15A corresponds to Case 6 in Table 2, and Figure 15B corresponds to Special Case 2.

2. The dips of S_0 and S_1 are measured consistently, clockwise from the horizontal.

To illustrate the derivation of dip pairs from a data set $(\beta,\delta_0,\delta_1)$, the situation shown in Figure 14 is quantified in Table 1.

Note that the calculation of ϕ (Equation 1) in this analysis reduces to $|D_0 - D_1|$ or its supplement $|D_0' - D_1'|$.

Having calculated the two dip pairs we now insert them into a routine which tells us the appropriate vergence for each pair. The routine is shown in Table 2, columns 1 to 5. This has been compiled by visually assessing vergence in situations comparable to Figure 14, according to the principles shown in Figure 13, for all possible combinations of β, D_0, and D_1 angles. Once the vergence for each dip pair is determined (column 5), we then apply the appropriate younging (if available) observed in the drillcore (column 6) to obtain the stratigraphic facing of the sequence (column 7) in each case.

To distinguish between the two sets of results we must apply a boundary condition. In practice this will generally be a narrow range of permitted cleavage orientations, obtained from surface mapping. For example if we know that the cleavage is subvertical, with D_1 ranging from 80^oE to 80^oW (i.e. $80^o \leqslant D_1 \leqslant 100^o$), we will usually be in a position to reject one of the calculated (D_0, D_1) pairs before we commence the routine. This will allow a unique solution for the dips of bedding and cleavage, the vergence, and the stratigraphic facing.

DISCUSSION

APPLICABILITY OF THE VARIOUS METHODS

It will be apparent that the methods developed in this paper are as limited as the assumptions on which they rest. The importance of these assumptions is underlined. While some terrains are too complex to permit the necessary assumptions to be made, the methods are generally applicable to folded sedimentary basins, slate belts, and to the more highly deformed complexes where the latter are divisible into small domains of cylindrical folding. Of all the factors affecting the applicability of the methods, the most critical is perhaps the scale of folding. For example deformed complexes in which strong folding exists on a mesoscopic scale are unlikely to prove suitable subjects for vergence analysis.

The general applicability of the methods discussed in this paper is summarized in Table 3. The table is self-explanatory, but several comments are pertinent.

Fold Axis Methods

The method of bedding-poles is dependent on fold cylindricity, whereas the bedding/cleavage intersection method may be used to test cylindricity of folding. In a drillhole containing poor to moderate cleavage, the two methods may be used in a complementary manner, the latter method testing whether the former method may be used overall to determine the fold axis.

Vergence Method

The initial conditions may appear too restrictive for the method to be of practical importance. However, drilling programs in cleaved terrains as a rule tend to require drillholes oriented perpendicular to the strike of the regional cleavage. If the fold axis is subhorizontal then the necessary conditions are automatically fulfilled. As mentioned earlier, the visual vergence method has been applied successfully in a relatively complex metamorphic terrain.

Facing Determination

Although presented in this paper as a natural extension of the vergence method, the determination of stratigraphic facing may of course be made independently of the method by which the vergence of the segment of drillcore is determined (e.g. the vergence may be obtained by extrapolation from surface mapping).

USE OF COMPUTER PROGRAMMING

The methods developed in this paper are applicable to any individual segment of drillcore, given the limitations discussed above. An important supplementary aim has been to introduce techniques for quantifying the analysis, so that time taken in repetitive logging of drillholes is reduced to a minimum. The structural elements of vergence, facing and fold axis orientation have been defined in terms of numerical parameters, all of which are easily measured from drillcore. These numerical parameters may then be used in a computer program to determine the values of the respective structural elements.

An appropriate data set would be as follows:

Drill depth	β	δ_0	δ_{min}	δ_1	α	γ	ε	Younging

The various methods may use these data, in conjunction with a boundary condition such as a specified range of cleavage orientations, to determine the following:

Drill depth	D_0	D_1	F	ϕ	Vergence	Facing

A simple example is shown in Table 4, and the interpreted structure is depicted in Figure 16.

Exström et al., (1975) outline a data system for drillcore named COREMAP, which includes a "Tectonics" file. The data set shown above is readily incorporated into this file and makes a valuable addition to COREMAP. Given the data set and the relevant boundary conditions, a suitable program would determine the variables tabled above, with the exception of the fold axis F. The stereographic techniques involved in determining the fold axis are also amenable to programming, albeit a more complex task.

ACKNOWLEDGEMENTS

The writer wishes to acknowledge fruitful discussion with John Parker, which led to a better understanding of the method of bedding-poles in determining the fold axis, and discussions with John Cottle on computing a subroutine embodying Table 2. I also wish to thank Roger Marjoribanks, Dick Glen, Trish Mooney and John Parker, and the reviewer D.P. Gold, for many constructive comments on the manuscript.

The writer is being supported by an Australian Commonwealth Postgraduate Research Award.

REFERENCES

Addie, G.G., 1962, A simplified stereographic solution of the two drill hole problem: ECON. GEOL., v. 57, p. 1122-1126.

Badgley, P.C., 1959, Structural methods for the exploration geologist: Harper and Brothers, New York, 280 p.

Bucher, W.H., 1943, Dip and strike from three not parallel drill cores lacking key beds: ECON. GEOL., v. 38, p. 648-657.

Exström, T.K., Wirstam, Åke, and Larsson, L.E., 1975, COREMAP - A data system for drill cores and boreholes: ECON. GEOL., v.70, p. 359-368.

Fisher, D.J., 1941, Drillhole problems in the stereographic projection: ECON. GEOL., v. 36, p. 551-560.

Fleuty, M.J., 1964, The description of folds: Geol. Assoc. Proc., v. 75, p. 461-492.

Gilluly, J., 1944, Dip and strike from three not parallel drill cores lacking key beds: Discussion in ECON. GEOL., v. 39, p. 359-363.

Haddock, M.H., 1931, Deep borehole surveys and problems: McGraw-Hill Book Co. Ltd., New York, 296 p.

Hobbs, B.E., Means, W.D., and Williams, P.F, An outline of structural geology: John Wiley & Sons, New York, 571 p.

REFERENCES (cont'd)

Johnson, C.H., 1939, New mathematical and 'stereographic net' solutions to problems of two tilts - with applications to core orientation: Bull. Amer. Assoc. Petroleum Geologists, v. 23, p. 663-685.

Laing, W.P., 1976, Structural and metamorphic geology of a critical area adjacent to the Broken Hill orebody, Willyama Complex, Australia: Unpublished Ph.D. Thesis, University of Adelaide.

McClellan, H., 1948, Core orientation by graphical and mathematical methods: Bull. Amer. Assoc. Petroleum Geologists, v. 32, p. 262-277.

Mead, W.J., 1921, Determination of attitude of concealed bedded formations by diamond drilling: ECON. GEOL., v. 21, p. 37-47.

Means, W.D., 1963, Mesoscopic structures and multiple deformation in the Otago Schist: N.Z. J. Geol. Geophys., v. 6, p. 801-816.

Mertie, J.B., Jr., 1943, Structural determinations from diamond drilling: ECON. GEOL., v. 38, p. 298-312.

Mills, J.W., 1963, A simplified stereographic projection solution of the two drillhole problem: Discussion in EC ON. GEOL., v. 58, p. 618-621.

Phillips, F.C., 1971, The use of stereographic projection in structural geology: Edward Arnold Ltd., London, 86 p.

Ragan, D.M., 1973, Structural geology; an introduction to geometrical techniques: John Wiley & Sons, New York, 2nd Ed., 208 p.

Ramsay, J.G., 1967, Folding and fracturing of rocks: McGraw-Hill Book Co., New York, 568 p.

Shackleton, R.M., 1958, Downward-facing structures of the Highland Border: Q. J. geol. Soc. London, v. 113, p. 361-388.

Stein, H.A., 1941, A trigonometric solution of the two-drillhole problem: ECON. GEOL., v. 36, p. 84-94.

REFERENCES (cont'd)

Wilson, G., 1961, The tectonic significance of small scale structures and their importance to the geologist in the field: Ann. Soc. Geol. Belg., v. 84, p. 423-548.

Wisser, E., 1932, An aid in the interpretation of diamond drill cores: ECON. GEOL., v. 27, p. 437-449.

Zimmer, P.W., 1963, Orientation of small diameter drill core: ECON. GEOL., v. 58, p. 1313-1325.

TABLE 1: Parametral values for the situation shown in Figure 14, determined from $(\beta,\delta_0,\delta_1)$ using equations (2), (3) and (4) in text.

β	δ_0	δ_1	δ_0'	δ_1'	D_0	D_1	D_0'	D_1'	$\phi = \lvert D_0 - D_1 \rvert$
40^o	100^o	150^o	80^o	30^o	50^o	100^o	30^o	160^o	50^o (130^o)

TABLE 2: Determination of vergence and stratigraphic facing in drillcore, using the parameters β, D_0 and D_1 and sedimentary younging data. The relationship between drillhole, bedding and cleavage is described in columns 1 and 2, and translated into the expressions x and y in columns 3 and 4. These completely define the vergence in column 5. Column 6 provides the alternative possible youngings (U = uphole, D = downhole) for each vergence situation. The resultant stratigraphic facing is shown in column 7. East is defined as the direction from which β is measured (see Figure 14). Note the cases in which a sequence which youngs uphole is actually inverted (2, 8, 10, 12, 15).

	1	2	3	4	5	6	7
Case	Relationship of cleavage to drillhole	Relationship of cleavage to bedding	$x = \beta - D_0$	$y = D_0 - D_1$	Vergence - where is antiform?	Younging	Facing
1	$\beta < D_1$	$D_0 < D_1$	$x > 0^o$	$y < -90^o$	Downhole	U D	Upwards Inverted
2				$-90^o < y < 0^o$	Uphole	U D	Inverted Upwards
3			$x = 0^o$	$y < -90^o$	Downhole	East West	Upwards Inverted
4				$-90^o < y < 0^o$	Uphole	East West	Upwards Inverted
5			$x < 0^o$	$y < -90^o$	Downhole	U D	Upwards Inverted
6				$-90^o < y < 0^o$	Uphole	U D	Inverted Upwards
7		$D_0 < D_1$	$x < 0^o$	$0^o < y < 90^o$	Downhole	U D	Upwards Inverted
8				$y > 90^o$	Uphole	U D	Inverted Upwards
9	$\beta = D_1$	1. Cannot differentiate between $x > 0$ and $x < 0$. 2. Younging and facing in this category are equivalent.					
10	$\beta > D_1$	$D_0 < D_1$	$x > 0^o$	$y < -90^o$	Uphole	U D	Inverted Upwards
11				$-90^o < y < 0^o$	Downhole	U D	Upwards Inverted
12		$D_0 > D_1$	$x > 0^o$	$0^o < y < 90^o$	Uphole	U D	Inverted Upwards
13			$x = 0^o$	$0^o > y > 90^o$	Uphole	East West	Inverted Upwards
14				$y > 90^o$	Downhole	East West	Inverted Upwards
15			$x < 0^o$	$0^o < y < 90^o$	Uphole	U D	Inverted Upwards
16				$y > 90^o$	Downhole	U D	Upwards Inverted

Special cases

1. $y = 0^o$ Cleavage parallel to bedding. Vergence not applicable.
2. $y = \pm 90^o$ Fold hinge. Vergence is neutral.

TABLE 3: Features of the various methods discussed in this paper which influence their applicability to drillcore analysis.

OBJECTIVE:	DETERMINATION OF FOLD AXIS		DETERMINATION OF VERGENCE AND FACING		
METHOD:	Method of bedding-poles	Bedding/cleavage method	Angle between bedding and cleavage	Vergence	Facing
ASSUMPTIONS:	1. Cylindrical folding 2. Non-linear drillhole	1. Fold axis coincides with bedding/cleavage intersection. 2. Orientation or at least strike of cleavage is known.		1. Cylindrical folding 2. Drillhole subperpendicular to fold axis and to strike of axial plane.	1. Vergence is known
EFFECTIVENESS DEPENDENT ON:	1. Fold style 2. Scale of folding	1. Presence of cleavage 2. Presence of measurable bedding/cleavage intersection.	1. Presence of cleavage	1. Fold axes being sub-horizontal or 1a. Hole drilled perpendicular to plunging fold axis. 2. Known range of axial plane orientation.	1. Presence of sedimentary criteria.
EFFECTIVENESS INCREASED BY:	1. Drilling subperpendicular to fold axis. 2. Gaining maximum curvature of drillhole.	1. Measuring the intersection lineation on the cleavage surface rather than on the bedding surface.	1. Taking a large number of measurements.		
PARTICULAR ADVANTAGES:	1. May be used in rocks lacking cleavage.	1. Does not depend on fold cylindricity. 2. May be used to test fold cylindricity. 3. Only requires a single segment of drillcore. 4. May be applied in a linear drillhole. 5. May be used to obtain information on bedding orientation.	1. No assumptions necessary.	1. The necessary condition (drillhole subperpendicular to fold axis) is readily ascertained from drillcore. 2. If rocks lack cleavage the method may be applied to parasitic folds.	

TABLE 4: Example of a set of structural results determined at a number of points down the drillhole of Figure 16, by the methods discussed in this paper.

Boundary condition from surface mapping: Cleavage dips uniformly to west at moderately steep angle; say $100^{o} \leqslant D_1 \leqslant 140^{o}$.

Drill depth (m)	D_0	D_1	F	ϕ	Vergence - where is antiform?	Younging	Facing
50	$110^{o}(70^{o}W)$	$115^{o}(65^{o}W)$	$10^{o} \rightarrow 360^{o}$	5^{o}	Uphole	D	Upward
100	$110^{o}(70^{o}W)$	$115^{o}(65^{o}W)$	$5^{o} \rightarrow 350^{o}$	5^{o}	"	D	"
150	$100^{o}(80^{o}W)$	$120^{o}(60^{o}W)$	$10^{o} \rightarrow 350^{o}$	20^{o}	"	D	"
200	$170^{o}(10^{o}W)$	$120^{o}(60^{o}W)$	$10^{o} \rightarrow 355^{o}$	50^{o}	Downhole	U	"
250	$130^{o}(50^{o}W)$	$125^{o}(55^{o}W)$	$5^{o} \rightarrow 180^{o}$	5^{o}	"	U	"
300	$130^{o}(50^{o}W)$	$125^{o}(55^{o}W)$	$15^{o} \rightarrow 360^{o}$	5^{o}	"	U	"
350	$130^{o}(50^{o}W)$	$125^{o}(55^{o}W)$	$20^{o} \rightarrow 355^{o}$	5^{o}	"	U	"
400	$150^{o}(30^{o}W)$	$125^{o}(55^{o}W)$	$0^{o} \rightarrow 360^{o}$	25^{o}	"	U	"
450	$30^{o}(30^{o}E)$	$120^{o}(60^{o}W)$	$0^{o} \rightarrow 010^{o}$	90^{o}	Here	?	
500	$80^{o}(80^{o}E)$	$120^{o}(60^{o}W)$	$5^{o} \rightarrow 010^{o}$	40^{o}	Uphole	D	"
550	90^{o}(vert)	$115^{o}(65^{o}W)$	$10^{o} \rightarrow 180^{o}$	25^{o}	"	D	"
600	$100^{o}(80^{o}W)$	$115^{o}(65^{o}W)$	$10^{o} \rightarrow 180^{o}$	15^{o}	"	D	"
650	$110^{o}(70^{o}W)$	$115^{o}(65^{o}W)$	$10^{o} \rightarrow 180^{o}$	5^{o}	"	D	"
700	$110^{o}(70^{o}W)$	$115^{o}(65^{o}W)$	$5^{o} \rightarrow 185^{o}$	5^{o}	"	D	"
750	$100^{o}(80^{o}W)$	$110^{o}(70^{o}W)$	$0^{o} \rightarrow 360^{o}$	10^{o}	"	D	"
800	90^{o}(vert)	$110^{o}(70^{o}W)$	$0^{o} \rightarrow 360^{o}$	20^{o}	"	D	"

LIST OF FIGURE CAPTIONS

FIG. 1. Four fold profiles showing styles most commonly found in nature. The parameters expressing fold style are the interlimb angle (L) and a ratio reflecting the proportion of limb area to hinge area (R). The equal area projections illustrate the pattern of poles to bedding for each fold.

FIG. 2. Stereographic diagram representing a single drillhole of orientation DH intersecting a fold with axis F. Points A,B,C....are the poles to bedding around the fold, lying in the bedding-pole girdle (BPG). For unoriented drillcore their loci are the small circles, of angular radius δ_A, δ_B, δ_C.... For explanation of δ_{min} see text.

FIG. 3. Illustrating the intersection of a curved drillhole (curved in a plane) and a cylindrical fold of full girdle type.

A. Relationship of folded surface to the bedding-poles and to the plane of the drillhole.

B. As above but with fold abstracted into its components, viz. the fold axis normal to the plane defined by the fan of bedding-poles (the bedding-pole girdle BPG).

FIG. 4. Diagram illustrating the method of determining the fold axis by bedding-poles, as applied to the situation represented in Figure 3. Small circles of angular radii δ_{min} are drawn corresponding to drillhole orientations 1 to 7 and 7a. The disposition of the δ_{7a} small circle indicates that the dashed bedding-pole girdle (BPG) and fold axis (F) are spurious (see text).

FIG. 5. A. Relationship of the angle δ_0 to the bedding angle observed in drillcore; $\delta_0 = (90^o$ - bedding angle).

B. Diagram illustrating the concept of a particular δ_{min} for a segment of drillcore aa' passing through folded bedding.

FIG. 6. Diagram showing the four apparent bedding-pole girdles obtained from two non-intersecting δ_{min} small circles. R = real girdle, A = apparent girdle.

A. The pattern obtained when the drillhole "passes through" the (real) bedding-pole girdle (at 5).

B. The pattern obtained when the drillhole does not "pass through" the (real) bedding-pole girdle.

FIG. 7. Relationship between drillpath XZ and the bedding-pole girdle BPG if the folding is of partial girdle type. For explanation see text.

FIG. 8. Relationship between bedding (S_0) and the bedding/cleavage intersection lineation (I) in drillcore. I and I' represent alternative orientations of the intersection lineation for a given angle γ.

A. Parameters used in the method which employs bedding/cleavage intersection on the bedding surface.

B. Stereographic representation of the loci of I and P_0 for unoriented drillcore.

FIG. 9. Relationship between cleavage (S_1) and the bedding/cleavage intersection lineation (I) in drillcore. E is the minor axis of the cleavage ellipse in the drillcore.

A. Parameters used in the method which employs bedding/cleavage intersection on the cleavage surface.

B. Stereographic representation of the method.

C. Determination of cleavage orientation using the small circle locus of P_1 and the known strike of S_1.

FIG.10. Appearance of drillcore when the drillhole is perpendicular to the fold axis.

FIG. 11. Profile of a fold showing relationship between bedding and the axial plane (AP) in terms of three different parameters. Parameter "a" is the angle between bedding and cleavage, "b" is the sense of the bedding/cleavage relationship, and "c" is the sense of rotation of bedding in parasitic folds.

FIG. 12. Segment of core showing parameters used to determine ϕ, the angle between bedding (S_0) and cleavage (S_1), and α, the angle between bedding and cleavage in a plane perpendicular to the core axis.

FIG. 13. Determination of vergence by inspection of drillcore. Drillcore is subperpendicular to fold axis. Arrows indicate direction of anti-formal closure.

A. Drillcore in one permitted orientation, with cleavage parallel to the line of sight.
B. Drillcore in the other permitted orientation, i.e. "A" rotated through 180^{o}.

FIG. 14. Illustrating the conventions adopted in measuring (β,δ_0,δ_1). Drillcore is subperpendicular to fold axis.

A. Drillcore in one permitted orientation, with cleavage (S_1) parallel to the line of sight.
B. Drillcore in the other permitted orientation, i.e. "A" rotated through 180^{o}.

FIG. 15. Illustrating two structurally distinct situations which nevertheless yield identical core angles (left hand column) in normal drill logging practice. The conventions outlined in the text (giving the results in the right hand column) are designed to remove this sort of ambiguity.

FIG. 16. Drillhole intersecting folded strata, with the subsurface structure synthesized from data at individual points down the drillhole (see Table 4). Arrows represent younging directions.

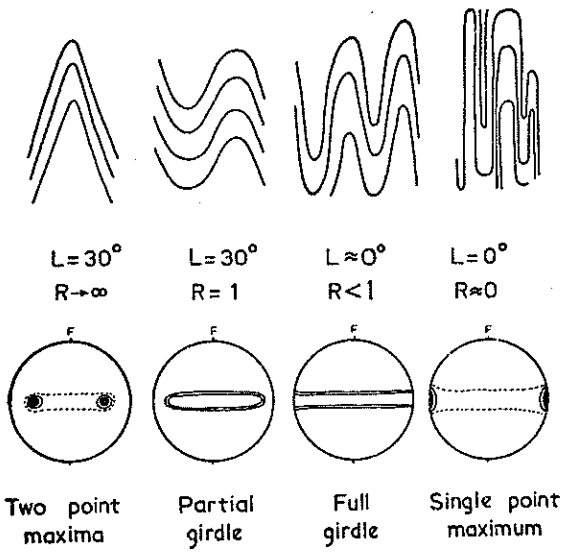

FIG. 1

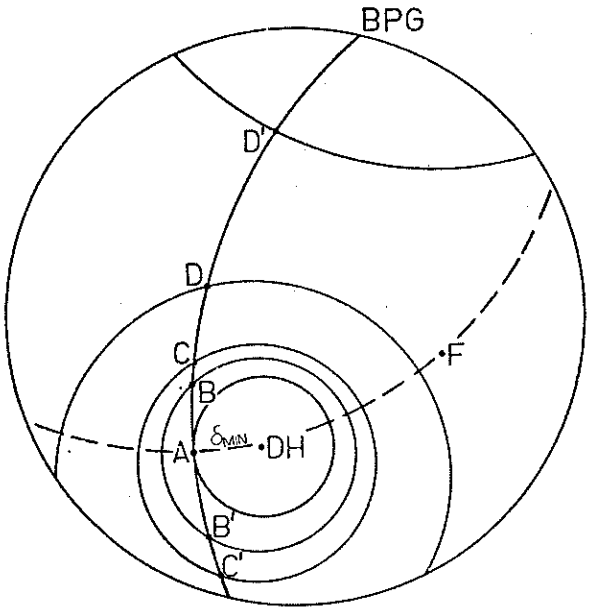

FIG. 2

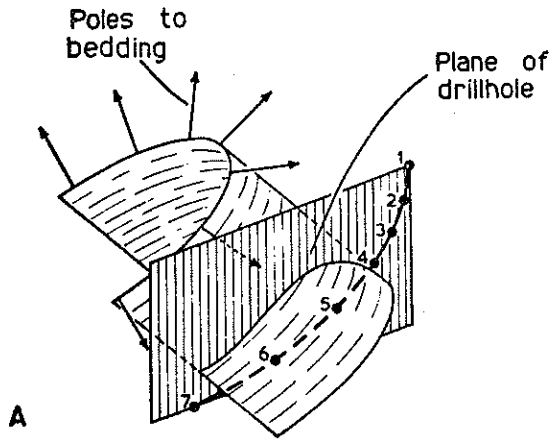

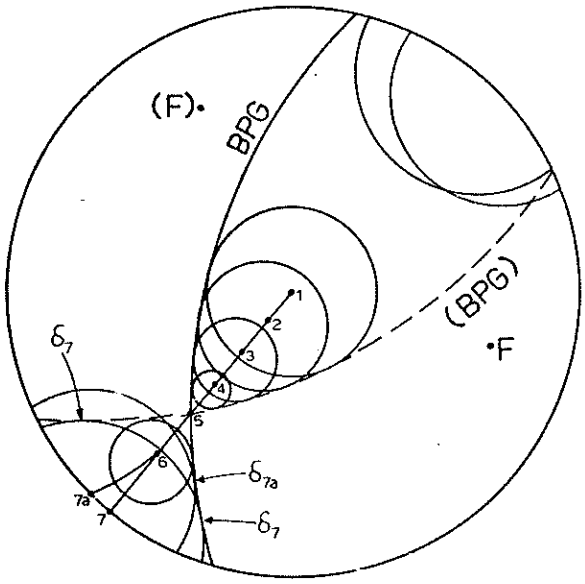

FIG. 4

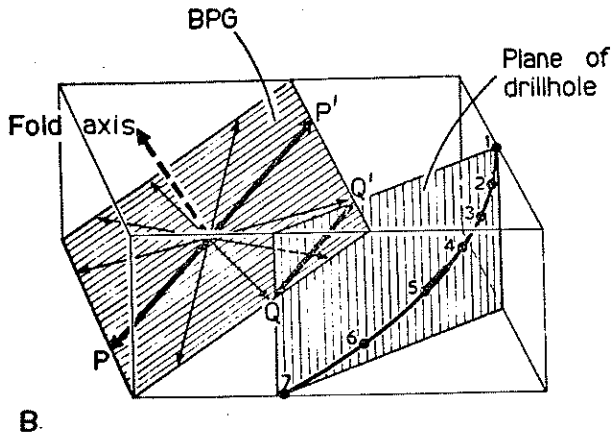

FIG. 3

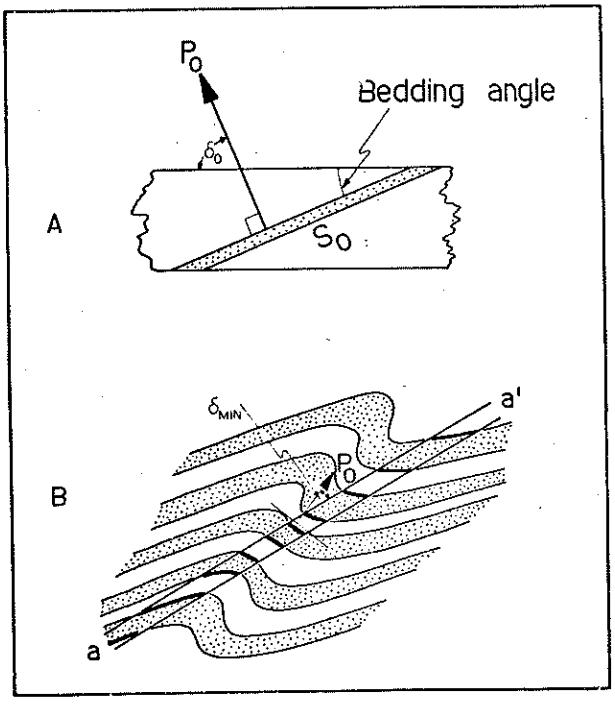

FIG. 5

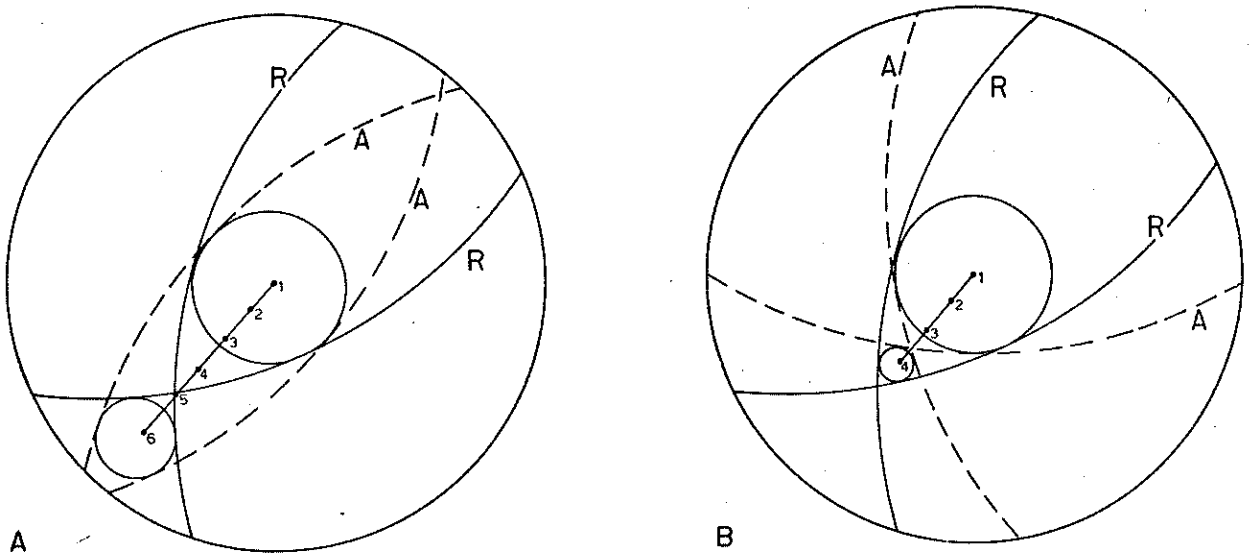

FIG. 6

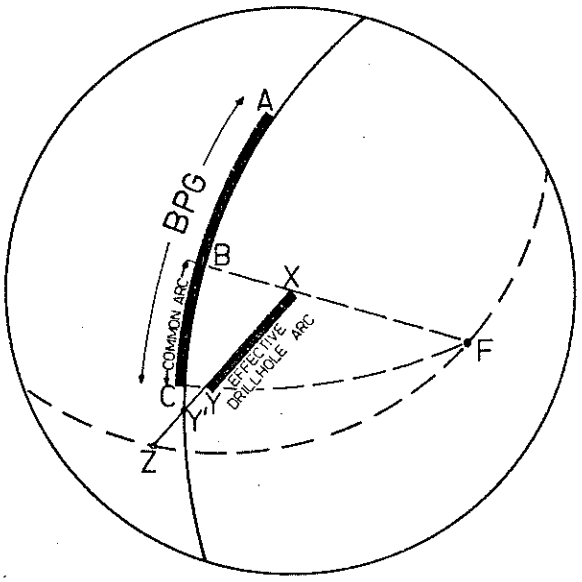

FIG. 7

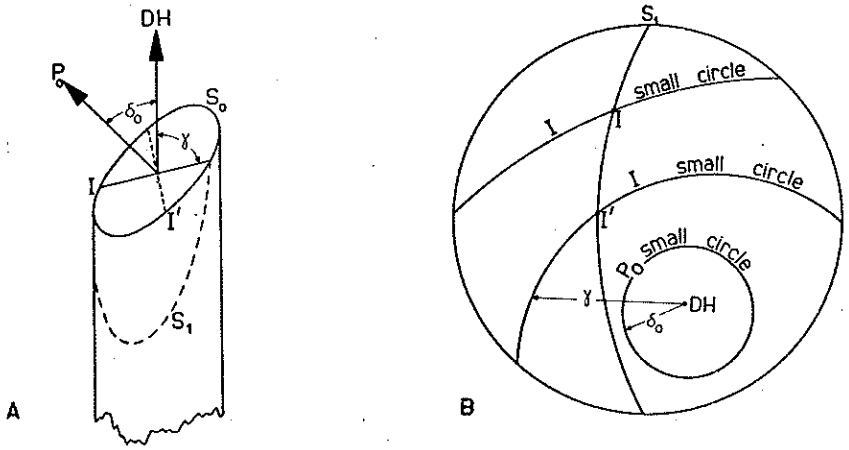

FIG. 8

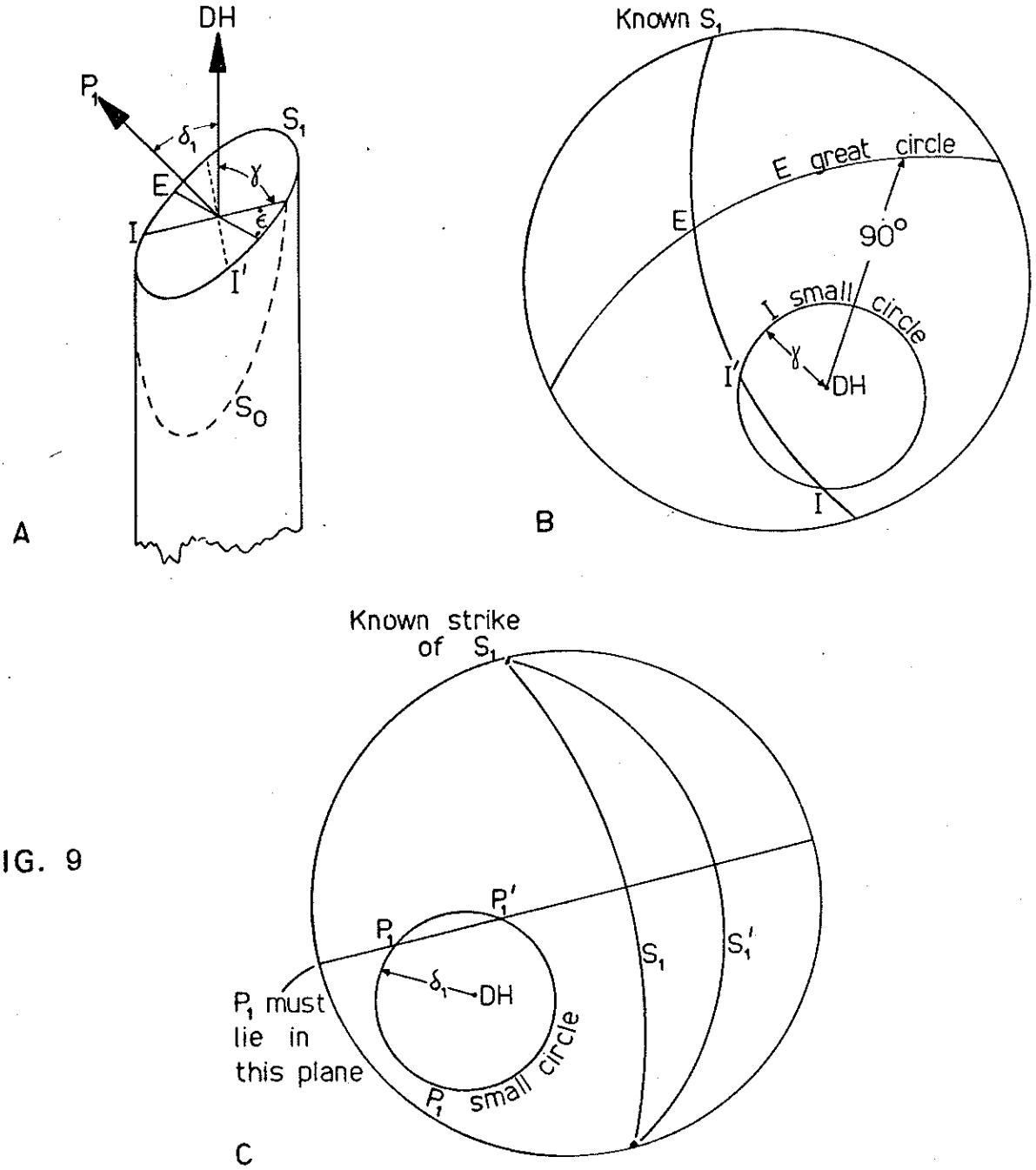

FIG. 9

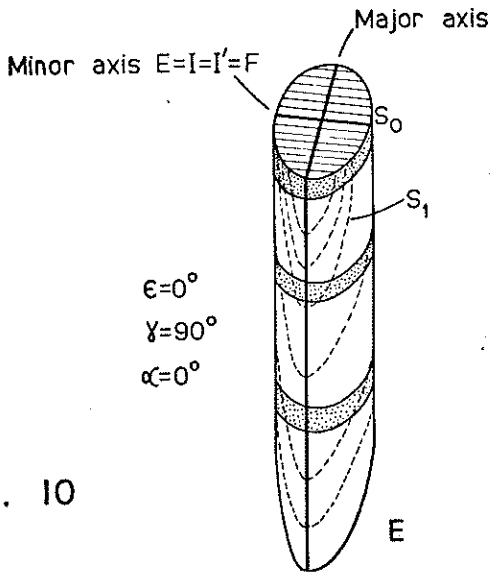

FIG. 10

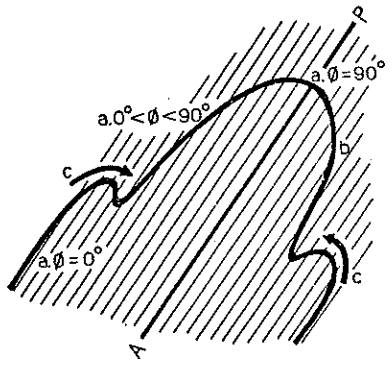

FIG. 11

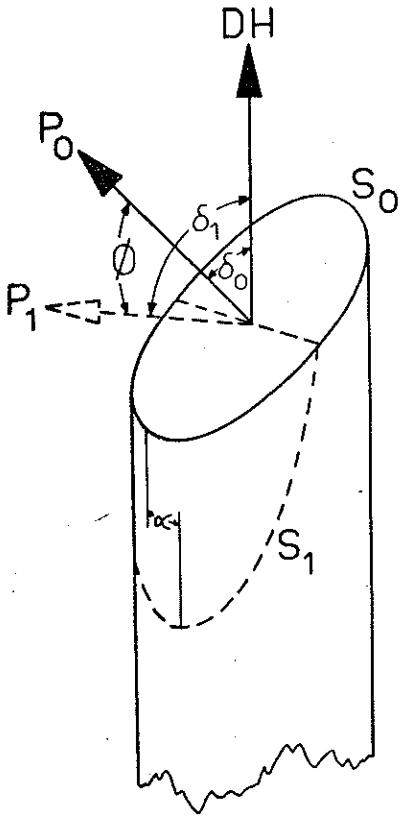

FIG. 12

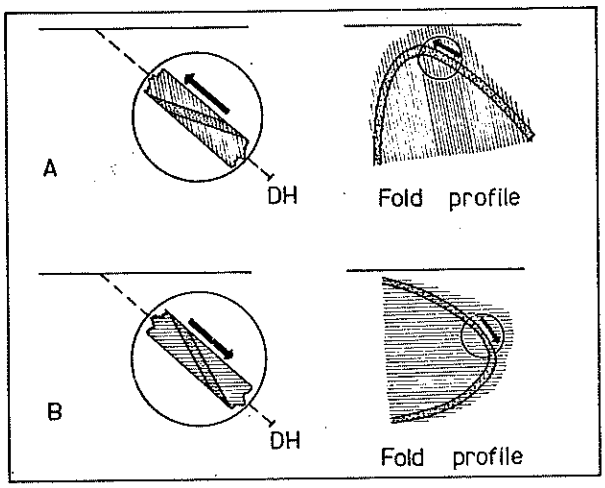

FIG. 13

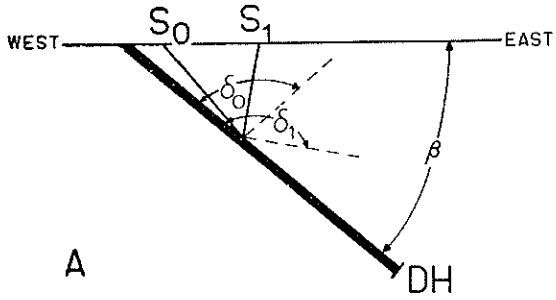

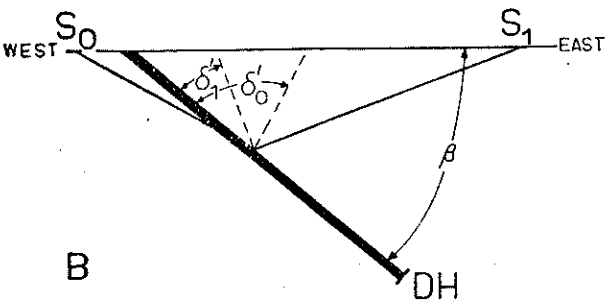

FIG. 14

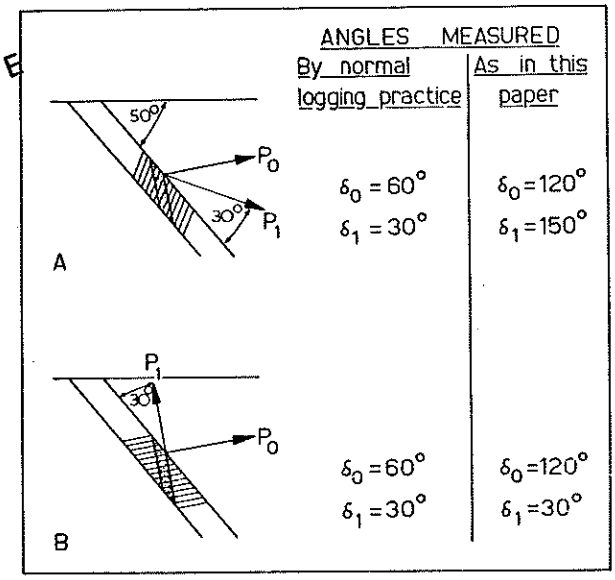

FIG. 15

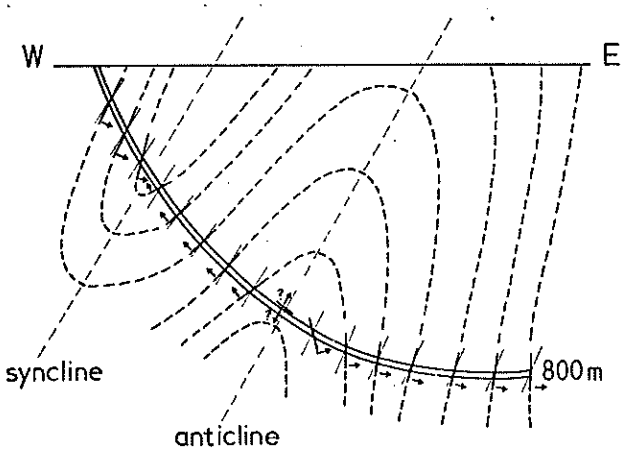

FIG. 16

APPENDIX C

F_1 FOLDS IN THE PARNELL TRACK AREA[1]

This area was mapped in detail at the beginning of the study, being at that time the best known example of superimposition of the "regional" schistosity on an earlier schistosity in an area of layered sillimanite schist. One small fold had been observed with the earlier schistosity parallel to its axial plane (Hoff, 1971).

Rutland and Etheridge (1973, pp.262, 270) discussed the varying expressions of the superimposed relationship in this and nearby areas, referring to the schistosities as S_1 and S_2 and noting that a sillimanite lineation (L_1) observed in S_1 is folded around F_2 folds and that S_2 in places contains a new sillimanite lineation (L_2).

Subsequent work by the writer in the Northern Leases and by R.W. Marjoribanks on a regional scale (see Marjoribanks et al., 1977) suggests that relations between schistosities in the Parnell Track area are more complex than originally inferred during the detailed mapping. A schistosity equivalent to S_3 in the Northern Leases is probably present, and further microfabric study is required to distinguish S_2 and S_3. A preliminary model of the overall geology is presented below, followed by a brief account of the established relations between D_1 and D_2 structures, with particular emphasis on the geometry of F_1 folds.

The area is bounded on all sides by alluvium, except for a narrow join to an area of poor outcrop and negligible structural information on the NW margin. Similar layered sillimanite schist occurs about 1 km to the W and SW, in the Southern Cross mine area (see inset, Map 5).

Layering is very well developed throughout the area, and is defined by alternating pelitic and psammitic bands which can commonly be traced for 100 m or more without significant change in thickness or character (Map 5). The bands range in thickness from 2-3 cm to over 1 m, averaging 5-15 cm. Many are strikingly reverse-graded, from medium-grained

---

[1] See pp.3,16 of thesis for location and basis of mapping.

psammitic material to coarse-grained pelitic material, similar to the graded beds observed in the Northern Leases (Section 2.2; see Figs. 2-12 and C-6). The bedded sedimentary origin of the grading and of the layering is not in doubt.

The area is divided naturally into two subareas, separated by a N-S trending retrograde schist zone (Fig. C-1). The western subarea contains a large E-W trending F_1 fold in layering, whose hinge-plane trace has been mapped over a distance (unfolded) of 300 m. The fold is tight, though not isoclinal, with a steeply dipping hinge plane. The hinge is visible in the western part of the subarea, where it has a steep plunge. However, over the larger part of the western subarea the geometry of the large F_1 fold is complicated by three factors:

(a) mesoscopic F_1 folds and the L_1 mineral lineation generally plunge obliquely to the apparent plunge of the large fold (see below);

(b) the S_1 schistosity in some areas, particularly around 13W 6N to 14W 7N, is relatively flatlying, although it appears to be congruent in sense to the fold structure in these areas;

(c) large-scale refolding by F_2 folds has distorted the shape of the fold in the eastern part of the subarea.

The inferred geometry of the macroscopic F_1 fold, taking into account these factors, is depicted in Fig. C-2. Consistent younging directions from reverse graded beds at numerous locations around the fold (see Map 5) indicate an easterly-facing fold, which is downward-facing where the fold axis is non-vertical and west-plunging (Fig. C-2).

Mesoscopic F_1 parasitic folds are congruent in sense to the major fold, but the flat, two-dimensional nature of much of the outcrop prohibits observation of their plunge. Where observed it varies from shallowly westward to almost vertical (Fig. C-3). This is a similar orientation to the plunge of

the L_1 lineation, but F_1 folds are rarely observed in association with the lineation and their parallel relationship is assumed. The style of F_1 small folds reflects that of the large fold, being tight to isoclinal but with rounded, only moderately thickened hinge zones (Fig. C-4,5). S_1 is more strongly developed in the more pelitic bands.

In the western subarea the elements comprising the F_1 fold - bedding, S_1 and L_1 - are folded openly about N-S trending axial planes which dip steeply to the W, vertically, or steeply to the E. On a micro-scale the S_1 schistosity is crenulated and locally overprinted by new grains of sillimanite and biotite in the S_2 orientation (Figs. C-4, 5, 6). The deformation of the L_1 lineation is complex, and involves flattening of fibrolite pods, with a tendency toward elongation in a gently-SW-plunging direction which defines a weak new lineation (L_2). The morphology and inferred mechanisms of overprinting are very similar to the development of S_2 in the Northern Leases, except for the growth of apparently post- D_2 coarse muscovite (see Section 4.2.1). On a mesoscopic scale the F_2 folds are open to tight, and generally steeply-plunging. Some refold a visible L_1 sillimanite lineation on a small circle pattern.

Several generations of acid pegmatite development are inferred in the western subarea. An early, pre- F_1 generation of pegmatite occurred parallel to bedding. A distinct preference for psammitic layers, and remarkable persistence of thin veins within the confines of a single layer (for example one vein with a thickness of 15-20 mm can be traced for 90 m), suggests that these pegmatites formed in situ by partial melting. A later generation of larger pegmatites crosscuts F_2 folds in a NNE direction and is probably related to development of the retrograde schist zone. These later pegmatites show extensive biotite $\pm$ tourmaline $\pm$ sillimanite aggregations on their margins.

The eastern subarea comprises a uniform sequence of W-dipping, E-younging (i.e. overturned) beds whose strike is N-S overall but varies

openly about two sets of folds. An early set of dextral parasitic folds in bedding is reclined, plunging moderately to the SW with a moderately-SW-dipping sillimanite-bearing axial-plane schistosity (Fig. C-3). On the eastern margin of the subarea, separated from the main part by a retrograde schist zone, a horizontal schistosity probably correlates with the moderately-dipping early schistosity (Fig. C-2). A later set of open sinistral parasitic folds is of variable, moderate to steep plunge about an axial plane striking N-S and dipping steeply W. The axial-plane surface is defined variably by the axial plane of crenulations, and of chevron or "herringbone" kinks (Fig. C-7) in the early schistosity or by a possible, though not positively identified, new schistosity in some layers. In some examples of chevron kinks, where adjacent layers contain alternate limbs of folds, it is reasonably inferred that the bedding has acted as a passive axial plane during the folding of the schistosity. This mechanism has also been inferred by Glen (1977) in D_3 deformation in the Mt. Franks area, NW of the Parnell Track area.

During field mapping no fabric earlier than the two detailed above was detected, and the structures in the eastern subarea were assigned respectively to the D_1 and D_2 events. However subsequent mapping in the surrounding region by R.W. Marjoribanks indicates that the early schistosity may correlate with S_2 in the mine area, and hence the later schistosity may be S_3. A recent field check by the writer failed to show evidence of any fabric, earlier than that mapped previously as S_1; hence the status of the early structures in the eastern subarea remains unresolved. However, in view of the fabric similarities with Glen's D_3 and the similar relative orientations of D_3 and D_2 in the Parnell Track area and the Northern Leases (S_3 being more upright and trending more east of north), there is little doubt that the later structures in the eastern subarea correlate with D_3 on a regional basis.

One of several matters which thus remains to be resolved is the relationship between D_3 structures in the eastern subarea and D_2 structures

in the western subarea: the almost identical orientation suggests some correlation. It is possible that the complex overlapping relationship postulated between D_2 and D_3 in the Northern Leases also applied in the Parnell Track area, with S_3 being moderately rich in sillimanite.

FIGURE C-1: Simplified map of the Parnell Track area, from the detailed Map 5 (see back pocket of thesis). The map shows bedding trends superimposed by trends of the later schistosity in each subarea. The trend of the early schistosity has been omitted for clarity; in the western subarea it trends approximately E-W and is congruent to the large F_1 fold, and in the eastern subarea it trends NW and is congruent to the dextral folds seen on the map.

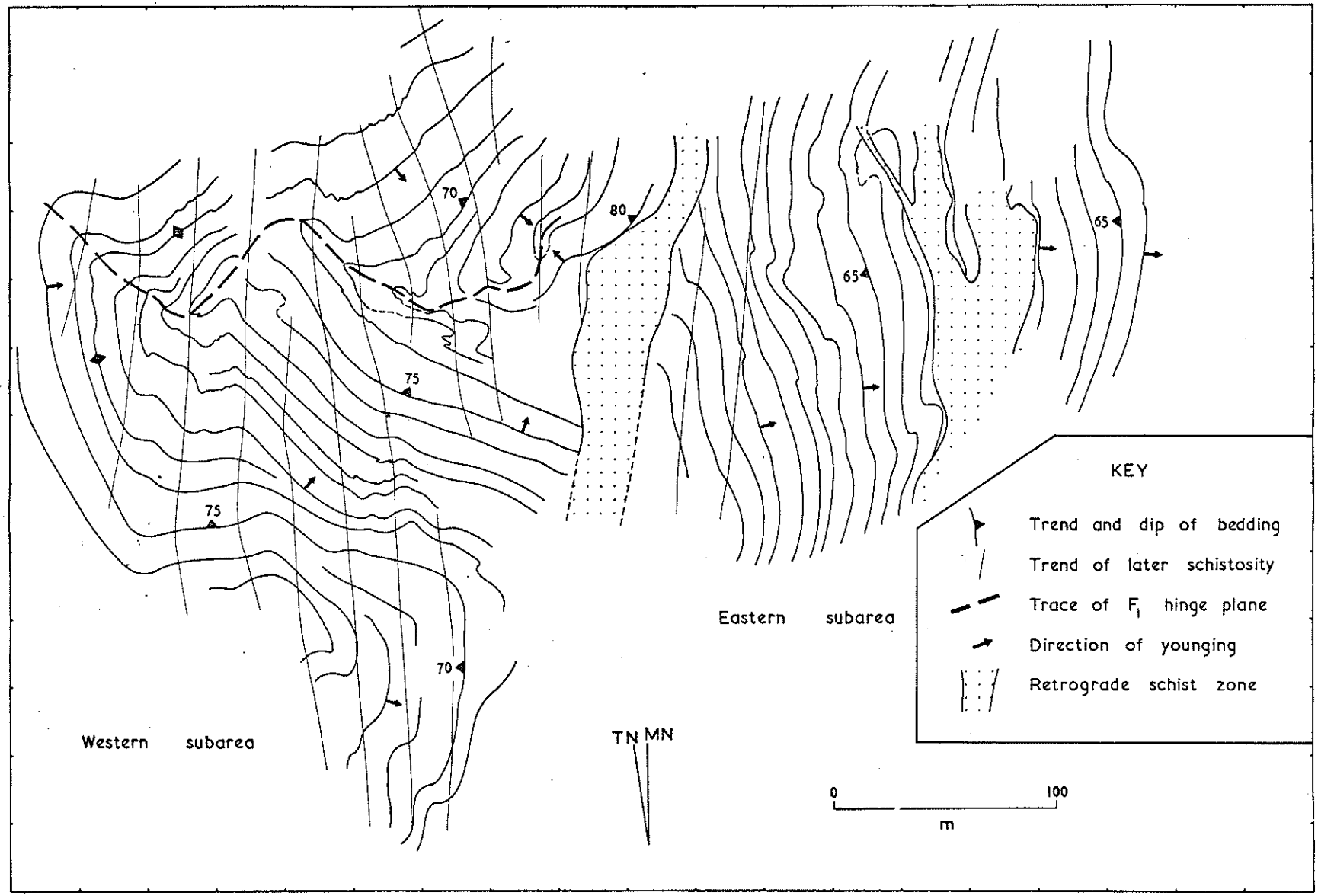
70
80
65
65
75
75
70
Western subarea
Eastern subarea
TN MN
KEY
Trend and dip of bedding
Trend of later schistosity
Trace of F_1 hinge plane
Direction of younging
Retrograde schist zone
0
100
m

FIGURE C-2: Simplified block diagram of the Parnell Track area. Bedding is heavily outlined, schistosity surfaces are stippled, and the two major retrograde schist zones are faintly stippled. The lineation L_1 which appears to be parallel to F_1 fold axes is shown on the bedding surface.

In the western subarea D_1 and D_2 nomenclature is used. In the eastern subarea the early structures are named D_{1-2} and the later structures are named D_{2-3}.

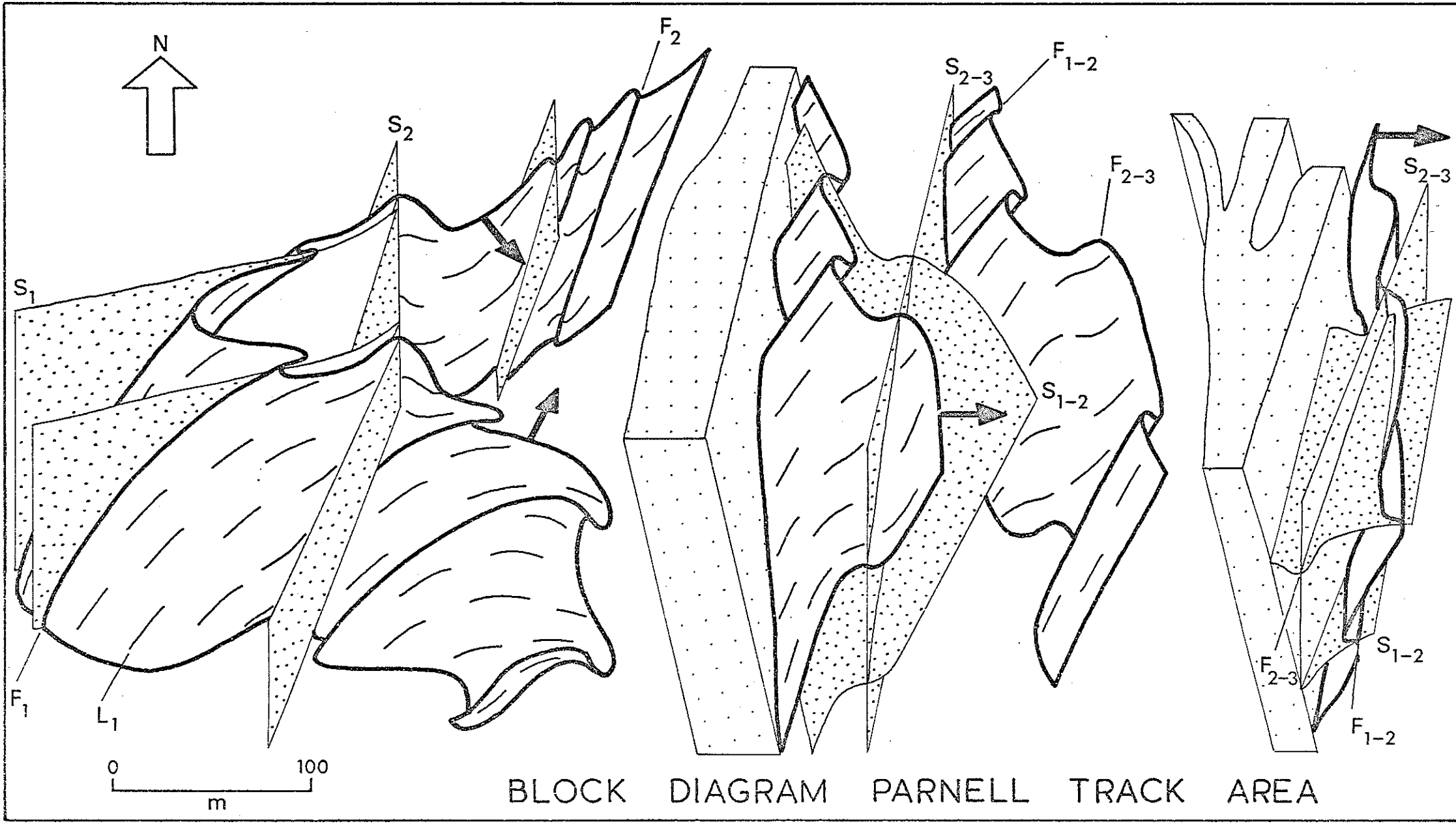

BLOCK DIAGRAM PARNELL TRACK AREA

FIGURE C-3: Orientation data for the Parnell Track area.

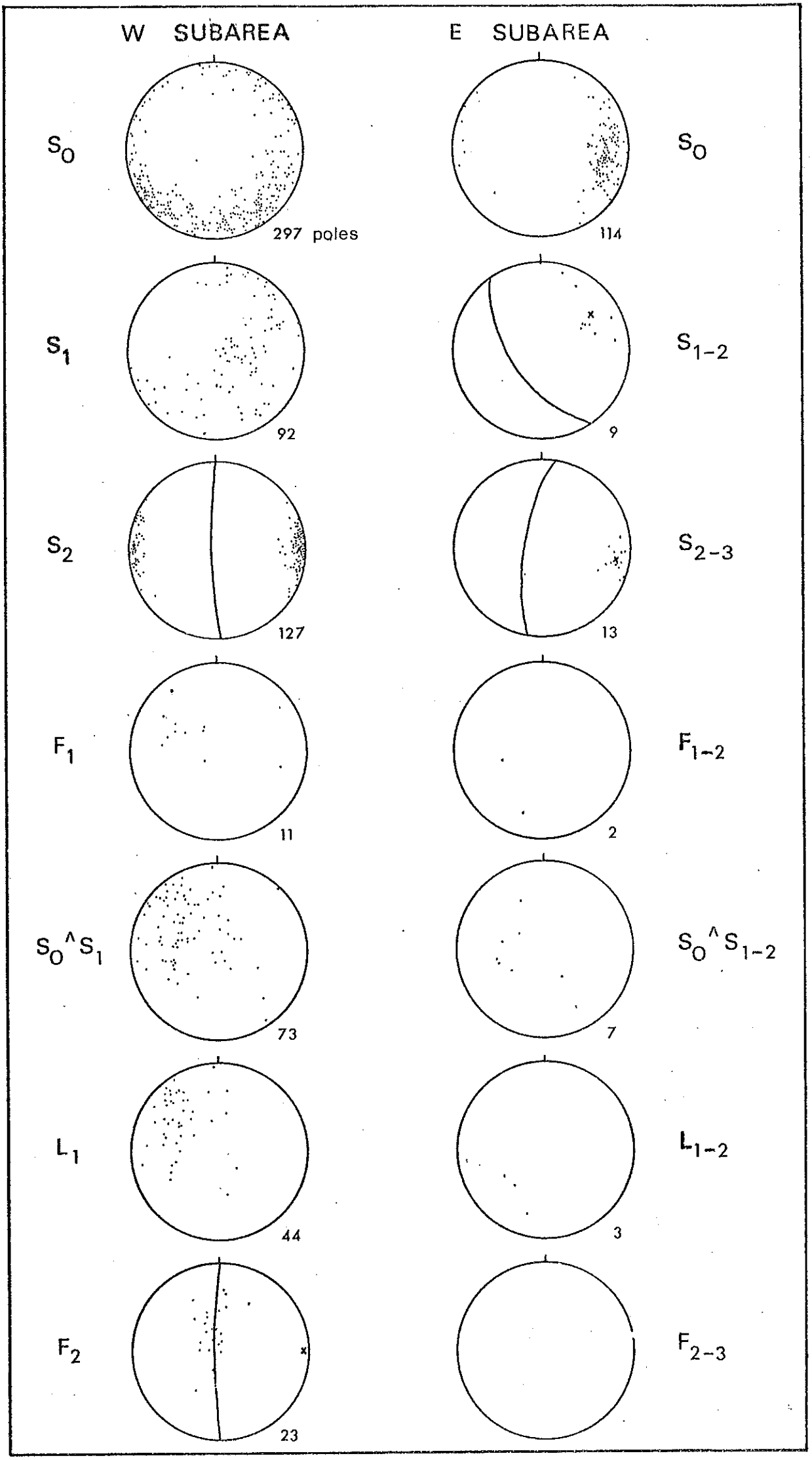
W SUBAREA
E SUBAREA
S_0
297 poles
114
S_0
S_1
92
9
S_{1-2}
S_2
127
13
S_{2-3}
F_1
11
2
F_{1-2}
$S_0 \wedge S_1$
73
7
$S_0 \wedge S_{1-2}$
L_1
44
3
L_{1-2}
F_2
23
F_{2-3}

FIGURE C-4 (left) Profile of F_1 fold with S_1 schistosity preserved in the psammitic core (but barely visible in the photograph). An irregular S_2 crenulation schistosity is developed in the sillimanite-rich pelitic layer and trends E-W across the photograph. Locality 153084.

FIGURE C-5 (right) Detail of the hinge of an F_1 fold, with S_1 in the psammite, and partly in the pelite, layer trending parallel to the rule, and a crenulation schistosity S_2 trending N-S in the pelite layer. The orientation of S_2 is variable, partly because S_2 consists dominantly of variably rotated, flattened plates of S_1 sillimanite (fibrolite).
Locality 126063.

FIGURE C-6: Strong S_1 schistosity oblique to bedding, crenulated about a steeply-dipping S_{2-3} axial plane in which rare new sillimanite is observed (eg. circled). The top of a strongly graded bed is marked by an abundance of sillimanite (white) and a thin selvedge of biotite (black). Bedding is E-W in photograph and S_1 is parallel to the rule.
Locality 127065.

FIGURE C-7: Herringbone structure, with the early schistosity S_{1-2} parallel to the long edge of the matchbox with an almost perpendicular rotated schistosity in the pelite.
Locality 066080.

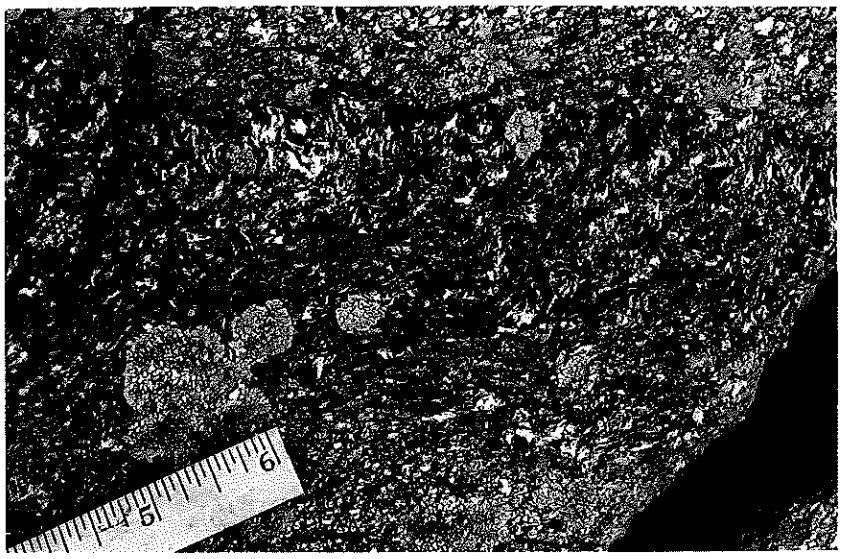
5
6

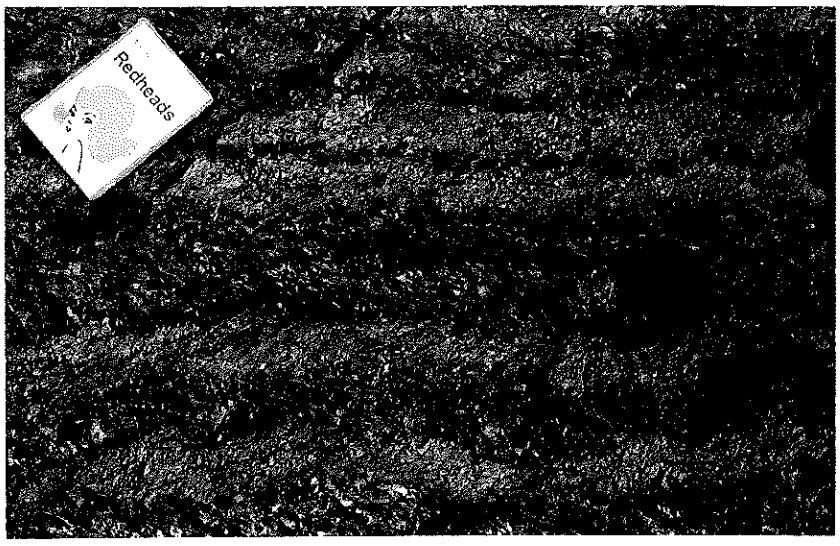
Redheads

THE AUSTRALASIAN INSTITUTE OF MINING AND METALLURGY

INCORPORATED BY ROYAL CHARTER 1955

THE SIGNIFICANCE OF SEDIMENTARY STRUCTURES IN THE WILLYAMA COMPLEX, NEW SOUTH WALES

By

R. A. GLEN and W. P. LAING

Reprinted from the Aus.I.M. & M. *Proceedings* No. 256, December 1975

Published by

The Australasian Institute of Mining & Metallurgy

Clunies Ross House, 191 Royal Parade, Parkville, Vic. 3052, Australia

Appendix D

APPENDIX E

NEW OBSERVATIONS ON THE STRUCTURE OF THE BROKEN HILL MINE AREA

by

R.W. Marjoribanks and W.P. Laing

(Manuscript of a short paper published in the Annual Newsletter of the Specialist Group in Tectonics and Structural Geology, of the Geological Society of Australia; December 1975.

RWM senior author).

NEW OBSERVATIONS ON THE STRUCTURE OF THE BROKEN HILL MINE AREA

Possibly more geological research has been done in the Broken Hill area than in any other mining province. This work has produced many notable controversies, but over the years a consensus has emerged about many aspects of the geology of the mines. For example, most now accept that the sulphide orebodies are spatially related to distinctive and unusual rock types whose origin may be connected with the origin of the ore, that the orebodies are at least grossly conformable with any definable lithological units within the enclosing wall rocks, and that they have undergone the same metamorphism as the wall rock metasediments. However, there has been little consensus about the structure of the mine area and successive attempts at a structural synthesis using marker units or detailed knowledge of orebody shapes (Andrews, 1922; Gustafson et al., 1950; Lewis et al., 1965) have had to be modified or rejected as mine exploration and development proceeded. Correlation of marker units has thus proved inadequate to the task of disentangling the complex geometry of an area shown by detailed observation of minor structures (Hobbs, 1966) to have suffered from the superimposition of more than one deformational event.

There is an abundance of minor structures in the Broken Hill area whose significance has hitherto remained unremarked, and which are in conflict with the existing structural models. These structures are: sedimentary facing (graded bedding identical to that described from elsewhere in the Willyama Complex by Glen and Laing, 1975), minor fold vergences and bedding-cleavage relationships. By careful mapping of these structures and by utilizing all possible information, the authors have been able to build up a model of the structure of the Broken Hill area consistent with all the data. Furthermore, the deformational events can be traced with consistent style and orientation over large areas of the

Willyama Complex. The results spring from studies supported by the Broken Hill Mine Managers Association and whose earlier results have been reported by Rutland (1973) and Rutland and Etheridge (1975).

Three major deformational and metamorphic events are identified, with the major fold structures of the mine area belonging to the second (F_2) and third (F_3) events. The earliest identifiable event (F_1) produced the dominant high-grade metamorphism of the Willyama, and was probably associated with large-scale isoclinal folding. Sedimentary facing indicates that the entire Broken Hill Mine area is developed on a single, inverted, limb of a major F_1 fold. F_2 synforms are thus anticlines and, conversely, F_2 antiforms are synclines.

Three major tight F_2 folds dominate the structure of the Broken Hill area. From northwest to southeast they are the Hangingwall Synform, the Broken Hill Antiform and the Broken Hill Synform. The folds plunge predominantly at moderate angles to the southwest and their axial planes have steep to shallow dips to the northwest. Folding was accompanied by high-grade metamorphism producing new sillimanite and biotite growth in the aluminous metasediments. The orebodies lie in, or adjacent to, the antiformal crest and the mine sequence rocks are repeated about the hinge trace of this fold. This last point is the central fact in the geology of Broken Hill. It can be demonstrated not only by the long-recognized mirror image of rock units about the line of lode, but also by a change in sedimentary facing about this line, by a change in minor F_2 fold vergence, and by a change in the layering/F_2-cleavage relationships.

F_3 folding was of lesser intensity than F_2 and was accompanied in the mine area by retrograde metamorphism. Axial planes of these folds are defined by the growth of biotite, chlorite and sericite and/or a crenulation cleavage. This surface is vertical or steeply dipping and is commonly parallel to, and appears to be genetically linked with, retrograde shear zones such as the Globe-Vauxhall or the Main Shear. West of the Globe-Vauxhall shear zone, the regional F_2 folds described above, have

been rotated about a major F_3 fold and are flat-lying. In the southern mines area (south of the British Shear) the Broken Hill Antiform is affected, and probably refolded by a large co-axial F_3 fold - the Western "Anticline". Much of the sulphide ore lies in the crest of this F_3 fold.

The structural model, briefly summarized here, has important implications for theories on the genesis of the orebodies. For example, a stratigraphy of the mine area, indispensable to any syngenetic theory, can only follow the disentanglement of the mine structure. The Broken Hill orebodies may well be syngenetic in ultimate origin, but their linear shape, and intimate relationship with the axes of F_2 and F_3 folds, strongly suggest that their present-day form and location owes at least as much to their long deformational history.

REFERENCES

ANDREWS, E.C., 1922: The geology of the Broken Hill district. Geol. Surv. of N.S.W., Mem. 8.

GLEN, R.A., and LAING, W.P., 1975: The significance of sedimentary structures in the Willyama Complex, New South Wales. Proc. Aust. Inst. Min. Met., 256, pp. 10-14.

GUSTAFSON, J.K., BURRELL, H.C., and GARRETTY, M.D., 1950: Geology of the Broken Hill ore deposit, N.S.W., Australia. Bull. geol. Soc. Am., 61, pp. 1369-1437.

HOBBS, B.E., 1966: The structural environment of the northern part of the Broken Hill orebody. J. geol. Soc. Aust., 13, pp. 315-338.

LEWIS, B.R., FORWARD, P.S., and ROBERTS, J.B., 1965: Geology of the Broken Hill lode, reinterpreted. 8th Cwlth. Min. metall. Cong., 1, pp. 319-332.

RUTLAND, R.W.R., 1973: A note on major structures in the Willyama Complex. Trans. Roy. Soc. S. Aust., 97, pp. 77-90.

RUTLAND, R.W.R., and ETHERIDGE, M.A., 1975: Two high grade schistosities at Broken Hill and their relation to major and minor structures. J. geol. Soc. Aust., 22(3), pp. 259-274.

APPENDIX F

STRUCTURAL EVIDENCE RELATING TO THE GENESIS OF THE BROKEN HILL OREBODY, AUSTRALIA

by

W.P. Laing, R.W. Marjoribanks and R.W.R. Rutland

(Manuscript of a paper submitted to the Bulletin of the Geological Society of America, February 1977.
WPL and RWM equal senior authors and RWRR junior author.)

CONTENTS

ABSTRACT

The structure of the Broken Hill Mines area is interpreted in terms of three major metamorphic and deformational events, the major fold closures present belonging to the second (F_2) and third (F_3) events. The earliest phase (F_1) produced the dominant high-grade metamorphic fabric of the Willyama Block and was associated with large scale isoclinal folding. In the Broken Hill Mines area all F_2 folds are downward-facing and it is inferred that they lie on a single inverted limb of a regional F_1 fold-nappe. The dominant high-grade mineral lineation (L_1) is attributable to the F_1 event.

Three macroscopic F_2 folds dominate the structure of Broken Hill. From NW to SE they are the Hangingwall Synform, the Broken Hill Antiform and the Broken Hill Synform. The folds plunge predominantly at moderate angles to the SW and their axial planes have steep to shallow dips to the NW. F_2 folding was accompanied by high-grade metamorphism producing new sillimanite and biotite growth in the aluminous metasediments. The core of the Broken Hill Antiform contains the "Mine Sequence" lithologies. Within the "Sequence" the hinge of the Antiform is established by a change in the vergence of mesoscopic F_2 structures and by a change in sedimentary younging directions. The "Mine Sequence" includes the conformable Lode Horizon, within which the orebodies form a stack of markedly linear bodies lying on the NW limb of the Broken Hill Antiform. The orebodies are everywhere parallel to the high-grade lineation L_1 and to F_2 fold axes. In North Mine the ore lenses occupy the hinge of a parasitic F_2 fold.

F_3 folding was of lesser intensity than F_2 and was accompanied in the Mines area by retrograde metamorphism. The axial planes of F_3 folds are vertical or steeply dipping and are commonly sub-parallel to, and

appear to be genetically linked with, retrograde shear zones such as the Globe-Vauxhall Shear and the Main Shear. In the Southern Mines the Western Antiform and Eastern Synform are due to the superposition of F_3 folding on F_2 structures, the Synform being in part replaced by the Main Shear. The six ore lenses of the southern part of the field lie within the hinges of these F_3 folds, or are developed as a vertical sheet within the Main Shear.

Because of the strain which the rocks have undergone, it is not possible to demonstrate the pre-deformational shape of the ore lenses. However the unravelling of the Mine structure enables the orebodies to be placed within an ordered stratigraphic sequence. The ore lenses and Lode Horizon occur within a psammopelitic sillimanite gneiss stratigraphically above rocks of probable volcanic origin. They are succeeded by a barren sequence of more pelitic sillimanite gneiss.

The following stages in the evolution of the orebody are proposed:

1) Deposition of metal sulfide in a zone of uncertain shape within a stratigraphic interval at the end of a phase of volcanism.
2) Strong accentuation of any original linearity into a direction parallel to L_1, during F_1.
3) F_2 and F_3 folding co-axial with L_1, with major drag-folding localized by the orebody. Successive lateral migration of ore into the hinges of these structures and into retrograde schist zones associated with F_3.

INTRODUCTION

The Broken Hill orebodies are among the world's great silver-lead-zinc deposits, having yielded 120 million tonnes of over 25% contained metal since their discovery in 1883 (Johnson and Klingner, 1976). A review of the literature up to 1973 concerning the origin of the orebody has recently been provided by Both and Rutland (1976). They point out that the recent consensus, based on geochemical evidence, has been towards an "exhalative sedimentary" origin (White, 1968) but that structural evidence and interpretations have generally suggested emplacement of the ore late in the structural and metamorphic history. It has even been suggested that the Lode 'Horizon' is discordant to the Mine 'Sequence' (Hobbs, 1966; Hobbs and others, 1968).

Resolution of the structural evidence is therefore critical to the interpretation of the origin of the orebody. During the past few years the authors and a number of colleagues have been involved in remapping the Broken Hill region and the Mine area with emphasis on mesoscopic structures and paying particular attention to the previously neglected metasedimentary rocks. This work has led to a new interpretation of the structure of the Mine area, which is the subject of this paper. The geometry now recognized is closer to that of Gustafson and others (1950) than to that of subsequent workers. It differs from Gustafson and others (1950) in two major respects: it interprets the geometry in terms of the superposition of three principal deformation episodes prior to the development of the discrete retrograde schist zones; and it demonstrates that the principal (F_2) folds in the mine area are stratigraphically 'downward-facing' (Shackleton, 1958).

Following over 75 years of intensive exploration and research, the shape of the orebodies, and the shape and distribution of units within the enclosing wall rocks, is now known in reasonable detail throughout the field (see Gustafson and others, 1950; King and O'Driscoll, 1953;

Carruthers and Pratten, 1961; Lewis and others, 1965; Johnson and Klingner, 1976). Knowledge of corresponding mesoscopic structures is by comparison limited, partly because early workers in the field did not distinguish or systematically record many of the structures present, and partly because of the nature of the exposure available. Surface outcrop within the Mines area is limited: adjacent to the ore lenses the rocks have suffered severe weathering and alteration. Underground exposures are in general restricted to the narrow segment of mine sequence rocks adjacent to the orebodies. Diamond drilling, which has been able to distingush the gross distribution of rock units throughout the field, has to date provided little additional information on mesoscopic structures.

The principal rock units are imperfect tools in distinguishing the large-scale structures, and cannot in themselves provide information on the nature and sequence of the deformations affecting the Mines area. Early work suffered from these twin defects. More recent studies (Hobbs, 1966; Ransom, 1968; Hodgson, 1974) have investigated the mesoscopic structures in some detail, and have provided important information on the nature and sequence of deformations present. These studies were however, restricted to relatively small areas of the Mines and were unable to relate the Mines structures to that of the surrounding region.

In this paper the known shape and distribution of the main rock units is used to provide the essential framework for the structural analysis. In seeking mesoscopic information to "flesh out" the framework, the authors have concentrated upon a layered sillimanite gneiss lithology because of the abundance of younging data, small folds, lineations and penetrative foliations which are preserved in this rock-type. Valuable structural data from this rock type have also been gathered for the first time from drillcore, using methods described by Laing (1977). In the synthesis, the continuity of the macroscopic features is largely established by knowledge of the distribution of the rock units. This information is drawn from the standard plans and sections of the mining companies, to some extent

supplemented by new observations by the authors. The significance of this distribution and the nature and relative ages of the deformations which it implies is determined from the mesoscopic evidence. This approach does not assume a complete stratigraphy of the Mines area; rather such a stratigraphy is a valuable by-product.

GEOLOGICAL SETTING

Regional Structure

The Broken Hill ore deposits lie within the Precambrian Willyama Block of New South Wales (Figure 1). The block consists predominantly of aluminous metasediments containing concordant horizons of amphibolitic and granitic rocks. All the rocks within the Broken Hill area were metamorphosed during a major regional event which reached the granulite facies in the Mine area (Binns, 1964) and which has been dated at 1695 $\pm$ 21 m.y. (Pidgeon, 1967; Shaw, 1968). This date is most reasonably correlated with the first major deformation episode which produced a strong schistosity and gneissosity (S_1) which is almost everywhere parallel to the lithological units and to preserved bedding.

Fig. 1

The central part of the Willyama Block, within which the ore deposits lie, is occupied by a number of major NE-trending folds (Figure 16)*. These folds and associated structures were also formed under high grade metamorphic

---

* The regional structural geology is described more fully in Marjoribanks, Glen, Laing and Rutland, 1977 (in press).

---

conditions but they can be correlated as belonging to a second deformational episode (F_2) on the basis of consistent style, orientation and overprinting on the earlier metamorphic fabric (S_1). Two of the regional folds are outlined by the outcrop of granite gneiss and amphibolite horizons and were recognized in early surveys of the district (Andrews, 1922) and named the Hangingwall Basin and Broken Hill Basin. The evidence indicates that

these structures are F_2 synforms and they will hereafter be called the Hangingwall Synform and Broken Hill Synform. The two synforms flank the zone of rocks which contains the Broken Hill orebodies and which must therefore be essentially antiformal. Structural mapping by the authors has defined the antiform which lies between these synforms as the Broken Hill Antiform, and the major F_2 antiform which lies to the NW of the Hangingwall Synform as the Sundown Antiform. All the F_2 folds have parallel NE-trending axial-plane traces and plunge overall at a moderate angle to the SW. They constitute the major mappable fold structures of the Broken Hill region.

Axial planes of the regional F_2 folds (S_2) dip to the NW at between 90° and 10° (Figure 16). This variation in dip of S_2 defines an open regional post-F_2 monoclinal fold (see section, Figure 1) of F_3 generation. The Mines area lies on the steep limb of the monoclinal flexure, with beds and S_2 surfaces flattening to the NW into the extensive shallow-dipping limb. North of Sundown S_2 steepens once again into the long limb of the F_3 fold. Thus, the Broken Hill Arch of earlier authors (e.g. Andrews, 1922; Gustafson and others, 1950) is essentially a consequence of this F_3 deformation which is associated locally with a penetrative retrograde axial plane schistosity (S_3). In places the retrograde surface forms intense planar retrograde schist zones, within which all earlier structures have been partly or completely obliterated.

Lithologies and Structural Geometry of the Mines Area

The Broken Hill orebodies lie within a distinctive suite of rocks known as the Mine Sequence (Carruthers and Pratten, 1961), consisting predominantly of aluminous psammo-pelitic metasediments - now layered sillimanite-garnet-biotite gneiss - within which are concordant horizons of amphibolite, granite gneiss and banded iron formation. In addition, more unusual rocks

column of different units without repetition by folding, and have generally supposed the sequence to be right way up, i.e. younging to the NW (Johnson and Klingner, 1976, p. 476).

The present work re-establishes an antiform in the 'sequence' but it will be convenient to retain the above nomenclature of units based on their present structural position. The units from the Lode Horizon to the Upper Granite gneiss will be considered together as the upper units while those structurally below the Lode Horizon will be referred to as the lower units of the 'sequence'.

Gustafson and others (1950) note that the absence of persistent "key 'horizons' everywhere distinguishable from all other rock layers and the inability to recognise top and bottom of beds were the greatest obstacles to the complete solving of either rock succession or folded structures". They recognized metamorphosed graded bedding locally but did not make use of this tool for structural interpretation. In the present work widespread use of metamorphosed graded bedding has been made both regionally and in the Mine area. The evidence obtained not only confirms the change of stratigraphic younging direction between the upper and lower units but also shows that the principal F_2 fold structures are structurally downward-facing.

Within the "Lode Horizon" itself a total of six ore lenses may be present, each with a characteristic mineralogy and generally separated from each other by narrow widths of country rock. Only in the Southern Mines area are all six lenses developed. In order of superposition they are:

A Lode	Collectively known as the zinc lodes
B Lode	
Upper No. 1 Lens	
Lower No. 1 Lens	
No. 2 Lens	Collectively known as the lead lodes
No. 3 Lens	

No. 2 and 3 Lens are the only lenses which occur throughout the field and are the only lenses present in significant volume in the Central and Northern Mines. Throughout the field No. 2 lens almost always occurs structurally above No. 3 lens. The individual lenses are highly-elongated bodies within the planar Lode Horizon, with the lead lodes, the most extensive, having a strike length of approximately 7 km and a maximum width, measured around the centre line of their complex cross-sectional shape, of approximately 1 km.

As already noted the macroscopic structural geometry of the Mine area is known in considerable detail throughout the field. Only a brief summary is given here in relation to our analysis, which has allocated the principal fold structures to three main phases of folding all of which antedate the discrete retrograde schist zones.

The principal macroscopic fold observed within the mine area is the Hangingwall Synform and this is allocated to F_2. It can be traced throughout the mine area as shown in the maps of Figures 4 and 5 and the sections of Figures 6 to 13. The plunge variation from about 35° to the SW to about 45° to the NE clearly illustrates the plunge culmination in the mine area which also affects the orebody (Figure 3).

Figs. 3 to 5

No other major folds are clearly evident from the distribution of rock units on the map. In particular, no rock units can be mapped around the hinge of the Broken Hill Antiform. This F_2 structure has been re-established by the study of mesoscopic structures and from drillhole data.

Recent work (French, 1976, pers. comm.) has shown that the ABM Potosi Gneiss contains a major F_2 antiform.

Major folds have also been re-established in the lower units, structurally below the orebody, but as discussed below there is some doubt whether these are F_1 or F_2. These folds correspond broadly with the Alma Anticline and the

Footwall Syncline of Gustafson and others (1950) and are isoclinal.

The principal structures folding the orebody itself do not have a strong surface expression but they are well defined by sub-surface data as the Western Anticline and Eastern Syncline of Gustafson and others (1950). These names are retained here as the Western Antiform and Eastern Synform. These folds have a variable plunge averaging about 20^{o} - 25^{o} to the SW in the Southern mines. In the Zinc Corporation and NBHC Mines, the folds affect all units from the Lode Horizon to the Lower Granite Gneiss (Figure 7) but the folds die out up-plunge and do not affect the outcrop pattern of the Lower Granite Gneiss. Northwards, as the British Shear is approached, the plunge of the folds in the orebody decreases and becomes horizontal, and a complex of smaller antiforms and synforms replaces the fold pair. These folds are closely correlated with the shape of the ore lenses. The lenses are stacked parallel to the axial planes of the folds, they are elongated parallel to the plunging axes of the folds and, in general, the greatest thickness of ore is found in the fold hinges.

Some of these folds have the appropriate sense for congruence with the Broken Hill Antiform but the continuity and orientation of their axial planes derived from drill sections shows that they must in part be F_3 folds superposed on the major F_2 structure. Their interpretation (and the geometry of the ore lenses) is complicated by their relation to both the Belt of Attenuation and the Main Shear of Gustafson and others (1950) (Figure 14). The evidence discussed below suggests that the Belt of Attenuation is a second generation structure associated with the F_2 Broken Hill Antiform. The Main Shear was defined by Gustafson and others (1950) as "the most conspicuous (plastic) shear plane at any place within the Belt of Attenuation" but it is often accentuated by retrograde zones superposed on the Belt of Attenuation during or after F_3 folding.

Adjacent to the British Shear the ore lenses are attenuated and show a sharp sinistral displacement. Within the Shear Zone itself there is a thick development of No. 3 lens known as the Brown Shaft Ore Shoot. This

lens of ore has its elongation within the schistosity of the Shear Zone and has a steep plunge to the south, parallel to the mineral lineation within the Zone and in contrast to the NE-plunging ore lenses immediately north and south of the Shear.

North of British Shear the orebodies plunge NE at around 45° within the broadly planar, steep northwest-dipping Lode Horizon. Below 24 level in North Mine, the plunge steepens as the orebodies approach and finally enter Globe-Vauxhall Shear at 27 level. Their pitch in the Shear below this level is sub-vertical.

Two sets of folds have long been recognized in the North Mine orebodies (Gustafson and others, 1950; O'Driscoll, 1968, Figures 19 to 22). An early group of large folds plunges 42° to the NE parallel to the overall plunge of the orebodies, and is overprinted by a group of folds whose average plunge is 36° to the west. The early folds are consistently dextral with axial planes steeper than the orebodies; they are outlined not only in the orebody/wallrock interface but also in the interface between low and high-grade sections within the orebodies (W. Widdop, personal communication, 1975). The folds are tight, and show appreciable thickening in the hinges and thinning on the limbs. They have commonly been correlated with the Western Antiform and Eastern Synform south of the British Shear (see Both and Rutland, 1976) but they are here interpreted as essentially F_2 structures whereas the macroscopic structures south of the British Shear show substantial F_3 components. The later set of folds in the North Mine orebodies is also consistently dextral, with axial planes shallower than the orebodies and characterized by a fracture surface. They are open folds, without the hinge thickening apparent in the early folds, and are interpreted as F_4 structures. They do not appear to have a large effect on the macroscopic geometry of the orebodies.

Figs. 6 to 14

EVIDENCE FROM MESOSCOPIC STRUCTURES

Lithological layering - S_0

This layering is common within the sillimanite gneiss of the Mines area. It is most prominent where picked out by surface weathering but is also easily seen in drill core and, with more difficulty, underground. The layers consist of psammite horizons from 1 cm to several metres thick and with generally sharp contacts against the pelitic country rock. The layers are parallel to each other and to the contacts of the major lithological units of the Mine Sequence. The spacing of the layers is irregular, with regularly-banded psammite/pelite sections alternating with thicker sections of more uniform pelite, in which only occasional psammite layers are present. Except where affected by folds the layers in general maintain a constant width and can be traced for the extent of the outcrop.

A few of the psammite layers show marked mineralogical gradation from a sharply-defined pure quartzite base to a pelitic sillimanite-biotite-garnet top (Figure 19). These beds are generally 2-10 cm, but up to 30 cm, thick. The graded units are considered to represent metamorphosed sedimentary graded beds and to give a younging direction for the strata. They can be observed on the surface and in drillcore: occurrences average approximately one graded bed or closely-adjacent group of graded beds, for every 500 m of core logged. The distribution of the graded beds is not uniform, tending to occur in groups within the regularly-banded sillimanite gneiss.

Early workers such as Andrews (1922) and Gustafson and others (1950) recognized the metasedimentary nature of the sillimanite gneiss of the Mines area and assumed that this prominent psammitic layering represented original sedimentary bedding. In a series of papers, Hobbs (1966), Ransom (1968), Hobbs and others (1968) and, following these authors, Hodgson (1974), postulated that much of this layering was the direct result of deformational and metamorphic processes, and could not be regarded as bedding.

However, following Glen and Laing (1975) the presence of sedimentary structures within the layering, its continuity in outcrop and the lack of any evidence for widespread transposition by folding on a mesoscopic scale, are considered as good evidence for its sedimentary origin. The lithological layering as described above is hence considered to represent original bedding and is labelled S_0.

The presence of sedimentary graded beds allows stratigraphic younging directions to be established throughout the Mines area. These directions have been established at six different localities on the surface and at nearly 400 localities underground; the results are summarized in Figures 4 and 5 and in Figures 6 to 13. The younging directions are consistent with, and provide independent confirmation of, the major fold structures of the Mines area. Thus, to the NW of the axis of the Hangingwall Synform beds young predominantly to the NW; between the axis of the Hangingwall synform and the axis of the Broken Hill Antiform, beds young to the SE, and to the SE of the Broken Hill Antiformal axis the beds again young predominantly to the NW. The youngest rocks are thus contained in the core of the Antiform and the oldest rocks in the core of the Synform, that is, the F_2 structures face downward (for example, see inset in Figure 10). This can only be explained by supposing that these F_2 folds were developed in beds lying on the overturned limb of a large pre-existing fold. The presence of a pre-F_2 deformational episode resulting in recumbent isoclinal folds (F_1) can be independently deduced (see below). The entire Mines area is believed to lie on a single, extensive, overturned limb of a large F_1 recumbent fold or nappe.

Within the SE limb of the Broken Hill Antiform in the North Mine area, the isoclinal Footwall Synform and complementary Alma Antiform are postulated mainly from two broad changes in younging directions about the ABM Potosi Gneiss and Lower Amphibolite units, as shown on Figure 10. By contrast, in the Southern Mines younging directions in this limb are dominantly to the NW. Units in the equivalent or approximately equivalent

stratigraphic position in the Southern Mines (the Lower Potosi Gneiss and the Lower Amphibolite) do not outline any obvious folds. However, local anomalies in younging direction do occur (for examples, Figures 6 and 7) and are probably related to small-scale isoclinal folds. Such folds may be of either F_1 or F_2 age. It is possible therefore that the Footwall Synform and the Alma Antiform are present throughout the Mines area, but have become attenuated and appressed in the Southern Mines due to the intensity of folding in these areas.

The First Deformational Event - F_1

The dominant mesoscopic fabric of the area is a well-developed schistosity defined by the orientation of planar aggregates of sillimanite and fibrolite and by the preferred orientation of sillimanite needles and biotite laths. Garnet and orthoclase porphyroblasts and the inclusions within them are also typically elongate within the schistosity. This penetrative surface is the oldest deformational fabric that can be identified and is labelled S_1. It is most strongly developed in pelitic metasediments and is commonly only weakly developed in psammitic units. In every outcrop where S_1 is observed it is parallel to the lithological layering (Figure 19) and to the contacts of the major marker units of the Mine Sequence. No folds (F_1) with S_1 as an axial-plane surface have been observed within the Mines area, although rare F_1 folds have been identified in the surrounding region. The parallelism of S_1 with S_0 indicates that F_1 folds are isoclinal and, together with the lack of observed hinges, suggests that F_1 folding may have been accompanied to some extent by transposition of bedding, in the sense of Hobbs (1966) (see Figure 15 for a model of F_1 folding). However, the general consistency of younging directions throughout the Mines area supports the conclusion of Glen and Laing (1975) that transposition did not occur on a mesoscopic scale during F_1 folding.

Within granite gneiss, S_1 is defined by a metamorphic segregation foliation composed of regularly-alternating quartzofeldspathic and mafic laminae up to 1cm thick (Figure 21). The preferred orientation of biotite, muscovite and, where present, sillimanite also helps to define the S_1 surface. Within

amphibolite units a similar, though generally finer, metamorphic differentiation foliation defines S_1 in places, along with the preferred orientation of biotite and of the long axes of hornblende.

In the pelitic metasediments the elongation of sillimanite and fibrolite defines a prominent lineation within S_1, labelled L_{1-2}. In the granite gneiss units this lineation is marked by a streaking of quartzofeldspathic and mafic material within S_1 and by the preferred orientation of the long axes of feldspar augen. Over most of the area the lineation plunges to the SW at 30°-50°. From the SW margin of South Mine toward the British Shear, the plunge of this lineation becomes progressively less and adjacent to the British Shear the high-grade lineation is sub-horizontal.

In a domain extending NE from British Shear to Imperial Ridge and part way along Turpins Ridge, two high-grade lineations are commonly present in a single outcrop or even on a single outcrop face. This domain of complex lineations is discussed in detail in a following section; at this point it is sufficient to note that the lineations are referrable respectively to F_1 and F_2, and that L_1 plunges to the NE at a variable angle (Figure 18). L_1 is best preserved in granite gneiss: in the ABM Potosi Gneiss, a strong L_1 lineation plunges at 30°-70° to the NE; in Potosi Gneiss outcrops at Martins Bore a mesoscopically folded L_1 has an overall plunge to the NE, and in the Lower Granite Gneiss at the southwestern end of Turpins Ridge a strong L_1 pitches subvertically within the S_1 gneissosity.

The geometric relationship between L_1 and F_1 fold axes is unknown. The most reasonable assumption in view of the probable high strain associated with the F_1 event, is that the F_1 axes are parallel to L_1.

The Second Deformational Event - F_2

Fig.15 Throughout the Mines area numerous mesoscopic folds are present which affect S_0 and S_1 and possess a new, penetrative high metamorphic grade, axial-plane schistosity. These folds are termed F_2 and the axial-plane surface is

termed S_2 (Figure 15).

Where fully developed, S_2 is defined by folded and flattened aggregates of fibrolite or sillimanite and by the preferred orientation of new sillimanite and biotite (Figure 20). It is thus similar in appearance to the S_1 surface. However, S_2 is typically only developed within or adjacent to the hinges of F_2 folds and in many outcrops (for example, adjacent to Zinc Corporation Mine at 1* and in North Mine at 2) the different stages in the progressive development of a penetrative S_2 from tightly-crenulated S_1 can be observed. In one common occurrence, layer-parallel S_1 is preserved within psammite layers while being obliterated and replaced by penetrative S_2 oblique to the layering in adjacent pelitic units. Even where in hand specimen S_2 has completely obliterated S_1, the flattened fibrolite aggregates defining S_2 can frequently be resolved under the microscope into tightly-crenulated S_1 fibrolite which has been transposed into the orientation of S_2. New sillimanite needles which have grown during F_2 cut across this tightly-folded S_1 fibrolite (Figure 22).

Within granite gneiss, quartzofeldspathic segregation veinlets have frequently formed in the axial planes of F_2 folds and form a penetrative S_2 surface which may be developed away from the vicinity of the folds. These veinlets are in detail irregular and possess gradational contacts with the surrounding granite gneiss (Figure 21). In spite of this they form a constantly-oriented surface oblique to the S_1 gneissosity and parallel to the axial plane of macroscopic F_2 folds.

---

* Reference localities within the Mines area are indicated on Figures 4 and 5.

With the exception of a domain running north from the British Shear to Imperial Ridge, mesoscopic F_2 folds plunge to the SW and are parallel to the high-grade lineation (L_{1-2}) developed within S_1. F_2 folds in the Upper Granite Gneiss of Block 10 Hill plunge to the SW at around 35°. F_2 folds on both sides of the British Shear have very low or horizontal plunges. F_2 folds from northeast of British Shear to Imperial Ridge plunge at varying angles to the NE, with steepest plunges around De Bavay Shear. At Imperial Ridge the F_2 folds are sub-horizontal, and further to the northeast at Round Hill they revert to the regional SW plunge. The variation of F_2 fold plunges from British Shear to Imperial Ridge is related to the complex lineation relationships observed in this area (see below).

The large-scale F_2 folds have similar attitude and style to the mesoscopic F_2 folds throughout the field. The Hangingwall Synform and Broken Hill Antiform are identified as macroscopic F_2 folds, because the sense of asymmetry of mesoscopic F_2 folds, layering-S_2 relationships and S_1-S_2 relationships changes across their respective axial-plane traces.

The Broken Hill Antiform

The Mine Sequence occupies the core of the F_2 Broken Hill Antiform. Although closure of marker units can be inferred only in the North Mine area, and there only in the subsurface, vergence information and the concomitant changes in younging direction throughout the field serve to indicate the approximate position of the Broken Hill Antiformal axis. Outcrops where the Broken Hill Antiform can be deduced from mesoscopic F_2 structures occur in the South Mine around localities 3 and 4 in Figure 4. In the Southern Mines the axial plane of the Broken Hill Antiform lies within or adjacent to the Belt of Attenuation. This planar zone of high strain on the eastern side of the ore-lenses is marked within the sillimanite gneiss wallrocks by tight "M" vergence F_2 folds (Figure 20).

By contrast, in North Mine the position of the antiform is well to the

SE of the ore-lenses. Vergence observations in the area between the Hangingwall (locally the Lords Hill) and the ABM Potosi Gneiss (e.g. at localities 5 and 6 in Figure 5) although very limited, are consistent with the NE-plunging NW flank of the antiform. About a line through the centre of the ABM Potosi Gneiss French (1976) reports a vergence change in NE-plunging F_2 relations, indicating the axial-plane trace of the Broken Hill Antiform. There are no exposed metasediments on the SE side of the ABM Potosi Gneiss. In the subsurface the core of the antiform is outlined by a unit of pelitic sillimanite gneiss structurally below the relatively psammopelitic sillimanite gneiss and quartzites of the Mine Sequence (Figure 10).

Several problems concerning the geometry of the Broken Hill Antiform in the North Mine remain unresolved, partly because of the extreme paucity of outcrop and surprizingly, of drilling data, and partly because of complexities in the structure itself. The first problem is evident in the anomalous slight divergence of lithological units on the surface in a NE direction, where, because of the NE plunge, convergence toward the macroscopic F_2 hinge might be expected (Figure 5). This may be due to superimposed shape change (interference) from later F_3 folding or from movements on the De Bavay and British Shears. Alternatively it may be a function of the known fanning of S_2 axial planes, measured from S_2 schistosity surfaces across the structure.

The second problem concerns the structural interpretation of the SE flank of the antiform and its hinge zone in the ABM Potosi Gneiss. Mesoscopic data from the ABM Potosi Gneiss indicate that the unit occupies the hinge area of a north-east-plunging <u>antiform</u> of F_2 age (see above). F_2 fold axes and the mineral lineation within the unit plunge uniformly to the north-east. However, the outcrop of the unit terminates at its south-western end in an apparent closure (Figure 5) which, if real, indicates that a north-easterly plunging fold in the unit would necessarily be

synformal as inferred by Gustafson and others (1950) (see below).

The apparent contradiction would be removed if it could be demonstrated that the outcrop termination is not, in fact, a closure in layering but a facies change (of sedimentary, diagnetic, or metasomatic origin) or a fault-bound termination of some kind; or, failing this, that the Potosi Gneiss represents the coincidence of two folds, possibly of different ages. Unfortunately the Potosi Gneiss termination is bounded by an area of no outcrop; furthermore it is not possible to show layering closing in sympathy with the outcrop termination (French, 1976). The surface evidence for a fold closure is therefore inconclusive. However data from the single drill section through the ABM Potosi Gneiss (Figure 10) throw some light on the problem, at the same time exposing structural complexities on the SE flank of the antiform. In the centre of the drill section the thick unit of pelitic sillimanite gneiss in the subsurface coincides with a major reversal of younging directions, and is interpreted as the core of the Broken Hill Antiform of F_2 age. The hinge line marked by the younging reversal is correlated with the F_2 hinge in the ABM Potosi Gneiss on the surface. However, southeast of the axial-plane trace thus established there exist two subsidiary reversals of younging in this drill section. The more south-easterly of these reversals is coincident with the Lower or Consols Amphibolite. Although manifest in only four younging directions (there are no younging data on the surface) the reality of the reversal is not in doubt, and its location within or on the margin of the amphibolite is relatively precise. However, along strike from this drill section the lack of drillholes and surface outcrop preclude verification of this reversal about the Lower Amphibolite. The second subsurface younging reversal lies between the above reversal and the major reversal defining the hinge of the Broken Hill Antiform. Although the paucity of younging data makes its location less than precise, this reversal of younging occurs in the subsurface in the vicinity of the ABM Potosi Gneiss (Figure 10).

The apparent conjunction of the subsidiary younging reversals with two lithological units suggests that the units respectively mark the hinge areas of two folds, possibly modified by dislocations. The configuration of the Lower Amphibolite and the ABM Potosi Gneiss is consistent with this idea. A lenticular, and in

places anastomosing outcrop pattern of the Lower Amphibolite (from mapping by North Broken Hill Ltd.) is consistent with the existence of a closure in that unit, while the possibility of an additional, synformal fold hinge in the ABM Potosi Gneiss has been discussed above. A synformal hinge in the ABM Potosi Gneiss certainly provides the most reasonable explanation for the break in outcrop of Potosi Gneiss between the North Mine and the southern mines. This break lies opposite a similar break in outcrop of the Upper Granite Gneiss (Figure 2) which is known to represent a plunge culmination of the Hangingwall Synform.

Thus the relationship between mesoscopic structures, particularly graded bedding, and the shape of rock units gives support to the existence of two major folds southeast of the Broken Hill Antiform. Such folds were postulated by Gustafson and others (1950) on the sole basis of rock unit shape, but they have been ignored in subsequent published interpretations. Following Gustafson and others (1950) the postulated folds are named the Footwall Synform and the Alma Antiform. It remains to be determined how the folds fit into the multiphase deformation history.

Two interpretations are possible. The fold pair can be interpreted as parasitic F_2 folds on the south-eastern limb of the Broken Hill Antiform. The tightness of the folds is consistent with the greater strain (vide the Belt of Attenuation) in this limb, which was probably associated with sliding. However, the apparent contradiction between the shape of the Potosi Gneiss and its internal mesoscopic F_2 structures (see above) suggests another possible interpretation, in which the fold closure in the southwestern end of the ABM Potosi Gneiss represents a synform unrelated to the closure of the F_2 antiform, i.e. of a different age to the F_2 antiform. The tightness of this synform (the Footwall Synform), and the associated isoclinal Alma Antiform, suggests that the fold pair is of F_1 age in this interpretation. The near coincidence of F_1 and F_2 axial-plane traces in the ABM Potosi Gneiss might simply reflect an erosional level at their line of intersection, or else it might be due to convergence of structures from F_2 sliding. It seems reasonable to suppose that the F_1 fold axes would be

parallel or sub-parallel to the moderately NE-plunging L_1 lineation in the Potosi Gneiss.

There is insufficient evidence, in outcrop or in the sub-surface, to distinguish between the respective hypotheses of F_1 or F_2 age for the subsidiary fold pair. Such distinction rests partly on whether the SW end of the ABM Potosi Gneiss body represents a fold closure, a question unsolved at present. One objection to the F_1 interpretation is that the folds (in particular the changes in sedimentary younging) cannot be detected folded around the Broken Hill Antiform on its NW limb. In any event it is almost certain that large, virtually layer-parallel dislocations conjointly with folding have played an important role in determining the complex geometry of the southeastern limb of the Broken Hill Antiform. It is worth noting that the complexities in this area have only come to light because of the attention paid to graded bedding preserved in the rocks (contrast Ransom's (1969, p.213) statement that "the structure of the footwall of the orebody is more simple than that of the hanging wall"). The dislocations or slides would serve to explain the absence of significant slices of the stratigraphic sequence, evident in the non-repetition of some marker units about the hinge of the antiform. The sliding was probably operative in both the F_1 and F_2 deformations.

Northeast of De Bavay Shear the Broken Hill Antiform occupies a belt of very poor outcrop and negligible sub-surface information. Two drillholes appear to intersect the pelitic sillimanite gneiss in the core of the fold (Figure 11) with appropriately high angles between bedding and the S_2 schistosity. There is some doubt as to whether the hinge of the antiform is located along the side of Round Hill within the Round Hill Slide or to the SE of the slide in the area of no outcrop along the Barrier Highway. The latter interpretation is favoured because F_2 folds in the areas immediately east of Round Hill and the Barrier Main Shaft have dominantly sinistral, SW-plunging vergence. The De Bavay Shear marks a reversal of plunge of mesoscopic F_2 folds, presumably reflecting a plunge reversal in the Broken Hill Antiform, from moderately NE on the SW side of the Shear to gently SW on the NE side of the Shear (Figure 18).

The Hangingwall Synform is well exposed northeast of De Bavay Shear in the Imperial Ridge and Round Hill areas. The Round Hill Slide along its SE flank is the continuation of the F_2 slide inferred in the same structural location in the Mines area. The major plunge change of the Hangingwall Synform corresponding to that of the Broken Hill Antiform takes place NE of De Bavay Shear, in the Imperial Ridge area (Figure 18).

Relation of Orebody to Major Folds

Southern Mines

In the area south of the British Shear the position of the axis of the Broken Hill Antiform is established mainly on graded bedding evidence from drill core. Most of this evidence comes from the southern part of the field and permits a precise definition of the axial plane only on the deeper levels of drill section CC_1 (Figure 8). Projection of the axial-plane trace into the vicinity of the ore lenses is made difficult by the superimposed effects of F_3 folding, particularly the tight Eastern Synform-Main Shear structure, which may disrupt, and in part replace, the F_2 hinge. Nevertheless there is sufficient evidence to show that the orebodies lie close to the antiformal axis, but that all of the zinc lodes, and at least a part of the lead lodes, lie on the NW limb of the fold.

In the central part of the field, little evidence from mesoscopic structures is available and it is necessary to interpret the position of the Broken Hill Antiform solely on known orebody shapes. Thus in a section such as that of Figure 14$_1$ where No. 3 lens structurally overlies No. 2 lens, it is possible to suggest that they lie on the SE limb of the F_2 antiform. Throughout most of the field, however, No. 2 lens occurs structurally above No. 3 lens, this consistent relationship indicating a consistent position of the orebodies on the NW limb of the Broken Hill Antiform.

Throughout the central and southern parts of the field the plunge of the linear ore lenses is parallel or sub-parallel to that of F_2 folds and to the high-grade lineation L_{1-2}, in the country rock. As far as can be defined,

therefore, the ore lenses are parallel to the axis of the Broken Hill Antiform, although slight obliquity could be present.

North Mine

The limited surface exposure in North Mine shows that S_2 in this area is vertical or steeply NW-dipping (Figure 17). This is a similar orientation to that which would be expected of the S_3 schistosity if developed. Identification of this surface as S_2 rather than S_3 is provided in three forms:

(a) The high-grade assemblage and distinctive crenulation microfabric.

(b) The axial-plane surface to the Hangingwall Synform at Lords Hill in the granite gneiss is a quartzofeldspathic segregation banding identical to the "type" S_2 surface in granite gneiss at Block 10 Hill. This type of surface has not been identified in F_3 folds.

(c) The very distinctive oblique relation between F_2 fold axes and the L_2 sillimanite lineation has been observed directly and indirectly in several outcrops. This relation is observed in the "type" area of F_2 folding SE of Round Hill, and is unknown in F_3 folds.

The North Mine orebody occupies, and outlines, a tight asymmetric fold whose plunge and dextral sense of asymmetry are consistent with the adjacent F_2 Hangingwall Synform at Lords Hill (see p.9). Although there is very little information on whether a layer-parallel schistosity is folded around the noses of the orebody folds, Hobbs (1966, p.332), Hobbs and Vernon (1968, p. 1425) and Hobbs and others (1968, p. 306) stated that the orebody is folded around the same high-grade axial-plane schistosity as the small folds in the wallrocks. It is clear from the above-listed considerations that this schistosity is S_2 and that the orebody folds are F_2 in age.

Figs.16 to 18

The High-grade Lineations L_1 and L_2

Throughout the Mines area there is one dominant high-grade mineral lineation defined principally by sillimanite, which plunges moderately to the SW (Figure 17). Generally it is parallel to mesoscopic F_2 fold axes but lies within S_1, and is thus labelled L_{1-2}. However, from its occurrence in F_2 folds without an axial-plane schistosity it is believed to have largely resulted from the earlier (F_1) deformation.

Within a domain extending from British Shear to Imperial Ridge, the dominant high-grade SW-plunging mineral lineation is oblique to F_2 fold axes. This lineation, however, lies within the axial-plane schistosity S_2, and is therefore labelled L_2. In some critical outcrops (for example, Figure 23) the SW-plunging L_2 is associated with a NE-plunging high-grade lineation, parallel to F_2 fold axes and lying in S_1. The latter is thus inferred to be L_1. Rare F_2 folds contain a high-grade lineation folded around their axes; this lineation is also L_1. Some exposures do not possess an axial-plane S_2 schistosity, and contain only a single, NE-plunging lineation, parallel to the F_2 fold axes. By analogy with the above cases L_2 appears to be absent and the lineation is inferred to be L_1.

To summarize, L_2 plunges constant to the SW. L_1 is generally parallel to L_2, but L_1 plunges to the NE in a domain of complex lineations between British Shear and Imperial Ridge. Evidence at both extremities of this domain shows that L_1 reverts to the regional SW-plunge through the horizontal. The geometry of the lineations in the Mines area is depicted schematically in Figure 18.

The relationship between the lineations and the F_2 fold axes is correspondingly complex. F_2 folds are parallel to the SW-plunging high-grade mineral lineation, except for an important category of folds in which a specifically identifiable L_2 retains its SW-plunging orientation within S_2, but F_2 fold axes vary within the S_2 axial plane (Figure 24). These folds are observed in the domain of complex lineations, in the small belt of outcrop between Round Hill and the Flying Doctor Base, and in the Browne Hills area in the Northern Leases. On the other hand, F_2 folds are parallel to L_1 (with only rare exceptions) even where the same folds are oblique to L_2.

The observed relations between the lineations of two separate deformations and the fold axes of the second deformation invite two questions: (a) why is F_2 generally parallel to L_1; and (b) what does the relationship between F_2 and L_2 tell us about strain during F_2? A complete discussion of these problems is outside the scope of this paper (Laing, 1977, unpublished thesis, gives a fuller treatment). However, in relation to the first question, one possibility is that the anisotropy due to the pre-existing L_1 lineation was sufficiently strong to control the orientation of the mesoscopic and macroscopic F_2 fold axes, notwithstanding the likelihood that the principal strain axes were not co-linear from F_1 to F_2.

In relation to the second question, the variation of F_2 fold axes within S_2 about a constant L_2 lineation direction is considered to indicate that L_2 represents the X direction and F_2 represents a direction of strain intermediate between Y (the intermediate axis of the strain ellipsoid) and X. If it is assumed that the fold axes rotated within the XY plane during the deformation (e.g. Borradaile, 1972; Roberts and Sanderson, 1974), the regionally dominant relation, in which F_2 is parallel to L_2, represents the highest state of strain, and the rarer folds in which F_2 is sub-perpendicular to L_2 represent a lower strain state, in that the fold axes remained sub-parallel to Y. Alternatively, the variation of F_2 may be due to local variation in the type of strain, without necessarily invoking passive rotation of fold axes. Presumably the strain associated with the parallel relation would be more constrictional than the strain associated with the oblique relationship (e.g. Borradaile, 1972). The second alternative is favoured by the localization of the non-parallel relationship to the region between the De Bavay and British Shears.

The Third Deformational Event - F_3

F_3 folds can be identified by their effect on F_2 structures and can be correlated throughout the Mines area on consistency of style and orientation. Overprinting on F_2 is best seen in the surface outcrops of the Belt of Attenuation. A fine, close-spaced cleavage, defined by the preferred orientation of sericite and dipping at moderate to steep angles to the SE, cuts across the coarser, NW-dipping S_2 schistosity of these outcrops. At the northern end of the old BHP Open Cut (locality 8), this cleavage is axial-plane to a large open sinistral fold, which plunges very gently to the SW and refolds the complex of F_2 folds in the Belt of Attenuation. This open fold can be correlated with the Western Antiform, which is therefore of F_3 generation. The F_3 folds are co-axial with F_2 folds - both structures plunging parallel to the high-grade lineation, and showing a steepening plunge when traced south from the British Shear. However the axial planes of the F_3 folds are nearly vertical so that they transect the NW-dipping axial-plane orientation of the F_2 folds.

The lower units of the Southern Mines area show that the Western Antiform is flanked to the SE by the Eastern Synform, thus forming a sinistral F_3 fold pair. In the vicinity of the ore lenses, the complementary F_3 synform

is difficult to distinguish due to the occurrence in this structural location of the tight F_2 folds in the Belt of Attenuation, and to the presence of a retrograde zone - the Main Shear. It is probable that much of the synformal fold shapes of the ore lenses referred to as the Eastern Synform represent ore in or adjacent to the nose of the Broken Hill Antiform, which has been refolded to lie on the short common limb of the Western Antiform-Eastern Synform fold pair. This interpretation is illustrated in Figure 14.

F_3 folds are generally absent from the North Mine area. A large warp in layering and S_2 axial planes is observed immediately NE of British Shear (Figure 10), and the axis of warping is parallel to the NE-plunging L_1 lineation and F_2 fold axes. Although there is no apparent axial-plane schistosity associated with the warp, the axial plane is vertical, and the parallelism of the axis with L_1 and F_2 strongly suggests that the fold is F_3 in age; the axial plane of the Broken Hill Antiform is inferred to be folded around the warp, in a structure analogous to the Western Antiform-Eastern Synform of the Southern Mines area. F_3 folds and S_3 schistosity are well developed NW of the Globe-Vauxhall Shear (Figure 25) and can be identified by overprinting of F_2 structures (see left-hand inset, Figure 12).

Post-F_3 Deformations

An important group of mesoscopic folds common in the North Mine area and the Northern Leases has axial planes dipping moderately to the west, distinctly shallower than layering, and axes plunging to the SW or W. They are open asymmetric folds lacking an axial-plane schistosity, although characteristically containing pegmatite veins in their axial plane, and they refold earlier structures including F_2 folds and L_1 and L_2 lineations (Figures 15 and 26). Their very constant, inclined axial-plane orientation, whose dip shallower than layering leads to a consistent dextral south-plunging asymmetry, is in contrast to the sub-vertical orientation of F_2 and F_3 axial planes in the North Mine area. Folds of this style and orientation can be traced beyond the

Mines area to the north, where they overprint F_3 structures. The folds are therefore assigned an F_4 age. Open, dextral west-plunging folds with no penetrative axial-plane structure also occur in the opencut area south of the British Shear and are of probable F_4 age.

Although in the Northern Leases F_4 refolds L_2, in North Mine F_4 axes and L_2 lineations are generally parallel (Figure 23). This reflects a change in attitude of L_2 across the De Bavay Shear, concomitant with a change in strike of S_2 from NE to ENE (Figure 17, subareas 3 and 4). This strike change is the consequence of a large open dextral north-plunging fold, of probable F_3 age, which is apparent on the regional map (Figure 1) and which affects all the lithological units and S_1 and S_2 surfaces on the NW limb of the Broken Hill Synform.

Figs.19 to 26

The Retrograde Schist Zones

A late phase of deformation is represented in the Mines area by two main sets of retrograde schist zones: the Globe-Vauxhall set, trending NE and dipping at 60°-70° to the SE, and the British-De Bavay set, trending N-S and dipping at 65° to the E. It has long been recognized that these schist zones represent ductile faults, but several workers (Hobbs and Vernon, 1968) have cautioned against assuming that the deformation or displacement within the retrograde schist zones took place by shearing. The following discussion summarizes more detailed argument in Marjoribanks and others (1977) which indicates that simple shear has played a significant role in the deformation. The zones are thus legitimately termed retrograde shear zones.

The orebody and other lithological units are displaced across the British Shear, as also are various lithological units across the De Bavay Shear (Figure 2). The displacement in each case was inferred to be sinistral, NE-block-up by Gustafson, Burrell and Garretty (1950), the vertical movement being inferred mainly from the repetition of the proposed synformal closure in the ABM Potosi Gneiss. However, the uncertainty of this proposed closure (see above) weakens the argument of these authors. Nevertheless,

Boots (1972) recently estimated from displacement of rock units that the movement plan was sinistral, NE-block-up with horizontal and vertical components of 335 m and 610 m respectively.

The orebody becomes progressively closer to the Globe-Vauxhall Shear in a northeasterly direction, and finally enters the shear in the deeper levels of North Mine. Its drastic attenuation at this point, and its possible reappearance in sheared ground to the northeast (from recent exploration by NBHL), emphasizes the importance attached to estimates of displacement on the Globe-Vauxhall Shear. The horizontal displacement is difficult to assess because the shear is sub-parallel to lithological trends; most workers have proposed dextral movement, with strongly varying estimates of its magnitude (e.g. Gustafson and others, 1950; Garretty, 1957; Johnson and Klingner, 1976). Most workers suggest that the vertical component of movement is SE-block-up, from meagre evidence to date.

The relative orientations and movement plans of the British/De Bavay Shears and the Globe-Vauxhall Shear have prompted the notion that the two sets represent conjugate shears (Gustafson and others, 1950; Henderson, 1956; Ransom, 1969, p. 183). The attendant movement perpendicular to their steeply-plunging line of intersection would require a horizontal component of movement greater than the vertical component in each shear.

Consideration of structures within the shear zones themselves as a guide to movement direction has only recently been attempted. The results however have been of limited application. Ransom (1969) and Offler (1972) argued that the extensional microfabric of the retrograde mineral lineation indicated that it represented the direction of maximum extension in the deformational strain ellipsoid.

A study of schistosity, lineation and folds within the Globe-Vauxhall and associated shears in the northern leases, has permitted a re-evaluation of all the available information on the British, De Bavay and Globe-Vauxhall Shears. Detailed discussion of the evidence is presented in Marjoribanks

and others (1977), but the main conclusions are as follows:

(1) Contrary to reports by previous workers (e.g. Ransom, 1969) the retrograde schistosity is not invariably parallel to the walls of the shear zones. The pattern of orientation of schistosity and lineation within the zones is compatible with ductile simple shear (Ramsay and Graham, 1970), and the direction of maximum extension is sub-parallel to the lineation and thus is steeply-plunging within both sets of shear zones.

(2) Newly established lithological and structural correlations across the Globe-Vauxhall Shear indicate that the vertical displacement of marker units across the shear in the Northern Leases is 600-1000m, SE-block-up, with a possible "scissors" movement accounting for a decrease in vertical displacement along the shear in a southwesterly direction toward the Mines area. The horizontal displacement cannot be gauged from marker units.

(3) The sense of vertical displacement estimated from marker units is compatible with the direction of ductile simple shear inferred from the pattern of schistosity and lineation. The steep attitude of the shear direction suggests that the vertical component of movement is distinctly larger than the horizontal component. The steep-NE plunge of the shear direction in the Globe-Vauxhall Shear provides a dextral sense of horizontal movement.

(4) The evidence casts doubt on a conjugate shear relationship between the British/De Bavay Shears and the Globe-Vauxhall Shear, suggesting instead that most of the ductile movement has been parallel to their line of intersection.

(5) Microstructural, mesoscopic and large-scale relations all indicate that at least some of the deformation in the retrograde shear zones is related to D_3 deformation outside the zones. The shears may

represent the restriction of ductile deformation into narrow planar zones as the country rocks became more rigid in the waning phase of D_3 metamorphism and deformation. To the NW of Broken Hill these ductile zones tend to be concentrated in the hinge areas of tight antiforms separating broad, open F_3 synforms, and may represent water accumulation, and consequent weakening of the rocks, in these structural locations.

(6) A 70° south-plunging lineation on the Main Shear adjacent to the orebodies indicates that the dominant component of movement on this shear, as on the parallel Globe-Vauxhall Shear, was vertical.

STRATIGRAPHY

The presence of a tight to isoclinal fold, the Broken Hill Antiform, within the Mine Sequence necessitates a revision of this long-standing structural sequence. Furthermore, the determination of younging from graded bedding at numerous points permits the revised sequence to be stratigraphically ordered. The stratigraphic sequence in the Broken Hill Mines area is as follows:

Pelitic sillimanite gneiss

Psammo-pelitic sillimanite gneiss (Contains units of the Mine Sequence: Lode Horizon, BIF, amphibolite, Potosi Gneiss.

Granite gneiss

Thicknesses are very variable and are meaningful only in a comparative way: the pelitic sillimanite gneiss is at least 2 km thick in the Northern Leases, the psammo-pelitic sillimanite gneiss is of the order of 500 m thick, and the granite gneiss is of the order of 200 m thick.

The marker units within the psammo-pelitic sillimanite gneiss have not been stratigraphically ordered. This is for three reasons:

(1) F_1 folding has had an unknown effect on this part of the sequence.

(2) The relationship of the Potosi Gneiss lithology to the overall layering of the sequence is obscure, and may be transgressive in places. The Potosi Gneiss is believed to be partly the product of diagenetic c metasomatic alteration post-dating the formation of the stratigraphic sequence, hence original correlations may be masked. There is evidence that there may have been alteration of other units (V. Wall, personal communication, 1976), complicating the picture still further.

(3) The structural model of the Mines area suggests that in the North Mine area, BIF horizons on the SE limb of the Broken Hill Antiform may be stratigraphically equivalent to Lode Horizon on the NW limb. Similar lateral correlations can be made in the Southern Mines. For example, Johnson and Klingner (1976) point out that the Middle Potosi Gneiss has a gradational relationship with the upper zinc lodes and that BIF horizons may occur in the along-strike stratigraphically equivalent position to both lead lodes and zinc lodes.

Local sequences may be erected where structural data and graded bedding data provide sufficient control, but at our present state of knowledge the inadvisability of correlations over the whole Mines area should be stressed. Several correlations are, however, implicit in the structural model. Specifically these are the Upper Granite Gneiss with the Lower Granite Gneiss; the Lode Horizon with the Burke Street lode NW of the Hangingwall Synform (Southern Mines); and "Main" Lode Horizon with "Upper" Lode Horizon (North Mine).

Nevertheless the Lode Horizon is only known to the NW of the Broken Hill Antiformal axis and has no definite correlatives on the SE limb. This can be explained by supposing that units on the SE limb of the Antiform are attenuated and dislocated along an F_2 slide surface and that the Lode Horizon will appear again at depth on the SE side of the slide, as illustrated in the

block diagram of Figure 27. The presence of such a slide is indicated by the intense S_2 schistosity of the Belt of Attenuation though there is no direct evidence of any F_2 displacement along it. It is probably analogous to the F_2 slide, for which good evidence exists, along the SE limb of the Hangingwall Synform. An alternative or complementary hypothesis, which will be elaborated upon in the concluding section, is that the thick Lower and ABM Potosi Gneiss units and associated BIF units, which occur only on the SE limb of the Broken Hill Antiform, are the stratigraphic equivalents of the Lode Horizon, and represent a facies change which has controlled the position of the Antiformal axis.

SUMMARY AND SYNTHESIS OF THE STRUCTURE

Figs. 27 and 28

1. Three major metamorphic and deformational episodes, each resulting in macroscopic folds, can be defined in the Mines area. These episodes and the penetrative structures associated with them are labelled F_1, F_2 and F_3. F_1 and F_2 were accompanied by the growth of high-grade metamorphic minerals of sillimanite-grade: F_3 was accompanied by a retrograde metamorphic event leading to the growth of biotite, muscovite and chlorite.

2. The entire Mines area lies on the single inverted limb of a regional isoclinal F_1 fold-nappe. The hinge of the nappe lies outside the Mines area.

3. Since F_1 folds are isoclinal and recumbent, the attitude of rock units, bedding surfaces and S_1 schistosity is principally a reflection of the second and third deformational events. Three major F_2 folds are present in the Mines area and its immediate vicinity. From NW to SE they are the Hangingwall Synform, the Broken Hill Antiform and the Broken Hill Synform. The folds have axial planes dipping at steep to moderate angles to the NW and, with the exception of a domain between British Shear and Round Hill, plunge to the SW. In the latter area, F_2 folds plunge to the NE, the

reversal of plunge from the regional plunge direction taking place through the horizontal.

4. The Mine Sequence occupies the core of the Broken Hill Antiform. In the Southern Mines area the Antiform is very tight and has a restricted hinge area. Closure of rock units about this hinge cannot be demonstrated, but the hinge is defined by a change in the sense of asymmetry of minor parasitic F_2 folds and a change in stratigraphic younging directions across the Mine Sequence. In the North Mine and the Northern Leases, similar mesoscopic structures define the axis of the Broken Hill Antiform, but in these areas the fold is more open and can also be demonstrated by a sub-surface closure of rock units. The SE limb of the Antiform contains a zone of high strain called the Belt of Attenuation. The strain is less intense in the North Mine where a macroscopic fold pair of uncertain age, called the Footwall Synform and Alma Antiform, can be distinguished.

5. F_2 structures were refolded and overprinted by the F_3 event. F_3 folds are generally open with vertical or steep SE-dipping axial planes and are associated with the development of intense, planar, retrograde schist zones. The schistosity in these zones is parallel or sub-parallel to S_3. The regional F_3 fold structure is defined by the progressive shallowing of the dips of S_2 when they are traced to the NW away from the Mines area. This open folding is part of a regional F_3 monocline, the other steep limb of which is located in the Sundown area 5 km to the NW of Broken Hill. A smaller but tighter F_3 fold pair is located in the Southern Mines area, in the area of the Western Antiform and Eastern Synform, which plunges to the SW parallel to adjacent F_2 axes. The Synform is a tight structure which may be replaced by a retrograde shear zone known as the Main Shear. The F_3 fold pair is not positively identified north of the British Shear, although in North Mine the open fold in S_2 schistosity may correspond to the F_3 fold pair.

6. Numerous post-F_3 mesoscopic folds are present throughout the Mines area. These folds are the dextral SW-plunging F_4 folds prominent in North Mine and the Northern Leases, and dextral west-plunging folds (possibly equivalent to F_4) present in the Southern Mines. The post-F_3 folds have no associated macroscopic structures or penetrative schistosities.

7. The orebodies lie within a conformable horizon known as the Lode Horizon. Within this horizon the individual orebodies form a stack of markedly elongate lenses. In the Zinc Corporation and NBHC Mines, the elongation of these lenses is coincident with the hinges of co-axial F_2 and F_3 folds, and is everywhere parallel to the dominant high-grade mineral lineation L_{1-2} within the enclosing rocks. In addition, ore also occurs within transgressive retrograde schist zones, such as the Main Shear, which are sub-parallel to the F_3 axial plane. Graded beds indicate that in the Southern Mines all of the zinc lodes and at least part of the lead lodes lie on the NW limb of the Broken Hill Antiform, close to its hinge-plane. The lead lodes lying in the Belt of Attenuation may be in the antiformal hinge itself.

In North Mine the Lode Horizon is not affected by any major F_3 folds and the ore lenses lie within the hinges of, and outline, a NE-plunging parasitic F_2 fold pair on the NW limb of the Broken Hill Antiform. The elongation of the ore lenses is coincident with the hinges of these folds and is parallel to the NE-plunging high-grade mineral lineation L_1 in the enclosing rocks. Thus, although in both North Mine and in the Southern Mines the orebodies plunge parallel to the high-grade mineral lineation and to F_2 fold axes, they occupy different positions in the two areas with respect to the Broken Hill Antiform hinge. The transition between the two areas must take place in the central part of the field, south of British Shear - an area where unfortunately little mesoscopic data is available. It is thus not known whether the transition from ore in the structural location of NBHC and Zinc Corporation Mines, to ore in the

structural location of North Mine, takes place through a gentle but progressive obliquity between ore lens and F_2 axis throughout the field, or whether the progression takes place over a more limited area in the central part of the field. If the F_2 belt of attenuation represents a slide, this may be responsible for bringing the orebody into the dislocated hinge area of the Broken Hill Antiform at the south end of the field.

8. The new structural model of the Mines area is presented in the sections of Figures 6 to 13 and in the block diagrams of Figures 27 and 28. The block diagrams represent a synthesis of information derived from lithological mapping, mesoscopic deformational fabrics and stratigraphic younging directions.

IMPLICATIONS FOR THE GENESIS OF THE OREBODY

During the past twenty-five years there has been an increasing body of opinion in favour of the view that the Broken Hill orebody is stratiform and essentially syngenetic. An exhalative sedimentary process (White, 1968) is usually envisaged but the relative importance of volcanic and non-volcanic processes in the generation of the exhalative fluids is debatable (for example, Stanton, 1972; Both, 1973).

Various aspects of the structural relations have been discussed by many authors and the various hypotheses have been reviewed by Both and Rutland (1976). Most authors have favoured structural control of the emplacement of the ore (for example, Andrews, 1922; Kenny, 1932; Gustafson and others, 1950; Lewis and others, 1965; Hobbs, 1966), but King and O'Driscoll (1953, p. 600) first suggested that the "ore deposition preceded rather than followed the development of the structure which the deposit now occupies". The conclusions of Hobbs (1966) and Hobbs and others (1968) were quite incompatible with this view in inferring not only that the orebody in North Mine was probably originally unconformable but also that the folds in the orebody in North Mine were unrelated to those in the Southern Mines.

The present studies go far towards resolving the apparent contradictions between the geochemical and structural evidence relating to the genesis

of the orebody, and some of the main points are now discussed.

Stratigraphic Conformability of the Orebody

Most authors have accepted the view that the linear orebody lies in a conformable Lode Horizon, since the Lode Horizon is evidently concordant with gross layering of the enclosing lithologies. This view has been contested by some on the grounds that the apparent conformability may be due to structural transposition (Hobbs, 1966; Ransom, 1968). However, the recognition of metamorphosed graded bedding in the metasediments has allowed the layering to be definitely identified as deformed bedding which shows consistent younging over large areas. The apparent conformability is therefore real and not due to transposition. The present structural studies have also allowed this conclusion to be re-asserted in the North Mine area where Hobbs (1966) had provided further persuasive evidence that the orebody was probably stratigraphically unconformable.

Hobbs' (1966) structural interpretation of the North Mine area rested on the assumption that folds, which he called Group 1 and defined as representing the first recognizable deformation, were everywhere parallel to the SW-plunging sillimanite lineation in the wallrocks. This meant that the NE- plunging orebody was grossly discordant to the Group 1 folds in the wallrocks. In the light of his assertion that the orebody plunge also reflected a Group 1 fold axis, the orebody was evidently grossly discordant to layering prior to the first recognizable deformation. Hence the orebody was either originally stratigraphically unconformable, or Group 1 folding was preceded by a phase of deformation which by some process rendered the orebody discordant to layering.

Proponents of a stratigraphically conformable, syngenetic origin were forced to the latter conclusion. Hobbs presented a hypothetical model in which strong deformation prior to Group 1 folding created a new transposed layering in the wallrocks, juxtaposed in an axial-plane orientation against the orebody which was assumed to retain a folded-layer form. Subsequent Group 1 folding about appropriately oriented axial planes produced SW-plunging folds in

the wallrock layering and NE-plunging folds in the orebody. Hobbs stated, however that there was no evidence for this model of early transposition, thereby implying that the original orebody was stratigraphically unconformable.

Hobbs' measurements of structural features in the North Mine area provide a framework in which we can reinterpret the structure in the light of the new observations presented in this paper. The F_2 fold pair outlined by the orebody is parallel to the overall NE plunge of mesoscopic F_2 folds in surface outcrop. These folds, and the orebody, are inferred to be parallel to the L_1 mineral lineation and strongly oblique to the SW-plunging L_2 mineral lineation in the wallrocks. The open folds (Hobbs' "Group 2" folds) which refold small F_2 folds and the orebody are F_4 folds, with axial planes dipping moderately to the west and lacking any penetrative S-surface. These folds account for most of the refolded lineations (now known to be L_1 and L_2) observed by Hobbs.

There is now undisputed evidence of a strong deformation (F_1), mainly in the form of a widespread layer-parallel schistosity, which predated the first recognizable deformation of Hobbs (now F_2). The effect of this deformation on the ore, apart from the probability that it strongly localized the mineralization in an L_1 orientation, is unknown. Nevertheless, the evidence that the tabular orebody lies within the conformable lode horizon, and is parallel to, and folded around F_2 axes, indicates that it is concordant with layering in the enclosing wallrocks. The confirmation, from sedimentary structures, that the layering represents bedding establishes the gross stratigraphic conformability of the North Mine orebody. It should perhaps be emphasized that the present study gives no information on the detailed relationships which may indicate local discordance between ore and bedding (for example, Maiden, 1976).

Stratigraphic position of the Lode Horizon

Thus it is now beyond dispute that the orebody lies in a restricted stratigraphic interval known as the Lode Horizon. The further demonstration that the major F_2 fold structures are downward-facing permits recognition of the fact that the lead lodes were deposited above the zinc lodes, thus removing an apparent geochemical anomaly. Moreover the Lode Horizon is seen to lie at the position of an important change in the stratigraphic succession. The rocks of possible volcanic origin (Potosi Gneiss, granite gneiss and amphibolites) almost all lie stratigraphically below or within the Lode Horizon in association with more siliceous metasediments. According to the present structural interpretation only the Middle Potosi of Johnson and Klingner (1976) may be stratigraphically above the orebody, and even then, there is a very close relationship. The metasediments stratigraphically above the Lode Horizon on the other hand are distinctly more pelitic and lack possible meta-volcanic rocks. It is therefore possible to envisage a simple model of sedimentary-exhalative formation of the orebodies during the final stages of a phase of volcanism.

The recognition of a distinctive, thick unit of pelitic sillimanite gneiss stratigraphically overlying the Mine Sequence highlights the more psammitic nature of the latter and in particular the "halo" of siliceous country rocks (quartzites) around the Lode Horizon (Johnson and Klingner, 1976). This increase in pelitic character upward and away from the psammo-pelitic and siliceous rocks enclosing the sulfide mineralization, is comparable with the environment of sulfide mineralization in the Zambian Copperbelt. In the latter province, economic concentrations of sulfides occurring in psammitic rocks are thought to be partly dependent on permeability characteristics of the enclosing sediments, specifically greater permeability in the original arenitic lithologies (Binda, 1969; van Eden, 1974). In any approach to regional exploration at Broken Hill involving theories of dependence of sulfide deposition on the host lithology, recognition of the boundary between

the two units would be an important objective.

Original Sedimentary and Volcanic Lateral Facies Variations

The nature of original lateral facies changes is much more difficult to assess. The rocks have suffered high strains during several deformation episodes and dislocations of the original succession are also present. One of the most important problems in this connection is provided by the present linearity of the orebody. This is clearly regarded by some authors as essentially a primary sedimentary feature (for example Johnson and Klingner, 1976) although it conforms to the trend and plunge of late generation folds.

Since No. 2 lens almost always lies NW of No. 3 lens in a NW-dipping succession throughout the field it is clear that the orebody lies in the south-east limb of the Hangingwall Synform. Moreover the plunge variation exhibited by the orebody appears to be similar to that of the Hangingwall Synform. This is especially notable in the anomalous region between the British and de Bavay shears where the present work shows that F_2 fold axes diverge from L_2 lineations. The orebody follows the F_2 fold axes rather than the principal strain direction represented by the lineation. Since F_2 axes are also shown to be parallel to L_1 it seems likely that the linearity of the orebody was already present during F_1. Thus the linearity may be a consequence of strain during F_1 or it may have been inherited from a pre-existing sedimentary linearity.

Some attempt at assessing the nature of primary sedimentary and volcanic facies variations can be made by comparing the stratigraphic developments in the different limbs of the major F_2 structures, that is of the Hangingwall Synform and the Broken Hill Antiform. The task is rendered difficult by the very high strain which is known to be present in the SE limb of the Broken Hill Antiform and the added possibility of an F_2 slide on this limb. This high strain, and the possibility of unknown F_1 strain effects, would be expected to have eliminated some stratigraphic units and to have anomalously thickened others. The following correlation of stratigraphic units across the Broken Hill Antiform is based on the assumption that these strain effects can be ignored, and is therefore highly speculative.

It is clear that the thickest developments of Potosi Gneiss and amphibolites are in the south-eastern limb of the Broken Hill Antiform. Moreover thick developments of the Potosi Gneiss are limited to that part of the succession southeast of the main orebody. The main outcrop of Potosi Gneiss is a linear body plunging parallel to F_2 fold axes and the L_{1-2} lineation. The gap in outcrop between the two members, the Lower Potosi Gneiss in the south (SE of Zinc Corporation) and the ABM Potosi Gneiss in the north (SE of North Mine), is simply due to the main plunge culmination. The thick development of Potosi Gneiss in the S.E. limb of the Broken Hill Antiform correlates with the occurrence of the orebody in the NW limb of the Antiform. The significance of this correlation is enhanced by strong development of BIF units in the SE limb of the Antiform and only negligible development in the NW limb.

The relations can be interpreted as a facies change across the hinge of the Broken Hill Antiform. The Lode Horizon and associated thin Middle and Upper Potosi Gneisses in the NW limb may be laterally equivalent to the succession containing the thicker Lower and ABM Potosi Gneisses in the SE limb. The thin Upper and thick Lower Potosi are both stratigraphically below the orebody and are probably stratigraphic correlatives.

If the thickening is sedimentary in origin then the orebody could be regarded as originally fringing the thickest part of the Potosi Gneiss. This concept agrees well with the view of Mackenzie (1968), that on a more local scale there may be an inverse correlation between orebody and Potosi Gneiss development. Such arguments would support the view that sedimentary and volcanic facies boundaries were approximately parallel to fold trends, so that the linearity of the orebody may be based on an original sedimentary feature. It can hardly be doubted however, that it has been strongly accentuated and modified during the subsequent deformation episodes, and it is probable that had the orebody not been linear before the deformation, then it would have been so afterward (see below).

The alternative interpretation of the observed relations across the hinge of the Broken Hill Antiform is that the thickening of the Potosi Gneiss on the SE limb is purely structural, due to folding, and that any mirror

relationship with ore development on the NW limb is a result of structural control during F_1 or F_2 folding.

Structural Controls on the Orebody

The evidence discussed above indicates a primary stratigraphic control on the orebody in its restriction to a particular stratigraphic interval and, possibly, in its linearity within that interval. There can be no doubt however, that there have been substantial movements of ore and consequent modifications of the form of the ore lenses during the deformation history.

The structural controls on the position of the orebody can be summarized as follows:

1. There is a close relationship of the orebody to a fold culmination of macroscopic F_2 folds. The culmination is best demonstrated by the outcrop pattern of the Hangingwall Synform. The outcrop pattern of the Potosi Gneiss in the SE limb of the Broken Hill Antiform is here interpreted as an effect of the same F_2 culmination in a parasitic F_2 or coaxial F_1 fold structure.
2. Within the SE limb of the Hangingwall Synform the orebodies are related to a system of drag-folds which are here interpreted as F_2 folds in the northeast and as F_3 folds, co-axial with F_2, in the south-west. The superposed ore lenses are stacked between parallel axial-plane traces of these drag-folds, and follow their plunge. There is a tendency for the ore lenses to be substantially thickened in the fold hinges.
3. One of the more notable features of the structural control of the ore-body is the en echelon arrangement of No. 2 and No. 3 lens (the lead lodes) and the zinc lodes at the southern end of the field. Early development of the orebody was in No. 3 lens and subsequent development has followed the general plunge of 20°-25° to the south-west. However, the reduction of No. 3 lens and the incoming of No. 2 lens and of the zinc lodes all tend to be controlled by local plunges in the Western Antiform and Eastern Synform of about 40° (see O'Driscoll, 1953). The termination

of lead lodes in the eastern limb of the Eastern Synform follows a similar plunge of about 40°. Mackenz ie (1968) remarked that the steep plunge of the overwall of the Western Antiform in the lead lodes of NBHC Mine is related to the sedimentary pinching out of a body of garnet quartzite within the lode. Johnson and Klingner (1976, p. 477) also inferred that the thickly developed portions of both their Lower and Middle Potosi Gneisses, which plunge south-westwards at about 40°, reflected sedimentary thickenings. However the Lower and Middle Potosi Gneisses are now interpreted to lie in opposite limbs of the Broken Hill Antiform. The 40° plunges are therefore not easily interpreted as being due to primary sedimentary variations, since in that case the plunges should be different in opposite limbs of the F_2 fold about which they have been folded. It is therefore tentatively inferred that the plunge variations are purely a structural feature reflecting inhomogeneous strain during or following the F_2 deformation. As such they are analogous to the macroscopic F_2 plunge culmination of the whole Mines area.

4. A zone of attenuation is generally present on the SE side of the orebodies and is attributed to both F_2, superposed F_3 and retrograde schist zone effects which together produced a dislocation in the hinge of the Broken Hill Antiform at the SW end of the field. The discontinuous Main Shear can be correlated with the F_3 event and with development of the retrograde schist zones. The ore shows its greatest vertical extent within the Main Shear and the ore shoots generally have nearly vertical axes. The late deformation has also controlled the development of steeply pitching rhodonitic zones in the North Mine orebodies.

5. The orebody is related to a distinct strike change, which in turn is closely related to the principal retrograde schist zones. Thus the plunge culmination in the orebody occurs where the Lode Horizon becomes parallel to the Globe-Vauxhall Shear Zone. The north-east

plunging segment of the orebody occurs where the strike has the largest easterly component, between the British and De Bavay Shears.

At first sight the concept that the linearity of the orebody may be based upon a primary stratigraphic feature appears to be incompatible with the fact that the orebody now has a doubly plunging form, approximately within the axial plane of the structures formed subsequent to the major stratigraphic inversion of F_1. An important conclusion of the present work however has been that L_1 lineations are essentially co-axial with F_2 fold plunges and with the orebody not only in the Southern Mines but also in North Mine. The L_2 lineation on the other hand is not parallel to these structures in the anomalous region around North Mine, but maintains the more normal SW plunge.

It follows therefore that the anomalous NE plunge in North Mine is largely unrelated to strain associated with F_3 or retrograde schist deformations since L_2 has not been rotated. Rather the plunge variation apparently reflects inhomogeneous strain of L_1 during the F_2 deformation. The margins of the zone in which the anomalous plunge developed became the locus of the later British and De Bavay retrograde schist zones.

Thus it is clear that the present linearity of the orebody has existed at least since the F_2 deformation. Some migration of the ore undoubtedly occurred during this phase to produce the observed thickening in F_2 fold hinges. It is possible that much larger migration of ore took place during this phase so that the linearity of the orebody is essentially an F_2 feature. However, since the ore follows the F_2 fold axes and the L_1 lineation even where these diverge from the L_2 lineation, it seems more likely that the linearity of the orebody was already present during F_1. If this is accepted it is also possible, but by no means necessary, to suppose that the linearity is based on a primary stratigraphic feature.

The stages of evolution of the orebody can be summarized as follows:

(1) Deposition of metal sulfide in a zone of uncertain shape within a stratigraphic interval at the end of a phase of volcanism.

(2) Strong accentuation of any original linearity of the mineralization in a direction parallel to L_1, during F_1, when the stratigraphic succession was inverted.

(3) F_2 folding coaxial with L_1, with major drag-folding localized by the orebody. Formation of main plunge culmination and strike variation. Migration of sulfide mineralization into hinge zones.

(4) F_3 drag folding co-axial with F_2 but with different axial-plane dip, modifying main orebody folds at southern end of field. Migration of sulfide mineralization into hinge zones with gentle or moderate plunges.

(5) Development of retrograde schist zones probably associated with F_3, and of Main Shear ore with steeply pitching ore shoots. Local modifications of trend and plunge of F_2 and F_3 drag folds.

(6) Recrystallization of ore in retrograde schist zones.

CONCLUSIONS

The first important result of this work is the re-establishment of an antiformal structure between the Broken Hill and Hangingwall Synforms in broadly the same way as was envisaged by Andrews (1922) and by Gustafson and others (1950). This has been possible because of the recognition and separation of phases of superposed folding: the folds which were thought to disprove the existence of the Broken Hill Antiform (for example Lewis and others, 1965) are now seen as superposed on it.

Even more important however is the recognition, for the first time, that the major F_2 folds are downward-facing. This leads to a completely new reconstruction of the environment of deposition of the orebody in keeping with the new stratigraphy. The orebody formed at the end of a period of volcanism

and was succeeded by deposition of a thick unit of non-volcanogenic sediments.

The evidence that F_1, F_2 and F_3 are generally co-axial largely removes contradictions between the geochemical and structural evidence relating to the origin of the orebody. Furthermore the new interpretation of the anomalous area between the British and de Bavay Shear Zones re-establishes the stratigraphic conformability of the orebody and the enclosing Lode Horizon. The way is thus now open for a combined stratigraphic and structural approach to exploration.

Implicit in the postulated sequence of events is the general localization of the orebody by primary stratigraphic features. The details of orebody thickness and shape however are controlled by the subsequent deformation history. The present orebody occurs on the NW limb of the Broken Hill Antiform. The possibility of a similar body occurring in the SE limb of the Broken Hill Antiform due to either stratigraphic or structural controls, deserves further consideration in spite of the structural complexity there.

ACKNOWLEDGEMENTS

We wish to acknowledge many discussions with and whole-hearted co-operation from Mines personnel, particularly Ralph Burkett, Duncan Archibald, Wolf Leyh and Bill Widdop (North Broken Hill Ltd.), David Klingner and Geoff Scott (CRA Exploration Pty. Ltd.), and Trevor Stevenson (Minerals Mining and Met allurgy). These companies gave permission to use and publish mine data, particularly drilling sections. John Anderson and Geoff Scott collected some of the drillcore younging data in the Southern mines. We also thank our colleagues in the Department of Geology at the University of Adelaide for helpful discussions, particularly Dick Glen. We are indebted to Milly Swan and Judy Laing for their painstaking drafting.

The research was funded largely by the Broken Hill Mining Managers' Association, to whom we record our thanks. One of us (W.P.L.) was supported by an Australian Postgraduate Research Award.

REFERENCES CITED

Andrews, E.C., 1922, The geology of the Broken Hill district: Geol. Survey N.S.W. Mem. 8, 432 pp.

Binns, R.A., 1964, Zones of progressive regional metamorphism in the Willyama Complex, Broken Hill district, New South Wales: Jour. Geol. Soc. Aust., v. 11, p.283-330.

Boots, M.K., 1972, The textural, mineralogical and chemical effects of retrograde metamorphism on the main lode horizon, Broken Hill, N.S.W.: Unpubl. Ph.D thesis, Univ. of N.S.W.

Borradaile, G.J., 1972, Variably oriented co-planar primary folds: Geol. Mag., v. 109, p. 89-98.

Both, R.A., 1973, Minor element geochemistry of sulphide minerals in the Broken Hill Lode (N.S.W.) in relation to the origin of the ore: Mineral Deposita, v. 8, p. 349-369.

Both, R.A., and Rutland, R.W.R., The problem of identifying stratiform ore bodies in highly metamorphosed terrains: the Broken Hill example (in press).

Carruthers, D.S., and Pratten, R.D., 1961, The stratigraphic succession and structure in the Zinc Corporation Ltd, and New Broken Hill Consolidated Ltd, Broken Hill, New South Wales: Econ. Geology, v. 56, p. 1088-1102.

Garretty, M.D., 1957, Another lode at Broken Hill ...? : Chem. Eng. Min. Review, v. 50, p. 36-41.

Glen, R.A., and Laing, W.P., 1975, The significance of sedimentary structures in the Willyama Complex, New South Wales: Proc. Aust. Inst. Min. Metallurgy, v. 256, p. 15-20.

Gustafson, J.K., Burrell, H.C., and Garretty, M.D., 1950, Geology of the Broken Hill ore deposit, Broken Hill, N.S.W., Australia: Geol. Soc. America Bull., v. 61, p. 1369-1438.

Henderson, Q.J., 1953, North Broken Hill mine: Fifth Empire Min. Met. Congress, v. 1, p.627-649.

Henderson, Q.J., 1956, Geological exploration at North Broken Hill Ltd: Proc. Aust. Inst. Min. Metallurgy, v. 180, p. 1-37.

Hobbs, B.E., 1966, The structural environment of the northern part of the Broken Hill orebody: Jour. Geol. Soc. Aust., v. 13, p. 315-338.

Hobbs, B.E., Ransom, D.M., Vernon, R.H., and Williams, P.F., The Broken Hill orebody, Australia. A review of recent work: Mineral. Deposita, v. 3, p. 293-316.

Hodgson, C.J., 1974, The geology and geological development of the Broken Hill lode in the New Broken Hill Consolidated mine, Australia. Part I: structural geology: Jour. Geol. Soc. Aust., v. 21, p. 413-430.

Johnson, I.R., and Klingner, G.D., 1976, Broken Hill ore deposit and its environment: In Economic Geology of Australia and Papua New Guinea, ed. C.L. Knight, p. 476-491.

Kenny, E.J., 1932, The Broken Hill lode - its geological structure: Proc. Aust. Inst. Min. Metallurgy, v. 87, p. 217-245.

King, H.F., and O'Driscoll, E.S., 1953, The Broken Hill lode: Fifth Empire Min. Met. Congress, v. 1, p. 533-577.

Laing, W.P., 1977, Structural interpretation of drillcore from folded and cleaved rocks: Econ. Geology, v. 72 (in press).

Lewis, B.R., Forward, P.S., and Roberts, J.B., 1965, Geology of Broken Hill lode, reinterpreted: Eighth Commonwealth Min. Met. Congress, v. 1, p. 319-332.

Mackenzie, D.H., 1968, Lead lode at New Broken Hill Consolidated Ltd: In Broken Hill Mines - 1968, ed. M. Radmanovich and J.T. Woodcock, Monograph Series No. 3, Aust. Inst. Min. Metallurgy, p. 161-169.

Maiden, K.J., 1976, Piercement structures formed by metamorphic mobilisation of the Broken Hill orebody: Proc. Aust. Inst. Min. Metallurgy, v. 257, p. 1-8.

Marjoribanks, R.W., Glen, R.A., Laing, W.P., and Rutland, R.W.R., 1977: Structure of the Willyama Block and of the Broken Hill orebody. Spec. Publ. Centre for Prec. Research, Univ. of Adelaide (in press).

O'Driscoll, E.S.T., 1968, Notes on the structure of the Broken Hill lode, and its tectonic setting: In, Broken Hill Mines - 1968, ed. M. Radmanovich and J.T. Woodcock, Monograph Series No. 3, Aust. Inst. Min. Metallurgy, p. 87-102.

Pidgeon, R.T., 1967, A rubidium-strontium geochronological study of the Willyama Complex, Broken Hill, Australia. Jour. Petrology, v. 8, p. 283-324.

Ramsay, J.G., and Graham, R.H., 1970, Strain variation in shear belts: Can. Jour. Earth Sci., v. 7, p. 786-813.

Ransom, D.M., 1968, The relationship of lode shape to wall-rock structure in the southern half of the Broken Hill orebody: Jour. Geol. Soc. Aust., v. 15, p. 57-64.

Roberts, J.L., and Sanderson, D.J., 1974, Oblique fold axes in the Dalradian rocks of the Southwest highlands: Scottish Jour. Geol., v.9, p. 281-296.

Shaw, S.E., 1968, Rb-Sr isotopic studies of the mine sequence rocks at Broken Hill: In Broken Hill Mines - 1968, ed. M. Radmanovich and J.T. Woodcock, Monograph Series No. 3, Aust. Inst. Min. Metallurgy, p. 185-198.

Stanton, R.L., 1972, A preliminary account of chemical relationships between sulfide lode and "banded iron formation" at Broken Hill, New South Wales: Econ. Geology, v. 67, p. 1128-1145.

Stillwell, F.L., 1922, The rocks in the immediate neighbourhood of the Broken Hill lode and their bearing on its origin: Geol. Survey N.S.W. Mem. 8, p. 354-396.

White, D.E., 1968, Environments of generation of some base-metal ore deposits: Econ. Geology, v. 63, p. 301-335.

Additional Reference:

French, D., 1976, Structural, petrological and geochemical aspects of the Potosi gneiss and Lower amphibolite at Broken Hill, New South Wales. Unpubl. B.Sc (Hons) Thesis, Univ. of Adelaide.

PHOTOGRAPHIC FIGURES

For Fig. 19 see thesis Fig. 2-16
For Fig. 21 see thesis Fig. 3-19
For Fig. 23 see thesis Fig. 3-24
For Fig. 24 see thesis Fig. 3-30
For Fig. 25 see thesis Fig. 3-34
For Fig. 26 see thesis Fig. 3-40

OPPOSITE: Fig. 20 (top)
Fig. 22 (bottom).

FIGURE CAPTIONS

Figure 1. Geological map and section of Broken Hill region. Gn = granite gneiss, AG = "Alma" augen granite gneiss, P = Potosi granite gneiss; for other symbols see Figure 4.

Figure 2. Simplified geological map of the Broken Hill mines area after Johnson and Klingner (1976). The inferred trace of the Broken Hill Antiform is also shown. Ornamentation as in Figure 4.

Figure 3. Simplified longitudinal profile of the Broken Hill orebody looking northwest.

Figure 4. Geological map of the Southern Mines area. Structural data simplified from detailed mapping. Circled numbers are localities referred to in text.

Figure 5. Geological map of the North Mine and the Northern Leases. Structural data simplified from detailed mapping. For legend see Figure 4.

Figures 6 to 9. Serial geological sections from south to north through the Southern Mines area. Lithological data from CRA Exploration Pty. Ltd: younging data and structural interpretation from this study. For location of sections see Figure 4 and for legend see Figure 9.

Figures 10 to 13. Serial geological sections from south to north through North Mine and the Northern Leases. Lithological and structural data from this study, with insets demonstrating the kinds of structural interpretation employed. For location of sections see Figure 5 and for legend see Figure 9.

Figure 14. Geological section through Kintore shaft, South Mine, looking northeast (see Figure 4). Diagram shows possible relations between the ore lenses and the main structures in the southern and central parts of the field.

Figure 15. Generalized illustration of the main fold groups. The F_1 fold is hypothetical. Not depicted here (but see Figure 24) is the less common type of F_2 fold in which the lineation is oblique to the fold axis.

Figure 16. Orientation diagrams for the main structural elements in the Broken Hill region.

Figure 17. Orientation diagrams for the main structural elements in the Mines area. Sub-areas 1, 3, 4 and 5 represent the entire length of the Hangingwall Synform.

Figure 18. Relations between lineations and fold axes in the Mines area. In the "section", which represents a composite view of sections XX_1' and YY_1', the heavy line represents the F_2 fold axes and the fine lines represent the lineations as labelled. The crosses indicate granite gneiss units.

Figure 19. Two graded beds in drillcore, immediately above scale. Note strong S_1 schistosity parallel to bedding in pelitic bands.

Figure 20. F_2 fold profile, with penetrative S_2 schistosity defined by sillimanite and biotite. Belt or Attenuation, 21 level, Zinc Corporation Ltd.

Figure 21. S_1 metamorphic segregation foliation in granite gneiss, folded about F_2 folds. S_2 is defined by intermittent quartzo-feldspathic veins. ABM Potosi Gneiss, North Mine.

Figure 22. Crenulated fine sillimanite of S_1 overgrown by coarse sillimanite parallel to the axial plane of the crenulations (S_2). Scale represents 0.5 mm.

Figure 23. Outcrop showing S_1 schistosity face with L_1 sillimanite lineation plunging steeply to the right (NE) and L_2 lineation plunging moderately to the left (SW). L_1 is folded about an open F_4 fold (coaxial with L_2) at top of photograph. De Bavay quarry, North Mine.

Figure 24. Outcrop showing S_2 schistosity face in which the F_2 fold axis (parallel to the trace of layering) is oblique to the moderately-plunging L_2 sillimanite lineation (parallel to the pen). Location 7, Figure 5, looking southeast.

Figure 25. F_3 fold profiles in drillcore with finely penetrative S_3 schistosity defined by muscovite, biotite and chlorite. White aggregates are retrogressed aggregates of sillimanite from S_1 or S_2.

Figure 26. F_4 folds (plunging toward viewer and to the left) refolding F_2 fold in layering and S_1 (plunging gently to right, parallel to pen). Note diamond-shaped interference pattern under pen and the pegmatites marking the trace of the S_4 axial plane. NW of Lords Hill, North Mine.

Figure 27. Block diagram of the Southern Mines area, showing interpreted relations between the main marker units and the main structures. For simplicity the Globe-Vauxhall Shear and British Shear are shown dipping vertically and the Broken Hill Synform is omitted.

Figure 28. Block diagram of the North Mine area, showing interpreted relations between the main marker units and the main structures. For simplicity the pelitic sillimanite gneiss in the core of the Broken Hill Antiform, and the Broken Hill Synform are omitted.

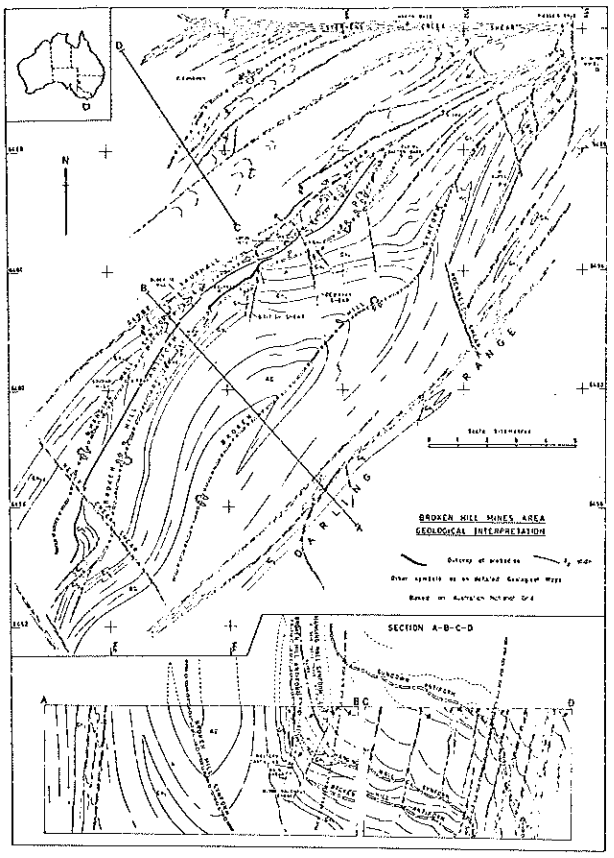

FIG. 1

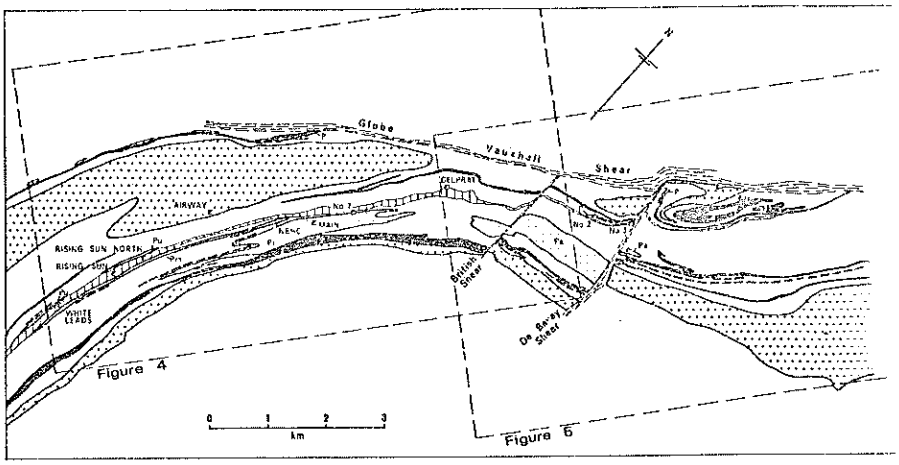

FIG. 2

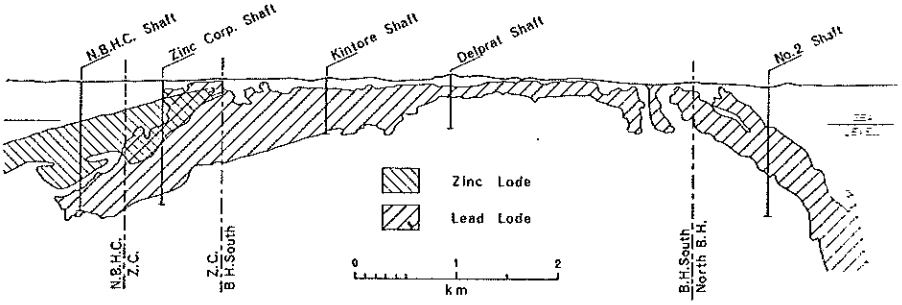

FIG. 3

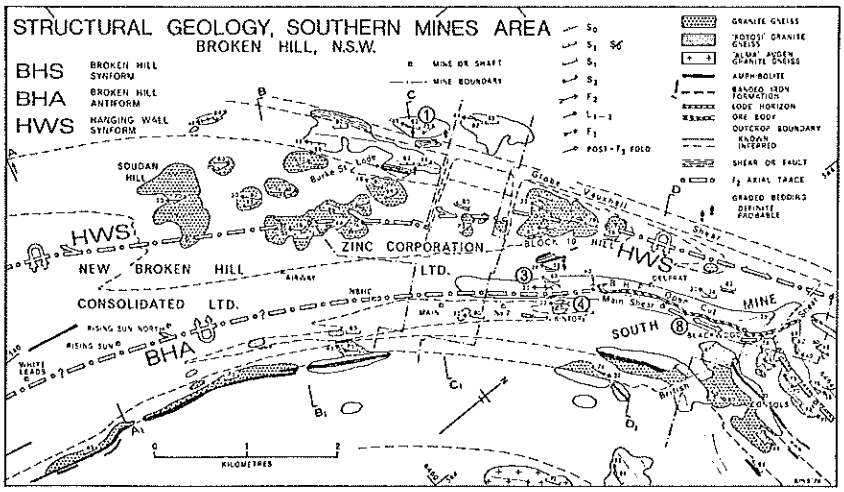

FIG. 4

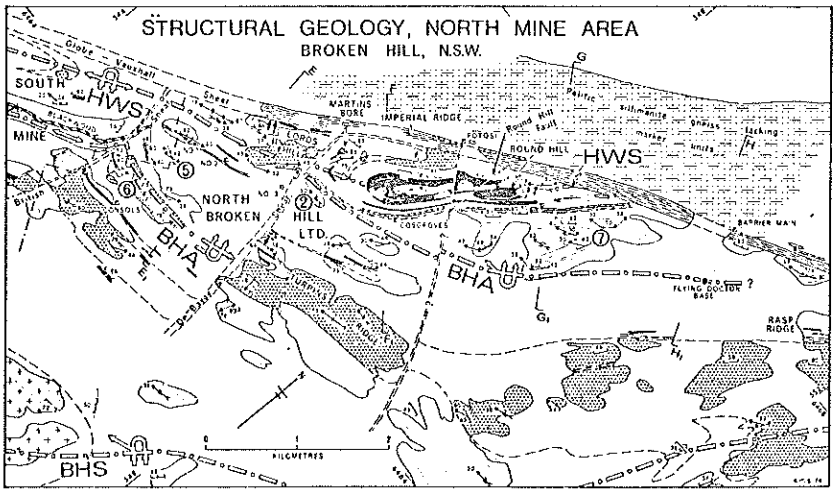

FIG. 5

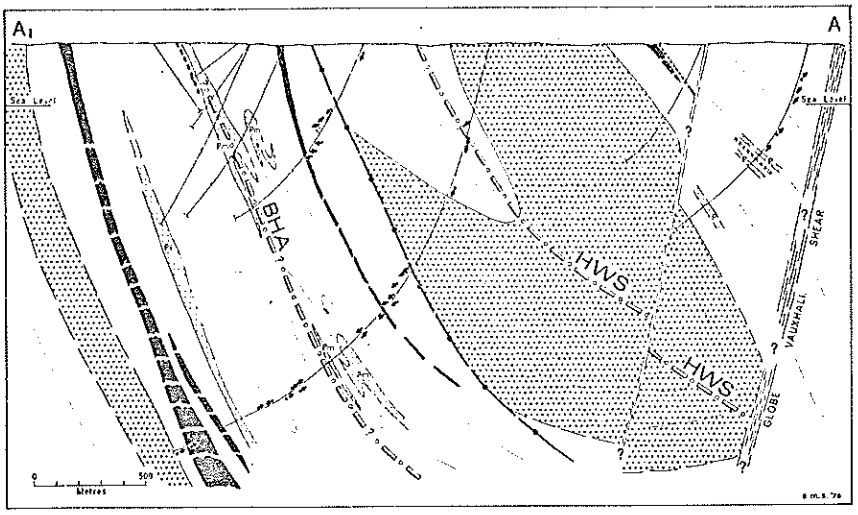

FIG. 6

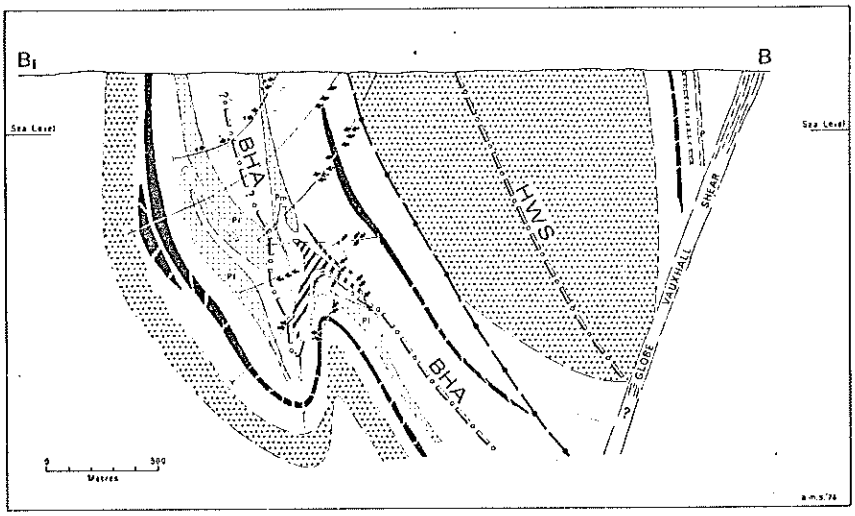

FIG. 7

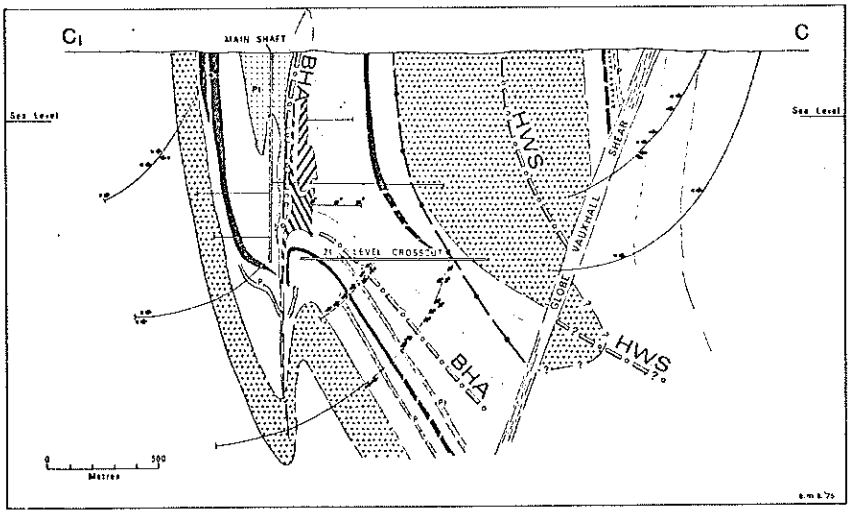

FIG. 8

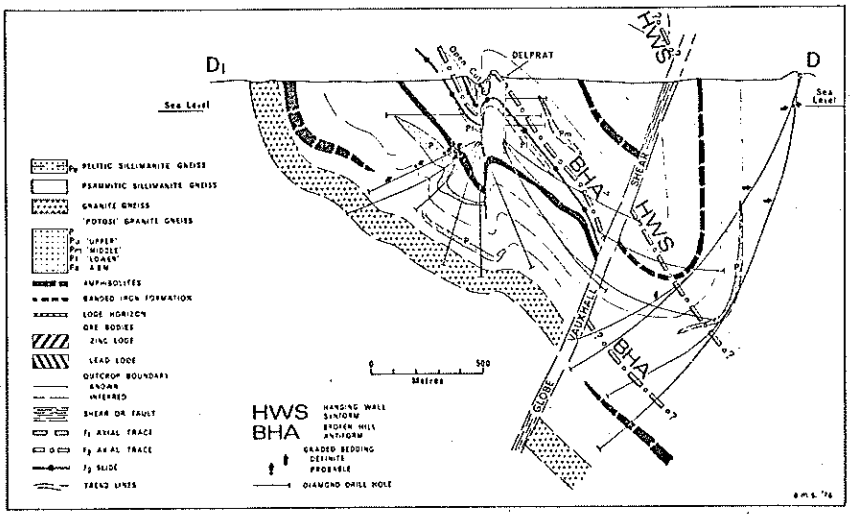

FIG. 9

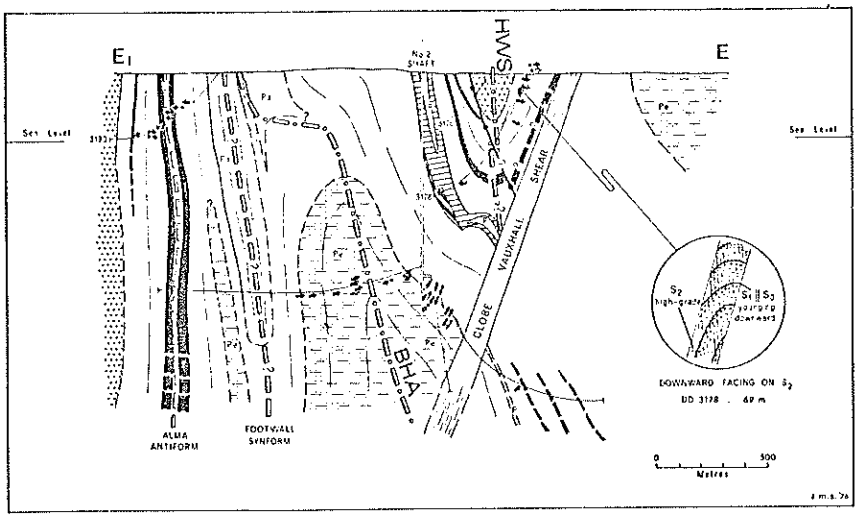

FIG. 10

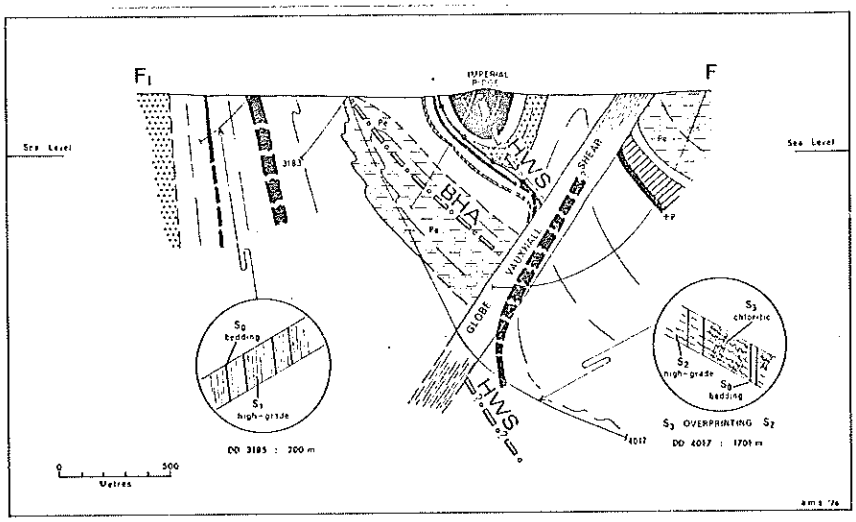

FIG. 11

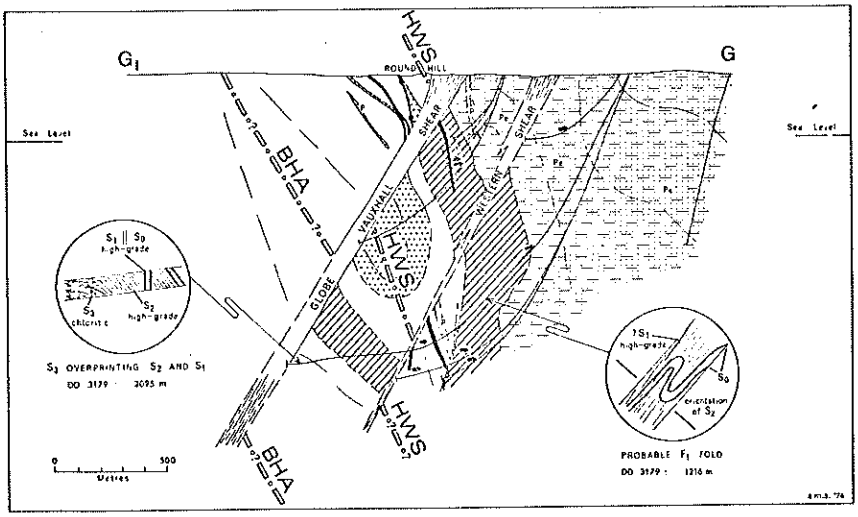

FIG. 12

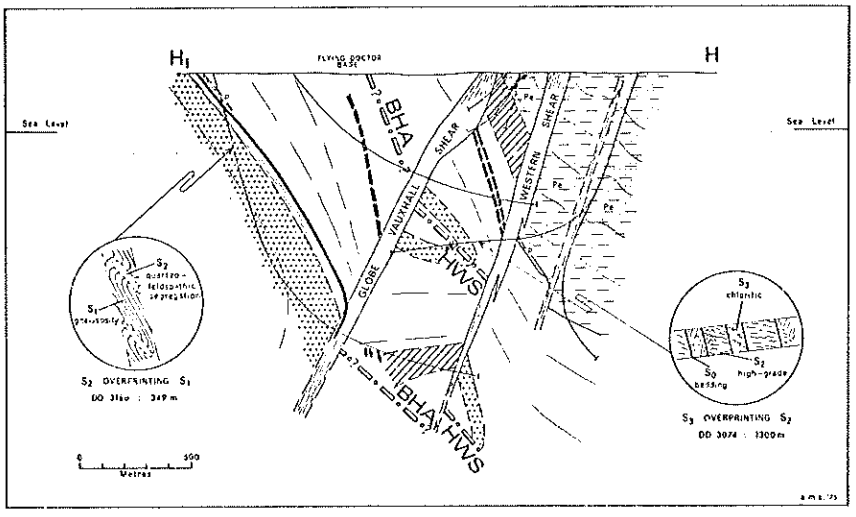

FIG. 13

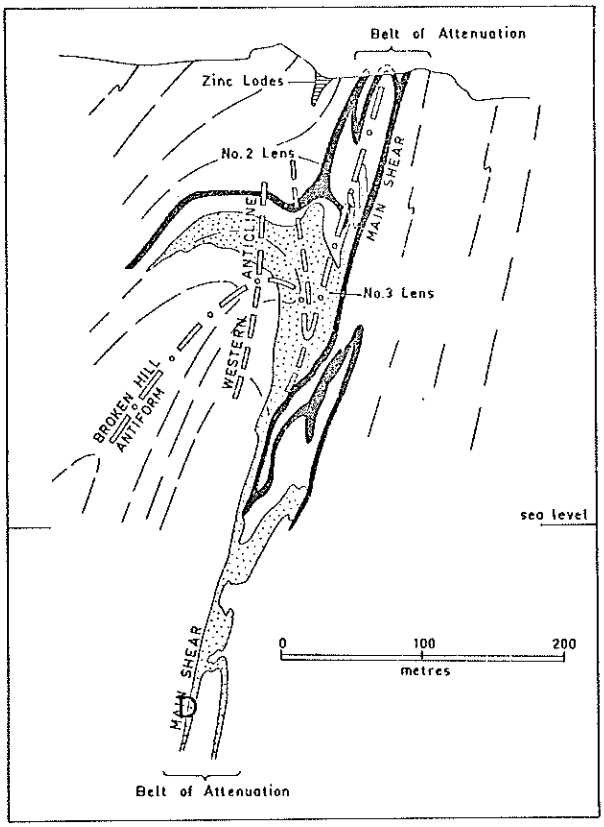

FIG. 14

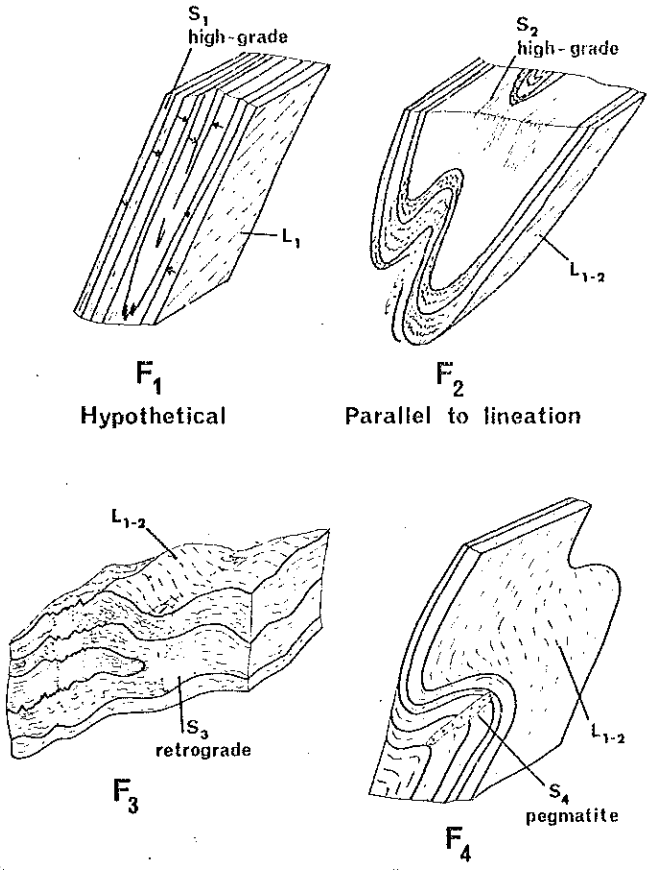

FIG. 15

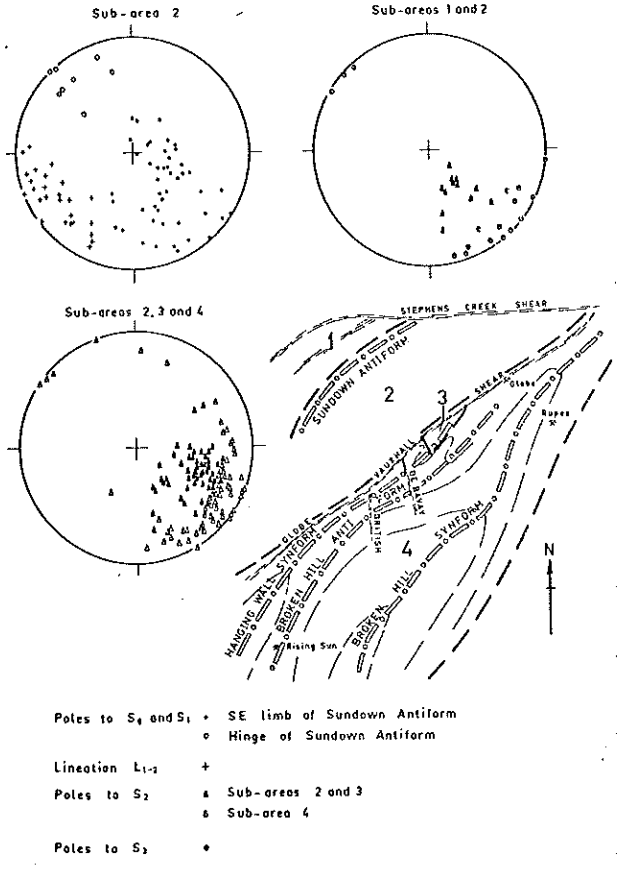

FIG. 16

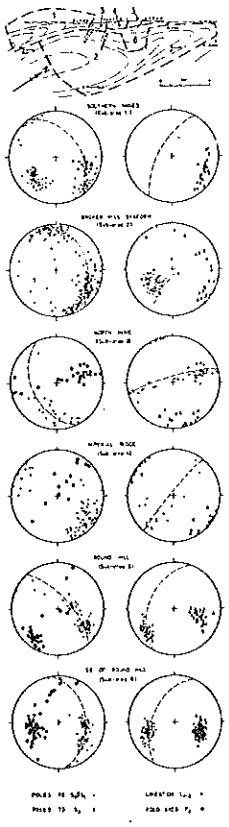

FIG. 17

FIG. 18

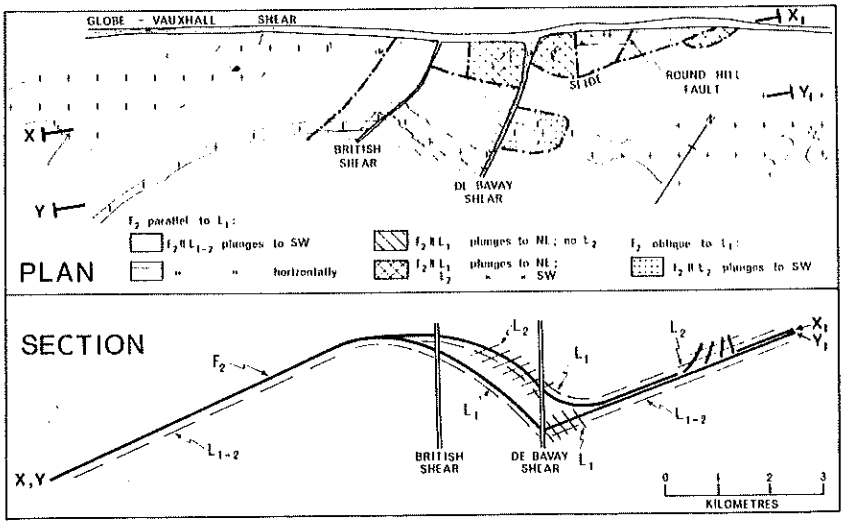

FIG. 27

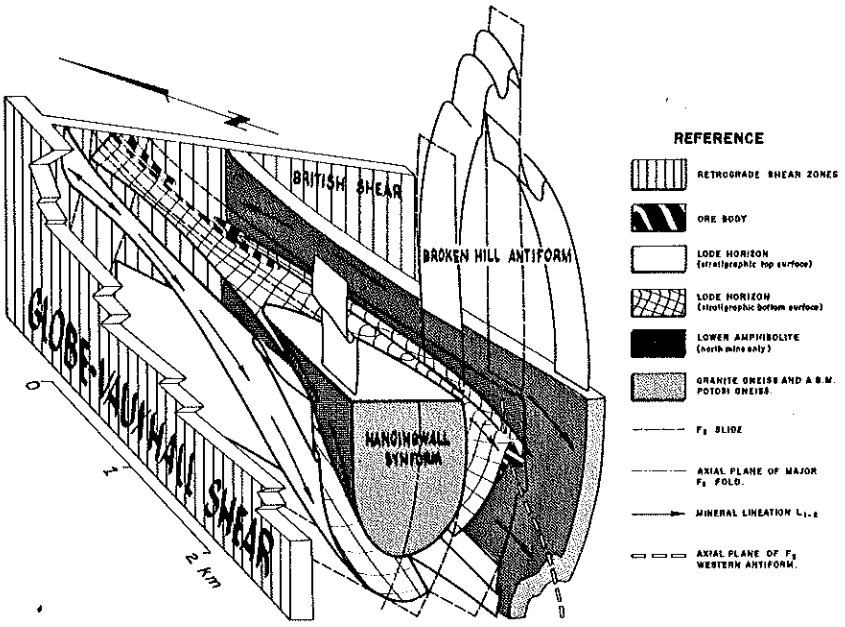

FIG. 28

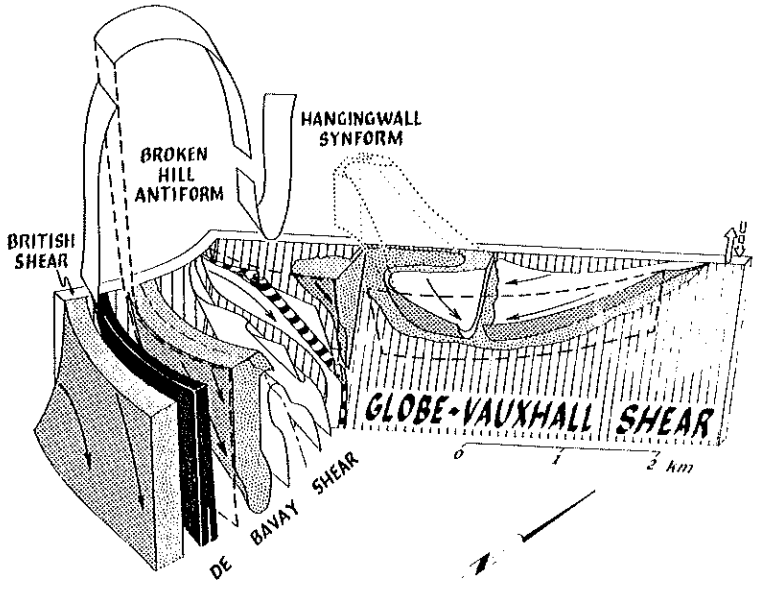

APPENDIX G

TECTONIC RELATIONSHIPS BETWEEN THE PROTEROZOIC GAWLER AND WILLYAMA OROGENIC DOMAINS, AUSTRALIA.

by

R.A. Glen, W.P. Laing, A.J. Parker and R.W.R. Rutland

(Manuscript of a paper published in the Journal of the Geological Society of Australia, vol. 24, no.1, 1977 under equal authorship.)

TABLE OF CONTENTS

ABSTRACT

Stratotectonic and morphotectonic data from the two principal exposed domains (pre-Adelaidean rocks) of the Gawler sub-province are used to characterise the Proterozoic Olarian Orogeny and to distinguish its effects from those of the later Phanerozoic Delamerian Orogeny.

The principal meta-sedimentary sequences in the Gawler domain and in the Willyama domain are inferred to have been deposited in a single broad zone of early Proterozoic shallow water sedimentation on older (presumed Archaean) continental crust. The sequence becomes more pelitic upwards and can be interpreted as a transgressive sequence with more distal facies to the east.

Three main phases of deformation can be recognized, and each phase has similar characteristics and age in both domains. D_1 and D_2 can be dated between 1850 and 1650 Ma, while D_3 appears to be about 1650-1540 Ma.

In high grade rocks D_1 gave rise to a layer-parallel schistosity, while D_2 is characterised by tight folds with a high grade axial plane schistosity. The whole sub-province was characterised by high geothermal gradients so that medium to high-grade metamorphism affected the lower parts of the succession before and during the D_1 and D_2 deformation episodes. No distinct tectonic zones can be recognized but large-scale stratigraphic inversions (i.e. nappe tectonics) during D_1 have been recognised only in the east of the Willyama domain. The higher parts of the stratigraphic succession are generally less deformed and exhibit only low-grade metamorphism.

D_3 produced relatively open, upright macroscopic folds and is characteristically associated with retrogression, but is demonstrably of

pre-Adelaidean age. The Gawler domain exhibits D_3 structures although it lies in the platform west of the Adelaide Geosyncline and was not affected by deformation during Adelaidean sedimentation or by the subsequent Delamerian Orogeny. A network of retrograde shear zones is the principal expression of post-Olarian deformation in the Willyama domain which forms part of the basement to the Adelaide Geosyncline

The trends of D_2 and D_3 folding in the two domains are similar and it is shown therefore that no large scale rotations have been produced by the Delamerian Orogeny. Large scale translations are not easily ruled out but are not required by the stratotectonic and morphotectonic characters of the two domains.

The Olarian Orogeny may have occurred in close proximity to a continental margin to the east and may thus be related to subduction processes. It differs from linear gneissic belts in Phanerozoic orogenies since it occurs in a more stable stratotectonic environment and over a wider area.

TECTONIC RELATIONSHIPS BETWEEN THE PROTEROZOIC GAWLER AND WILLYAMA OROGENIC DOMAINS, AUSTRALIA

1. INTRODUCTION

The Precambrian rocks of South Australia and adjacent New South Wales have long been divided into an older basement complex and a younger cover sequence of relatively undeformed and unmetamorphosed Precambrian sediments. This paper is concerned with the tectonics of the older basement complex and is based on studies of the two principal areas of exposure.

Within the Gawler Block, the platform basement has not been tectonically re-worked since the Olarian orogeny terminated about 1500 m.y. ago. The limits of the block are now defined where platform basement disappears under thick platform cover of various ages. Within the Block thin undeformed Adelaidean platform cover is preserved in the east, in the Gawler Platform. The platform basement (much observed by superficial cover) occupies the remainder of the Block and is known as the Gawler orogenic domain[1]. It is best exposed in the area of the Eyre Peninsula adjacent to Spencer Gulf.

East of the Torrens Hinge Zone (fig. 1) the Adelaidean cover sequence thickens into a major depositional area, commonly known as the Adelaide Geosyncline, which was folded in the Delamerian Orogeny. The Willyama orogenic domain (Tectonic Map of Australia and New Guinea, 1971) is the largest inlier within the Delamerian fold belt and forms the basement to the folded Adelaidean rocks in the Willyama Block. It is convenient to divide the Willyama orogenic domain into the Broken Hill and Olary sub-domains.

---

[1] The term 'orogenic domain' is used here (as on the Tectonic Map of Australia and New Guinea, 1971) to refer to individual exposed areas of basement rocks, the limits of which are now defined by younger cover of various ages. A hierarchy of tectonic units is also distinguished in the basement rocks. The largest are tectonic provinces, and these are sub-divided into sub-provinces and then into zones. Boundaries between zones are often obscured by younger cover but they may sometimes be exposed within the orogenic domains. Thus a domain is a geographic entity only and it may contain portions of different zones. Conversely a single tectonic zones may be recognised in more than one orogenic domain (cf. Rutland, 1976).

General correlation between the strongly deformed and metamorphosed rocks of the Gawler and Willyama domains was first proposed by Browne (1922) and a broad time equivalence has since been demonstrated on the basis of limited, but reliable, isotopic data (Compston and Arriens, 1968; Thomson, 1970, p. 195). Thomson (1969) noted "The approximate matching of the Olarian (Willyama) Orogenic Cycle with four phases of tectonism in the Eyre Peninsula area ... although the subtle age differences may indicate a migration of orogenic belts during the Precambrian". He also suggested (Thomson, 1976a) that "the apparent (Willyama) succession has some points in common with the Cleve Metamorphics of Eyre Peninsula".

The two domains are grouped on the Tectonic Map of Australia and New Guinea (1971) in the Central Australian Orogenic Province. Rutland (1973a) suggested a reclassification of the main Proterozoic tectonic province of Australia into three main divisions, the Arunta sub-province in the North being separated from the Gawler sub-province in the south by the younger Musgrave-Fraser sub-province. The Arunta and Gawler sub-provinces both display a major Proterozoic orogeny, characterised by plutonism, metamorphism and deformation in the range 1850-1650 Ma, and both show a tendency for isotopic dates of plutonism and metamorphism to decrease from west to east.

In the Arunta sub-province, the major orogeny affects an early Protero zoic ('Nullaginian' of Dunn, Plumb and Roberts, 1966) mobile belt sequence which generally displays only moderate metamorphism and deformation and below which an Archaean basement can locally be recognised.

In the Gawler sub-province, to which both the Gawler and Willyama domains belong, gneissic rocks and granites are much more abundant, and the sedimentary sequence is much more strongly deformed and metamorphosed.

Nevertheless the sedimentary sequence appears to be thinner and to have a much more platformal character than that in the Arunta sub-province.

Tectonic phases have been given different local names in the various orogenic domains (e.g. Thomson, 1969) but following Thomson (op.cit. p. 33) we refer to the sequence of deformational, metamorphic and plutonic events, recognised throughout the Gawler sub-province, as the Olarian orogeny.

The Gawler and Willyama domains are now approximately 300 km apart in a direction oblique to their regional strike and together they allow the stratigraphic succession and structural style to be observed for several hundred kilometres both along and across stike. Their study therefore offers the possibility of assessing the nature of Proterozoic orogeny for comparison with Phanerozoic orogeny. Moreover, since the Gawler domain lies outside, and the Willyama domain inside, the Delamerian fold belt, the study also allows an assessment of the effects of the Delamerian orogeny on the basement rocks (cf. Talbot, 1969). These effects include possible translations and rotations of basement blocks, as well as internal strains. In this paper we present a preliminary discussion of these problems, based on a summary of the stratigraphic and structural history of the Gawler and Willyama domains in the light of the recent work of the authors. Sedimentary and igneous rocks which post-date the Olarian orogeny are in places not discussed except in relation to the orogeny.

2. STRATIGRAPHIC RELATIONSHIPS

2.1 General nature of the sequence

Both the Gawler and the Willyama domains are characterized by high grade metamorphic basement rocks ranging from the lower amphibolite facies into the granulite facies (Binns, 1964; Tilley, 1921). The majority are of undoubted sedimentary origin since the lithological layering can be

shown to be not metamorphically derived, but original bedding, albeit deformed. In the Broken Hill sub-domain, lithological layering in a predominantly monotonous pelitic unit is defined as bedding by the presence of sedimentary structures (Glen and Laing, 1975). In the Olary sub-domain the recognition of sedimentary structures is obscured by large amounts of migmatites and pegmatites, but primary structures have been found (Parker, 1972; G. Pitt, pers. comm.; R. Wiltshire, pers. comm.). In the Gawler domain layering is more enigmatic. However, it is believed to represent deformed bedding because -

(1) individual units can be traced for tens of kilometres,

(2) a variety of primary rock types are recognised (quartzite, dolomite, pelite, iron formation), and

(3) local sequences can be correlated over large areas.

The rocks have been subjected to periods of intense deformation, and consequently much of their original character has been destroyed. Detailed structural and lithological mapping in local areas combined with the use of sedimentary facing criteria in the Willyama sub-domain has allowed the erection of local successions. These can be correlated over wide areas. The mapping of R.W. Marjoribanks has formed part of the basis of this correlation in the Broken Hill sub-domain.

In addition to the metasedimentary sequences, a variety of granitic rocks occurs. Some of these are syn- or post-orogenic granites and have been dated at 1500 to 1600 Ma (e.g. Thomson, 1969). Others such as the granitic gneisses in the mine area at Broken Hill are inter-layered with the metasediments and have taken part in all the deformation episodes which affect the metasediments. Isotopic studies by Pidgeon (1967) and Shaw (1968) show that these granitic gneisses conform to the isochrons and initial $^{87}Sr/^{86}Sr$ ratios of the enclosing metasediments and have a metamorphic age of ca 1700 Ma. They may be of volcanic origin (e.g. Johnson and Klingner, 1976) or they may be pre-tectonic intrusions.

Other areas of granite gneiss especially in the Olary sub-domain and in Eyre Peninsula probably represent the original basement to the metasedimentary

sequences, although corroboration from isotopic evidence has not yet been published, and they have also been interpreted in other ways (e.g. Tilley, 1921; Campana and King, 1958). The elucidation of the stratigraphy of the metasediments has an important bearing on this problem in that it demonstrates that the gneisses lie at the base of the succession. However, the gneisses have been extensively reworked and remobilised during the Olarian orogeny and no major stratigraphic unconformity has been recognised between them and the metasediments.

2.2 Gawler Orogenic Domain

The regional geology of the Gawler Block has recently been reviewed by Thomson (1976b) who defined three major tectonic units - an Older Precambrian Basement, a Younger (Middle Carpentarian) Precambrian Basement, and an Adelaidean Cover. Metasedimentary rocks of the Older Precambrian Basement are broadly classified as the Cleve Metamorphics (Thomson, 1969, p.27).

However, for the purpose of this paper we prefer to use the term Hutchison Group for the main sequence of metasedimentary rocks, Flinders "Gneiss" for the inferred basement to these, and to refer to younger granites and granite gneisses of intrusive origin by their locality names. Previously, all granite gneisses, granulites and many quartzo-feldspathic gneisses have been referred to as the Flinders "Group" or "Gneiss Complex" (Miles, 1954; Johns, 1961) but this has led to confusion because they are not all genetically related: some are basement to the Hutchison Group metasediments, some are granulite facies metasediments, while others are pre-Hutchison Group granites which have been subsequently deformed. Recent isotopic work has shown that some of the granulite facies sediments are Archaean (Cooper et al. 1976) and further work is now in progress. Our usage of Hutchison Group follows that defined by Coin (1976) for southern Eyre Peninsula, and can be justified in the Cowell-Cleve district. Here, in the centre of the main belt of exposed Hutchison Group and Flinders "Gneiss", a sequence has been established which appears to be consistent over the length of the Peninsula, and which is therefore inferred to be upward facing.

North of Mt. Pony (Fig. 2) in the core of a refolded F_2 anticline a basal unit of granite augen gneisses and amphibolites (Flinders "Gneiss") underlies a thick pile of quartzites (Warrow Quartzite, Thomson, 1969, p. 28), which are

particularly feldspathic low in the succession but contain more schist intercalations higher up. Conglomeratic rocks have been reported within this quartzite by Jack (1914) and Thomson (1969).

Immediately overlying the quartzite is a relatively thin association of dolomite, banded iron formation (BIF) and amphibolite. Above this is a sequence of schists and gneisses which become phyllitic (i.e. less quartzo-feldspathic) toward the top. West of Cleve several amphibolite horizons occur within the schists, together with a second BIF consisting of massive weathered ironstone, jaspilites, banded quartzites and dolomitic horizons. This BIF is overlain by more schists and phyllites. The inferred thickness of this succession is shown in Figure 3.

In the Middleback Ranges a similar succession has been recognized by Miles (1954) and Furber and Cook (1976). Here, two BIF's are separated by the Cook Gap schists, a unit which is 330 metres thick in the South Middleback Range but which thins appreciably to the north. The lower BIF is underlain by dolomitic cherts and dolomites and at least on the eastern side of Iron Prince these appear to be further underlain by a sericitic quartzite. The base of this sequence is the "Gneiss Complex" (Miles, 1954) but whether this represents an older gneissic terrain or a younger granite is not definitely known.

In southern Eyre Peninsula a similar succession is recognised by Coin (1976), and Whitten (1966), who identified two BIF's within the Hutchison Group and correlated them with BIF's in the Middleback Ranges.

2.3 Willyama Orogenic Domain

The Willyama domain consists of two sub-domains of strongly outcropping basement - the Olary sub-domain in South Australia and the Broken Hill sub-domain in New South Wales - which are separated by a belt of dominantly Cainozoic cover (Fig. 4). Apart from Mawson's pioneering study of 1912, work had been confined to one or other of the segments with little correlation between them until Thomson (1969, 1976a) treated the two segments as one block in a tectonic

synthesis. The synthesis, however, was based on lithological, as opposed to stratigraphic (sequential) similarities. No combined stratigraphic sequence has been published.

2.3.1 Olary sub-domain

A detailed stratigraphy for this sub-domain has yet to be established but consideration of work by Whitten (1966), Robertson (1972), Parker (1972) and G. Pitt (pers. comm.) of the South Australian Geological Survey makes it possible to refine the informal succession which was described in the antiformal, and presumed anticlinal, Weekeroo area by Talbot (1967).

Talbot's succession is the reverse of that previously proposed by Campana and King (1958) and consists of four gneissic units (1-4) overlain by two schist units (5 and 6). This succession has since been confirmed by further structural studies supported by limited sedimentary structures (Parker, 197?; Wiltshire, 1975). The basal leucogneiss (1) is a massive to macro-layered granofels which grades into a layered gneiss and which is overlain by a quartzo-feldspathic schist with pegmatite schlierer (2). Overlying these, (G. Pitt, pers. comm.) are a granodiorite gneiss (3), and an upper unit of layered gneiss and schist (4). Within this upper unit are several quartzite horizons and a BIF. Whitten (1966) noted that amphibolites are also present adjacent to the BIF.

Occurrences of calc-silicates mark a gradation from the gneiss units into the schist units. In the lower schist unit (5) sillimanite predominates in the lower part and gives way to andalusite higher up. The overlying bedded unit (6) is a low grade sequence of fine grained, well bedded metasediments which are quartzitic at the base, and which show well preserved cross-bedded ripple structures (Talbot, 1967 p.50 and plate 1, Fig. 2). Talbot suggested the possibility of an unconformity between the two schist units. The succession is summarized in Fig. 5.

2.3.2 Broken Hill sub-domain

Although the Broken Hill sub-domain has been intensively studied, previous stratigraphic reconstructions (Gustafson, Burrell and Garretty, 1950; King and Thomson, 1953; Lewis, Forward and Roberts, 1965) have been based on simple structural models which are now known to be inadequate to explain even the local succession. Recent detailed structural mapping has made substantial progress in elucidating the structure of the medium and high grade rocks (Hobbs, 1966; Rutland, 1973b; Rutland and Etheridge, 1975; Marjoribanks, Glen, Laing and Rutland, in preparation) and has also permitted important re-interpretation of the stratigraphic succession in the mine area (Laing, Marjoribanks and Rutland, in prep. In the structurally less complex low grade rocks the sequence has been described in a number of unpublished theses over the past decade (e.g. Tuckwell, 1975). Correlation across the whole area still presents some difficulties and it is convenient to recognise three local successions:

(1) the high grade sequence of the Broken Hill mine area (with prograde sillimanite);

(2) the medium grade sequence of the Mt. Franks district (with prograde andalusite) and

(3) the low grade sequence of the Kantappa area.

These are outlined in Figure 6.

The high grade succession, which includes the mine sequence, has been established from surface mapping and study of drill core. The structure of the mine area is analysed in detail by Laing, Marjoribanks and Rutland (in prep.) The succession passes upwards from the 'Alma' augen gneiss through sillimanite schist and amphibolites into a granitic gneiss. Overlying this is the mine sequence of quartz-rich sillimanite schist, containing amphibolites, 'Potosi' gneiss and the lode horizon with associated BIF's. It is important to note that the single granite gneiss underlying the mine sequence is the well foliated, medium grained granitic gneiss previously referred to by mine geologists and others as the separate Upper and Lower Granite Gneisses. Stratigraphically

above the mine sequence is a thick succession of pelitic sillimanite schist. Numerous examples of graded bedding in the mine sequence and the pelitic schist establish the validity of this stratigraphic succession.

In the Mt. Franks district the succession begins with sillimanite schist and passes upwards into andalusite schist, black chiastolite schist, followed by a quartzitic unit which contains local bands rich in chiastolite or calc-silicate. The sillimanite/andalusite isograd generally parallels bedding and is closely associated with other calc-silicates and amphibolites. The basal sillimanite schist of the Mt. Franks district, although garnet poor, resembles the pelitic schist at the top of the high grade succession. They are similar mineralogically, texturally and structurally. Hence we tentatively link the two sequences together as shown in Figure 7.

The upper part of the Mt. Franks succession is similar to the lower part of the Kantappa succession, which consists of a basal andalusite schist, containing a dark chiastolite schist and a calc-silicate unit near the top, followed by quartzite. The sequence is continued by mica schists, phyllite and minor fine grained quartzites. King and Thomson (1953) recognised that the low grade rocks in the Kantappa area presented a problem in regional correlation. The considered the possibility that there was a major stratigraphic break between the high grade rocks and these low grade rocks, but stated that there was no evidence for such a break. Our work suggests that there is a progressive lithological and metmamorphic transition from the low grade rocks to the high grade rocks through the Mt. Franks area, without recognizable unconformities.

However, it may be noted that amphibolites are restricted to the high grade and the base of the medium grade parts of the Mt. Franks succession. Tuckwell (1975) has also suggested a minor depositional hiatus at a somewhat higher stratigraphic level in the Bijerkerno area.

The validity of stratigraphic reconstruction in all areas is confirmed by facing obtained from graded bedding in the sillimanite schist, cross bedding and graded bedding in the andalusite schist and quartzites, and ripple marks and cross bedding in the phyllites.

The combined succession presented above, represents only part of the original sequence: there are quartzo-feldspathic units, including the Thorndale gneisses, the augen and aplitic gneisses and the Redan gneisses (e.g. Vernon, 1969), which must be added to this succession. Basement to the metasediments has not been established but the Redan gneisses which occupy a belt along the southern margin of the Broken Hill sub-domain, possibly represent a reworked older basement complex. They are well foliated augen gneisses with intercalated amphibolites and have a very distinctive magnetic signature. They are similar to gneisses at the base of the sequence in the Olary sub-domain (Fig. 5). Other augen gneisses such as the 'Alma' augen gneiss and 'Yanco Glen' augen gneiss might also represent basement to the metasedimentary succession.

2.4 Comparison of Stratigraphic Sequences

The above descriptions indicate a broad similarity of successions in different parts of the Willyama domain (Fig. 7) and it appears reasonable to make stratigraphic correlations between them.

Similar basal gneiss units occur in each sub-domain and may represent reworked older basement on which the metasedimentary sequences were deposited. The overlying layered gneiss and sillimanite schist contain the BIF horizons and associated amphibolites. The sillimanite, andalusite and (bedded) mica schist units also display broad similarities, although the calc-silicates near the base of the mica schist at Olary have no counterpart in the equivalent stratigraphic position at Broken Hill. Rather, they may be represented by nodular epidote bearing quartzites occurring in, and at the top of, the mine sequence. Bands of calc-silicates at the top of the sillimanite schist unit in the Mt. Franks district have no obvious correlatives in the Olary sub-domain.

Two other differences are apparent:

(1) At Broken Hill, although the mine sequence is quite quartzofeldspathic, it lacks distinct quartzites and the transition into the overlying pelitic schist is more subtle than the corresponding transition into the mica schist unit at Olary.

(2) The BIF of Broken Hill is associated with a sulphide facies (of the lode horizon) and with possible meta-volcanic rocks (e.g. the 'Potosi' gneiss) which have not been recognised in the Olary sub-domain.

These differences suggest that while this part of the succession was everywhere deposited in shallow water, the Broken Hill mine sequence represents a more distal environment than the Olary sequence. The sulphide mineralization may indicate that reducing conditions as found in central regions of restricted basins or behind barred shelves were operating in the Broken Hill area (e.g. Carruthers and Pratten, 1961); or it may indicate that a volcanic exhalative supply overwhelmed the existing sedimentary environment (Stanton, 1972).

The upper parts of the Mt. Franks sequence, the sequence of the Kantappa area and the bedded mica schist of the Olary sub-domain are more directly correlable. Both at Kantappa and Olary the base of the bedded sequence is particularly quartzitic with prominent calc-silicates. These, the minor quartzite horizons and the phyllites and schists, are all fine grained and finely bedded and are marked by the preservation of delicate sedimentary structures. These characteristics are possibly due to a general decrease of metamorphic grade and of penetrative deformation in the uppermost units of the stratigraphic column.

These correlations within the Willyama domain can reasonably be extended to the Gawler domain by the strong similarities in rock associations and types of sedimentation: both domains are characterized by granitic basement and/or basal rocks; both contain sequences which are psammitic near the base and which become more pelitic upwards (i.e. broadly transgressive sequences), and both have notable BIF/amphibolite associations in equivalent stratigraphic positions. The BIF horizons of the Middleback Ranges in the Gawler domain have mineralogies representing a silica-iron oxide facies (Whitten, 1966) similar to that of the Olary BIF. One difference between the two domains is that there is no comparable development in the Willyama domain to the dolomites and calc-silicates of the Gawler domain. This kind of variation, however, only emphasises the general shallow depositional environment.

Thus in spite of the present distance between the two domains it seems

reasonable to infer that they belonged to a single stratotectonic zone of wide areal extent. The zone was characterised by shallow water sedimentation on older continental crust (as has also been suggested by Thomson, 1976a). There is some variation in facies from more proximal to more distal environments and according to our crude estimates this is associated with an increase in the thickness of the sequence from SW to NE (Fig. 7).

Estimation of the age of this widespread stratigraphic sequence is not closely controlled. The sequence is evidently older than the ca. 1700 Ma regional metamorphism. By analogy with the Arunta sub-province of northern Australia (p. 2) there is a strong presumption that the sequence is of comparable early Proterozoic ('Nullaginian') age, and rests on an Archaean basement. This presumption is supported by Whitten's (1966) suggestion that all the older BIF's in South Australia are equivalent and resemble those of the 'Nullaginian' Hamersley Group in Western Australia (Trendall and Blockley, 1970). It may also be noted that parts of the Hamersley Group are characterised by dolerite sills which rarely cross the bedding and which are of very wide lateral extent. This strengthens the view that the amphibolites in the Gawler and Willyama domains are probably of basaltic igneous derivation. They were most probably emplaced as sills in a tensional tectonic environment, after the deposition of the sediments, but before the Olarian orogeny.

3. MORPHOTECTONIC RELATIONSHIPS

The stratotectonic unity of the Gawler and Willyama domains is strongly reinforced by similarities in their morphotectonic history of deformation, metamorphism and plutonism. Most of the relations presented below stem from new work, carried out by the authors in each domain.

3.1 Gawler Domain

The first deformational event (D_1) is represented by the formation of a high grade schistosity, S_1, which is always observed parallel to bedding. No folds associated with S_1 have been found. In the metasediments S_1 is defined

by the alignment of sillimanite and biotite and in the basal granites by biotite. Fibrolite parallel to S_1 occurs in distinct clots wrapped around by the biotite laths, raising the possibility that it represents pseudomorphs after pre-S_1 porphyroblasts (e.g. andalusite or staurolite).

The second deformational event (D_2) was a fold-forming event. Folds on all scales are isoclinal and overturned to the east. They are characterized by the development of a strong axial plane schistosity, S_2, which in the hinges is observed overprinting the layer-parallel schistosity S_1. In the limbs however, there is only one schistosity, which is layer-parallel and which represents the combined effect of D_1 and D_2 strain. S_2 is also defined by sillimanite and biotite, and contains a strong lineation, parallel to the fold axes, defined by individual minerals and by elongate aggregates of quartz and feldspar. Other thermal effects gave rise to the syntectonic Middlecamp granite, near Cowell, which displays a strong S_2 schistosity.

The third deformation (D_3) was also a fold forming event, which produced large relatively open upright folds. These have a sub-vertical axial-plane schistosity trending north to north-east. They deform F_2 and S_1 structures and the Middlecamp granite. The S_3 fabric is weakly developed and restricted to F_3 fold hinges. It is characterised by incomplete recovery and recrystallisation, and is defined by muscovite, biotite and chlorite, which indicate that the metamorphism accompanying D_3 was of lower grade than that during D_1 and D_2. A large mylonite zone in the eastern part of Eyre Peninsula is associated with this event and is characterised by the recrystallisation of quartz and feldspar and the retrogression of biotite to chlorite. The late tectonic Narridy Creek and Carpa granites which locally display an S_3 foliation, are also allocated to D_3.

Late stage minor folds and crenulations, generally trending E-W, affect the above structures including the mylonite schistosity. Post-tectonic events include the intrusion of further granites (e.g. the Charleston Granite) and dolerite dykes.

3.2.1 Willyama domain: Olary sub-domain

A pre-tectonic thermal event (M_1) is recognised in the low and medium grade rocks of the Olary sub-domain. Talbot (1967) referred to andalusite as pre-sillimanite in age, while A. Spry (pers. comm., 1975) observed pre-tectonic, pre S_1, andalusite.

Although rare F_1 folds have been found (R. Wiltshire, pers. comm.), D_1 is generally characterised by a schistosity parallel to bedding (Talbot, 1967; Parker, 1972; G. Pitt, pers. comm.). This schistosity, S_1 is outlined by sillimanite and biotite in the higher grade rocks, and by muscovite in the low grade rocks. Pegmatite veins are developed parallel to S_1 (Parker, 1972).

Folds associated with the second deformation are tight and now upright (Parker, 1972; R. Wiltshire, pers. comm.) and have an axial plane schistosity (S_2) defined by sillimanite and biotite in the high grade rocks. The sillimanite also defines a lineation parallel to F_2 fold axes. This deformation was accompanied by the emplacement of pegmatites.

The third deformational event produced shear zones and upright open F_3 folds both generally trending NE to ENE. The folds are dominantly dextral in sense and steeply plunging. The accompanying S_3 mica schistosity is dominantly a rotational fabric formed by the crenulation of S_1 or S_2. Numerous small to large granite and pegmatite bodies were emplaced during D_3.

Younger structures are restricted to small scale crenulations of S_3 and earlier schistosities.

3.2.2 Willyama Domain: Broken Hill sub-domain

The separation of the various phases of deformation and of their effects in the Broken Hill sub-domain has been a slow process and is still incomplete (see e.g. Hobbs, 1966; Williams, 1967; Rutland 1973, Rutland and Etheridge, 1975). However it is now clear that schistosities and associated folds of three main generations are present (S_1, S_2 and S_3 of this paper, correspond broadly to S_{1p}, S_{1n} and S_2 respectively of Rutland and Etheridge, 1975). The full basis for the revised classification and correlations is given in

Marjoribanks, Glen, Laing and Rutland (in preparation).

There is compelling evidence in the low and medium grade rocks of the Broken Hill sub-domain for a period of andalusite and biotite growth before the first deformational event. Andalusite and chiastolite porphyroblasts are enveloped by S_1, and were altered, at least partially, to sericite and quartz during D_1, which induced the observed preferred orientation of sericite. In some areas in the medium grade rocks, the crystallisation of andalusite overlapped into D_1. The first up-grade appearance of fibrolite, which is at the top of the sillimanite schist unit, occurs within these andalusite-quartz-sericite aggregates, and it is seen as clots surrounded by S_1.

In the high grade rocks, the tendency of sillimanite and fibrolite to aggregate in clots suggests similar pre-deformational growth of andalusite (cf. Hodgson, 1974, Fig. 16).

The existence of extensive areas showing high angle bedding/schistosity relations in the first deformation in the low and medium grade rocks is in distinct contrast to the layer-parallel S_1 in the high grade rocks. S_1 is outlined by muscovite in the lower grade rocks, and by sillimanite and biotite in the high grade rocks. It contains a weak to strong mineral lineation. Pegmatites and migmatites are developed parallel to S_1.

The consistency of stratigraphic facing over large areas and the continuity of bedding led Glen and Laing (1975) to suggest that any folding associated with D_1 would necessarily be on a large scale. This is now confirmed. In the high grade rocks R.W. Marjoribanks (pers. comm. 1975) has defined macroscopic domains of upward and downward facing beds. These he regards as limb areas of large isoclinal F_1 folds. On these limbs occur very rare small F_1 fold pairs which are characteristically isoclinal. In the medium and low grade rocks, Glen (1975) has reconstructed a large F_1 syncline which has limbs tens of square kilometres in extent and an axis lying approximately north-south. This fold is non-isoclinal in the low and medium grade rocks, but becomes isoclinal in the underlying sillimanite schist. The hinge of the fold has been rotated by F_3

folding into a more upright attitude and is cut off by the Apollyon Valley retrograde schist zone, but can be found further north in the low grade rocks of the Kantappa area where it was recognised as a more open, upright F_1 syncline by Tuckwell (1968), and later workers. Other andalusite schists in the Broken Hill sub-domain at Bijerkerno (Tuckwell, 1975) and in the Yanco Glen area (G. Corbett pers. comm.) show a non-parallel early schistosity. All occurrences of low and medium grade rocks may thus be connected by large scale F_1 folding.

The second deformation (D_2) in the Broken Hill sub-domain, resulted in the formation of large scale F_2 folds in the high grade rocks, but there is no comparable fold development in the medium and low grade rocks. Microstructural complexities in S_1 in the low grade rocks north of the Kantappa Lineament (Laing, 1969; Price, 1969) may possibly be explained in terms of S_2 development. F_2 folds in the high grade rocks are tight and are upright or overturned to the east. A sillimanite-biotite S_2 schistosity is observed in the hinges where it overprints S_1, but in the limbs the layer-parallel schistosity probably represents the combined effect of D_1 and D_2 strain. S_2 contains a strong mineral lineation which is generally, but not always, parallel to F_2 fold axes. Axial planes of small F_2 folds are characterised by quartzo-feldspathic segregations.

The third deformation (D_3) produced both large and small scale F_3 folds which refold D_1 and D_2 structures in high grade rocks and D_1 structures in medium and low grade rocks. S_3 formed by crenulation of earlier schistosities and is variably defined by either the axial plane of the crenulations or by new mineral growth. At its highest grade S_3 contains sillimanite although generally it is defined by mica and/or chlorite. Its orientation is relatively constant over the sub-domain, striking north to north-east with a subvertical dip. Thermal effects inferred to be related to D_3 (see below) resulted in the generation of pegmatite and the Mundi Mundi granite. Associated patchy retrogressive metamorphism produced cross-cutting muscovite (the M_2 event of Binns, 1963), staurolite, garnet and chloritoid.

All previous fold structures were overprinted by a late stage crenulate deformation (D_4) which produced small scale kinks and folds.

A notable feature of the Broken Hill sub-domain is the presence of a network of retrograde schist zones (Vernon, 1969) in a variety of orientations. The largest retrograde zone in the Broken Hill sub-domain is the ESE trending Thackaringa-Pinnacle shear which Thomson (1969) recognised in the Olary sub-domain. This appears to be a late stage feature, disrupting early structure and have a possible dextral sense of movement (Andrews, 1922). Other zones parallel to it form a definite group which cause D_3 structures to be rotated (R.W. Marjoribanks, pers. comm). Two other prominent trends in the Broken Hill sub-domain are NNE to NE (Globe-Vauxhall, Apollyon Valley, Mt. Franks, Mundi Mundi) and NNW (De Bavay, British). The NE trending set is also present in the Olary sub-domain.

The Globe-Vauxhall, Apollyon Valley and Mt. Franks zones are characterised by a retrograde schistosity whose strike is generally parallel to the zone boundaries whose strike in turn is parallel to that of S_3 in the surrounding rocks. The retrograde schistosity contains a steeply pitching mineral lineation, which is also shared by S_3 immediately adjacent to the zones. The retrograde schistosity is axial plane to small folds which plunge parallel to adjacent F_3 folds. The only sub-surface information on these zones comes from the Globe-Vauxhall (Laing, 1977). This shows that although the zone boundaries crosscut and dip more shallowly than S_3, the retrograde schistosity within the zone varies from parallel to S_3 to parallel to the boundaries. An apparent systematic change in orientation of schistosity across the schist zone can be explained in terms of the incremental strain model of Ramsay and Graham (1970). The above features suggest a possible relationship between one group of retrograde schist zones and D_3. In the medium grade rocks the mineral assemblage which defines the retrograde schistosity of

the Mt. Franks zone is the same as that which defines S_3 although the grainsize is smaller in the former. The intensity of S_3 deformation in the surrounding rocks increases towards the zone (Glen, 1977). In the high grade rocks, there appears to be a continuous, though rapid, change in mineralogy and metamorphic grade towards the retrograde zones. We would thus suggest that one group of retrograde schist zones may represent a late stage of D_3 deformation, although we recognise that the features described above may have resulted from a later, independent retrograde deformation superimposed on, but controlled by D_3 structures. The other groups of retrograde schist zones with different orientations transect D_3 folds and are evidently younger. The tectonic significance of this later ductile deformation is discussed in a following section.

3.3 Comparison of Morphotectonic Relationships

The previous section has summarised the morphotectonic histories of the several areas established on the basis of independent mapping. Comparison of these morphotectonic histories across the Gawler sub-province (Table 1) reveals striking similarities and reinforces the stratotectonic similarities between the Gawler and Willyama domains.

Correlations between the different areas are made on the basis of two factors:

(1) Similar deformational styles and associated metamorphism of individual events.

(2) Similar sequences of events.

It is not inferred that either the individual events or the sequences are strictly synchronous across the region. However, since isotopic dates across the region are broadly comparable it is believed that only limited diachronism is involved. The available evidence suggests that comparable events in the Olarian Orogeny may be somewhat younger in the Willyama than in the Gawler domain. For example late-tectonic granites in the Gawler domain (Tarcoola granite suite, Thomson, 1976b) have been dated at 1580 Ma while the Mundi Mundi granites in the Willyama domain yield an age of 1540 Ma (Shaw, 1968). An age of 1780 ± 120 Ma for

TABLE 1

MORPHOTECTONIC RELATIONSHIPS ACROSS THE GAWLER SUB-PROVINCE

	GAWLER DOMAIN	WILLYAMA DOMAIN			
		Olary Sub-Domain	Broken Hill Sub-Domain		
			Broken Hill Mine Area	Mt. Franks District	Kantappa Area
	Charleston granite	-	-	-	-
M_5 D_4	kinks crenulations	crenulations	F_4 folds, kinks	F_4 folds, kinks	-
M_4 D_3	S_3 mica; weak. NE trend.	S_3 mica; NE trend	S_3 mica, sillimanite; strong. NE trend	S_3 mica; NE trend	No S_3
	F_3 upright, open. NE trend. mylonite zone	F_3 upright, open. NE trend. Some RSZs**	F_3 upright, open. NE trend Some RSZs	F_3 upright open, kink type NNE to NE trend Some RSZ	F_3 upright, open, kink type NE trend Some RSZ
	Narridy Creek granite	Granitoids	Granitoids	Granitoids late	Mundi Mundi granite late
M_3	S_2 sillimanite, biotite; dip to W	S_2 sillimanite, biotite; vertical	S_2 sillimanite, biotite; dip to NW	S_2 a plane to tight crenulations dip to NW	S_2 local muscovite generally crenulations
D_2	F_2 isoclinal, over-turned to E. Co-axial lineation	F_2 tight upright	F_2 tight to isoclinal overturned to NW Co-axial lineation	F_2 very local. tight, overturned to NW	F_2 very local tight
	Middlecamp granite	Pegmatite	Q/F* veins, granitoids		
M_2 D_1	S_1 sillimanite, biotite; layer parallel.	S_1 sillimanite, biotite/ mica; layer parallel.	S_1 sillimanite, biotite; layer parallel.	S_1 sillimanite, biotite/ muscovite layer parallel and non parallel.	S_1 muscovite; non parallel.
	F_1 not seen	F_1 rare	F_1 macroscopic facing variation isoclinal	F_1 macroscopic facing variation. non upright macroscopic syncline	F_1 macroscopic rightway up upright syncline
			Granitoids, migmatites	Migmatites, granitoids	
M_1	Possible andalusite or staurolite	andalusite	possible andalusite	andalusite	andalusite

*Q/F veins: quartzo-feldspathic veins

**RSZ : retrograde schist zone

the main metamorphism in the Gawler domain based on limited evidence (Compston & Arriens, 1968) compares with approximately 1700 Ma in the Willyama domain (Pidgeon, 1967; Shaw, 1968). But much more detailed work is required to confirm these indications.

The evidence summarized above (in sections 3.1 and 3.2) suggests that a pre-tectonic metamorphism may have characterised much of the Gawler sub-province. Pre-S_1 andalusite is preserved only in the medium and low grade rocks of the Willyama domain. These rocks occur at the top of the sedimentary pile where later deformational and metamorphic events were less intense. However, textural relations in S_1 fibrolite clots in the high grade rocks from all areas suggest the presence of a pre-S_1 andalusite phase. Granitic gneisses carrying the S_1 schistosity may represent intrusions accompanying this metamorphism.

The first major deformational event (D_1) gave rise to a layer-parallel schistosity in high grade rocks throughout the sub-province. Evidence from the Broken Hill sub-domain indicates that this schistosity was related to the formation of macroscopic recumbent isoclinal folds (nappes), while in the medium and low grade rocks S_1 was axial-plane to large non-isoclinal folds. The metamorphism (M_2) accompanying D_1 was associated with syntectonic migmatites and pegmatites.

In all high grade areas a second deformational event (D_2) is recognised, characterised by tight folds with a high grade axial plane schistosity. Quartzofeldspathic segregations (particularly along axial planes) developed in all domains but there are apparently no analogues in the Willyama domain of the syntectonic Middlecamp granite in the Gawler domain. In the medium and low grade rocks D_2 is represented only by local developments of folds and schistosity. It is possible that the D_1 and D_2 fold phases in the high grade rocks may be represented by a combined fold phase in the low grade rocks, which is consistent with a high structural level of the low grade sequence during the early, main orogeny.

A third deformational stage recognised in all areas, is the production of

relatively open, upright macroscopic folds (D_3) associated with waning metamorphism (M_4). Recrystallisation during M_4 was characteristically incomplete and S_3 shows a wide variation in character from weak crenulations to strongly penetrative schistosity. Locally, in the highest grade sillimanite-bearing rocks, granitic pegmatite segregations are developed in axial planes. Generally, however, S_3 is defined by biotite and muscovite, both old and new. At its lowest grade it is defined by chloritic, retrograde assemblages.

In both the Gawler and Willyama domains D_3 fold axial planes are subvertical and have a dominantly NE trend, but there is substantial variation about this trend in both areas (Figures 2 and 4).

Syn- and post-tectonic pegmatites and generally discordant granite bodies are present sporadically throughout the sub-province. These are typified by the Carp- and Narridy Creek granites near Cowell and by the Mundi Mundi granite north of Broken Hill. Later small-scale folds and crenulations are present over most of the sub-province.

In the Gawler domain a major mylonite zone was developed during the D_3 deformation, but otherwise there is an absence of the network of retrograde schist zones which characterise the Willyama domain.

As discussed above, some of the zones in the Willyama domain may also be associated directly with D_3 but the discordant sets are superimposed on D_3 and could be significantly younger. Whenever they were initiated, they certainly continued to be active during the deposition of Adelaidean rocks and during the subsequent Delamerian orogeny (see below).

Apart from this difference in development of retrograde schist zones it seems clear from the correlations and similarities summarized above that the Gawler and Willyama domains were subjected to essentially the same orogenic events, - the Olarian orogeny. The recognition of D_1 structures in high, medium and low grade rocks of the Broken Hill sub-domain indicates that no major morphotectonic unconformities are present. Such unconformities as may exist are stratotectonic unconformities developed prior to the deformational events of the

Olarian orogeny. This conclusion applies to the unconformities which have been proposed below the lowest grade schist sequences described in section 2.

3.4 Age of the Deformations

In the Broken Hill sub-domain, potassium-argon data from whole-rock and mica analyses (Richards and Pidgeon, 1963) indicate that the total rock system became closed at ca 500 Ma. This date can be reasonably correlated with the cessation of ductile movement on the retrograde schist zones, coinciding with the end of the Delamerian orogeny (see Table 2).

The D_3 deformation in the Gawler domain cannot be directly dated but its age is closely bracketed by other morphotectonic and stratotectonic events whose ages have been determined with relative precision. The lack of imprint of these later events in the Willyama domain not only reflects significant tectonic differences between the two domains (see below) but also renders dating of D_3 more difficult.

D_3 structures in the Gawler domain are broadly synchronous with the intrusion of granites, e.g. Burkitt granite, ca 1590-1680 Ma (Compston and Arriens, 1968; Thomson, 1976a). Regional D_3 folds are overlain unconformably by the Gawler Range Volcanics dated at ca 1535 Ma. (Compston and Arriens, 1968). In the Cowell-Cleve area the Narridy Creek granite which is internally massive, has its margins strongly foliated parallel to the S_3 schistosity of the enclosing schists. The later stages of D_3 deformation can therefore be bracketed between the intrusion of the Narridy Creek granite and the extrusion of the Gawler Range Volcanics. It is clear that D_3 structures in the Gawler domain are not related to the Delamerian orogeny.

In the Willyama domain there are no equivalents of the Gawler Range Volcanics, and the Upper Proterozoic (Adelaidean) cover rocks are strongly folded as a result of the Delamerian orogeny. A younger age limit to D_3, and in particular the relationship between D_3 folding and cover folding, is therefore not immediately clear. Talbot (1967), working in the Olary sub-domain concluded that folds in the Adelaidean cover rocks post-dated the youngest macroscopic folds of layering (our D_3) in the Willyama Complex. Amphibolite dykes which cut across these folds were emplaced prior to Adelaidean deposition (Talbot, op.cit. pp.50-51;54-55). Folds in the Adelaidean cover are related to lithological variation in the basement and to

reactivation of the pre-existing (S_3) basement schistosity (Talbot, 1969, p.64).

In the Broken Hill sub-domain a marked unconformity surface between the Willyama Complex and the Adelaidean rocks is not grossly deformed despite the presence of regional D_3 folds in the former. Andrews (1922) suggested that the cover folding post-dated the main deformation in the Willyama Complex and corresponded to renewed movement in retrograde schist zones (his "crush zones"). Binns (1963) also related cover folding to strong movement on the retrograde schist zones. These conclusions have been supported by the more detailed work of Laing (1969). The evidence therefore indicates that D_3 folding in the Willyama Complex was not related to folding of the Adelaidean cover rocks, but points to a long deformation history in the retrograde schist zones.

Relationships between D_3 structures and the Mundi Mundi suite of intrusive granitic bodies, suggest a broadly similar time of formation. Laing (1969) showed that pegmatite veins emanating from a massive, discordant body of Mundi Mundi granite were folded around D_3 folds. Other bodies of Mundi Mundi granite in the north-western part of the Willyama sub-domain are post-tectonic, although their margins are in part foliated parallel to S_2 in the surrounding rocks. Pegmatite and granite bodies of the Mundi Mundi type in various places cut across layering and lie within the axial planes of D_3 folds. Anderson (1971) inferred that the intrusion of Mundi Mundi pegmatites accompanied his Group 3 deformation (our D_3). It is to be noted that the slight metamorphism associated with the pegmatites (see Binns, 1963) is consistent with the general low-grade conditions prevailing during D_3.

The association of D_3 deformation with a phase of granite emplacement is analogous to the situation in the Gawler domain. The comparison is reinforced by the dating of the Mundi Mundi granite suite at ca.1540 Ma (Shaw, 1968). This confirms the broad correlation of D_3 between the domains, and establishes that D_3 in the Willyama domain was, like its counterpart in the Gawler domain, an integral part of the Olarian orogeny.

The difficulty of spearating the ages of the early deformations in the

Broken Hill sub-domain has been noted by Rutland and Etheridge (1975). D_1 and D_2 structures - schistosity and lineation - are defined by similar, high grade minerals, and it is reasonable to infer that the dating of high grade assemblages at 1780 $\pm$ 120 Ma in the Gawler domain and 1695 $\pm$ 21 Ma in the Willyama domain, reflects an age of metamorphism associated with one, or both, of these deformations. We may conclude only that the age of D_1 is not younger and D_2 is not older than these isotopic dates. Textural relations between D_1 and D_2 fabrics, and the relations between D_1 lineations and D_2 folds (Laing, Marjoribanks and Rutland, in prep.) suggest that the two deformations may have been part of a single complex event. This is consistent with Shaw's (1968) suggestion that the ca 1700 Ma metamorphism took place over a protracted period or else that it was followed by a milder metamorphism prior to ca 1540 Ma. Thomson (1976b) gave a date of ca 1680 Ma for the post-tectonic Burkitt granite in the Gawler domain and this gives a younger age limit for the D_2 deformation there. A lower limit for D_2 is inferred by an age of 1855 ($\pm$ 10) Ma given by Cooper et al. (1976) for the Kirton Point granite gneiss which antedates at least D_2.

3.5 Post-D_3 Tectonic History

The parallelism of tectonic events in the Gawler and Willyama domains broke down following the D_3 phase (Table 2). The intrusion of the Tarcoola granite suite heralded the beginning of a complex phase of igneous activity in the Gawler domain which lasted over 100 Ma (Thomson, 1976b, p.465), whereas the intrusion of the Mundi Mundi granite suite in the Willyama domain appears to have been a relatively simple, shortlived event. In the Gawler domain the Tarcoola granites were accompanied by extrusion of acid volcanics (Nuyts Archipelago and Moonabie volcanics). The Corunna Conglomerate and the dominantly clastic Tarcoola Beds were then deposited unconformably on the previous units, and were accompanied by extrusion of the massive, dominantly acid Gawler Range Volcanics at ca 1535 Ma (Lemon and Gostin, 1975). The latter in turn were intruded by granites of the Charleston suite at ca 1500 - 2450 Ma. This terminated a complex igneous phase characterized by volcanic extrusion as well as plutonic intrusion. The evidence thus suggests that subsequent to the Tarcoola acid intrusive phase, the Gawler Block was at a relatively high crustal level. This conclusion is consistent with the undeformed,

flatlying nature of the Gawler Range Volcanics, the younger Roopena basic volcanics (ca 1345 Ma, Compston et al., 1966), and the overlying Adelaide System on the Stuart Shelf, and confirms Thomson's (1970, p. 206) suggestion that the Charleston granite phase "represents the final igneous event that marked ... consolidation of the Gawler Craton".

Cratonisation of the Gawler domain contrasted with continued instability in Adelaidean time of the Willyama domain and the reminder of the basement lying east of the Torrens Hinge Zone (Figure 1). Where the Adelaidean cover rests on the Gawler domain, viz. the Stuart Shelf on the northeastern margin, the cover rocks are undeformed, whereas Adelaidean cover rocks on the Willyama domain are strongly deformed. The general absence of retrograde schist zones from the Gawler domain, and the fact that many retrograde schist zones are demonstrably younger than D_3 in the Willyama domain, suggests that the retrograde schist zones in the latter domain were largely a consequence of the younger tectonic activity which produced the highly unstable basement on which the rocks of the Adelaide Geosyncline were deposited.

Several tectonic phases can be recognised in the development of the Adelaide Geosyncline (Rutland and Murrell, 1975, and in preparation). An early phase of tensional faulting and basaltic magmatism accompanied Willouran deposition. Strong faulting was also particularly important in controlling Sturtian deposition. In the Broken Hill region, the Sturtian deposits show very great thickness changes across faults which appear to follow the trend of retrograde schist zones in the Willyama Complex (Laing, 1969; Thomson, 1969). It follows therefore that some zones were already established at this time. The zones, and locally the D_3 schistosity, were also clearly reactivated and modified during the Delamerian orogeny. Cleavage in the Adelaidean rocks is commonly parallel to retrograde schistosity in their underlying basement and examination of ERTS 1 photographs shows that extensions of some retrograde schist zones can be traced trhough Adelaidean rocks (cf. Scheibner, 1973a). This type

of evidence has led some workers to infer that D_3 and the schist zones were themselves initiated during the Delamerian orogeny, although Andrews (1922) and Talbot (1967) recognised their pre- and post-Adelaidean history. Further evidence of the post-Adelaidean history of the retrograde schist zones is provided by potassium-argon data from the retrograde schist zones, which suggest that the system remained open until about 500 Ma, the time of the Delamerian orogeny.

Episodes of mafic and ultramafic magma emplacement also provide evidence of the extended history of these zones. Uralitised dolerite dykes occur in the southern part of the Willyama domain and clearly post-date the high-grade metamorphism. In the Stirling Vale area, two trends at about 125° and 150-155° can be observed, the latter set being parallel to a retrograde schist zone. Gustafson et al., (1950, pp. 1416-1417) recognised three sets of dislocations associated with the retrograde events and considered that the dolerites occupied faults of the oldest set and were displaced by those of the younger sets. Williams (1967) Watson (1968) and Maiden (1972) also reported offset of post-D_3 dolerite dykes by retrograde schist zones. Ross (1971) reported that where a dolerite dyke was intersected by a retrograde schist zone in the North Broken Hill Limited mine it was extensively converted to biotite schist. Small ultramafic intrusions in the Willyama Complex have also been shown to post-date the higher grade regional metamorphism but to be affected by retrograde schist zones (Crase, 1969; Giles, 1974). Andrews (1922) noted that some retrograde zones show a brittle phase of brecciation superimposed on the ductile fabric. That some retrograde schist zones have acted as faults is evident from the fault scarps, of Tertiary to Recent age, of the Globe-Vauxhall (Mulga Springs fault), Mundi Mundi, and other zones. In general, however, it is notable that relatively ductile deformation was maintained in the retrograde schist zones throughout their history notwithstanding the fact that this deformation was expressed, in part, by faulting in the cover.

It seems reasonable to correlate the mafic magmatic activity with extensional

tectonics during the development of the Adelaide Geosyncline, most probably in Willouran time. This is consistent with our inference that much of the development of the retrograde schist zones correlates with later faulting during Sturtian deposition and with the Delamerian orogeny[1]. But as already noted some of the retrograde schist zones were initiated during the final stages of the Olarian orogeny. This is particularly clear for the mylonite zone associated with D_3 deformation in the Gawler sub-province, where Delamerian effects can be ruled out.

The apparent continuity of deformation history represented by the retrograde schist zones in the Willyama Block is therefore partly illusory. That deformation history is divided between two major orogenic episodes, the Olarian orogeny terminating ca 1500 Ma (see below) and the Delamerian orogeny culminating ca 500 Ma ago. The episode of emplacement of mafic dykes and ultramafic intrusions serves to separate the effects of the two orogenic cycles.

3.6 The effect of the Delamerian orogeny on Olarian orogenic structures

There has recently been considerable discussion in the literature of the arcuate structure of the Mt. Lofty-Olary fold belt produced during the Delamerian orogeny (Crawford and Campbell, 1973; Scheibrer, 1973b; Coward, 1976). Both the Fleurieu and Nackara arcs have been interpreted as oroclinal folds although these interpretations have also been strongly opposed (e.g. Daily, Jago and Milnes, 1973). Other authors have suggested large horizontal translations on inferred major faults, either before or after Adelaidean deposition (e.g. Harrington et al. 1973, Dunnett, 1976).

The discussions have generally not taken account of the structure of the Gawler sub-province, which does in fact provide important evidence.

---

[1] An isotopic event at ca 870 Ma. has also been recognised in the Houghton Inlier near Adelaide (Cooper and Compston, 1971) and it is possible that some of the deformation of the retrograde schist zones following the mafic dyke phase should be correlated with this.

Both the Gawler and Willyama domains show a considerable variation in fold trends, especially of D_3. However, it is notable that the range of variation is about the same in both domains and the overall trend is north-easterly in both domains[1]. It also appears that D_2 trends are more constant in both domains than D_3. In the Gawler domain in particular (Figure 2) it can be seen that both NNW and NE D_3 trends are superposed on relatively constant N to NNE D_2 trends. This suggests therefore that the variations in D_3 trends are original and not due to subsequent bending of an originally straight trend.

Since substantial variation in D_3 trends occurs in the Gawler as well as the Willyama domain it is clear that much of the variation cannot be due to the Delamerian orogeny which did not affect the Gawler domain; it must in fact be a product of the Olarian orogeny. This evidence has important bearing on the various hypotheses of oroclinal deformation of the Mt. Lofty-Olary fold belt.

The hypothesis of Crawford and Campbell (1973) that the Willyama Block was torn off from the Mt. Painter Block and rotated through about 70° is clearly untenable since the Olarian trends in the Gawler and Willyama domains are similar. (Giddings and Embleton (1974) have also provided palaeomagnetic evidence against the large-scale rotation of the Yorke Peninsula postulated by Crawford and Campbell).

It is less easy to rule out hypotheses of large-scale translation of one domain relative to the other since it is not possible to establish conclusively that the two domains are now in their original relationship (see below). However, it is clear that any such translation on discrete faults must have occurred prior to Adelaidean deposition since continuity of

---

[1] Northerly or north-easterly trends also characterise the inliers within the Delamerian fold belt. The only exception is in the extreme north of the Mt. Painter domain where the east-west trends may represent a later effect due to the Musgravian orogeny, which may extend to this region via the Muloorinna Ridge.

Adelaidean deposition is established across possible fault lines, such as the Torrens Hinge Zone (cf. Harrington, 1974) and the MacDonald Fault. In the latter case also there appears to be a reasonable correlation of the basement rock units of the Olary sub-domain across the fault line. Translation integrated across broad zones of simple shear in the basement is again less easily discounted (Scheibner, 1973b; Coward, 1976) since these are not necessarily reflected by parallel structures in the cover.

A full discussion of Adelaidean tectonics is beyond the scope of this paper but there is considerable evidence that the three main retrograde schist zone directions in the Willyama domain, play a part in controlling fold trends in the Delamerian fold belt.

Two points are here emphasised.

(1) The Adelaidean fold trends are usually approximately parallel to those in the underlying basement especially when the latter are associated with a retrograde schistosity.

(2) Variation in basement fold trends in the Willyama domain appears to be related to spatial variation in the relative importance of the different retrograde schist zone trends.

Thus, on the north side of the Willyama Block the faults (e.g. Corona Fault) limiting the Adelaidean outliers are related to the retrograde schist zones of NNW trend, which have a sinistral strike slip component. The northward increase of importance of this sinistral NNW trend appears to be associated with a change in trend of the Willyama structures from 030° to 360°; and the Adelaidean fold trends are also about 360°. Within the main part of the Broken Hill sub-domain the NE trending shear zones are most prominent and fold trends are similar to those in the Gawler domain. However, an important E-W zone occurs within the domain, and the very large dextral Thackaringa-Pinnacles zone occurs towards the southern margin. It can be suggested that the swing of both Olarian and Adelaidean fold structures to ENE within the Olary sub-domain is associated with the dominance of the dextral E-W retrograde schist direction.

Thus it seems reasonable to postulate that the swing in Olarian and Adelaidean trends from N-S through NE-SW, to ENE-WSW as one progresses from north to south in the Willyama domain is at least partly due to the operation of conjugate zones of simple shear (Fig. 8). This, however, does not demonstrate that the variations in Adelaidean fold trends are the consequence of deformation during the Delamerian orogeny. As indicated above the retrograde schist zones have both a pre-Adelaidean and Adelaidean history. Much of the rotation of Olarian fold structures may have occurred before Adelaidean deposition, in which case the Adelaidean trends are largely inherited. This problem is discussed in more detail with respect to both the tectono-stratigraphic and deformational aspects of the Adelaidean rocks by Rutland and Murrell (1975, and in preparation).

Since this paper was submitted for publication a paper by M.B. Katz (1976) has appeared which interprets the whole orogenic history of the Willyama Block in terms of lineament tectonics. The paper is based on the assumptions (op.cit. p. 275, 276) that the lineaments belong to a major fundamental fracture zone known as the Darling River lineament system (DRL) dating from the early Precambrian and that movements along the component lineaments of the DRL are the primary controls of the structural, metamorphic, igneous and mineralization events in the Willyama Block. As discussed above, the influence of discrete shear zones cannot be recognised until late stages (D_3) in the Olarian Orogeny. In our opinion, there is no valid evidence that the 'DRL' was the 'primary control' of the earlier history. Interpretations of the observed pattern of retrograde schist zones in terms of the control by the DRL also appear to us to be not strongly based. Katz (1976) has also suggested that the Adelaide 'aulacogene' was "the result of the separation of the Willyama Block from the Gawler Block" by translation of the Willyama Block ENE along the Darling River lineament by 70-80 km. According to Katz (op.cit. p. 282) this event "is reflected in the Willyama Block by the Willyama metamorphism (1700 m.y.) and the Mundi-Mundi granite

(1560 m.y.)." It will be clear from the above discussion that the latter two events relate to the Olarian orogeny which affected both the Willyama and the Gawler orogenic domains and that both events antedate the inception of the Adelaidean depositional basin. Moreover, while the present authors recognise the influence of extensional tectonics during the early stages of Adelaidean deposition they reject the concept of separation of blocks by many tens of kilometres with the implicit development of a flow of oceanic crust to the Adelaidean basin in the Flinders Ranges. A full discussion of the tectonics of the Delamerian fold belt has been provided by Rutland and Murrell (1975, and in preparation).

4. THE OLARIAN OROGENY: CONCLUDING DISCUSSION

The relationships summarized above in sections 2 and 3 suggest a number of generalisations concerning the nature of the Olarian orogeny, which bear on the general problem of remobilisation of Precambrian terrains and on the extent to which Precambrian orogeny can be interpreted in terms of Phanerozoic orogeny.

4.1 Dimensions of the sub-province

The most striking feature is that the orogeny has been imposed on a relatively uniform sequence of platformal sediments which were apparently deposited on stable continental crust. The original extent of this re-working of older crust is not clear since the exposed domains are now bounded on all sides by younger cover. The tectonic regime is clearly different from that north of the Amadeus Transverse Zone (Rutland, 1973a) but it could extend westwards under the younger platform cover which covers much of the Gawler Block. Thomson (1976b, Figs. 1 & 2) suggests that magnetic anomalies and isolated outcrops in the extreme west of the Gawler Block reflect the presence of B.I.F. and therefore of an extension of the Gawler sub-province. It could also have extended eastwards and there is no definite evidence of any relationship to an active continental margin.

The exposed width of the orogenic belt is about 200 km across strike in both the Gawler and the Willyama domains. The Willyama domain represents a more distal sedimentary facies than the Gawler domain so that it is possible that the total width of this orogenic belt exceeded the combined widths of the

two domains (Case 3, Figure 9). However, in view of the observed variations in fold trends and the possibility of post-orogenic strike-slip faulting, it is also conceivable that the two domains were originally developed along the morpho-tectonic strike from each other (Cases 1 and 2, Figure 9). In this case the total width of the tectonic regime represented would be about 200 km. The choice between the various alternatives would be made easier if the domains could be subdivided into distinct tectonic zones but this has not yet been possible.

4.2 Evidence for zonation and polarity of the sub-province

The syn-orogenic and post-orogenic plutons have not yet been sufficiently well studied to recognised any definite polarity in either composition or age, although as already noted, available dates do suggest that comparable events took place somewhat later in the Willyama than in the Gawler domain. However, one feature worthy of examination is the distribution of granulite facies rocks. These appear to be concentrated on the SE side of each domain and could conceivably be part of a single linear zone of high heat flow and geothermal gradient. However, such an interpretation must be treated with reservation at present for a number of reasons. First, the sub-province generally appears to be characterized by a high geothermal gradient: there is a general correlation between metamorphic grade and height in the structural succession so that the rocks at the base of the section are generally in high amphibolite facies. Thus the isograds are generally flat and a rather sporadic distribution of granulite facies conditions might be expected. Secondly, in the Broken Hill sub-domain recent work has shown that the isograds proposed by Binns (1964) need substantial revision (Rutland and Etheridge, 1975; N. Phillips, pers. comm. 1975). There has been substantial retrogression of early high grade rocks during and and after D_3 so that their present limits do not reveal their original extent and cannot be used to make inferences about areas of high heat flow (cf. Katz, 1976). As more information becomes available other relicts of granulite facies rocks may be discovered. Moreover it is not clear how far the granulite facies metamorphism is associated with both D_1 and D_2, but in any case the isograds must have been folded by D_3. Thirdly, it may be noted that small domains of high grade rocks occur well to the east of the Gawler domain in the coastal exposures of the Yorke Peninsula and in the inliers near Adelaide. Although the latter are generally

strongly retrogressed, there are occurrences of coarse granitic gneisses. In the Yorke Peninsula, the rocks are broadly similar to those in the Gawler domain. They are metamorphised to high amphibolite facies but NW structural trends are common. Finally, the gravity map of South Australia shows a strong positive gravity anomaly extending from the Broken Hill domain southwards across the Murray Basin. There is therefore some reason to suppose an even greater width to the sub-province than is indicated by the exposed domains.

There is therefore no compelling morphotectonic evidence that the Gawler and Willyama domains are laterally equivalent. The evidence for F_1 nappe structures in the Willyama domain only, suggests otherwise, and in view of the evidence that the two domains are not equivalent in sedimentary facies, it seems more probable that the two domains were not formed along the orogenic strike from each other.

4.3 Structural characteristics of the sub-province

The style of deformation and sequence of deformational events in the Gawler sub-province is not unlike that observed in some high grade zones of Phanerozoic orogenies. Superposed folding in high grade rocks including early nappe structures is characteristic of such tectonic zones as the Pennine zone of the Alps or the Nordland zone of the Scandinavian Caledonides among Phanerozoic collision orogenies. These zones also display comprehensive re-working of a granitic basement like the Gawler sub-province. Moreover in the Nordland zone the morphotectonic phenomena occur in a sequence of mature sediments, including a very important carbonate facies. Similar zones are much less prominent in Cordilleran orogenic belts and the closest analogy may be the Omineca zone in the Canadian Rockies.

These analogies would suggest a possible close connection of the Gawler orogeny with an active continental margin. The evidence for decrease in sotopic ages moving eastwards, the polarity indicated by the sedimentary facies and the appearance of possible meta-volcanic rocks in the Broken Hill area all suggest that any such active continental margin lay to the east of the sub-province. Rutland (1973a & b) suggested that the main phase of Proterozoic plutonism and metamorphism had a similar relationship to ocean floor spreading within a long term chelogenic cycle as does the circum-Pacific, Phanerozoic plutonism. However, the analogy cannot

be pressed too far. From what has been said it will be evident that the Olarian orogeny apparently occurred in a more stable stratotectonic environment, displayed a lesser degree of crustal mobility, and occurred over a wider area than the Phanerozoic examples. These differences may imply significant secular changes in tectonic activity, perhaps consequent on declining radioactive heat production (e.g. Rutland, 1973a).

Rather similar tectonic sub-provinces do occur in the Proterozoic provinces of Canada (e.g. Davidson, 1972) and Scandinavia (e.g. Simonen, 1971) but a comparative analysis of these provinces is beyond the scope of this paper.

Ultimately the interpretation of the Olarian orogeny must also take into account the different character of the roughly coeval Arunta sub-province in northern Australia (Rutland, 1973a, 1976). The Arunta sub-province generally shows a more variable and thicker sedimentary facies of mobile belt character and it usually displays a lower grade of metamorphism associated with upright cleavage and folding. Most of the sub-province was stabilised by ca 1700 Ma, with subsequent deposition of the platformal 'Carpentarian' sequence. Only in the Mt. Isa zone on the east of the sub-province did orogenic activity affect the equivalents of the Carpentarian rocks with plutonism at ca 1600 and 1425 Ma (e.g. Plumb and Derrick, 1976).

The sequence of orogenic events here grouped together as the Olarian orogeny apparently embraced the period of Carpentarian deposition and of both pre-Carpentarian and post-Carpentarian orogeny in North Australia. The main metamorphism associated with D_1 and D_2 deformations appear to have been of much the same age as the pre-Carpentarian metamorphism in North Australia. However these events were not followed by deposition of a platform sequence equivalent to the Carpentarian. Instead the D_3 deformation and associated plutonism corresponds roughly in age to the deformation and plutonism of the Mt. Isa orogenic zone. Thus the Gawler Range volcanics dated at 1535 Ma bear some analogy with the acid volcanics at the base of the Carpentarian sequence and also represent a period of transitional tectonism but in age they, and the associated plutons, such as the Charleston granite (1450-1500 ma) are closer to

the late plutonic activity of the Mt. Isa zone of the Arunta sub-province. This relatively young volcanic and plutonic activity in the Gawler sub-province, like that in the Mt. Isa zone, provides a further indication that an active continental margin lay to the east (Rutland, 1973a and b).

The apparent absence of a sedimentary sequence aged between 1700 and 1500 Ma and the relative paucity of younger pre-Adelaidean sequences suggests that, in general the Gawler sub-province was a more positive area after the Olarian orogeny than the Arunta sub-province after the pre-Carpentarian orogeny there.

The most important problem requiring further research in the Gawler sub-province concerns the nature and evolution of the basement underlying the probable 'Nullaginian' meta-sedimentary sequence. The granitic gneisses pose similar problems to those in Archaean greenstone terrains in that they often show local intrusive relations to the overlying meta-sediments. Nevertheless the nature of the meta-sediments demands the presence of an older continental basement (cf. Moorbath, 1975). Much more detailed petrological and isotopic studies than those at present available are required, and some are now in progress.

ACKNOWLEDGMENTS

This work has been carried out while Glen and Laing have been supported by Australian Commonwealth Postgraduate Research awards, and Parker by an Adelaide University Research Grant. Glen and Parker were on study leave from the New South Wales and South Australian Departments of Mines, respectively.

We wish to thank Bren Thomson of the South Australian Department of Mines for helpful discussions and for providing pre-prints of his 1976 papers. Roger Marjoribanks has kindly allowed us to make use of some as yet unpublished results, and also read an early draft of the paper. We also thank Graham Pitt and Bob Wiltshire for useful discussions on the Olary sub-domain.

REFERENCES

Anderson, D.E., 1971: Kink bands and major folds, Broken Hill, Australia. Bull. geol. Soc. Am., 82, pp. 1841-1862.

Andrews, E.C., 1922: The geology of the Broken Hill district. Geol. Surv. N.S.W. Mem., 8, 432 pp.

Binns, R.A., 1963: Some observations on metamorphism at Broken Hill, N.S.W. Proc. Australas. Inst. Min. Metall., 207, pp. 239-261.

Binns, R.A., 1964: Zones of progressive regional metamorphism in the Willyama Complex, Broken Hill district, New South Wales. J. geol. Soc. Aust., 11, pp. 283-330.

Browne, W.R., 1922: The petrological evolution of the Willyama Complex. D.Sc. thesis, (unpublished), University of Sydney, 34 pp.

Campana, B., and King, D., 1958: Regional geology and mineral resources of the Olary province. Geol. Surv. S.A. Bull., 34, 134 pp.

Carruthers, D.S., and Pratten, R.D., 1961: The stratigraphic succession and structure in The Zinc Corporation Ltd. and New Broken Hill Consolidated Ltd., Broken Hill, New South Wales. Econ. Geol., 56, pp. 1088-1102.

Coats, R.P., Horwitz, R.C., Crawford, A.R., Campana, B., & Thatcher, D., 1969: Geol. Surv. S.A. Geological Atlas Special Series, Sheet, Mount Painter Province 1:250,000, 426.

Coin, C.D.A., 1976: A study of the Precambrian rocks in the vicinity of Tumby Bay, Southern Eyre Peninsula. Ph.D. thesis, University of Adelaide.

Compston, W., and Arriens, P.A., 1968: The Precambrian geochronology of Australia. Can. J. Earth Sci., 5, pp. 561-683.

Compston, W., Crawford, A.R., & Bofinger, V.M., 1966: A radiometric estimate of the duration of sedimentation in the Adelaide geosyncline, South Australia. J. geol. Soc. Aust., 13, pp. 229-276.

Cooper, J.A., and Compston, W., 1971: Rb-Sr dating within the Houghton Inlier, South Australia. J. geol. Soc. Aust., 17, pp. 213-219.

Coward, M.P., 1976: Large scale Palaeozoic shear zone in Australia and present extension to the Antarctic ridge. Nature, Phys. Sci., 259, pp. 648-649.

Crase, N.J., 1969: An investigation of some of the younger basic and ultra-basic rocks to the west of Broken Hill, N.S.W. B.Sc. (Hons) Thesis, (unpublished), University of Adelaide.

REFERENCES (cont'd)

Crawford, A.R., & Campbell, K.S.W., 1973: Large-scale horizontal displacement within Australo-Antarctica in the Ordovician. Nature Phys. Sci., 241, pp. 11-14.

Daily, B., Jago, J.B., & Milnes, A.R., 1973: Large-scale horizontal displacement within Australo-Antarctica in the Ordovician: a reply. Nature,Phys. Sci., 244, pp. 61-64.

Davidson, A., 1972: The Churchill province. In Variations in tectonic styles in Canada (ed. R.A. Price and R.J.W. Douglas), Geol. Assoc. Can. Spec. Paper 11, pp. 381-433.

Dunn, P.R., Plumb, K.A., and Roberts, H.G., 1966: A proposal for a time-stratigraphic subdivision of the Australian Precambrian. J. geol. Soc. Aust., 13, pp. 593-608.

Dunnett, D., 1975: Some aspects of the Panantarctic cratonic margin in Australia. Philos. Trans. R. Soc. Lond., A280, pp. 641-654.

Furber, D.V. and Cook, J.N., 1976: Middleback Range iron ores. In Economic Geology of Australia and Papua New Guinea (Ed. C.L. Knight) pp. 945-951.

Giddings, J.W., and Embleton, B.J., 1974: Large-scale horizontal displacements in southern Australia - contrary evidence from palaeomagnetism. J. geol. Soc. Aust., 21, pp. 431-436.

Giles, C., 1974: The ultramafics of the Broken Hill district and their associated mineralisation. B.Sc. (Hons) thesis, (unpublished), University of Adelaide.

Glen, R.A., 1975: Geology of the Mount Franks district: Progress report. Unpublished report, Centre for Precambrian Research, University of Adelaide.

Glen, R.A., 1977: Structural studies and metamorphic relations between low, medium and high grade rocks in the Mt. Franks-Mundi Mundi area, Broken Hill, N.S.W. Ph.D. thesis (unpublished) University of Adelaide.

Glen, R.A., & Laing, W.P., 1975: The significance of sedimentary structures in the Willyama Complex, New South Wales. Proc. Aust. Inst. Min. Metall. 256, pp. 15-20.

Gustafson, J.K., Burrell, H.C., and Garretty, M.D., 1950: Geology of the Broken Hill ore deposit, Broken Hill, N.S.W., Australia. Bull. geol. Soc. Am., 61, pp. 1369-1438.

Harrington, H.J., 1974: The Tasman geosyncline in Australia. In The Tasman geosyncline - a symposium (ed. A.K. Denmead, G.W. Tweedale, and A.F. Wilson) Geol. Soc. Aust. Qd. Div., pp. 383-407.

REFERENCES (cont'd)

Harrington, H.J., Burns, K.L., and Thompson, B.R., 1973: Gambier-Beaconsfield and Gambier-Sorell fracture zones and the movement of plates in the Australia-Antarctic-New Zealand regions. Nature Phys. Sci., 245, pp. 109-112.

Hobbs, B.E., 1966: The structural environment of the northern part of the Broken Hill ore body. J. geol. Soc. Aust., 13, pp. 315-338.

Hodgson, C.J., 1974: The geology and geological development of the Broken Hill Lode in the New Broken Hill Consolidated mine, Australia: structural geology. J. geol. Soc. Aust., 21, pp. 413-430.

Jack, R.L., 1914: The geology of the County of Jervois, and of Portions of the Counties of Buxton and York, with special reference to underground water supplies. Geol. Surv. S.A. Bull., 3.

Johns, R.K., 1961: Geology and mineral resources of southern Eyre Peninsula. Geol. Surv. S.A. Bull., 37, 102 pp.

Johnson, I.R., and Klingner, G.D., 1976: Broken Hill ore deposit and its environment. In Economic Geology of Australia and Papua New Guinea, (ed. C.L. Knight), pp. 476-491.

Katz, M.B., 1976: Broken Hill - a Precambrian hot spot? Precambrian Research, 3, pp. 91-106.

King, H.F., and Thomson, B.P., 1953: The geology of the Broken Hill district. In Geology of Aust. Ore Deposits (ed. A.B. Edwards), pp. 533-577.

Laing, W.P., 1969: The geology of the Brewery Well area, northern Barrier Ranges, western New South Wales. B.Sc. (Hons.) Thesis, (unpublished), University of Sydney.

Laing, W.P., 1977: Structural geology of a critical area adjacent to the Broken Hill orebody. Ph.D. Thesis, (unpublished), University of Adelaide.

Laing, W.P., Marjoribanks, R.W., and Rutland, R.W.R., 1976: Structural evidence relating to the genesis of the Broken Hill orebody (in prep.).

Lemon, N., and Gostin, V.A., 1975: Sedimentology of the Corunna Conglomerate near Iron Knob, South Australia. Abstracts First Aust. Geol. Convention, geol. Soc. Aust., p. 74.

Leslie, R.B., and White, A.J.R., 1955: The "Grand" Unconformity between the Archaean (Willyama Complex) and Proterozoic (Torrowangee Series) north of Broken Hill, New South Wales. Trans. R. Soc. S. Aust., 78, pp. 121-133.

REFERENCES (cont'd)

Lewis, B.R., Forward, P.S., and Roberts, J.B., 1965: Geology of the Broken Hill Lode, reinterpreted 8th Comm. Min. and Metall. Congress, 1, pp. 319-332.

Maiden, K.J., 1972: Studies on the effects of high grade metamorphism on the Broken Hill orebody. Ph.D. thesis, (unpublished), University of New South Wales.

Mawson, D., 1912: Geological investigations in the Broken Hill area, Memoir Roy. Soc. S. Aust., 2, pp. 211-319.

Miles, K.R., 1954: The geology and iron ore resources of the Middleback Range area Geol. Surv. S.A. Bull., 33.

Moorbath, S., 1975: The geological significance of Early Precambrian rocks. Proc. Geol. Assoc., 86, pp. 259-279.

Parker, A.J., 1972: A petrological and structural study of portion of the Olary Province, west of Wiperaminga Hill, S. Australia, B.Sc.(Hons)thesis, (unpublished), University of Adelaide.

Parker, A.J., 1977: Structure and petrology of high grade metamorphics in the Cowell/Cleve area, Eyre Peninsula. Ph.D. thesis (unpublished),University of Adelaide.

Pidgeon, R.T., 1967: Rb-Sr geochronological study of the Willyama Complex, Broken Hill, Australia. J. Petrol. 8, pp. 283-324.

Plumb, K.A., and Derrick, G.M., 1976: Geology of the Proterozoic rocks of the Kimberley to Mount Isa region. In Economic Geology of Australia and Papua New Guinea (ed. C.L. Knight) pp. 217-252.

Price, G.P., 1969: The geology of the Cartwright's Creek area, northern Barrier Range, New South Wales. B.Sc. (Hons) thesis, (unpublished) University of Sydn

Ramsay, J.G., and Graham, R.H., 1970: Strain variation in shear belts. Can. Jnl. Earth Sci., 7, pp. 786-813.

Richards, J.R., and Pidgeon, R.T., 1963: Some age measurements on micas from Broken Hill, Australia. J. geol. Soc. Aust., 10, pp. 243-259.

Robertson, R.S., 1972: Petrological and structural investigation of Willyama Complex rocks, Wiperaminga Hill area, South Australia. B.Sc. (Hons) thesis, (unpublished), University of Adelaide.

Ross, A.F., 1972: Studies of Broken Hill geology: A. Relationships between dykes and sulphide ore of the Broken Hill lode: B. Structural elements in the northern leases. B.Sc. (Hons) thesis, (unpublished) University of Adelaide.

Rutland, R.W.R., 1973a: Tectonic evolution of the continental crust of Australia In Continental drift, sea floor spreading and plate tectonics: implications to the earth sciences (ed. D.H. Tarling and S.K. Runcorn), Academic Press, London, pp. 1003-1025.

REFERENCES (cont'd)

Rutland, R.W.R., 1973b: A note on major structures in the Willyama Complex. Trans. R. Soc. S. Aust., 97(2), pp. 77-90.

Rutland, R.W.R., 1976: Orogenic evolution of Australia Earth Sci. Reviews, 12 pp. 161-196.

Rutland, R.W.R., and Etheridge, M.A., 1975: Two high grade schistosities at Broken Hill and their relation to major and minor structures. J. geol. Soc. Aust., 22, pp. 259-274.

Rutland, R.W.R., and Murrell, B., 1975: Tectonics of the Adelaide Fold Belt. Abstracts First Aust. Geol. Convention, geol. Soc. Aust., pp. 3-5.

Scheibner, E., 1973a: ERTS-1 Geological investigations of New South Wales. Unpublished Report, Geological Survey of New South Wales (73/382).

b: Fossil fracture zones (transform faults), segmentation and correlation problems in the Tasman Fold Belt System. In The Tasman Geosyncline - a Symposium (ed. A.K. Denmead, G.W. Tweedale, and A.F. Wilson). Geol. Soc. Aust. Qd. Div., pp. 65-96.

Shaw, S.E., 1968: Rb-Sr isotopic studies of the mine sequence rocks at Broken Hill. In, Broken Hill mines - 1968 (ed. M. Radmanovich and J.T. Woodcock). Monograph Series, No. 3, Aust. Inst. Min. Metall., pp. 185-198.

Simonen, A., 1971: Das finnische Grundgebirge. Geol. Rundschau. 60(4), pp. 1406-1421.

Talbot, J.L., 1967: Subdivision and structure of the Precambrian (Willyama Complex and Adelaide System), Weekeroo, South Australia. Trans. R. Soc. S. Aust., 91, pp. 45-57.

Talbot, J.L., 1969: The effects of the Palaeozoic orogeny on the Precambrian Shield of South Australia. Geol. Assoc. Canada, Sp. Papers, 59-66.

Tectonic Map of Australia and New Guinea, 1971: Geological Society of Australia 1:5,000,000. Sydney.

Thomson, B.P., 1969: The Precambrian crystalline basement. In Handbook of South Australian geology (ed. L.W. Parkin).

Thomson, B.P., 1970: A review of the Precambrian and Lower Palaeozoic tectonics of South Australia. Trans. R. Soc. S. Aust., 94, pp. 193-221.

Thomson, B.P., 1976a: Tectonics and regional geology of the Willyama, Mount Painter and Denison Inlier areas. In Economic Geology of Australia and Papua New Guinea (ed. C.L. Knight) pp. 469-476.

Thomson, B.P., 1976b: Gawler craton - regional geology. In Economic Geology of Australia and Papua New Guinea, (Ed. C.L. Knight). p. 461-466

REFERENCES (cont'd)

Tilley, C.E., 1921: The granite-gneisses of southern Eyre Peninsula (South Australia) and their associated amphibolites. Quartz. Jour. Geol. Soc. Lond., 77, pp. 75-134.

Tuckwell, K.D., 1968: The geology of part of the western Barrier Range, north of Poolamacca Station, Broken Hill. B.Sc. Honours thesis (unpublished) University of New South Wales.

Tuckwell, K.D., 1975: Structural and Metamorphic studies in the Euriowie Block, Broken Hill. Ph.D. thesis (unpublished) W.L. & L.B. Robinson College, Broken Hill.

Vernon, R.H., 1969: Archaean or Lower Proterozoic rocks, the Willyama Complex, Broken Hill area. In The Geology of New South Wales (ed. G.H. Packham), J. geol. Soc. Aust., 16(1); pp. 20-55.

Watson, D.P., 1968: Structures and field relations of epidiorite dykes in the Broken Hill orebody. Proc. Aust. Inst. Min. Metall., 227, pp. 1-9.

Whitten, G.F., 1966: The geology of some South Australian iron deposits. M.Sc. thesis, (unpublished), University of Adelaide.

Williams, P.F., 1967: Structural analysis of the Little Broken Hill area, New South Wales. J. geol. Soc. Aust., 14, pp.317-331.

Wiltshire, R.G., 1975: Structural geology of the old Boolcoomata area, South Australia Ph.D. thesis (unpublished) University of Adelaide.

Wopfner, H., 1969: Depositional history and tectonics of South Australian sedimentary basins. ECAFE Document I and NR/PR. 4/57. Symposium on the development of petroleum resources of Asia and the Far East, Canberra.

Additional References

Cooper, J.A., Fanning, C.M., Flook, M.M., Oliver, R.L., 1976: Archaean and Proterozoic metamorphic rocks on southern Eyre Peninsula, South Australia. J. geol. Soc. Aust. 23, pp. 287-292.

Katz, M.B., 1976: Lineament tectonics of the Willyama Block and its relationship to the Adelaide aulacogene, J. geol. Soc. Aust. 23, pp. 275-285.

Marjoribanks, R.W., Glen, R.A., Laing, W.P., and Rutland, R.W.R., 1977: Structure of the Willyama Block and of the Broken Hill orebody, New South Wales (in prep.).

Stanton, R.L., 1972: A preliminary account of chemical relationships between sulphide lode and "banded iron formation" at Broken Hill, N.S.W., Econ. Geol., 67, 1128-1145.

FIGURE CAPTIONS

Fig. 1. Locality map showing tectonic subdivision (after Tectonic Map of Australia and New Guinea, 1971).

Fig. 2. Map of Eyre Peninsula showing relations between Gawler Domain (including young granites), and cover rocks of Middle Proterozoic and Adelaidean age. Subdivision of the orogenic domain (enclosed unhachured areas) into older Flinders Gneiss and younger Hutchison Group is provisional and is based on geophysical data in the western part of the domain and on data from Coin (1976) near Tumby Bay.

Fig. 3. Comparison of stratigraphic successions in Cowell-Cleve area and Middleback Ranges. Basal gneiss unit in both areas is Flinders Gneiss and overlying metasediments belong to the Hutchison Group. Thickness of sequence in both areas is approximate only and is not corrected for tectonic thickening or thinning. Bar scale represents 1 kilometre.

Fig. 4. Map showing major tectonic units of the Willyama Domain: Possible pre-Willyama Basement, Willyama rocks and Adelaidean cover. In the Broken Hill sub-domain, Kantappa, Mt. Franks, Bijerkerno and Yanco Glen are areas of low to medium grade metamorphism. Major 'shear' zones also marked: MM = Mundi Mundi; MF = Mt. Franks; AV = Apollyon Valley; GV = Globe-Vauxhall. Cover fold trends north of Olary from R. Wiltshire, (pers. communication).

Fig. 5. Composite stratigraphic succession in Olary sub-domain. Numbers refer to Talbot's (1967) succession. Thickness is approximate only and uncorrected for deformation effects. Bar scale represents 1 kilometre.

Fig. 6. Stratigraphic sections across three local successions in the Broken Hill sub-domain. Bar scale represents 1 kilometre. Thicknesses are approximate and are uncorrected for tectonic effects.

FIGURE CAPTIONS (cont'd)

Fig. 7 Schematic comparison of stratigraphic sequences across Gawler sub-province. Broken Hill sequence is a composite sequence after Figure 6.

Fig. 8 Relation of Adelaidean fold trends to basement domains dominated by particular trends of retrograde schist zones and later faults.

Fig. 9 Map to illustrate possible morphotectonic relationships between the Gawler and Willyama domains. Various trends and positions for possible pre-Adelaidean strike-slip faults could be postulated. There is no known evidence for pre-Adelaidean movement on the particular possible fault shown in this figure, but it has been drawn to coincide with the Norwest and Macdonald faults which were active during and after Adelaidean deposition.